

# **Integrated modelling of global environmental change**

**An overview of IMAGE 2.4**

Edited by

A.F. Bouwman, T. Kram and K. Klein Goldewijk

*Integrated modelling of global environmental change. An overview of IMAGE 2.4*  
© Netherlands Environmental Assessment Agency (MNP), Bilthoven, October 2006  
MNP publication number 500110002/2006

*Language editing*

R.E. de Wijs, M.P.M. Hartman

*Graphics*

M. Abels, C. Bartels, J. de Ruiter, A. Warrink, F. de Blois

*Design and layout*

Uitgeverij RIVM

ISBN-10: 90-6960-151-6

ISBN-13: 978-90-6960-151-9

The publication can be downloaded from the website ([www.mnp.nl/en](http://www.mnp.nl/en)) or a printed copy requested via email ([reports@mnp.nl](mailto:reports@mnp.nl)). Be sure to include the MNP publication number.

Parts of this publication may be reproduced provided acknowledgement is given to the Netherlands Environmental Assessment Agency. Include the following information:

For the book :

MNP (2006) (Edited by A.F. Bouwman, T. Kram and K. Klein Goldewijk), Integrated modelling of global environmental change. An overview of IMAGE 2.4. Netherlands Environmental Assessment Agency (MNP), Bilthoven, The Netherlands.

For an individual chapter:

[Author(s)] (2006). [Chapter title] in: MNP (2006) (Edited by A.F. Bouwman, T. Kram and K. Klein Goldewijk), Integrated modelling of global environmental change. An overview of IMAGE 2.4. Netherlands Environmental Assessment Agency (MNP), Bilthoven, The Netherlands, [page numbers].

The Netherlands Environmental Assessment Agency (MNP in Dutch) functions as the interface between science and policy, producing independent assessments on the quality of the environment for people, plants and animals to advise national and international policy makers.

Netherlands Environmental Assessment Agency

PO Box 303

3720 AH Bilthoven

Phone: +31 (0) 30 274 27 45

Fax: +31 (0) 30 274 44 79

E-mail: [info@mnp.nl](mailto:info@mnp.nl)

Website: [www.mnp.nl/en](http://www.mnp.nl/en)

## Contents

	Page
<b>Foreword</b>	5
<b>1 The IMAGE model: History, current status and prospects</b> T. Kram and E. Stehfest	7
<b>2 People in the pixel: Grid-based population dynamics using PHOENIX</b> H.B.M. Hilderink	25
<b>3 TIMER 2: Model description and application</b> D.P. Van Vuuren, B. Van Ruijven, M.M. Hoogwijk <sup>1</sup> , M. Isaac and H.J.M. De Vries	39
<b>4 Modelling agricultural trade and food production under different trade policies</b> B. Eickhout, H. Van Meijl <sup>2</sup> and A. Tabeau <sup>2</sup>	61
<b>5 Modelling livestock-crop-land use interactions in global agricultural production systems</b> A.F. Bouwman, K.W. Van Der Hoek <sup>3</sup> and G. Van Drecht	77
<b>6 HYDE 3: Current and historical population and land cover</b> K. Klein Goldewijk and G. Van Drecht	93
<b>7 Simulating carbon exchange between the terrestrial biosphere and the atmosphere</b> J.G. Van Minnen, B. Strengers and B. Eickhout	113
<b>8 Modelling the fate of nutrients through the soil and hydrological system</b> A.F. Bouwman, A.H.W. Beusen, K.W. Van Der Hoek <sup>3</sup> and G. Van Drecht	131
<b>9 Climate: Variability, predictability and interactions with land cover</b> B. Strengers, M. Schaeffer and B. Eickhout	153

<b>10</b>	<b>GLOBIO 3: Framework for the assessment of global terrestrial biodiversity</b>	<b>171</b>
	R. Alkemade, M. Bakkenes, R. Bobbink <sup>4</sup> , L. Miles <sup>5</sup> , C. Nellemann <sup>6</sup> , H. Simons <sup>7</sup> , T. Tekelenburg	
<b>11</b>	<b>FAIR: A model for analyzing environmental and cost implications of future commitment regimes</b>	<b>187</b>
	M.G.J. Den Elzen and P.L. Lucas	
	<b>References</b>	<b>207</b>

<sup>1</sup> Ecofys, Utrecht, The Netherlands

<sup>2</sup> Agricultural Economics Research Institute, Wageningen University and Research Centre, The Hague, The Netherlands

<sup>3</sup> Laboratory for Environmental Monitoring, National Institute for Public Health and the Environment, Bilthoven, The Netherlands

<sup>4</sup> Landscape Ecology, Faculty of Biology, Utrecht University, The Netherlands

<sup>5</sup> UNEP, World Conservation and Monitoring Centre, Cambridge, UK

<sup>6</sup> UNEP GRID Arendal, C/O NINA Lillehammer, Norway

<sup>7</sup> IUCN Netherlands Committee, Amsterdam, The Netherlands

## Foreword

Continued population growth and rising per capita income, leading to industrialization and ever-increasing flows of materials, are giving rise to concern about how to ensure more sustainable forms of global human development. It is widely accepted that following a similar development path in developing countries to the one taken in many industrialized countries for many decades will lead to an unsustainable future. In particular, problems associated with climate change, loss of biodiversity, water scarcity and the accelerated nitrogen cycle are encountered at global, continental and regional scales. Solving them will demand a comprehensive understanding of the Earth system. According to the Millennium Ecosystem Assessment, the challenge is 'to investigate what goods and services are provided to humans by the natural and managed ecosystems, and how the ability to provide those services is put at risk by human activities'.

Only through a better understanding of the global environment and how it responds to anthropogenic pressure, can policy makers make the decisions pertinent to a more balanced interaction between human development and the natural system. Giving sound advice to policy makers, who are challenged in their selection of the most effective and efficient measures against large-scale or even global environmental threats, requires a specific mixture of knowledge and innovative tools that are not immediately obvious. Recommendations should have a sound base in the natural sciences, recognizing the uncertainties of the complex Earth system but also drawing on the social sciences.

An Earth system model such as the Integrated Model to Assess the Global Environment (IMAGE) will be a helpful tool in investigating the global issues, and their causes and links, in a comprehensive framework. This will include the major feedback mechanisms in the biophysical system. The version of IMAGE presented here represents the result of many years of development at the National Institute for Public Health and the Environment (RIVM); work on IMAGE is continuing at the Netherlands Environmental Assessment Agency (MNP), now separate from the RIVM. MNP has been operating as an autonomous agency since 1 January 2006. The first, single-region version of IMAGE, called the Integrated Model to Assess the Greenhouse Effect, was developed in the late 1980s. Since then, updates, as presented in several publications, have culminated in the latest incarnation, the IMAGE 2.4 framework.

IMAGE 2.4 shares many of the basic structural components of its predecessors. Assuming change, population and the macro-economy as key drivers, the model establishes physical indicators for both the energy/industry system and the agriculture/land-use system for assessment of changes in land cover, climate, and the carbon and nitrogen cycles. Besides showing several improvements in IMAGE and the extension of issues offered, this book illustrates how IMAGE can be used to feed broader policy-exploring tools. Examples are tools for assessing impacts on biodiversity, global sustainability focused on vulnerability and food security, and comprehensive climate mitigation strategies.

The contributions of IMAGE to international assessments of global environmental problems and sustainable development illustrate the continuing desire to improve the model framework so as to address the issues raised. Recently, IMAGE results have played a key role in several global studies, including the IPCC Special Report on Emissions Scenarios (SRES), the UNEP Third Global Environment Outlook(GEO-3), the Millennium Ecosystem Assessment (MA), the Second Global Biodiversity Outlook, and the Global Nutrients from Watersheds project of the UNESCO Intergovernmental Oceanographic Committee. At the European level, IMAGE has been involved in the Eururalis study on future prospects for agriculture and the rural areas of the EU-25 countries, and the Greenhouse Gas Reduction Policy (GRP). At MNP, IMAGE is a major contributor to the Sustainability Outlook. In addition to its involvement in several projects funded by the European Commission, IMAGE 2.4 is currently employed in four global environmental assessments, all scheduled for release in 2007: the Fourth Assessment Report of the IPCC, the UNEP Fourth Global Environment Outlook, the IPCC Agricultural Assessment (IAASTD) and the OECD Second Environmental Outlook.

Following one of the recommendations of the IMAGE Advisory Board in 2000, model extensions and improvements are being increasingly pursued in close co-operation with institutions, both in the Netherlands and abroad, who have expertise complementary to the IMAGE team at MNP. Today a core network of partners is taking shape around IMAGE; within this setting, instrumental joint projects have been submitted with partner institutions to secure the necessary resources. The Netherlands Meteorological Institute (KNMI), the Potsdam Institute for Climate Impact Research (PIK) and various departments and institutes of Wageningen University and Research Centre (Wageningen UR) now work closely with MNP on a variety of topics. Other network partners also contribute their knowledge and expertise in bringing collaborative activities to fruition.

The current version of IMAGE, 2.4, offers valuable stepping stones in securing the position of IMAGE as one of the leading frameworks for integrated assessment of global sustainability issues. Further developments initiated within the network of collaborating institutions offer excellent prospects for the future of the IMAGE model framework in contributing to the analysis of crucial interactions between human well-being and ecological goods and services.

Professor N.D. van Egmond

Director of the Netherlands Environmental Assessment Agency (MNP)

# 1 THE IMAGE MODEL: HISTORY, CURRENT STATUS AND PROSPECTS

## 1.1 Introduction

The current version (2.4) of the Integrated Model to Assess the Global Environment (IMAGE) documented in this publication represents the latest incarnation of a development that goes back as far as the late 1980s, when a team at the National Institute for Public Health and the Environment (RIVM), Bilthoven, the Netherlands, embarked on developing a global model to explore relevant aspects of climate change, emerging in those years as an important case for internationally concerted policy deliberations. The first version (1.0), formerly known as the Integrated Model to Assess the Greenhouse Effect (IMAGE), was a global, single-region model describing global trends in driving forces and the ensuing consequences for climatic change and impacts on key sectors through a coupled set of modules representing the main processes involved (Rotmans, 1990). At the time, IMAGE 1.0 was among the first pioneering examples of Integrated Assessment Models addressing climate change.

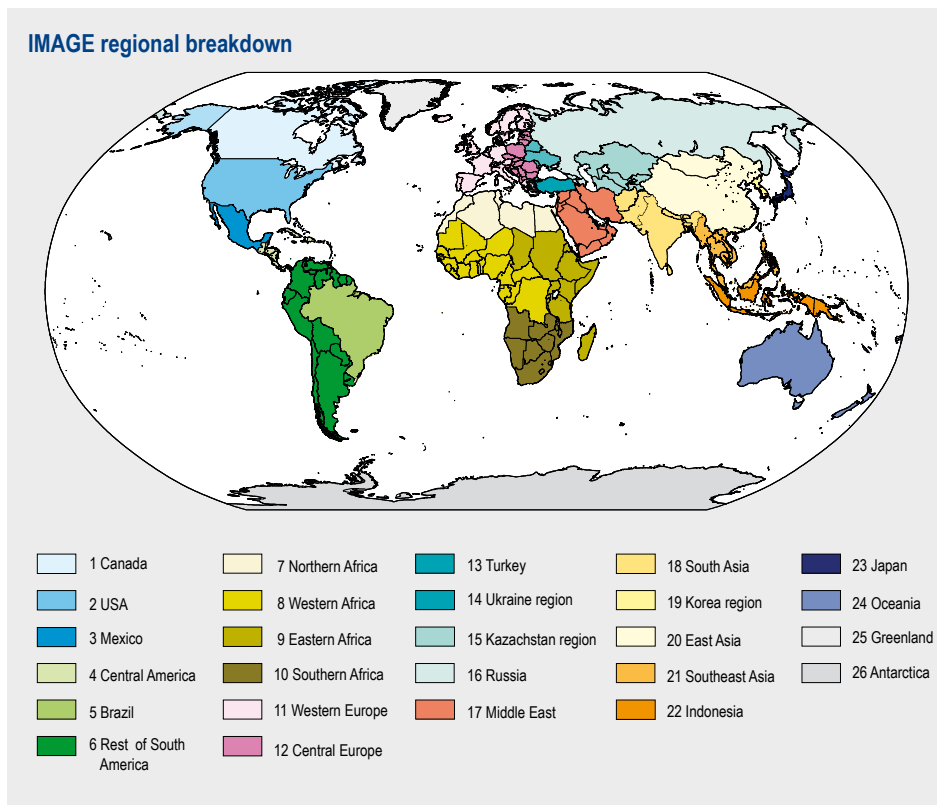


Figure 1.1. Breakdown in regions in IMAGE 2.4.

Since then, IMAGE has evolved through a series of new versions, each introducing major revisions, enhancements and extensions up to the current version (2.4) documented here. This version marks an important milestone on the development path towards a next generation model, referred to as IMAGE 3, aimed at capturing – to a larger extent – the different aspects and domains of sustainability, with emphasis on the ecological domain but also related to the economic and social domains.

Specific features of the IMAGE model include comprehensive coverage of direct and indirect pressures on human and natural systems closely related to human activities in industry, housing, transport, agriculture and forestry. Whereas socio-economic activities and drivers of change are elaborated at the 24-region level (Figure 1.1), the climate, land-cover and land-use change-related processes are represented in a geographically explicit manner on the 0.5 by 0.5 degree grid scale. It is this latter characteristic, relatively rare in integrated assessment models, that makes IMAGE particularly suited to exploring interactions between human and natural systems.

Key elements of sustainable development include provision of affordable energy while keeping air pollution and climate change under control; management of water systems in support of agriculture, industry and human settlements; increasing agricultural production while protecting soil, groundwater and surface water quality, and slowing down and eventually halting further loss of biodiversity. More generally, these issues can be described as the challenge to strike the balance between human development and the goods and services provided to humans by the natural and managed ecosystems, which are put at risk by human activities (Millennium Ecosystem Assessment, 2006a). An integrated assessment model like IMAGE 2.4 presents a helpful tool for investigating these interactions in a comprehensive framework, including the major feedback mechanisms within the biophysical systems.

As previously stated, the current version of IMAGE is the result of many years of development at the National Institute for Public Health and the Environment (RIVM), and –following a recent re-organization – the now separate Netherlands Environmental Assessment Agency (MNP). The development stages can be followed in a series of three books (Rotmans, 1990; Alcamo, 1994; Alcamo et al., 1998). Substantive further development work was undertaken between 1998 and 2001, resulting in the version 2.2 model used to elaborate the IPCC-SRES scenarios (Nakicenovic et al., 2000). The documentation on version 2.2 covering the implementation of the SRES scenarios is included on two CD-ROMs (IMAGE-team, 2001a; IMAGE-team, 2001b).

The main focus of this book, *Integrated modelling of global environmental change: an overview of IMAGE 2.4*, is to document the new developments in the IMAGE model between 2001 and 2006. More specifically, section 1.3 summarizes version 2.4 of the model (which the subsequent ten chapters of this book further elaborate). After highlighting the new key features of version 2.3 in the framework of a historical overview, this first chapter summarizes the current status of the development process up to mid-2006 (section 1.3). It goes on to compile uncertainty and sensitivity analyses carried

out for the main model components (section 1.4), which is followed by an overview of recent and current IMAGE applications (section 1.5). The chapter concludes with ongoing and planned initiatives for improvement beyond version 2.4 and on the way to IMAGE 3 (section 1.6).

## 1.2 History of the IMAGE model

The IMAGE model had its beginnings back in the mid-1980s, when RIVM decided to build a simple prototype model to capture the relationships between human activities and climate change. The experience gained from the prototype was subsequently used to build the Integrated Model to Assess the Greenhouse Effect (IMAGE 1.0, Rotmans (1990)). IMAGE 1.0 was a global (single-region) model to capture major cause-effect relationships making up the complex greenhouse problem. It constituted a global-averaged integrated structure combining energy and agriculture models for greenhouse gas emissions, a global carbon cycle model, parameterized global radiative forcing, temperature change and sea level rise. IMAGE 1.0 was used to explore global scenarios for further developing the first set of scenarios for IPCC. With regard to effects of climate change, and possible feedbacks, a regional set of modules was implemented to drive grid-based impact calculations as part of the ESCAPE framework (European Commission, 1992).

Building further on innovative approaches taken in the ESCAPE framework to estimate emissions resulting from energy and land use for world regions, IMAGE's focus was shifted to a regional base, and became known as version 2.0 (Alcamo, 1994). In this version land-cover and land-use modelling was done on a resolution of 0.5 by 0.5 degrees, drawing on experience with geographically explicit global models. At the time (1994), IMAGE 2.0 was the first published global integrated model having geographic resolution. All subsequent incarnations of IMAGE 2 have retained this two-strand approach of regional drivers and grid-based biophysical modelling.

In essence, IMAGE 2.0 consisted of three linked clusters of modules: the Energy-Industry System (EIS), the Terrestrial Environment System (TES) and the Atmosphere-Ocean System (AOS). The EIS generates industrial and energy emissions for 13 regions using simplified energy-economy relationships. TES, which has hardly changed in subsequent versions, establishes global land-cover change on the grid scale, taking (agro-)economic and climate factors into account. Changing land cover and other factors are used to compute the (net) flux of carbon dioxide (CO<sub>2</sub>) and other greenhouse gases to the atmosphere. The BIOME model (Prentice et al., 1992), the terrestrial carbon model and an FAO-based crop-growth model are important determinants of the changes in land-cover and associated emissions. The collective emissions from EIS and TES are then fed into AOS, which subsequently computes the build-up of greenhouse gases in the atmosphere. The zonal average temperature and precipitation patterns are calculated from the atmospheric composition changes.

Guided by recommendations from international review meetings, further refinements and extensions were implemented in IMAGE 2.1 (Alcamo et al., 1998). Here, the aim was to enhance the model's performance and broaden its applicability. Major steps included improved computation of future regional energy use in EIS. Since the development of IMAGE 2.1 future fuel prices have influenced the selection of fuels in the model, depending on resource depletion on the supply side and price-dependent energy conservation on the demand side. The initial land-cover map, from which the global simulations start, was updated on the basis of DISCover version 1 (Belward and Loveland, 1995), together with improved allocation of agricultural land, computation of vegetation responses to climate change. The map also included the demand of land for timber production.

The third session of the IMAGE Advisory Board in 1999 resulted in a list of recommendations and suggestions for further development work on IMAGE (Tinker, 2000). The board recommended making Global Change the target area, extending it beyond climate change, and building on integration of socio-economic and natural systems. While development up to IMAGE 2.1 had up to this point been largely an in-house effort by RIVM staff, collaboration with other domestic and international research groups was now suggested for further steps. Scientific recommendations included the development of cost curves for land-use emission reductions, meta-models and scanner models to address policy discussions and a revision of agro-economic modelling to be more in concert with approaches in other sectors. Furthermore, it was recommended to include interannual climate variability in relation to vegetation and water, and its effects on climate impacts, and to replace the zonal-mean climate-ocean model with a two-track approach. Here, a fast track would employ a simple climate model and a second track, a climate model of intermediate complexity. In addition, a list of more detailed recommendations and suggestions proposed concrete steps to consider in the development of IMAGE 2. As previously was the case, the recommendations and suggestions from the Advisory Board formed a welcome guide for the IMAGE team, with the majority of recommendations being incorporated in the subsequent work.

One of the major changes in IMAGE 2.2 concerned the recommended two-track strategy for the climate model. The earlier zonal-mean climate-ocean model in IMAGE was replaced by a combination of the simple MAGICC climate model and the Bern ocean model. In the new approach, the resulting global average temperature and precipitation changes were scaled using temperature and precipitation patterns generated by complex, coupled Global Circulation Models (GCMs). The widely accepted method of Schlesinger et al. (2000) for scaling patterns of aerosol-induced climate change was also adopted. This new approach is now the standard method for the first, simple and fast tracks to deal with climate change in the IMAGE model. A specific advantage is that patterns from different GCMs can be used to explore the uncertainties in the behaviour of the global climate system (IMAGE-team, 2001b). Parallel to this development, a second track – aiming to couple a climate model of intermediate complexity – was explored in co-operation with the Netherlands Meteorological Institute (KNMI). To date, this track currently operates in a parallel mode through the ECBilt model (see chapter 9) and more recently the SPEEDY model.

On the economy–energy side, the linkages between the TIMER energy model, which had replaced the EIS, and the macro-economic model Worldscan were improved; this included down-scaling from the 12 regions in Worldscan to the – by then – 17 active regions in TIMER and the rest of the IMAGE framework.

This IMAGE 2.2 version (IMAGE-team, 2001a) was used to contribute to the work on the Special Report on Emissions Scenarios of the Intergovernmental Panel on Climate Change (Nakicenovic et al., 2000), in particular the B1 scenario (De Vries et al. 2000). Besides changes in the model structure, much effort was therefore devoted to generating model input parameters in line with the overall story lines and the required harmonization of key input data of the SRES exercise. Special efforts were made to attune emission factors to available data in the start-year and their scenario-specific development over time. In this sense, the participation in the IPCC-SRES process has greatly enhanced the capacity of both the model and the IMAGE team to explore scenarios and obtain results geared to the requirements of various international assessment processes.

After completion of version 2.2 and the SRES scenarios, the model and model results were published in the form of a CD-ROM, facilitated by the development of the User Support System (USS) and allowing for interrogation of the model structure, input data and the vast number of results through a user-friendly interface.

The experiences gained from the SRES process had, however, reinforced the desire to seriously reconsider the future of the IMAGE model. It had become abundantly clear that further major steps in model development would be beyond the capacity of the IMAGE team, both in terms of expertise to support in-house development and in resources to simultaneously pursue further applications of the model. This tension had already been flagged by the Advisory Board in 1999 and required firm decisions on priorities and operational structures to pursue the overall goals and ambitions. As part of the process, the Dutch Ministry of Housing, Spatial Planning and the Environment (VROM) was involved in setting out strategic directions for IMAGE. The combined result of the Advisory Board report, the internal discussions within MNP and the consultations at the Ministry of VROM was put together in a strategy report entitled 'An IMAGE of the Future' (Kram, 2003).

One of the main conclusions in the report is that the IMAGE framework had received adequate international recognition to warrant or justify further investment in parallel with policy-relevant applications. Furthermore, broadening the scope to serve the emerging demand for analyses in support of global sustainability debates was adopted as the main challenge, and a more active stand taken on setting up co-operative arrangements with other research groups was seen as indispensable. A set of model enhancements was identified and later initiated; these enhancements taken jointly will constitute the next generation model, IMAGE 3. However, parallel to this, a small set of model changes, internally referred to as version 2.3 and mainly concerned with the integration of energy crops and carbon plantations, was implemented for the analysis of mitigation options (Van Vuuren et al., 2006).

The main milestone on the road to realizing IMAGE 3, however, is the IMAGE 2.4 version described in this book, which already addresses much of the overall development strategy and new challenges.

### 1.3 IMAGE 2.4

In the last couple of years a series of improvements, enhancements and extensions of the IMAGE model have been initiated and framed in an overall model strategy towards broader coverage of sustainable development issues. The development activities increasingly take place in close collaboration with national and international partner institutes, with the aim of jointly benefiting from shared expertise and models. A scheme of the current model structure is given in Figure 1.2. The subsequent chapters of this book will follow the main model components, describing in more detail the new developments in IMAGE 2.4 and the challenges offered by the envisaged IMAGE 3.

Looking at the top of the scheme in Figure 1.2, we see a description of the basic driving forces, including demographics (chapter 2), energy supply and demand (chapter 3), and agricultural demand, and trade and production (chapter 4). All of these interact through land use and emissions with the Earth systems. Subsequently, important elements in the biophysical modelling of land cover and land-use processes are also addressed, i.e. land cover and land use (chapter 5), contemporaneous and historical land cover (chapter 6), the carbon cycle (chapter 7) and nutrients (chapter 8), followed by climate and climate variability, including its interaction with land cover (chapter 9). Finally, the use of data and information from IMAGE as input for broader policy-exploring tools is discussed for both global biodiversity (chapter 10) and comprehensive climate mitigation strategies and regimes (chapter 11). Several chapters, notably 9, 10 and 11, present model components that are not strictly integrated with IMAGE 2.4.

The scheme of the IMAGE 2.4 model framework in Figure 1.2 shows many of the basic structural components of its predecessors. The key drivers of change, population and the macro-economy, can be derived from various external and internal sources. For macro-economic drivers the exogenous source depends on the study in which IMAGE 2.4 is applied. One of the most important challenges for IMAGE is the integration of a macro-economic model in the modelling framework in order to be able to address feedbacks from the environmental system to the economy. In the remainder of this section the main model components, and their improvements and extensions incorporated in IMAGE 2.4, are summarized.

#### *Demographics*

Population projections (chapter 2) are taken primarily from authoritative exogenous sources like the UN or IIASA, but may also be adopted from the in-house demographic model PHOENIX (Hilderink, 2001). In IMAGE 2.4, grid-based population dynamics have been improved by introducing a new downscaling algorithm. Population within a grid cell is calculated with a proportional method using available country-specific data

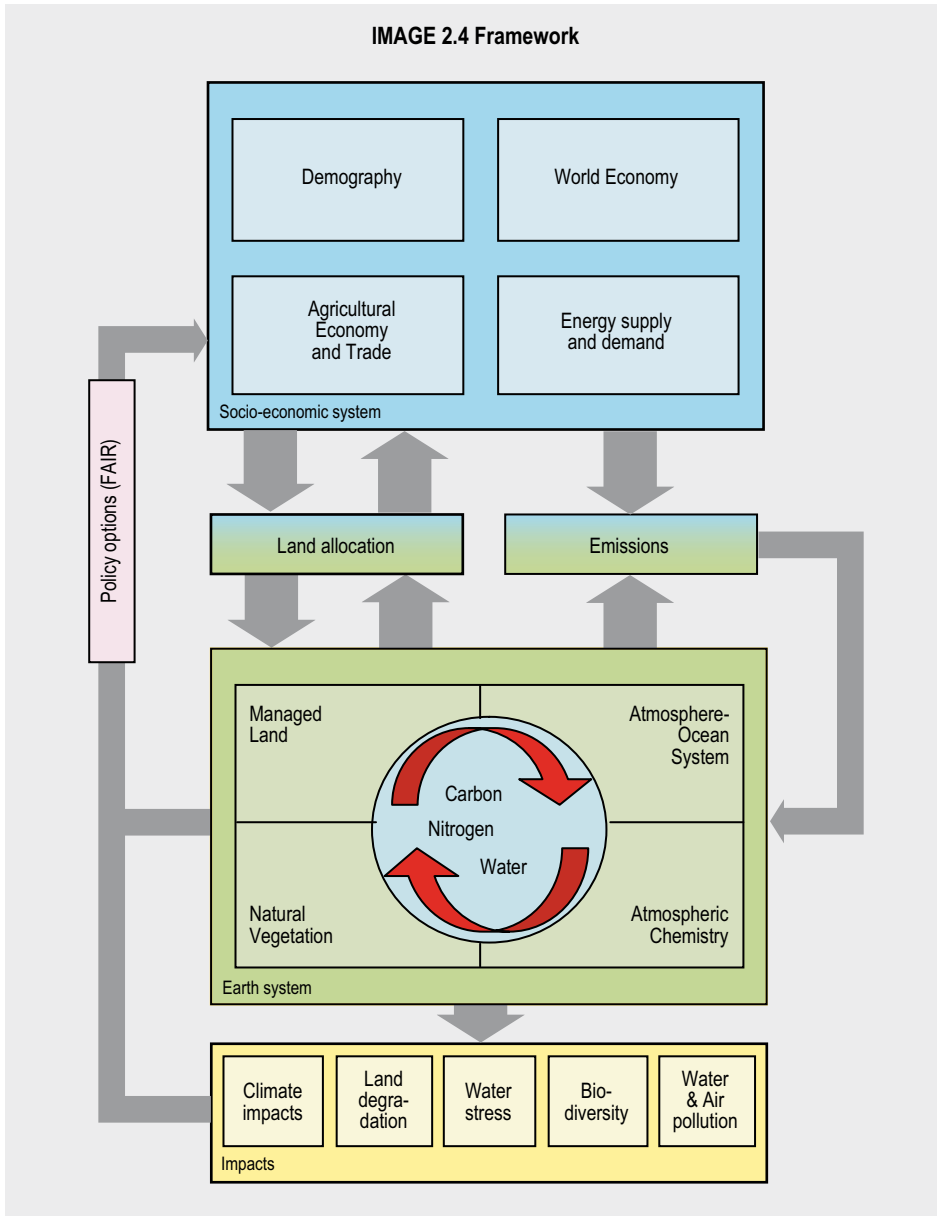


Figure 1.2. Schematic diagram of IMAGE 2.4.

combined with the trends on the level of world regions, as determined by PHOENIX. This approach allows for simulating shifts in population within IMAGE regions.

### **Energy supply and demand**

In the TIMER model (chapter 3), aggregated economic indicators like GDP, household consumption and value added in industry, services and agriculture are used to estimate the demand for energy services. Energy supply chains with substantial technologi-

cal detail are then selected on the basis of relative costs to meet the resulting final energy demand after autonomous and price-induced energy savings. Market shares for energy resources and technologies are calculated via a multinomial logit distribution function (De Vries et al., 2001). TIMER includes explicit treatment of traditional biofuels, vintages of capital stock, learning-by-doing (i.e. technologies improve with their cumulative build-up of installed capacity) and resource depletion (driving up costs for extraction of exhaustible energy resources). It generates primary and final energy consumption by energy type, sector and region; capacity build-up and utilization; cost indicators, and greenhouse gas and other emissions. Important new elements that have been introduced in the TIMER 2.0 model (part of IMAGE 2.4) are hydrogen production and more detailed descriptions of the electric power system and renewable energy, including bioenergy.

### ***Agricultural demand and trade***

Demand for and production of agricultural products on the basis of population changes and economic developments are simulated through a linkage to the global trade analysis project (GTAP) model (see chapter 4). GTAP calculates consumption and trade of agricultural products by taking into account regional and world market prices, which are calculated explicitly from production functions including capital, labour and land prices. In return, IMAGE 2.4 provides land-supply curves, yields and yield changes, which result from climate change and expansion of agriculture to less productive areas, and simulates the geographically explicit environmental impacts. This iterative coupling between GTAP and IMAGE allows assessment of the economic and environmental consequences of specific trade policies.

### ***Land use and land cover***

One of the most striking parts of IMAGE 2.4 is the geographically explicit land-use modelling, considering both cropping and livestock systems on the basis of agricultural demand (chapter 4) and demand for energy crops (chapter 3). The rule-based allocation accounts for crop productivity (Agro-Ecological Zones approach; FAO, 1978-1981), and other suitability factors like proximity to existing agricultural land and water bodies. The land-cover type 'energy crops' is now included in IMAGE 2.4. A more detailed description of animal production systems has been introduced in IMAGE 2.4 to portray the spatial variability in grazing systems, and to address the rapid development of intensive ruminant production on managed grassland and the rapidly increasing use of various feedstuffs (chapter 5). Moreover, a new initial land-use map for 1970 is incorporated on the basis of satellite observations combined with statistical information (chapter 6). Historical land cover (HYDE 3) for the period 1700-1970 (chapter 6) is based on census data, the land's suitability for agricultural production and historical population density distributions. Changes in natural vegetation cover on undisturbed or abandoned land are simulated in IMAGE 2.4 on the basis of a static natural vegetation model (Prentice et al., 1992).

### ***Carbon cycle***

The consequences of these land-use and land-cover changes for the carbon cycle are simulated by a geographically explicit terrestrial carbon cycle model (chapter 7). If

agricultural land is abandoned, it is assumed to revert gradually to its more natural state, with implications for the carbon stock. The carbon cycle model, implemented in the IMAGE framework since version 2.0, has been subjected to a thorough evaluation, which showed that the model is suitable for simulating global and regional carbon pools and fluxes. The model accounts for important feedback mechanisms related to changing climate, CO<sub>2</sub> concentrations and land use. In addition, it allows for evaluating the potential for carbon sequestration in natural vegetation and carbon plantations (chapter 7).

### *Nitrogen cycle*

IMAGE 2.4 also includes a new module to assess the consequences of the changing population, economy, land use and technological development for surface-nutrient balances and reactive nitrogen emissions from point sources and non-point sources (chapter 8). These surface balances form the basis for describing the major fluxes in the global and regional nitrogen cycle, as well as the effects on water and air quality (Figure 2.1). Processes that are accounted for in this module are human emissions, wastewater treatment, surface nitrogen and phosphorous balances for terrestrial systems, ammonia emissions, denitrification and N<sub>2</sub>O and NO emissions from soils, nitrate leaching, and transport and retention of nitrogen in groundwater and surface water. In order to derive spatially explicit scenarios, tools were developed to translate regional or country-specific information to grid-specific input parameters.

### *Atmosphere – ocean system*

Emissions from the energy system (chapter 3) and emissions due to land-use changes (see chapters 7 and 8 for the terrestrial carbon and nitrogen cycle) determine the composition of the atmosphere. IMAGE 2.4 uses the Atmosphere–Ocean System model developed for IMAGE 2.2 (Eickhout et al., 2004). However, important non-linear interactions between the land, the atmosphere and the ocean cannot be studied with IMAGE 2.4 due to limitations of the current climate model and the natural vegetation module. Therefore a series of studies was carried out to explore a possible pathway to include a more detailed climate model in IMAGE (chapter 9). As an outcome of this exploration, the detailed climate circulation model (SPEEDY) coupled to the Dynamic Global Vegetation Model LPJ will be part of future IMAGE versions.

### *Biodiversity*

In addition to these environmental impacts of global change calculated within the core biophysical modules, results are also used as input to drive impact models in the broader IMAGE 2.4 framework, such as the biodiversity model GLOBIO 3. GLOBIO (chapter 10) can be used to assess the impacts of climate and land-use change, infrastructure, and nitrogen deposition on biodiversity and ecosystems. Likely effects of scenario assumptions or political interventions are estimated by calculating trends in mean species abundance.

### *Climate Policy options*

IMAGE results are also used for the evaluation of climate policies in conjunction with the policy decision-support model FAIR (chapter 11). FAIR is widely used to assess the environmental and abatement cost implications of international regimes for the differentiation of future emission reductions of greenhouse gases. The model links long-term climate targets and global reduction objectives with regional emission allowances and abatement costs, accounting for the Kyoto Mechanisms.

## 1.4 Uncertainty and sensitivity

Obviously, numerous sources of uncertainty in the various components of IMAGE 2.4 influence its analytical results, ranging from data imprecision and model uncertainties, to scenario assumptions in applications. To date, no comprehensive and systematic exploration has been performed of key uncertainties and how they are propagated throughout the entire IMAGE model to influence the final results. Currently, plans are being developed to undertake this demanding exploratory task. What has been done in many instances is to look at uncertainties in underlying data and model formulations in sub-systems of the overall framework, thus providing partial sensitivity analyses for IMAGE 2.4 framework. An overview of the available sensitivity studies for the main modules is given below.

An earlier version of the TIMER energy and emissions model was systematically examined to establish the most important parameter settings and model assumptions influencing model results. This exploration using the NUMeral Spread Assessment Pedigree (NUSAP) system (Van der Sluijs et al., 2005). Input variables and model components most sensitive to projected CO<sub>2</sub> emissions were population and economic growth; shifts in economic structure; technology improvement factors; fossil and renewable resource cost/supply curves, and autonomous and price-induced efficiency gains. Combined with the outcome of expert appraisal of the parameter 'pedigree', estimates of the 'strength' of the parameters were added to their sensitivity.

Obviously, any projection of future environmental conditions rests critically on the underlying emission factors and their relationship with relevant human activities or drivers. The IMAGE model has incorporated the most recent and authoritative sources. Despite ongoing efforts to collect data and enhance statistical procedures and modeling, many emission sources of greenhouse gases and other anthropogenic trace gases remain uncertain. Van Aardenne et al. (2001) have overviewed the qualitative analysis of activity data, emission factors and grid maps as in IMAGE. As a rule, emissions from large point sources like power plants tend to be of acceptable quality, while smaller and dispersed sources are typically poor to very poor. Whereas global or large-scale regional aggregate budgets are generally reasonably well known, the contribution of sectors and activities by geographic location is for the most part much more uncertain. Emission factors that depend on fuel properties, like CO<sub>2</sub> and sulphur dioxide (SO<sub>2</sub>), can be estimated within narrow ranges, but others are very sensitive to technological

details, local conditions like soil properties, and management practices. This induces not only uncertainties in the initial inventories, but also in future emission projections.

In the coupled application of the agro-economic GTAP model and IMAGE, land-supply curves play a crucial role in establishing agricultural demands, production and trade flows. Derived from biophysical properties in IMAGE, land-supply curves are used in GTAP to find solutions of equilibrium for agricultural land volumes and the associated land rental rate (see chapter 4). To test the sensitivity, simulation experiments were run with the asymptote 2.5% lower and 2.5% higher than the central estimate; the impacts on model results for land supply, the real land rental rate and production changes were investigated (Tabeau et al., 2006). Analyses show that changing the asymptote of the land supply function leads to significant changes of land supply for countries where agricultural land is relatively scarce. However, the induced production changes are rather low. The aggregated agricultural production elasticity with respect to the asymptote change varies from 0.1 for countries where agricultural land is abundant to 0.5 for countries where the agricultural land is scarce. This means that the simulation results for production development are rather robust with regard to the estimated land supply-curve parameters.

The sensitivity of ammonia ( $\text{NH}_3$ ) volatilization in agricultural production systems to variation in input parameters was investigated by Bouwman et al. (2006). Various parameters were selected, including nitrogen excretion per head, animal stocks, the distribution of production over pastoral, and mixed and landless systems, fertilizer inputs and the  $\text{NH}_3$  emission factors for animal housing, etc. The results suggest that on the global scale, excretion of nitrogen per head and animal stocks are the most important parameters in the model. However, the importance of the various parameters varies among world regions and countries. For example, in China fertilizer use is a far more important determinant for total ammonia loss than in other world regions, while in India the use of manure as fuel is a very important process. The overall conclusion is that nitrogen excretion per head merits our attention in future research. Research will focus on the difference between N excretion in extensive versus intensive systems, and modelling excretion as a function of production characteristics such as milk production per head and nutrient intake by feed category (see chapter 5). This study also made clear that the spatial modelling of nutrient use presented in chapter 8 allows for analysis of various policy alternatives and consequences for the nitrogen cascade.

A series of experiments examined the role of the terrestrial carbon cycle in overall climate change scenarios implemented in IMAGE 2.2 (Leemans et al., 2002). The experiments yielded a broad spectrum of atmospheric  $\text{CO}_2$  concentrations, ranging, for example, in the IPCC-SRES A1B scenario from 714 to 1009 ppmv in 2100. The spread of this range is comparable to the full range arising from the different SRES scenarios with respect to the IMAGE 2.2 default settings for the carbon cycle: 515-895 ppmv. The most important respective negative and positive feedback processes are  $\text{CO}_2$  fertilization and soil respiration. In recognition of the importance of a proper parameteriza-

tion of the major feedbacks on the carbon cycle and land use, and thus in determining the future state of the climate system, the issue has more recently been further pursued (see chapter 7).

With regard to the response of the climate system to changes in atmospheric composition and associated radiative properties, two core aspects were tested. The first parameter addressed was climate sensitivity, which describes by how many degrees the equilibrium global mean temperature will rise if the CO<sub>2</sub>-equivalent concentration of greenhouse gases in the atmosphere doubles compared to the pre-industrial level. The simple climate model in the Atmosphere-Ocean System (AOS) of IMAGE 2, attuned to represent the generally accepted central estimate for the climate sensitivity of 2.5 degrees, was adjusted to explore the range from 1.5 to 4.5 degrees. As expected, this amplified or reduced all climate-related impacts very tightly for any given emission projection. For climate change impacts, however, global mean effects are of limited significance. Therefore, a second sensitivity analysis addressed the spatial patterns of temperature and precipitation projections. IMAGE employs exogenous patterns from complex climate models (GCMs) to scale the impacts of the endogenously derived global mean temperature change. The robustness of regional impacts on different GCM patterns was tested by UNEP/RIVM (2004). Results indicate that while GCM outcomes for some regions are fairly consistent, in other regions the temperature effect is very different. With regard to annual precipitation the disagreement between models is even stronger. In some regions, e.g. South America, they do not even agree on the direction of change.

Estimates of the costs of emission reductions, even within a well-defined scenario context are subject to considerable uncertainties, as the potential contribution and cost of abatement options are spread across wide ranges. A sensitivity analysis was performed for a scenario that stabilizes at 550 ppm CO<sub>2</sub>-equivalent (Van Vuuren et al., 2006) in order to identify for which abatement options the alternative assumptions had a significant impact on overall abatement costs. Selected options were tested one by one, but also all together and simultaneously. Most individual options did not affect the total abatement costs by more than 10% (up or downwards) until 2050, with the exception of energy crops. When accepting the high end of the literature estimates on the supply potential, and introducing the option to capture and store CO<sub>2</sub> from bioenergy, costs dropped by up to 40%. The compounded effect of all options taken together, however, results in 40% lower to almost 100% higher costs in 2050. Beyond 2050 the impact of uncertainties in options increases further. This applied particularly to options that are expected to become viable on a large scale in the longer term, such as hydrogen ( $\pm 20\%$  in 2100). The compounded effect of all options considered collectively falls into the range of -40% to +250% by 2100.

## 1.5 Applications

In parallel with the development steps outlined in the previous section, the IMAGE model has been applied to a variety of global studies. The specific issues and questions addressed in these studies have inspired the introduction of new model features and capabilities, and in turn, the model enhancements and extensions have broadened the range of applications that IMAGE can address. Since the publication of IMAGE 2.1 (Alcamo et al., 1998), subsequent versions and intermediate releases have been used in most of the major global assessment studies and other international analyses, as listed below:

- **IPCC-Special Report on Emissions Scenarios (SRES):** implementation of the B1 marker scenario and calculation of the other harmonized set of comprehensive emissions scenarios up to 2100 (De Vries et al., 2000; Nakicenovic et al., 2000; IMAGE-team, 2001a);
- **UNEP Third Global Environment Outlook (GEO-3):** assessment of environmental impacts from four global scenarios to 2030 (UNEP, 2002; UNEP/RIVM (2004);
- **Millennium Ecosystem Assessment (MA):** development of four global scenarios for the development of ecosystem services up to 2050 (Millennium Ecosystem Assessment, 2006b);
- **EuRuralis-1:** assessment of future prospects for agriculture and the rural areas in the EU-25 countries (Eickhout et al., 2006);
- **Fourth Assessment Report of the IPCC (AR4):** comprehensive global mitigation scenarios explored using IMAGE/TIMER/FAIR (Van Vuuren et al., 2006). Besides participating in the mitigation scenarios study, several MNP experts serve as contributing/lead authors to the Working Group III report. A sensitivity study on the terrestrial carbon cycle was also done with IMAGE to obtain an adequate baseline against which to evaluate the potential for carbon sequestration options.
- **Greenhouse Gas Reduction Policy (GRP) study:** exploration of alternative climate change abatement goals and regimes in support of EU policy making using IMAGE/TIMER/FAIR (European Commission, 2005);
- **Second Global Biodiversity Outlook (GBO-2):** background report for the UN Convention on Biodiversity: evaluation of baseline trends in biodiversity loss and effects of policy actions in different fields with IMAGE/GLOBIO up to 2050 (Alkemade et al., 2006);
- **MNP Sustainability Outlook (DV):** assessment of sustainability issues in land use and energy resulting from different scenarios, reflecting various perspectives on future directions for Dutch society (Netherlands Environmental Assessment Agency, 2004a,b);
- **Global Nutrients from Watersheds (NEWS):** preparation of data on global nutrient surface balances for the UNESCO-Intergovernmental Oceanographic Committee NEWS project (Seitzinger et al., 2005).

Currently, IMAGE 2.4 is engaged in three global environmental assessments, all scheduled for release in 2007. In varying combinations with other teams, IMAGE forms part of a range of modelling frameworks, as outlined below:

- Fourth Global Environment Outlook of UNEP (GEO-4) will have 'Environment for Human Well-being' as the central theme, linking environment and development. IMAGE will play a major role, contributing to the energy outlook, land-use change and climatic consequences of the four updated GEO scenarios (see <http://www.grid.unep.ch>).
- International Assessment of Agricultural Science and Technology for Development (IAASTD) (<http://www.agassessment.org>) will be published in the autumn of 2007. Together with the International Food Policy Research Institute (IFPRI), the IMAGE team plays a pivotal role in the quantification of agricultural markets and environmental consequences. The scenarios of the Millennium Ecosystem Assessment (Millennium Ecosystem Assessment, 2006b) will be used as a basis.
- Second Environmental Outlook of OECD is to be published in 2007. IMAGE's task will be to develop the environmental baseline according to the economic projections of OECD's economic model ENV-Linkages for the first part of the Outlook. In the second part, the impacts of several policy packages will be analyzed, centering on the theme 'policy coherence'. This applies to coherence across different policy areas within OECD and to more coherence between OECD and non-OECD member states, with a special focus on major players, the so-called BRIICS countries (Brazil, Russia, India, Indonesia, China and South Africa).

In addition to these global assessments, IMAGE is also widely used in other projects and studies at sub-global scale, mostly European and more often than not in consortia, including the main partners of the IMAGE development network. Examples include Nitro-Europe, MATISSE (on sustainability assessment methods and tools) SCENAR2020 (agriculture scenarios), ADAM (EU climate-response strategies comprising balanced adaptation and mitigation) and Eururalis 2.

## 1.6 What comes after IMAGE 2.4?

Concrete steps are being taken to initiate the development of further enhancements and extensions of IMAGE beyond what is offered in version 2.4. Following one of the recommendations of the IMAGE Advisory Board in 1999, these developments are pursued in close co-operation with institutes in the Netherlands and abroad with expertise complementary to the IMAGE team at MNP. Today a core network of partners is being built around IMAGE, and, where instrumental, joint projects have been submitted with partner institutes to secure the necessary resources. The Netherlands Meteorological Institute (KNMI), the Potsdam Institute for Climate Impact Research (PIK) and various departments and institutes of Wageningen University and Research Centre (WUR) now work closely together with MNP on a variety of topics. In addition, other network

partners contribute their knowledge and expertise in collaborative arrangements. The most important activities are highlighted below.

### ***Emissions Reduction Allocation***

In co-operation with the Netherlands Organization for Applied Scientific Research (TNO), a new Emissions Reduction Allocation Module (ERAM) was developed that allows for a flexible approach to different classes of environmental problems (acidification, climate change). Separate and simultaneous emission targets can be imposed, with full feedback on structural and technological adjustments in TIMER. The ERAM model covers emissions from all sectors, but in its current form only feedbacks on energy-related emissions are fully implemented. In a following phase, ERAM will be expanded with explicit optimization routines, and land-use emission reductions will be implemented that are comparable to the energy sector emissions.

### ***Crop modelling***

In co-operation with WUR-Plant Production Systems a plan has been developed for improved crop modelling on the IMAGE grid scale. The new model will link crop growth to climate, soil, water, nutrients and management parameters and thereby mark a substantial improvement in the current, less integrated treatment of the various processes and linkages in IMAGE 2.4. The work is envisaged as a joint WUR/MNP PhD research project.

### ***Water supply and demand***

Further integration of water supply and demand with other parts of IMAGE being considered under a co-operative agreement with the WUR Centre for Water and Climate. Currently, the WaterGAP model of the University of Kassel (Alcamo et al., 2003) functions as a soft-link to IMAGE 2.4 in the form of an impact model to reflect changes in water supply and demand, and associated levels of water stress. The new model to be developed should provide a more integrated treatment of water in key processes like variable precipitation (SPEEDY), evapotranspiration (LPJ and the new crop model) and extraction for irrigation (the new crop model), households and industry.

### ***SPEEDY/LPJ climate-vegetation modelling***

The successor to the ECBilt model, the intermediate complexity 3D climate model SPEEDY has now, again in close co-operation with KNMI, been transferred to MNP to be linked to IMAGE. After several adjustments to make this coupling viable, the model was successfully coupled with the dynamic vegetation model LPJ at MNP. Test runs confirm the proper functioning of the coupled dynamic climate-vegetation system, although a few remaining flaws still need to be dealt with. Further work will involve a coupled ocean model, already ongoing at KNMI, and integration with the IMAGE framework. This integration will allow for capturing changes in climate variability and their implications for other sections of the model, e.g. natural vegetation, agricultural production and the hydrological cycle. It will also enable assessment of climatic impacts from changes in radiative forcing and land use.

In conjunction with the dynamic climate model SPEEDY (see above), the current BIOME vegetation model of IMAGE will be replaced by the dynamic vegetation model LPJ of the Potsdam Institute for Climate Impact Research. The LPJ model has been made available to MNP as part of a broader co-operation plan and has been adapted to fit into the IMAGE structure. The linkage to LPJ will allow a better representation of biogeochemical cycles and analysis of the compounded effect of changes in these cycles, and biogeophysical changes associated with land use and hydrology.

### ***Land allocation***

An improved and extended land-allocation module for IMAGE will be developed using the WUR-Soil Inventory and Land Evaluation, to start with, the collaborative research focused on the European region in the first Eururalis project (Eickhout et al., 2006). This research is currently being continued in Eururalis-2. A country-by-country representation of drivers and parameters of future land-use determinants will be implemented consistent with regional totals and country information from LEI's GTAP model. The main purpose is to better reflect determinants of spatial allocation process. A nested version of IMAGE has already been technically implemented as a start to achieving a better representation of Europe. This nested or 'zoom' version offers more intra-regional breakdown into smaller regions and countries and more spatial detail in one of the larger global IMAGE regions; all other regions are modelled at the standard IMAGE resolution and act as 'background'. A new land-cover base map with 5 by 5 minute resolution was developed from satellite-based data for this purpose (Klein Goldewijk et al., 2006), and 5 by 5 minute resolution maps of soil characteristics and derived soil properties were prepared for use in IMAGE by ISRIC-World Soil Information (Batjes, 1997; 2002).

### ***Bioenergy***

In cooperation with the WUR Agro-economic Institute (LEI), work has been initiated on the inclusion of the currently lacking land use for bioenergy in the overall agro-economic modelling. To capture relevant aspects of the demand for energy crops, this will most probably imply an extension to the GTAP-E model, with explicit representation of bioenergy in the relevant sectors, including land in the production functions. The GTAP-E model will have to be attuned to the more detailed TIMER model to ensure internal consistency.

### ***Global Integrated Sustainability model***

The Global Integrated Sustainability MOdel (GISMO) will be developed to quantitatively address, position and analyze global sustainability questions, with a focus on the link between development and the environment. GISMO will build mainly on the already existing (global) simulation models within the IMAGE framework, but will also seek collaboration with (modelling) groups outside the MNP. These groups include, for example, the University of Denver for economy modelling; the institute for Medical Technology Assessment (iMTA-Erasmus University Rotterdam) for health modelling; and the Institute for Environmental Studies (Vrije Universiteit Amsterdam) for analyses of the role of institutions. The project does not intend to create a large new model,

but rather to develop a framework to address broad sustainable issues and assess the trade-offs and co-benefits of specific policies in an integrated way. Topics to be covered include population and health, poverty and biodiversity, the role of institutions in sustainable development and, elaborating on the work of Lucas and Hilderink (2004), on vulnerability and food security.

Valuable steps are being taken in the development of IMAGE 2.4 to secure the position of IMAGE as one of the leading frameworks for integrated assessment of global sustainability issues. The further developments initiated within the network of collaborating institutes offer excellent prospects for the future, in which the IMAGE model framework will make an important contribution to the analysis of crucial interactions between human well-being and ecological goods and services.



## 2 PEOPLE IN THE PIXEL: GRID-BASED POPULATION DYNAMICS USING PHOENIX

- Population change and population distribution are important drivers of global environmental change. Population projections are either derived from external sources, or simulated within the IMAGE 2.4 framework by the PHOENIX model.
- In IMAGE 2.4, grid-based population dynamics have been improved by introducing a new downscaling algorithm. Population within a grid cell is calculated with a proportional method using available country-specific data combined with the trends on the level of world regions, as determined by PHOENIX. This approach allows for simulating shifts in population *within* IMAGE regions.
- For further improvement of grid-based population projections, an attractiveness function is proposed, which allocates population changes based on allocation factors varying in both time and space. This attractiveness function can be used to mimic higher urbanization rates in specific locations or initiate the formation of new urban areas.

### 2.1 Introduction

The proportion of the population living in urban areas is expected to increase in the coming decades. In 2007 roughly 50% of the world population will be living in urban areas, while in 1950 this was only about 30% (UN, 2003). Urbanization can result in the worsening of living conditions in urban areas. Crowding itself already increases opportunities for easily transmittable diseases such as tuberculosis (Gray, 2001). In addition, poverty and psychosocial health problems may occur in urban areas, including increased health risks from malnutrition and HIV/AIDS, but also higher lifestyle-related health risks such as smoking, addictive substances and limited social support (Harpam et al., 2003). Moreover, environmental problems such as inadequate water and sanitation, and various forms of contamination, can also affect health. The (long-term) effect of global environmental change on water and food availability through, for example, temperature increase, land degradation and changing precipitation patterns can worsen these environmental conditions and even affect demographic processes by increasing health risks (Parry et al., 2001). Similar to these urban-specific determinants of health and mortality, the other two basic demographic components, fertility and migration, are interlinked with socio-economic and environmental aspects (Hilderink, 2000b), which are different for urban than for rural areas. In developing countries, the total fertility rate (TFR) in cities with a population over 5 million is half of that in rural areas (Montgomery et al., 2003).

The pressure on the environment may also increase as a result of urbanization. Expansion of cities forces the production of bulk food to move away from where people live, making food supply more dependent on energy for transport and infrastructure. Production of vegetables and meat often takes place in peri-urban areas, where highly

intensive production systems act as point sources of emissions of ammonia, nitrate, methane and other pollutants. Water scarcity and deteriorating water quality are often difficult to prevent since a growing city generally depends on water supply within its area, provided by surface water or groundwater resources.

Both the environmental and socio-economic aspects are included in various population projections (Rotmans and De Vries, 1997; Hilderink, 2000b; Lutz and Goujon, 2001). However, spatially explicit population projections are rare. The European Union is one of the few exceptions, carrying out projections up to 2025 on sub-national level on the basis of the sophisticated cohort-component methodology (Eurostat, 2005).

In IMAGE, regional population changes are mostly obtained from exogenous sources, for example, the IPCC SRES scenarios (Nakicenovic et al., 2000) and the downscaling to the 0.5 by 0.5 degree grid cells under the assumption of uniform population changes. A limitation of IMAGE 2.4 (and earlier versions) is that the built-up (urban) area is assumed not to change in scenarios, and this may lead to unrealistic results of downscaling regional population estimates.

This chapter explores how the current methodology can be refined and improved in order to simulate spatially explicit population dynamics for urban and rural populations at a high resolution. First, data limitations related to population growth in rural and urban areas (section 2.2) and future population changes, components of population growth and modelling population changes (2.3) are discussed. Subsequently, we present a number of improvements to the modelling of population dynamics in IMAGE, and further possibilities for improvement (section 2.4).

## **2.2 Urbanization and population density: data limitations**

### ***Urbanization***

The possible impacts of urbanization, both on the human and the environmental system, are beyond dispute. However, the definition of what is considered to be urban area is rather ambiguous. The World Urbanization Prospects of the United Nations (2001) use data provided by National Statistical Offices (NSO) of all countries. As a result, definitions of urban area and urban population within UN projections show a very broad variation depending on the methodology applied by each NSO.

Most definitions are based on the number of inhabitants in a city. The threshold value of the number of persons to be counted as 'urban area' ranges between 200 (Norway, Greenland) and 20,000 (Nigeria). Other countries use a selection of their major cities (in Denmark this comprises the capital city and all provincial capitals, while, for example, in India a minimum population density of 390 persons per square kilometre is combined with indicators for the structure of the economy to define urban population. In

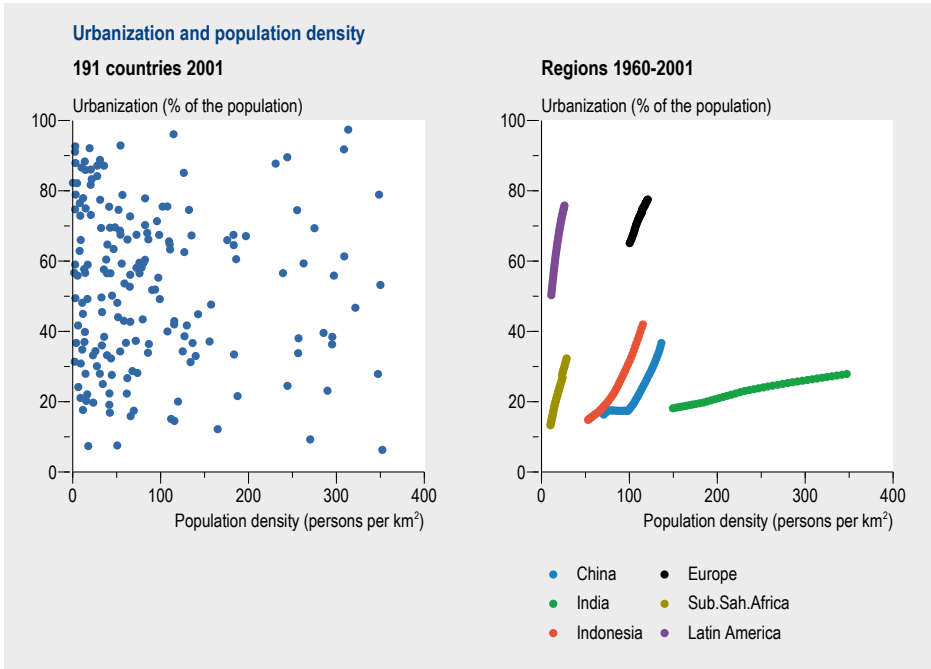


Figure 2.1. Urbanization and population density for 191 countries for the year 2001 and for selected countries and regions for the period 1960-2001 (World Bank, 2004).

addition to differences in interpretation, definitions also change over time in countries such as China, making comparisons difficult (White et al., 2003).

Population density and the level of urbanization do not seem to be correlated, at least on the national scale (Figure 2.1). Time-series analysis suggests, however, that the proportion of urban population increases with increasing population density.

### Population density

Instead of using the number of inhabitants of a city or other characteristics mentioned above, population density could be used as a proxy for urban area. The gridded population of the world (GPW) (CIESIN, 2005) provides population density data with a spatial resolution of 2.5 by 2.5 minutes for 1990, 1995 and 2000 from population census data for 399,747 administrative units. LandScan (2001) provides population density maps at an even higher spatial detail of 1 by 1 km. In addition to population census data, LandScan (2001) included other factors such as roads, slope, land cover, night-time lights and coastlines.

In IMAGE 2.4 urban area or built-up area is derived from the DISCover version 2 database (Loveland et al., 2000). Built-up areas are assumed not to be available for any other type of land use. IMAGE 2.4 does not simulate changes in the size of the built-up area. An implication of this assumption is that the urban population only increases with changes in the population living within the constant built-up areas.

## 2.3 Future population

### *Population change*

Changes in population size are the simplest way of dealing with demographic changes. The world population passed the number of 6 billion people in 1999 and is currently growing at a rate of 1.3% per year. Most of this growth occurs in Asia and Africa, while the growth of the population in the EU25 is only slightly positive (Eurostat, 2005); the population for Europe as a whole has even been decreasing since 1998 and may continue to decrease for at least the coming 50 years (UN, 2004). In Eastern Asia (dominated by China) a negative growth rate may be reached just before 2040. All growth percentages show a gradual decline in the coming decades. Some of the regions had their peaks in growing percentages in the 1950s (Northern America and Europe) and in the 1960s (Eastern and South-eastern Asia), while growth rates of Africa peaked in the 1980s.

The combination of these growth percentages with the population size yields the absolute change in population. Despite the fact that growth percentages are rapidly declining, the peak of population increase in absolute terms is still to come in some regions (Figure 2.2). Africa, for example, shows a growing increase of the population up to 2030. Around that year, the population is expected to increase by more than 25 million per year. The world population showed a growth of almost 80 million per year in 2002 and is expected to decrease to around 40 million per year in 2050.

For exploring future population changes we rely on the available population projections, mostly at national or regional level. Most of these projections do not distinguish between urban and rural population. One of the few exceptions is formed by the world urbanization prospects of the United Nations (UN, 2003), providing urbanization rates for 228 countries for the period up to 2030. The methodology applied to these projections was already used in the 1970s and 1980s (UN, 1974; 1980); it consists of projecting the urbanization ratio using a logistic pathway with a ceiling of 100%. Combining these ratios with the projections for the total population yields the urban population projections (UN, 2003).

Rogers (1985) developed a more advanced methodology, applying different growth rates for both the urban and rural populations and including migration flows between rural and urban populations. This method has been refined and used for analysis of causes of urban growth (White et al., 2003), taking into account different underlying population dynamics. Urban growth can be attributed to three causes: (i) overall population growth through natural increase; (ii) rural-to-urban migration; and (iii) reclassification of rural areas as urban areas.

Reclassification occurs when a certain population density threshold is exceeded and rural area becomes urban area, but also by changing the definition of urban area. Natural increase, i.e. the difference between births and deaths, along with reclassifica-

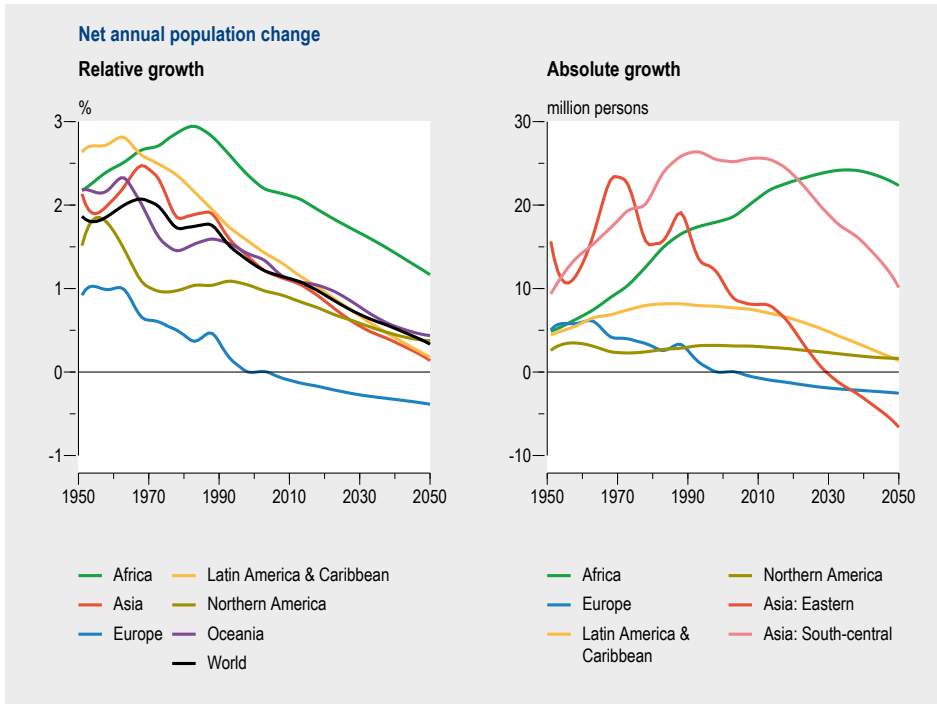


Figure 2.2. Net annual population change (annual growth percentage and absolute growth) for selected regions, 1951-2050, medium variant of the UN (UN, 2000).

tion, accounts for an average of 61% of urban population growth in developing countries, while rural-to-urban migration accounts for the other 39% (Gross et al., 1997).

### **Components of population change**

Calculating the changes in total population does not provide insight into the underlying components of such changes. The (natural) growth of the world population is a result of the difference between the total number of births and deaths. Births and death rates can be related to the total population size, which results in the crude birth rate (CBR) and the crude death rate (CDR), reflecting the numbers of births and deaths, respectively, per 1000 persons in a given year. The growth rate of the world population is thus determined by the difference between the CBR and CDR.

Another basic component of population change is migration, determined by external (international migration) and internal flows. External flows are usually applicable to the urban population, although the flow is often preceded by the internal migration within a country, the actual urbanization process. Socio-economic factors (e.g. income, employment opportunities and schooling) and health risks (e.g. pollution, crowding effects, access to safe drinking water, sanitation and food availability) have a major effect on the urban and rural population growth.

When more than one population is considered (e.g. urban and rural population), interactions can occur. The most relevant interaction in this context is people moving from one population to another. Population size and structure can vary because of differences in the initial population in combination with deviating fertility and mortality patterns. These processes are relatively simple, although the underlying factors and relationships are not fully understood.

In general, death rates are lower in urban than in rural areas, and lower in developed countries compared to developing countries (UNSD, 2003). The health transition (Frenk et al., 1993) is well under way in most cities in developing countries, which causes a gradual substitution of infectious diseases by chronic ones. In Bangladesh, for example, the urban infant mortality rate (IMR) is about 27% lower than that in rural areas, though the variation is greater, too. The IMR in urban slums is twice as high as the urban average, a pattern that is also seen in Nairobi (Harpam et al., 2003).

Birth rates are also lower in urban than in rural areas. Higher ages at marriage, use and awareness of modern contraceptives - aspects included in the concept of proximate determinants of fertility (e.g. Bongaarts and Potter, 1983; Hilderink, 2000b) - result in a substantially lower average number of children per female (Montgomery et al., 2003). While in rural areas in Sub-Saharan Africa, Latin America and North Africa this number still exceeds 5, in high urbanized areas this is down to only 2 to 3 children per woman (Montgomery et al., 2003).

Although CBR and CDR are often used to describe population dynamics, there is a serious problem when it comes to interpreting them. The CBR generally declines as a result of two forces: (i) the decline of fertility, referred to as de-greening of a population, measured in terms of the expected number of children born per woman and, (ii) the ageing of the population, which is a consequence of the reduction in mortality levels in combination with past fertility decline, reducing the proportion of women of fertile age.

Both CBR and CDR depend on the age structure of the population, which is the cumulative product of past mortality and fertility. Therefore, a correct analysis of mortality and fertility is only possible if the effects of a specific age structure are taken into account. Instead of crude birth and death rates, age-specific data are preferred for demographic analysis. Such data are commonly known in their aggregated forms, i.e. the total fertility rate (the number of children that a woman would have given birth to at the end of her reproductive life span if current age-specific fertility rates prevailed) and life expectancy (number of years a birth cohort may expect to live given the present mortality experience of a population).

The profound transformation of changing fertility and mortality patterns is generally referred to as demographic transition. It was classically defined by Notestein (1945) and Davis (1945), although its intellectual history goes back much further (Szreter, 1993). The demographic transition is not an isolated process; it is part of a much broader

transformation observed in a growing number of countries since the 18th century and is commonly referred to as ‘modernization’. In the economic domain, modernization involves a rise in real output and wide-ranging innovations and improvements in the production, transportation and distribution of goods. On the demographic and social side, modernization involves significant alterations in fertility, mortality and migration, as well as in family size and structure, education and the provision of public health.

At the level of the individual, modernization is characterized by an increased openness to new experiences, increased independence from authority, belief in the efficacy of science, and ambitions for oneself and one’s children (Easterlin, 1983). These inter-relations of manifold processes inevitably lead to a considerable variety in fertility decline between and within populations, although the pattern of the demographic transition is remarkably consistent in all parts of the world. Important differences exist in the position of individuals and groups on the trajectory of transition. The concept of demographic transition expresses plausible descriptions of the fertility decline in the idiom of post-war concerns with population and development (Cotts Watkins, 1987; Szreter, 1993).

Historical data indicate that fertility and mortality show rather gradual changes. The process of migration is less well understood because: (i) migration consists of two components, emigration and immigration, both with different dynamics, while still related to the migrant population; (ii) the relationship between the determinants, such as economic opportunities, conflict situations, extreme environmental events, and these migration components is often not fully understood; analyses of these relationships result in associative rather than causal connections and, (iii) some of these determinants have a high incidental nature, which causes difficulties in forecasting migration patterns.

## 2.4 Modelling population change

### *General*

Throughout history, people have tried to forecast the size of the population. Frejka (1996) provided an overview of existing long-range population projections dating from the time of Gregory King (1648-1719) at the end of the 17th century. Gregory had even made estimates right up to the year 20,000. The early long-range projections were based on mathematical extrapolation of total numbers or growth rates.

In the general component framework provided by Notestein (1945), different stages of demographic changes were distinguished by sex and age structure of a population. The population growth rates of the different stages are associated with assumptions on the components of fertility, mortality and migration. Since 1945, this cohort-component methodology has been refined and widely applied, with the United Nations being perhaps the most authoritative in the field of population projections (Lutz, 1996; Hilderink, 2000b; UN, 2004).

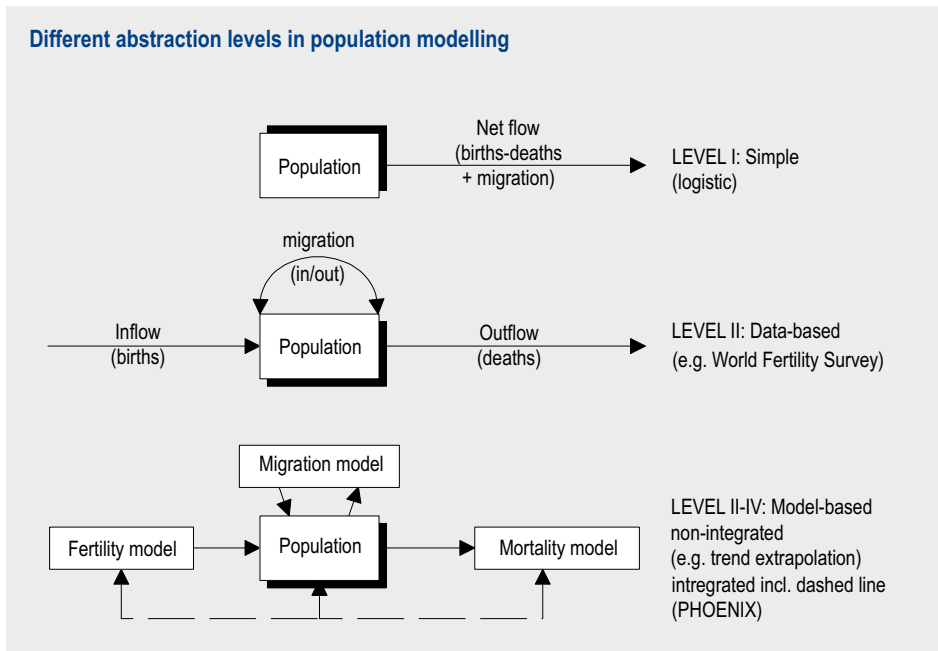


Figure 2.3. Different abstraction levels in population modelling (Sources: PHOENIX (Hilderink, 2000a), TARGETS (Rotmans and De Vries, 1997)).

Changes in growth of various (sub-)populations can be described with different levels of abstraction (Figure 2.3), varying from simple and static models to fully integrated approaches such as in the PHOENIX model (Hilderink, 2000b). At Level I of abstraction, the simplest description, the population changes are described on the basis of net flows, i.e. the number of births minus number of deaths and plus net migration (Figure 2.3). Level II involves a more dynamic approach by distinguishing population inflows and outflows based on exogenous data for total number of births and deaths. At a higher abstraction level, Level III, the non-integrated modelling approaches are used, in which the number of births and deaths are simulated based on endogenous model relations. All these approaches are classified as purely demographic models. The highest abstraction level (Level IV) is the fully integrated modelling approach characterized by interaction between mortality and fertility processes, and including interrelations of mortality, fertility and migration with environmental and socio-economic variables (Forrester, 1971; Millennium Institute, 1996; Rotmans et al., 1997; Hilderink, 2000a).

### **Modelling population change in the IMAGE framework**

In the IMAGE 2.4 framework, population projections are either taken exogenously or modelled using the PHOENIX model (Hilderink, 2000b; Hilderink, 2000a). PHOENIX is used to explore, develop and analyze different demographic scenarios at various geographical aggregation levels (i.e. regional, national and grid cell). This consistent way of dealing with various scales makes it perfectly suitable to be used within the IMAGE framework. The demographic core of PHOENIX is formed by a cohort-component model consisting of 28 major world regions, 100 one-year age groups and the two sexes.

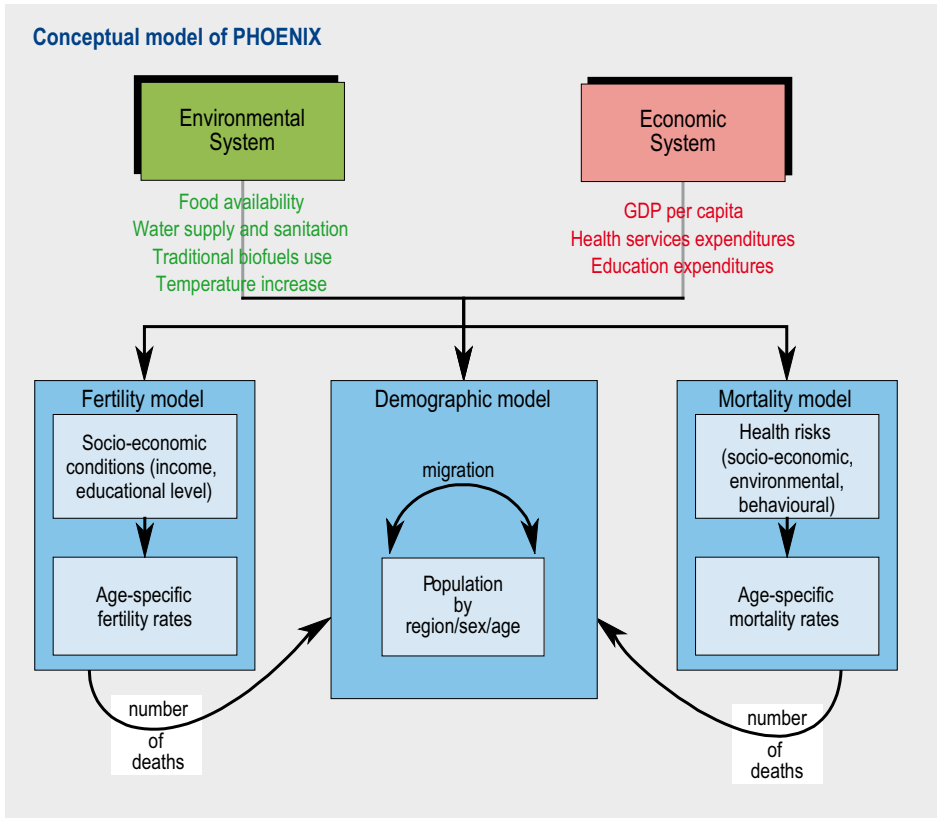


Figure 2.4. The conceptual framework of PHOENIX.

A fertility model is used in PHOENIX to describe age-specific fertility rates which are the result of a process of diffusion of innovation (Retherford and Palmore, 1983, Montgomery and Casterline, 1993, Rosero-Bixby and Casterline, 1993, Rodriguez and Aravena, 1991). Innovation is a concept comparable to Easterlin's modernization (see previous section; Easterlin, 1983). Innovation is modelled on the basis of the level of development, expressed by the Human Development Index (UNDP, 2005).

The fertility model provides the number of births, the inflow of the demographic model. The outflow is provided in PHOENIX by the mortality model, which calculates the age and gender-specific number of deaths based on a selection of health risks. The most important socio-economic (poverty and illiteracy), environmental (malnutrition, malaria, in and outdoor air pollution, lack of safe drinking water and sanitation), and behavioural risks (tobacco, blood pressure, obesity, HIV-AIDS) make up an age and gender-specific mortality rate. The level of health services determines to what extent a health risk contributes to these mortality rates. Migration, as the third demographic component, is taken exogenously. Figure 2.4 shows the PHOENIX model with the context, position and interrelationships.

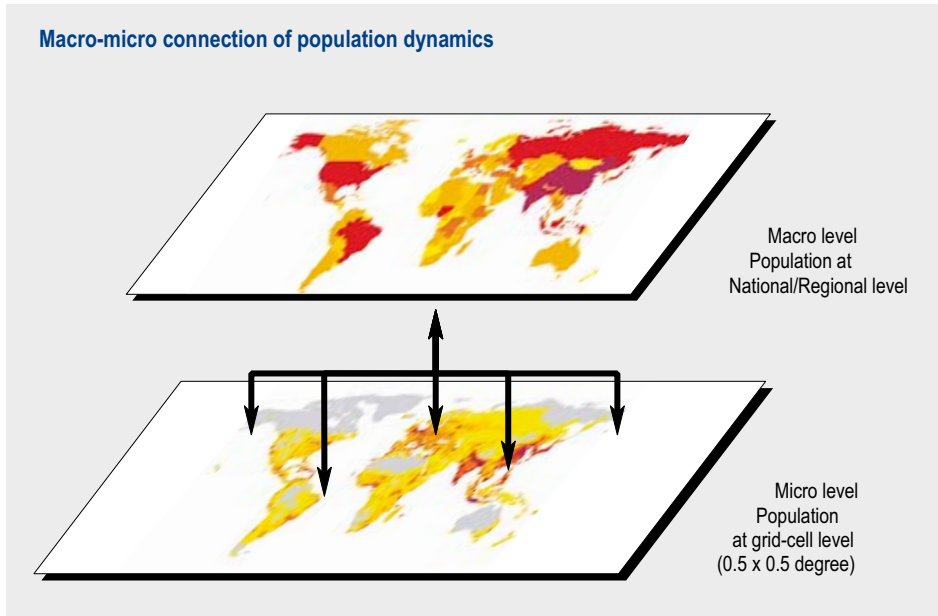


Figure 2.5. Macro-micro connection of population dynamics by interlinking population changes at the regional level to the grid cells.

### **Grid-based population projections in IMAGE**

The connection of the macro and micro aggregation levels is two-sided (Coleman, 1990; De Bruijn, 1999). At the macro level, the context of individual behaviour is assessed by distinction of the concept of social institution, which operates at different hierarchical levels like national and international levels. Population data is then provided at the macro level and used as boundary condition to describe population dynamics at the micro level (e.g. within a grid-cell).

Micro-level outcomes can be used to feed into (or even determine) macro-level modelling processes. For example, the availability of natural resources at the micro level may influence the mortality and migration intentions of individuals, thus influencing macro characteristics. Although this micro-macro connection is a crucial one, the lack of data and limited understanding impel us to take macro-micro connection as starting point. This is reflected in Figure 2.5 by the top-down approach.

Coupling the population projections at the macro level to the grid-cell population can be done by using various allocation algorithms. The basic equations for these allocation algorithms are:

$$\Delta p_i(t) = \lambda_i(t) \times \Delta P(t) \quad (1)$$

and

$$p_i(t+1) = p_i(t) + \Delta p_i(t) \quad (2)$$

Under the conditions:

$$\sum_i \lambda_i(t) = 1 \quad (3)$$

$$\sum_i p_i(t) = P(t) \quad (4)$$

where  $p_i$  is the grid-cell population,  $\lambda_i$  the allocation factor of the macro population change to the micro populations, and  $P$  the macro population. Taking Figure 2.3 as a guiding framework for describing population changes, the allocation algorithms of net population change can be distinguished. With these algorithms, net population changes, as one of the outcomes of integrated population projections of PHOENIX, are directly used as inputs to describe population changes in the related grid cell, represented by Level I in Figure 2.3.

Within this family of algorithms, the most commonly used approach is the proportional method, which assumes that increases and decreases in population are proportionally allocated to the grid-cell population as, for example, in GLOBIO 2 (UNEP, 2002). This assumption implies the following for the allocation factor  $\lambda_i$ :

$$\lambda_i(t) = \frac{p_i(t)}{P(t)} \quad (5)$$

The classification of the 24 world regions in IMAGE is based on a compromise of region-specific characteristics (land use, energy and economy). Demographic homogeneity was not a major determinant when compiling the regions. Applying this algorithm to the 24 heterogeneous world regions would allocate the population increase to those places where most people already live. This may lead to incorrect allocation. For example, most of the population growth of Mongolia, which is part of the East Asia region, is allocated to the Chinese coastal zone, where most of the people in this region live.

This problem was solved by combining regional scenarios with associated national data of World Population Prospects (Van Vuuren et al., 2005). The results of this new methodology are shown for the IPCC-SRES A2 scenario (Nakicenovic et al., 2000) for the year 2050 (Figure 2.6). The relative difference is highest in Lao People's Democratic Republic and the Philippines where the population increase is almost 60% higher than in the old method, while Indonesia has 26 million less people with the new method.

Figure 2.7 shows the results of the new methodology for the population density in persons per grid cell in 2050. The consequences of the population increases according to the A2 scenario result in a further increase of already densely populated areas in China and India. The increase in India and Bangladesh is concentrated along the Ganges River where many grid cells will be confronted with more than 1 million inhabitants who all need space, water and food.

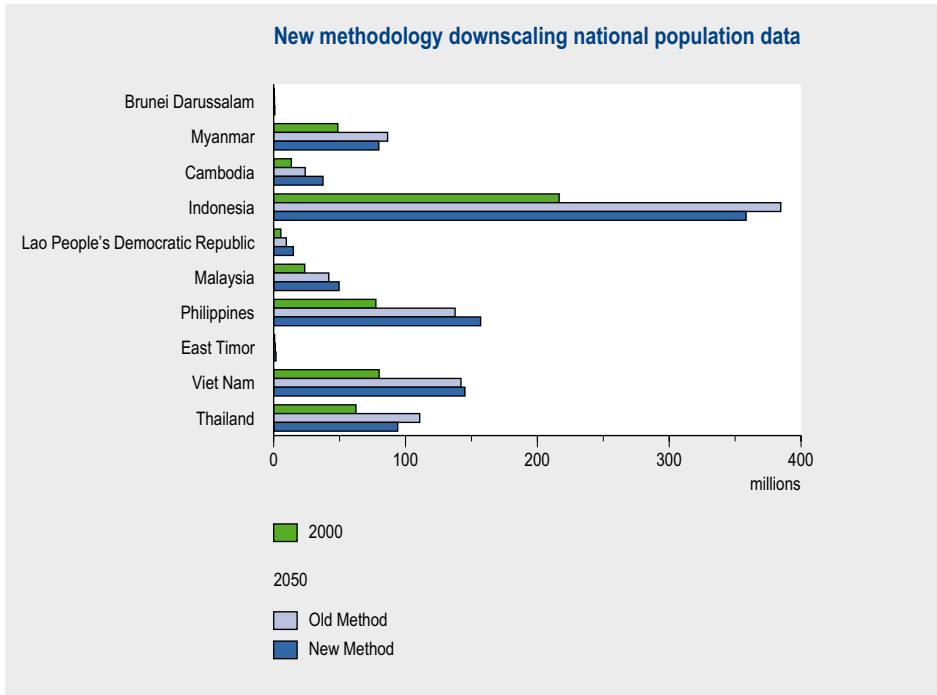


Figure 2.6. Population based on the new methodology using national level data to downscale compared to the old methodology using only regional level data for the A2 scenario for 2050.

This improved methodology enables a better understanding and analysis of the effects of population increase in relation to environmental conditions such as climate or water availability and changes in these. Accounting for the environmental conditions may improve the allocation of future population changes, for example, by introducing the concept of attractiveness. Population changes can then be allocated using different weights for the allocation factor  $\lambda_i$ . The arguments of this attractiveness function can include population density (enforcing higher urbanization rates), land-use patterns (initiating the formation of new urban area) and water availability (making water-stressed areas less attractive to live in).

## 2.5 Concluding remarks

Population represents an important driver of global environmental change. In the IMAGE framework, population projections are either taken exogenously or simulated with the PHOENIX model. One important aspect of population is its distribution. With almost half of the population living in urban areas and the importance of urbanization for the components of population changes, it is clear that we need to improve our understanding of the urbanization process. However, modelling urbanization is not a trivial task.

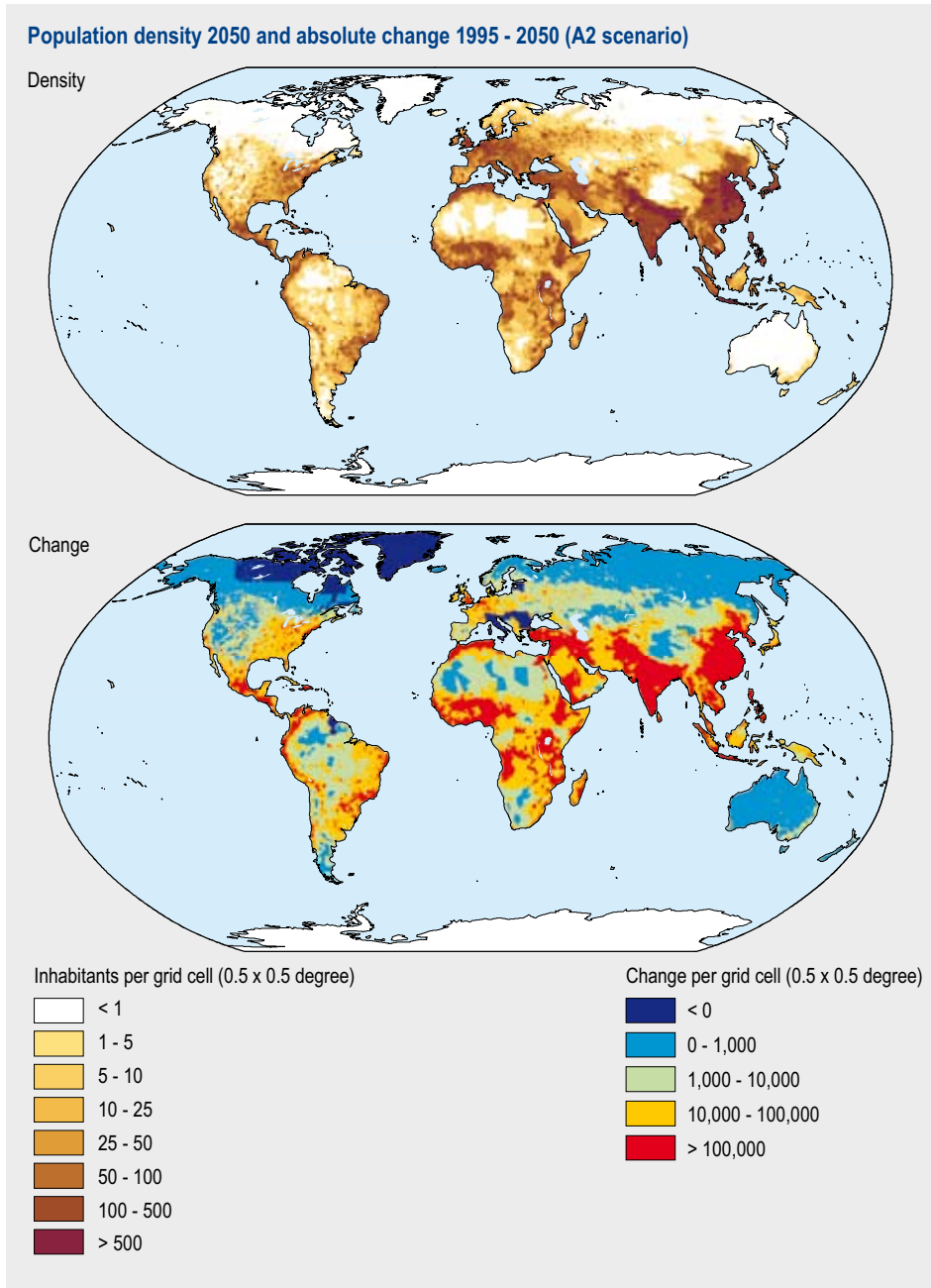


Figure 2.7. Population density for 2050 according to the A2 scenario and the increase in persons per grid cell compared to 1995.

In IMAGE, the population density is used as a proxy for urban and rural population. Change in population density is calculated for each grid cell with a proportional method, using available country-specific population data combined with the trends on the level of world regions as determined by, for example, PHOENIX. The proportional

method is attractive in its simplicity, but it also has several shortcomings related to urbanization and population density: (i) the proportion of the population living in urban areas is constant with this methodology if urban areas are not explicitly defined; urbanization only occurs if the population density in rural areas exceeds a certain threshold and the value of this threshold is rather arbitrary; (ii) there is no limit to population density and (iii) it is difficult to deal with decreasing population expected in certain world regions in the coming decades.

The method described addresses future urban populations and not urban areas. In this chapter an attractiveness function to allocate population changes with varying allocation factor  $l_i$  is proposed to describe future population changes in space. The attractiveness function can be used to mimic higher urbanization rates in specific places or initiate the formation of new urban areas. The approach for allocating urban area for historical projections (1700-2000) as discussed in chapter 6 is based on a similar concept using weighting maps to allocate urban area.

It is more difficult to deal with decreasing population, since up to now there has hardly been any experience with the patterns and consequences of a declining population. This could be explored by taking the underlying demographic components of population changes - birth, death and migration - as a starting point. The changes in these components make up the overall population change, safeguarding the macro-level changes.

Research on underlying determinants of birth and death provide clues to describe these processes, for example, for fertility (Bongaarts and Potter, 1983) and mortality (Frenk et al., 1993; Ezzati et al., 2002). Estimating migration flows is more difficult than birth and death rates. At the region or country level the migration flows represent international migration, while at the grid level intra-national migration should also be taken into account. However, the results of the allocation method discussed in this chapter can also be used to gain insight into detailed grid-level population dynamics regarding birth, death and migration.

Taken together, applying and exploring the currently available allocation methodologies in IMAGE and proposed improvements may be a valuable next step for assessing future global population dynamics at grid scale, using data from IMAGE and population projections. The resulting population densities are useful for improving our understanding of future urbanization patterns and as a tool for planning processes.

## 3 TIMER 2: MODEL DESCRIPTION AND APPLICATION

- The Timer 2 model describes long-term development pathways in the energy system in the broader context of impacts on climate change, air pollution and sustainable development. It is integrated into the IMAGE framework via energy-related emissions of greenhouse gases and air pollutants, the use of bioenergy and the role of the energy system in mitigation scenarios.
- Important new elements that have been introduced in the Timer 2 model are hydrogen production and more detailed descriptions of the electric power system and renewable energy (including bio-energy).
- The coupled TIMER-IMAGE-FAIR framework can be used to study different mitigation scenarios. In general, low greenhouse gas concentration scenarios (550 ppm CO<sub>2</sub>-eq. and less) were found technically achievable using the framework, with direct costs in the order of 1-2% GDP. A mix of options is needed to achieve the required reductions; options that might form very substantial overall reductions are in particular carbon-capture-and-storage (CCS), energy efficiency improvement and bioenergy.

### 3.1 Introduction

Energy forms a central element in discussions on sustainable development. First of all, the use of energy supports economic development. Securing affordable energy supply is an important element in the energy policies of many countries. Fossil fuel resources, which currently account for more than three-quarters of world's energy use, are slowly being depleted with especially oil and gas resources becoming more and more concentrated in a limited number of supply regions. At the same time, renewable energy sources also have limitations. Secondly, fuel combustion is the single most important cause of both air pollution and greenhouse gas emissions. The future of global energy use is highly uncertain and depends on uncertain factors such as technology and socio-economic development, resource availability and societal choices. Exploring different scenarios for the future energy system thus provides crucial information to decision-makers.

The IMage Energy Regional Model (TIMER) is an energy model that has been developed to explore different scenarios for the energy system but in the broader context of the IMAGE environmental assessment framework. TIMER is an energy-system simulation model, describing the demand and supply of 12 different energy carriers for 17 world regions (Figure 3.1). Its main purpose is to analyze the long-term trends in energy demand and efficiency and the possible transition towards renewable energy sources. Within the broader IMAGE context, the model describes energy-related greenhouse gas, as well as air pollution emissions and land-use demand for energy crops. The TIMER model focuses particularly on several dynamic relationships within the energy system, such as inertia, learning-by-doing, depletion and trade among the different

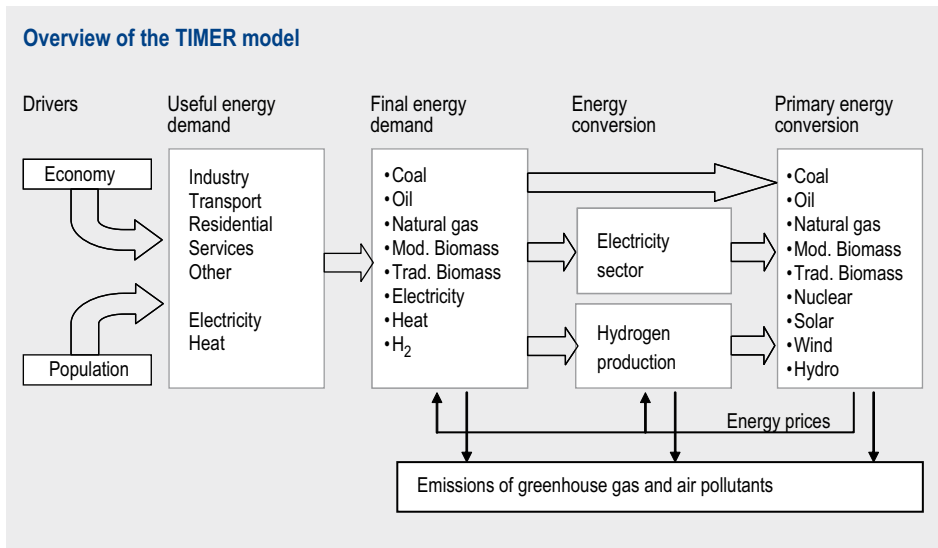


Figure 3.1. Scheme of the TIMER model.

regions. The TIMER model is a simulation model, which means results depend on a single set of deterministic algorithms instead of being the result of an optimization exercise. As such it can be compared to other energy system simulation models such as POLES (Criqui and Kouvaritakis, 2000).

The TIMER model was originally developed as a one-world model (TIME) for the TARGETS sustainable development model (Rotmans and De Vries, 1997). A model version comprising 17 world regions was developed (Timer 1.0) between 1997 and 2000 (De Vries et al., 2002). The Timer 1.0 model was applied, for example, to the development of the IPCC SRES scenarios (De Vries et al., 2000), exploration of climate policies (Van Vuuren and De Vries, 2001; Van Vuuren et al., 2003), country-level scenario assessment, and, together with IMAGE, global environmental scenario studies (UNEP, 2002; Carpenter and Pingali, 2006). More recently, improved modelling of renewable energy sources, revision of the electricity model and the development of a hydrogen sub-model led to the Timer 2 model. Thus far the Timer 2 model has simulated the energy system for 17 world regions. This model version was used to explore different stabilization strategies (Van Vuuren et al., 2006). Given the interest in results at the country-level for the main developing countries, a 26 region version of the model has been developed.

In this chapter we present an overview of the TIMER model and its recent developments. For a full documentation of the Timer 1.0 model see De Vries et al., (2002); here we concentrate on changes implemented in Timer 2. Section 3.2 overviews the model and discusses the sub-models on energy demand, conversion and supply. Section 3.3 discusses the common elements of the model, including technological development, depletion and substitution. Section 3.4 focuses on the major changes that were included in Timer 2, and finally, section 3.5 describes a typical application of TIMER in the recent stabilization scenarios study closely connected to the IMAGE and FAIR models.

## 3.2 Model outline and structure

The TIMER model describes the chain, going from demand for energy services (useful energy) to the supply of energy itself through different primary energy sources and related emissions (Figure 3.1). The steps are connected by demand for energy (from left to right) and by feedbacks, mainly in the form of energy prices (from right to left). The TIMER model has three types of sub-models: (i) the energy demand model; (ii) models for energy conversion (electricity and hydrogen production) and (iii) models for primary energy supply. An overview of some of the main assumptions for the different sources and technologies is listed in Table 3.1.

### *The Energy Demand sub-model*

The final energy demand (for five sectors and eight energy carriers) is modelled as a function of changes in population, economic activity and energy efficiency (Figure 3.2). The first two factors drive the demand for energy services (or useful energy). The energy-intensity development for each sector (i.e. energy units per monetary unit) is assumed to be a bell-shaped function of the per capita activity level (i.e. sectoral value added or GDP). This reflects an empirical observation that a changing mix of activities within a sector could, with rising activity levels, first lead to an increase and

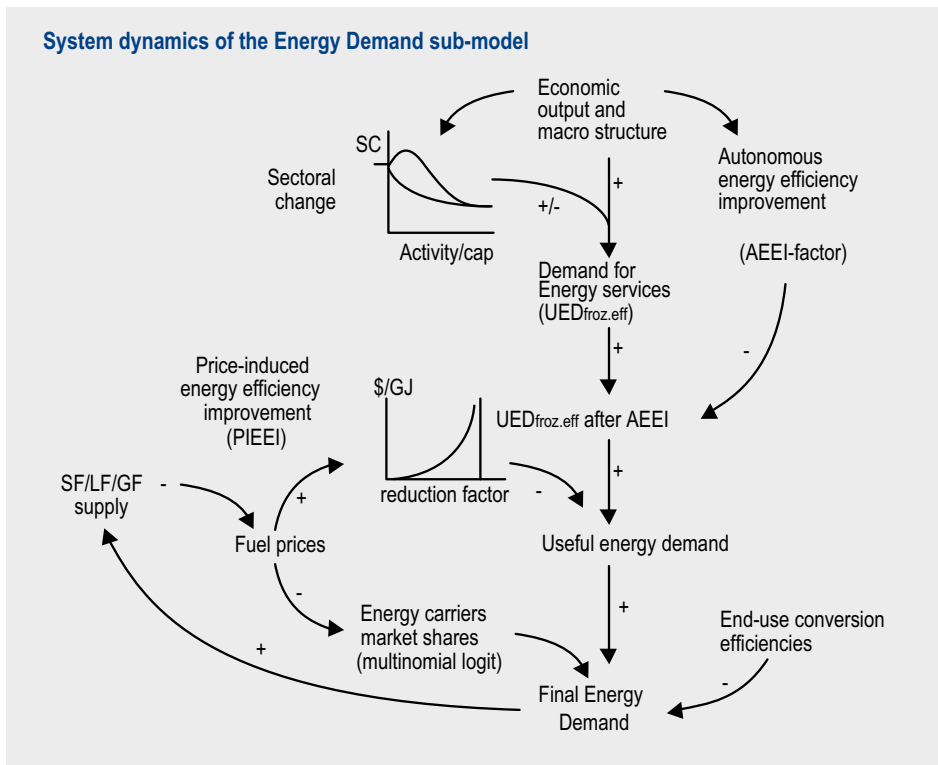


Figure 3.2. System dynamics representation of the Energy Demand sub-model. UED is Useful Energy Demand, i.e. the energy services delivered; SF/LF/GF indicate Solid Fuel, Liquid Fuel and Gaseous Fuel, respectively.

*Table 3.1. Assumptions within the TIMER model for various energy categories.*

Option	Assumptions	References
Fossil fuels	Regional resources and production costs for various qualities; global trade (coal, oil and natural gas resources equal 300, 45, and 117, respectively). Global average crude energy prices in 2050 are 1.4, 5.1 and 4.4 1995US\$/GJ for coal, oil and natural gas, respectively. In 2000, these prices are 1.1, 3.0 and 2.3 1995US\$/GJ.	Rogner (1997)
Carbon capture and storage	Regional reservoir availability and storage costs for various options (different categories of empty oil and natural gas reservoirs, coal reservoirs, coal-bed methane recovery, aquifers). Total capacity equals 1500 GtC. Transport and storage costs range, depending on category and region, from 10-150 US\$/tC.	Hendriks et al. (2002a)
Power plant efficiency and investment costs	Power plant efficiency and investment costs for 20 types of thermal power plants (coal, oil, natural gas, biomass) including carbon capture and storage defined over time.	Hendriks et al. (2004)
Energy crops	Potential and costs for energy crops defined by region on the basis of IMAGE 2.3 maps (including abandoned agricultural land, natural grasslands and savanna). Primary biomass can be converted into liquid biofuels (for transport) and solid bioenergy (for electricity). Technology development is based on learning-by-doing. Maximum potential equals 230 EJ in 2050 and 600 EJ in 2100. Production costs for liquid fuels varies from 12-16 US\$/GJ in 2000 to around 8-12US \$/GJ in 2050 (depending on scenario). Production costs for solid fuels is around 4 US\$/GJ.	Hoogwijk (2004)
Solar/wind power	Solar and wind power based on studies that assess global potential on the basis of 0.5 x 0.5 degree maps. Costs change over time as a result of depletion, learning-by-doing and grid penetration (declining capacity-credit and excess electricity production).	Hoogwijk (2004)
Nuclear power	Investment costs of nuclear power based on available information in the literature (most important references indicated). Investments costs are assumed to decrease over time. Fuel costs increase over time as a result of depletion.	MIT (2003); Sims et al. (2003)
Hydrogen	Hydrogen modelled on the basis of production from fossil fuels, bio-energy, electricity and solar power (including carbon capture and storage). Selection on the basis of a multinomial logit model.	Van Ruijven et al. (2006)

subsequently to a decrease in energy intensity (structural change). Evidence of this trend is more convincing in some sectors (e.g. industry) than in others (e.g. transport) (De Vries et al., 2002). In any case, the actual shape of this function (defined by sector and region) has a large influence on the demand for energy services in the model. The Autonomous Energy Efficiency Increase (AEEI) multiplier accounts for efficiency improvement that occurs as a result of technology improvement independent of prices. The AEEI is assumed to be linked to the economic growth rate.

A second multiplier, the Price-Induced Energy Efficiency Improvement (PIEEI), describes the effect of rising energy costs on consumers (Figure 3.2). This multiplier is calculated using a sectoral energy conservation supply cost curve and end-use energy costs. The demand for secondary energy carriers is determined by the relative prices of the energy carriers in combination with premium values. The premium values reflect non-price factors determining market shares, such as preferences, environmental policies, strategic considerations etc. Secondary fuel allocation is determined by a multinomial logit formulation for most fuels (see section 3.3). Alternative approaches are used for traditional biomass and secondary heat. The market share of traditional biomass is assumed to be driven by per capita income, where a higher per capita income leads to lower per capita consumption of traditional biomass. The market share of secondary heat is determined by an exogenous scenario parameter. Finally, non-energy use of fossil fuels is modelled on the basis of an exogenous-assumed intensity parameter (related to industry value-added) and a price-driven competition of the various energy carriers.

### *The Electric Power Generation sub-model*

The Electric Power Generation sub-model (Figure 3.3) simulates investments in various electricity production technologies and their use in response to electricity demand and to changes in relative generation costs (see also Hoogwijk, 2004). The demand for capacity is derived from the forecast for the simultaneous maximum demand and a reserve margin of about 10%. The first factor is calculated using assumptions on the load distribution, the net electricity demand, electricity trade and transmission losses. Different technologies compete for a share in investments based on their total costs (capital and operational costs). The operational strategy (use of existing park) is based

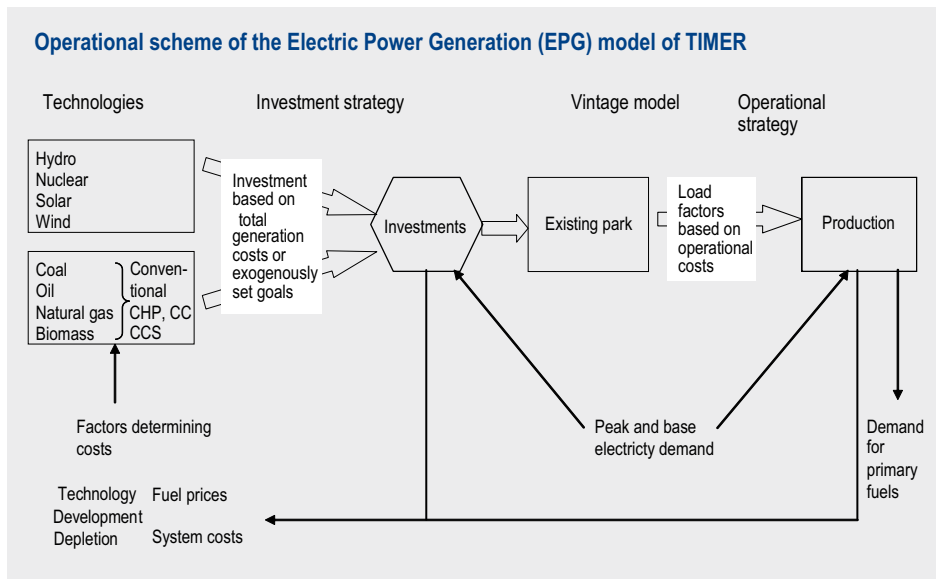


Figure 3.3. Schematic presentation of the Electric Power Generation model.

on operational costs for peak and base load. In both cases, a multinomial logit model is used.

Fossil fuels and bioenergy can be used in a total of 20 different plant types that represent different combinations of (i) conventional technology; (ii) gasification and combined cycle technology; (iii) combined-heat-and-power, and (iv) carbon-capture and storage (see also Hendriks et al., 2004). In addition, the model distinguishes hydro-power, solar power, wind power and nuclear power. The costs of technologies are described in terms of learning and depletion dynamics. For renewable energy sources with an intermittent character (wind and solar power), additional costs are determined for discarded electricity (if production exceeds demand), back-up capacity and additionally required spinning reserve (spinning reserve is formed by power stations operating below maximum capacity that can be scaled up in relatively little time to avoid loss of power if supply of wind and solar power suddenly drops). The required spinning reserve is assumed to be 3.5% of the installed capacity of the conventional park. If wind and solar photo-voltaic cells (PV) penetrate the market, the additionally required spinning reserve equals 15% of the intermittent capacity (but only after the additional spinning reserve exceeds the capacity already present in the system). Back-up capacity is added to account for the low capacity credit (its contribution to a reliable supply of electricity at any moment of time) of the intermittent sources. For the first 5% penetration of the intermittent capacity, the capacity credit equals the load factor of the wind turbines. If the penetration of intermittent sources increases further, the capacity credit decreases. The costs of back-up power are allocated to the intermittent source. Finally, a mismatch between supply of intermittent resources and electricity demand is also taken into account. Wind and PV electricity is discarded if it exceeds the electricity demand in a month as given by the load-demand curve.

### ***Supply of primary energy***

Supply of all primary energy carriers is based on the interplay between resource depletion and technology development. Technology development is introduced either as learning curves (for most fuels and renewable options) or by exogenous technology change assumptions (for thermal power plants). To model resource depletion of fossil fuels and uranium, several resource categories that are depleted in order of their costs are defined. Production costs thus rise as each subsequent category is exploited. For renewable energy options, the production costs depend on the ratio between actual production levels and the maximum production level. Details on modelling fossil fuels and bioenergy use are given below. Uranium is treated similarly to fossil fuels. The modelling of renewables is discussed in more detail in section 3.4.

TIMER includes three fossil-fuel production sub-models for solid, liquid and gaseous fuels, respectively. For each region these sub-models calculate the demand for secondary energy carriers, electricity generation, international transport (bunkers) and the demand for non-energy use and feedstocks (Figure 3.4). The calculated fuel demand accounts for losses (e.g. refining and conversion) and energy use within the energy system. In the next

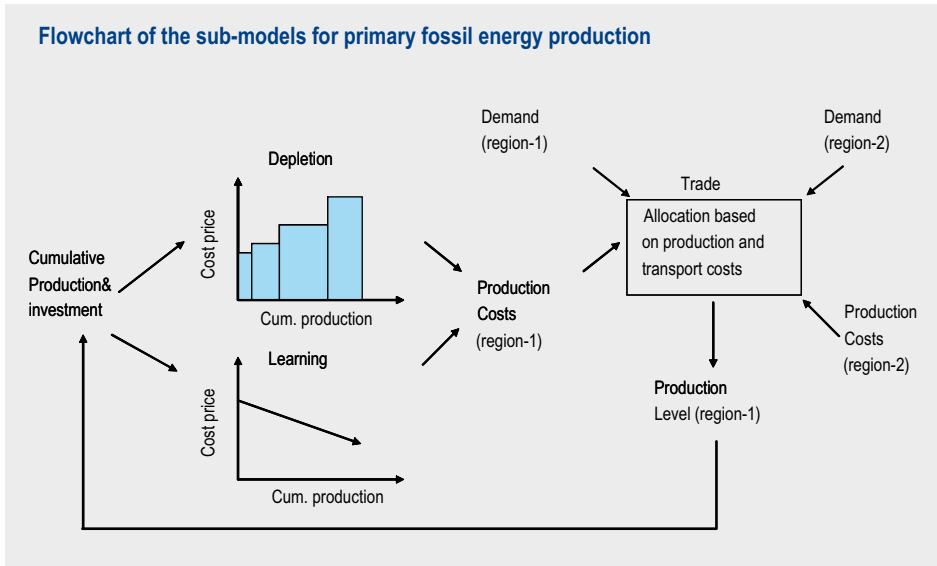


Figure 3.4. Schematic presentation of the sub-models for primary fossil energy production (2 regions are used to illustrate fuel trade).

step, demand is confronted with possible supply, both within the region and in other regions by means of the international trade model.

The allocation in the trade module is based on costs. These are governed, as indicated above, by the combined influence of learning-by-doing and resource depletion. The resource base is categorized in 10-14 different classes per fuel type and region, ranked according to production costs (based on Rogner, 1997). Meanwhile, the learning parameter leads to lower costs with increasing cumulated production.

In the trade formulation, each region imports fuel from other regions depending on the ratios between the production costs in the other regions plus transport costs, and the production costs within the region considered (multinomial logit). Transportation costs form the product of the representative interregional distances and time and fuel-dependent estimates of the costs per GJ per km. To reflect geographical, political and other constraints in the interregional fuel trade, an additional parameter is used to simulate the existence of trade barriers between regions.

The structure of the biomass sub-model is similar to that of the fossil fuel supply models but with a few important differences (see also Hoogwijk, 2004). First of all, in the bio-energy model depletion is not governed by cumulative production but by the degree to which available land is being used for commercial energy crops. Available land is defined as abandoned agricultural land and part of the natural grasslands in divergent land-use scenarios for the 21<sup>st</sup> century and is based on IMAGE scenario calculations. The land is categorized according to productivity levels which are assumed to reflect the cost of producing primary biomass. The biomass model also describes the conver-

sion of biomass (residues, wood crops, maize and sugar cane) to two generic secondary fuel types: bio-solid fuels (BSF) and bio-liquid fuels (BLF). The solid fuel is used in the industry and power sector, and the liquid fuel in other sectors, in particular, transport. The trade and allocation of biofuel production is determined by optimization rather than by the multinomial logit equation used elsewhere in TIMER, so as to avoid unstable, oscillating model behaviour.

### *The TIMER Emissions sub-model*

The TIMER Emissions Model (TEM) calculates the regional atmospheric emissions from energy and industry-related processes. The model covers carbon dioxide (CO<sub>2</sub>), methane (CH<sub>4</sub>), nitrous oxide (N<sub>2</sub>O), nitrogen oxides (NO<sub>x</sub>), carbon monoxide (CO), non-methane volatile organic compounds (NMVOC), sulphur dioxide (SO<sub>2</sub>) and emissions of halocarbons (CFCs, HCFCs, HFCs, etc.). Emissions are calculated by multiplying primary energy-use fluxes and industrial activity levels with time-dependent emission coefficients. Changes in these coefficients represent technological improvements and end-of-pipe control techniques for CO, NMVOC, NO<sub>x</sub> and SO<sub>2</sub> (FGD in power plants, fuel specification standards for transport, clean-coal technologies in industry, etc.)

## 3.3 Common model elements

The TIMER model has several elements that re-appear in various submodels. Two of these involve the dynamics of technology development and substitution. Another common element, which will not be discussed here, is the capital vintage structure for each process. This element describes the investment and lifetime of different capital stocks. Its use implies that changes in energy use and production can only be adopted by the system at a rate equal to new investment and the depreciation of existing capital.

### *Technology development*

An important aspect of the TIMER model is the endogenous formulation of technological development on the basis of 'learning-by-doing'. This phenomenon is considered to be a meaningful representation of technological change in global energy models (Azar and Dowlatabadi, 1999; Grubler et al., 1999; Wene, 2000). The general formulation of learning-by-doing is that a cost measure,  $y$ , tends to decline as a power function of an accumulated learning measure,  $Q$ :

$$y = \alpha Q^{-\pi} \quad (1)$$

where  $\pi$  is the learning rate,  $Q$  the cumulative capacity or output and  $\alpha$  a constant. Often  $\pi$  is expressed by the progress ratio  $\rho$ , which indicates how fast the costs measure,  $y$ , decreases with the doubling of  $Q$  ( $\rho=2^{-\pi}$ ). Progress ratios reported in empirical studies lie mostly between 0.65 and 0.95, with a median value of 0.82 (e.g. Argotte and Epple, 1990).

In the TIMER model, learning-by-doing influences the capital-output ratio of coal, oil and gas production, the specific investment cost of renewable and nuclear energy, the cost of hydrogen technologies and the rate at which the energy conservation cost curves decline. The value of  $\rho$  ranges between 0.7 and 1.0, based on historic values. The actual values used depend on the technologies and the scenario setting. The  $\rho$  of solar/wind and bioenergy have been set at a lower level than the values for fossil-based technologies, founded on observed historic trends (e.g. Wene, 2000; Junginger et al., 2005). There is evidence that in the early stages of development  $\rho$  is higher than for the technologies that have already been in use for long time periods. Other factors may also contribute to such faster learning in early phases, such as a relatively high investment in research and development (Wene, 2000).

It is interesting here to ask whether learning curves should be applied separately on the regional scale or for the world as a whole. On the one hand, technologies developed in one region will often also be available in other regions. On the other, a significant part of cost reduction comes from experience gained by applying the technology and developing the associated infrastructure that may not be so easily transferred. In TIMER, we postulate the existence of a single global learning curve. Regions are then assumed to either pool knowledge and ‘learn’ together or be (partly) blocked from this pool. In the latter case, only the obviously smaller cumulated production within the region itself drives the learning process.

#### ***Substitution of fuels and technologies***

Substitution among energy carriers and technologies is described in the model using the multinomial logit formulation:

$$IMS_i = \frac{\exp(-\lambda c_i)}{\sum_j \exp(-\lambda c_j)} \quad (2)$$

where  $IMS_i$  is the share of total investments for fuel or production method  $i$  (-),  $c_i$  the cost or price of production method  $i$  and  $\lambda$  the so-called logit parameter, which reflects the sensitivity of markets to relative differences in production costs.

The cost  $c_i$  may include other factors such as premium factors, additional investment costs and cost increases as a result of a carbon tax. The multinomial logit model implies that the market share of a certain technology or fuel type depends on costs relative to competing technologies. The option with the lowest costs gets the largest market share, but in most cases not the full market. We interpret the latter as a representation of heterogeneity in the form of specific market niches for every technology or fuel. The multinomial logit mechanism is used in TIMER to describe substitution among end-use energy carriers, different forms of electricity generation (coal, oil, natural gas, solar/wind and nuclear) and substitution between fossil fuels and bioenergy.

### 3.4 Important changes in the Timer 2 model

Several parts of the model have been changed since the publication of the Timer 1.0 documentation (De Vries et al., 2002). In this section we discuss two of these changes: the modelling of renewable energy sources and the hydrogen model.

#### *Renewable energy*

The potential of renewable energy (wind, solar photovoltaic and bioenergy) has been estimated generically on the basis of a methodology developed by Hoogwijk (2004). First, the relevant physical and geographical data for the regions considered are collected at the resolution of 0.5 by 0.5 degree. The wind and solar characteristics are taken from the digital database constructed by the Climate Research Unit (New et al., 1999). Land-use information for energy crops is taken from the IMAGE land-use model.

Subsequently, the model assesses which part of the grid cell area can be used for energy production given its physical-geographical (terrain, habitation) and socio-geographical (location, acceptability) characteristics. This leads to an estimate of the geographical potential. Next, the technical potential accounts for the fact that only part of the energy can be extracted in the form of useful secondary energy carriers (fuel, electricity), due to limited conversion efficiency and maximum power density. A final step is to relate this technical potential to the on-site production costs. The information at grid level is finally sorted and presented as cost-supply curves to TIMER. Cost-supply curves are used dynamically and change over time as result of learning effect. Producing more renewable energy also leads to changes along this curve, and thus to higher costs.

For bioenergy, the TIMER model includes several routes from energy crops to liquid biofuel (ethanol and Fisher-Tropsch diesel) and solid biofuel (section 3.2). The geographic potential of biomass production by energy crops is estimated using suitability/availability factors accounting for competing land-use options and the harvested rainfed yield of energy crops. A Cobb-Douglas function including capital, land and labour costs is used to calculate costs of production. Maps such as those shown in Figure 3.5 can be produced, indicating the electricity production costs (categories from  $<0.05$  \$/kWh to  $>0.15$  \$/kWh) for each 0.5 by 0.5 degree grid cell. In almost all scenarios there is a significant increase in economic potential between 2000 and 2050 due to cost decreases as a result of learning-by-doing, in the form of scaling up, mass production and innovations. Similar calculations are done for wind and PV. A comparison of the results was presented by De Vries et al. (2006).

#### *Hydrogen*

The hydrogen sub-model (Van Ruijven et al., 2006) simulates the demand for the model and production, infrastructure and technology dynamics of hydrogen-related technologies (see Figure 3.6). Hydrogen production costs are determined by capital and fuel costs and (if relevant) costs of carbon capture and storage. The costs of energy services from hydrogen for the end-user are equal to the production costs (taking into account end-use efficiency), and the costs of end-use capital and infrastructure. The market-share of

### Estimated costs of producing electricity for wind, solar-PV and biomass (A1 scenario)

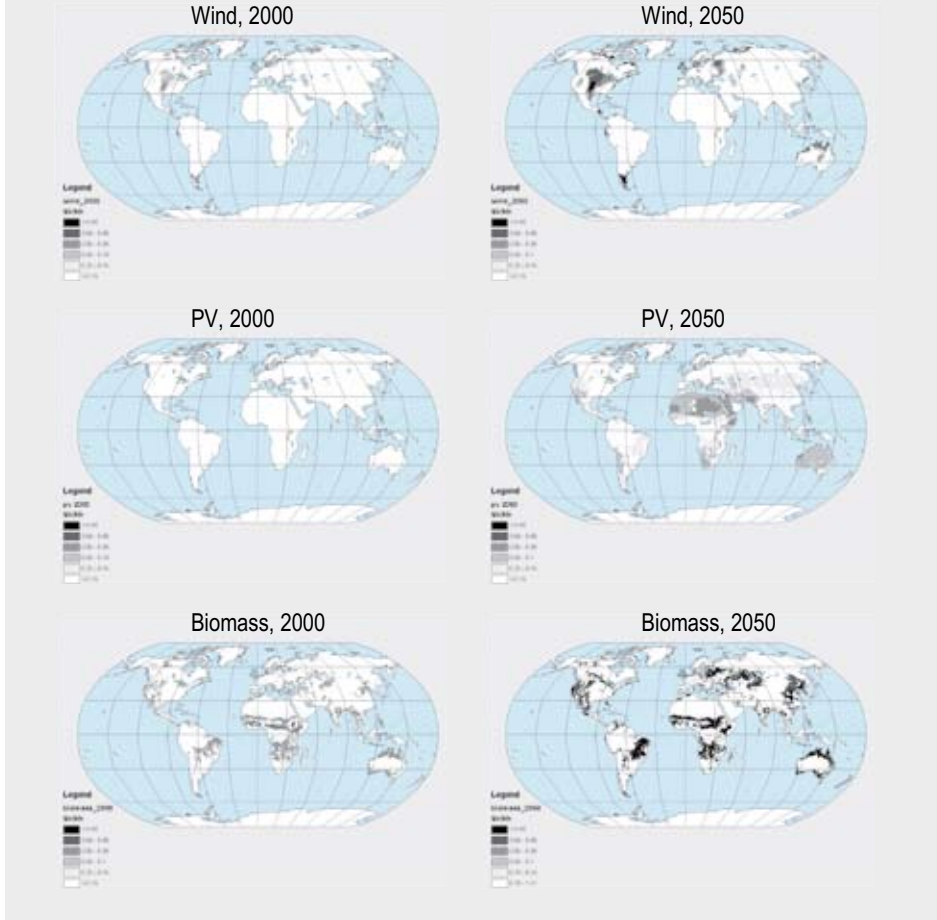


Figure 3.5. Estimated costs of producing electricity in the A1 scenario for wind, biomass and solar-PV in 2000 and in 2050 (De Vries et al., 2006).

hydrogen is determined by a multinomial logit formulation, using the difference of the energy service costs from hydrogen and from other energy carriers. A feedback loop due to technological learning tends to lower the hydrogen production costs as cumulative installed capacity increases.

In Timer 2, hydrogen can be produced by coal gasification, partial oxidation of oil, steam reforming of natural gas, gasification of biomass, electrolysis or direct solar-thermal production of hydrogen. For the production of hydrogen from natural gas, the model distinguishes between large-scale and small-scale Steam Methane Reforming (SMR). In this way a transition period can be simulated in which there is no infrastructure, and the more expensive small-scale SMR is the only available technology for stationary

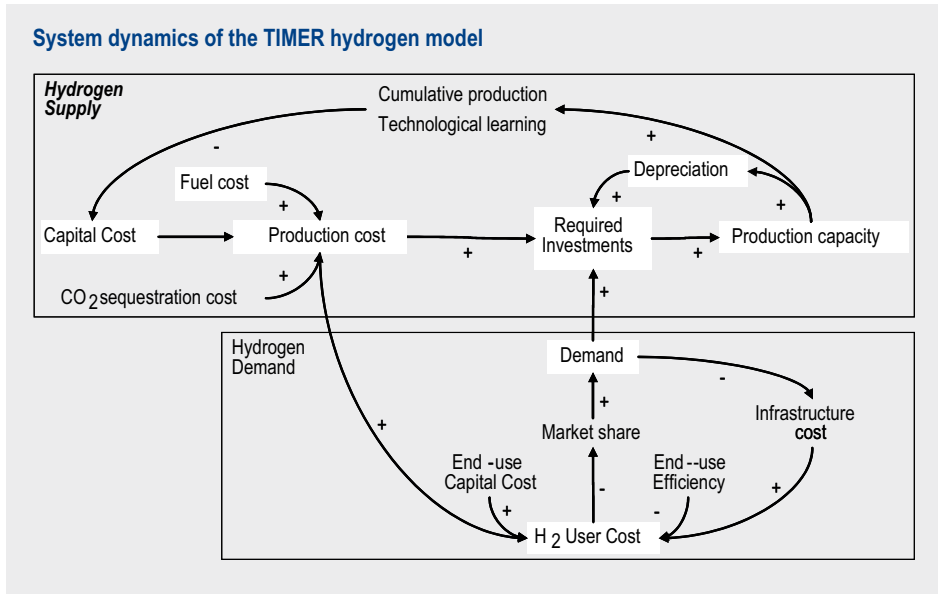


Figure 3.6. System dynamics representation of the TIMER-hydrogen model. Arrows indicate influence factors or inputs for calculation (Van Ruijven et al., 2006).

applications of hydrogen. The capital cost of production technologies declines through learning-by-doing (section 3.3).

Hydrogen can penetrate all five end-use markets. Another option is mixing up to 5% hydrogen (on an energy basis) into the natural gas grid for use in the residential and service sectors (Hendriks et al., 2002b). We assume exogenous cost decline for fuel cells, using Solid Oxide Fuel Cells in the industrial sector and Proton Exchange Membrane fuel cells in both stationary and mobile applications (Wurster and Zittel, 1994; Reijnders et al., 2001).

Transport and distribution of hydrogen is a major issue in the transition to a hydrogen energy system. Transport covers the distance from large-scale plants to residential areas or re-fuelling stations and is only considered for hydrogen produced on a large scale (this includes pipelines and trucks). Distribution includes the final distribution of hydrogen, i.e. the small-scale network in residential areas or the re-fuelling station itself. The costs of distribution are added to the cost of hydrogen. Since the development of a hydrogen transport infrastructure is expensive, hydrogen for stationary applications can initially only be produced by small-scale SMR plants near end-use locations. Investments in large-scale infrastructure (pipelines) will only be made when hydrogen demand density rises above a certain threshold. When this happens, stationary applications can be served by both small-scale and large-scale hydrogen plants. For the transport sector we assume that hydrogen can initially be produced on all scales, since demand is dispersed and transport can be provided by truck.

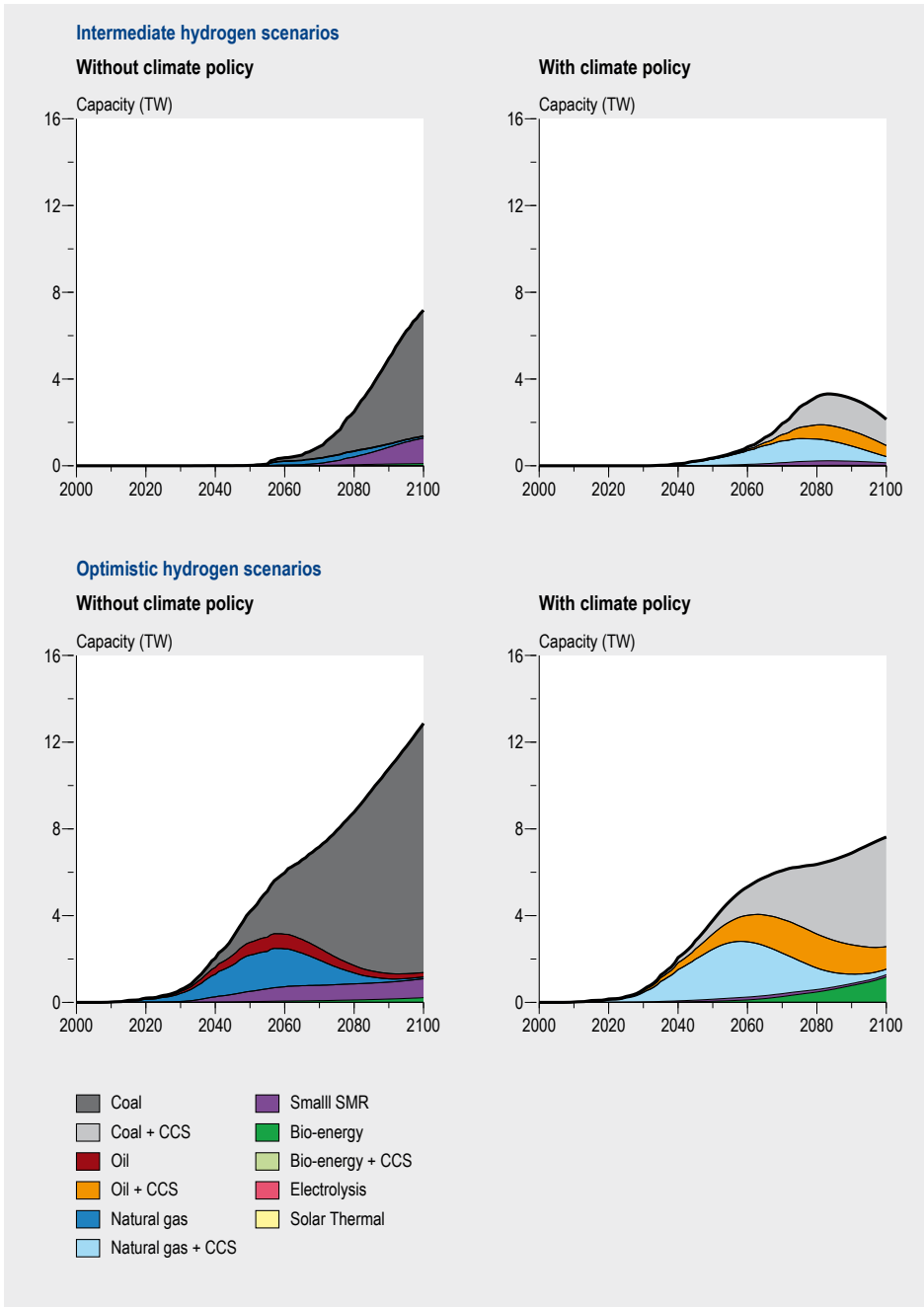


Figure 3.7. World hydrogen production capacity for the intermediate and optimistic hydrogen scenarios with and without climate policy (CP) (calculations are based on the SRES A1 scenario). No penetration occurs with pessimistic assumptions on hydrogen technology and cost (Van Ruijven et al., 2006).

The results of TIMER calculations show that under the default assumption, hydrogen is not likely to penetrate the world market before the mid-21<sup>st</sup> century, with or without climate policy, if only costs are considered (Figure 3.7). It could become a major secondary energy carrier later on, but only under optimistic assumptions. The transport sector provides the earliest opportunities. Urban air pollution could provide an important incentive to the use of hydrogen. The best prospects are in OECD Europe and Japan, where energy prices are relatively high due to high taxes and few indigenous energy resources.

Coal and natural-gas-based technologies seem to be the most economically attractive ones from the perspective of production. Partial oxidation of oil, biomass gasification, electrolysis and solar thermal hydrogen production are more expensive and hence show a lower degree of penetration. Under carbon constraints, the fossil-fuel-based hydrogen production technologies are still the most attractive if combined with carbon capture and storage; if this is not available, the preferred hydrogen path shifts towards biomass and natural gas. These outcomes reveal an ambiguous role for hydrogen in relation to climate policy. On the one hand, the most cost-effective production of hydrogen is from coal. As a result, CO<sub>2</sub> emissions from energy systems with hydrogen are likely to be higher than without hydrogen. On the other hand, energy systems with hydrogen can respond to constraints on CO<sub>2</sub> emissions more flexibly and at lower costs. This is because the use of hydrogen provides new and presumably cheap carbon emission reduction options in the form of centralized carbon capture and storage.

### 3.5 An application of TIMER: exploring low concentration stabilization scenarios

#### *Methodology*

A recent application of TIMER is the exploration of different pathways for stabilizing greenhouse gas concentration at low levels (Van Vuuren et al., 2006), the rationale being that climate change is one of the most prominent problems of sustainable development of this century (Carpenter and Pingali, 2006). Recent literature suggests that climate risks could already be substantial for an increase of 1-3°C compared to pre-industrial levels (Mastandrea and Schneider, 2004). Remaining temperature thresholds under low level with a high degree of certainty is likely to require stabilization at low greenhouse gas (GHG) concentrations. Meinshausen (2006), for instance, shows that remaining temperatures below the 2°C target with a 50% certainty requires stabilization below 450 ppm CO<sub>2</sub>-eq. Nevertheless, the number of studies looking at such low stabilization levels is very limited. The TIMER model was used in combination with the FAIR model (chapter 11), and the climate and terrestrial sub-models of IMAGE to develop scenarios that explore how such low greenhouse gas concentration stabilization levels could be reached. The links between the sub-models are indicated in Figure 3.8.

The overall analysis consists of three steps (Figure 3.8). First, a baseline emission scenario was constructed using IMAGE and TIMER. Both models were also used to provide informa-

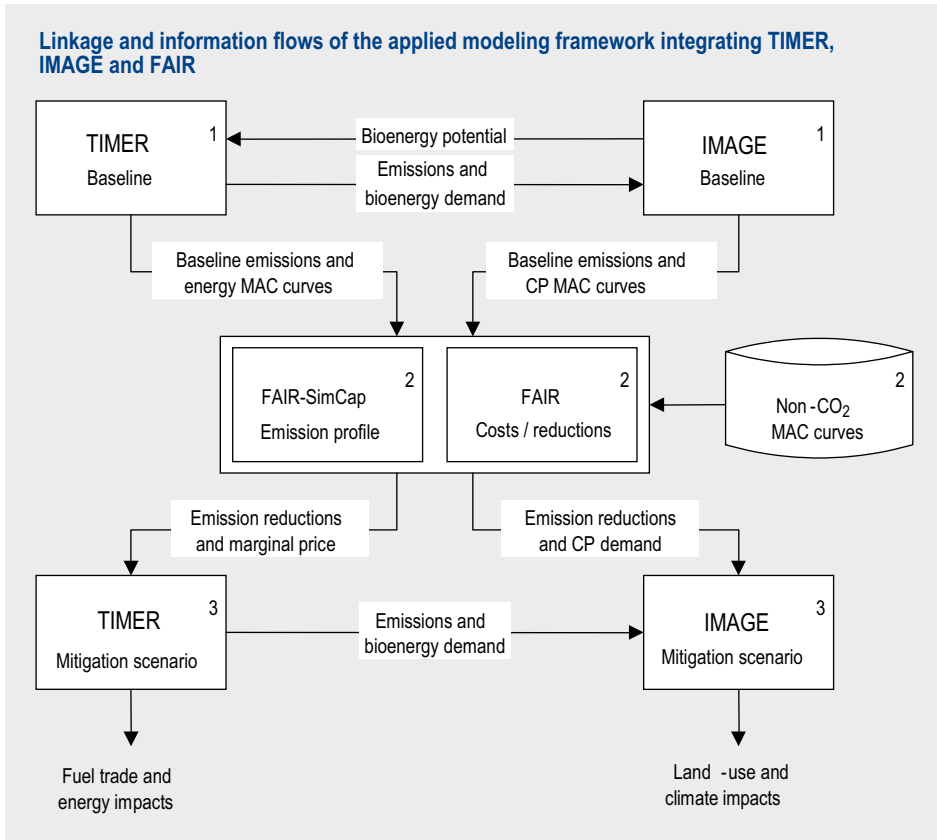


Figure 3.8. Linkage and information flows of the applied modelling framework integrating TIMER, IMAGE and FAIR (note CP = carbon plantations; MAC = Marginal abatement curve) (Van Vuuren et al., 2006).

tion on abatement by carbon plantation and measures in the energy system. Second, global emission pathways that lead to a stabilization of the atmospheric GHG concentration were developed using the FAIR model. The FAIR model distributes the global emission reduction among the different regions, gases and sources in a cost-optimal way, using the marginal abatement costs. Finally, the emission reductions and permit price determined in the previous step were implemented in the IMAGE/TIMER model to develop the final mitigation scenario (emissions, land use, energy system).

Estimates for reduction costs and potential from TIMER were made by imposing an emission permit price (carbon tax) and recording the induced reduction of CO<sub>2</sub> emissions. TIMER responds to the addition of an emission permit price in several ways. On the energy supply side, options with high carbon emissions (such as coal and oil) become more expensive when compared to options with low or zero emissions (such as natural gas, CCS, bioenergy, nuclear power, solar and wind power). The zero emissions therefore gain market-share. On the energy demand side, investments in efficiency become more attractive. Technology change can strongly influence the results. Differ-

ent sets of response curves to carbon tax levels were constructed to take this influence into account.

Apart from changes in energy use, there are other ways to reduce emissions. MAC curves for carbon plantations have been derived using the IMAGE model. For non-CO<sub>2</sub> gases, the starting point of our analysis consists of the MAC curves provided by the EMF-21 project of the Energy Modelling Forum (Weyant et al., 2006). Lucas et al. (2006) extended this set on the basis of a literature survey and expert judgement on long-term abatement potential and costs.

Finally, required emission reductions are estimated from information on multi-gas emission pathways constructed in FAIR (chapter 11). Three main criteria were used when developing the pathways: (i) a maximum reduction rate was assumed, reflecting the technical (and political) inertia that limits emission reductions. Fast reduction rates would require the early replacement of existing fossil-fuel-based capital stock, and this may involve high costs; (ii) the reduction rates compared to the baseline were spread over time as much as possible; (iii) the reduction rates were only allowed to change slowly over time.

### **Results**

Under a medium baseline (IPCC SRES B2 scenario) (see Van Vuuren et al., 2006) and without climate policy, worldwide primary energy use nearly doubles between 2000 and 2050 and increases by another 35% between 2050 and 2100. Most of this growth occurs in non-Annex I regions (about 80%). Oil continues to be the most important energy carrier in the first half of the century, and its demand is driven mainly by the transport sector. Natural gas dominates new capacity in electric power generation in the first decades, but starts to be replaced by coal from 2030 onwards due to increasing gas prices. As a result, coal becomes the dominant energy carrier in the second half of the 21<sup>st</sup> century. Energy-sector CO<sub>2</sub> emissions continue to increase for most of the century, peaking at 18 Pg C yr<sup>-1</sup> in 2080.

In order to reach the selected emission pathway that leads to stabilization of GHG radiative forcing at 650, 550 and 450 ppm CO<sub>2</sub>-eq, GHG emissions need to be reduced by 65%, 80% and 90%, respectively, in 2100, compared to the B2 baseline. Figure 3.9 shows the (cost-optimal) reduction in the mitigation scenarios for different gases (upper panel). In the short term, a substantial share of the reduction is achieved in all stabilization scenarios by reducing non-CO<sub>2</sub> gases while only 10% of the reductions come from reducing energy-related CO<sub>2</sub> emissions. The disproportionate contribution of non-CO<sub>2</sub> abatement is caused mainly by the relatively low-cost abatement options that have been identified for non-CO<sub>2</sub> gases. After 2015, an increasing part of the reduction will need to come from CO<sub>2</sub> emitted by the energy system.

The climate policies required to reach the stabilization pathways lead to substantial changes in the energy system compared to the baseline scenario (shown for 450 ppm CO<sub>2</sub>-eq) (Figure 3.10). These changes are more profound when going from 650 to 450

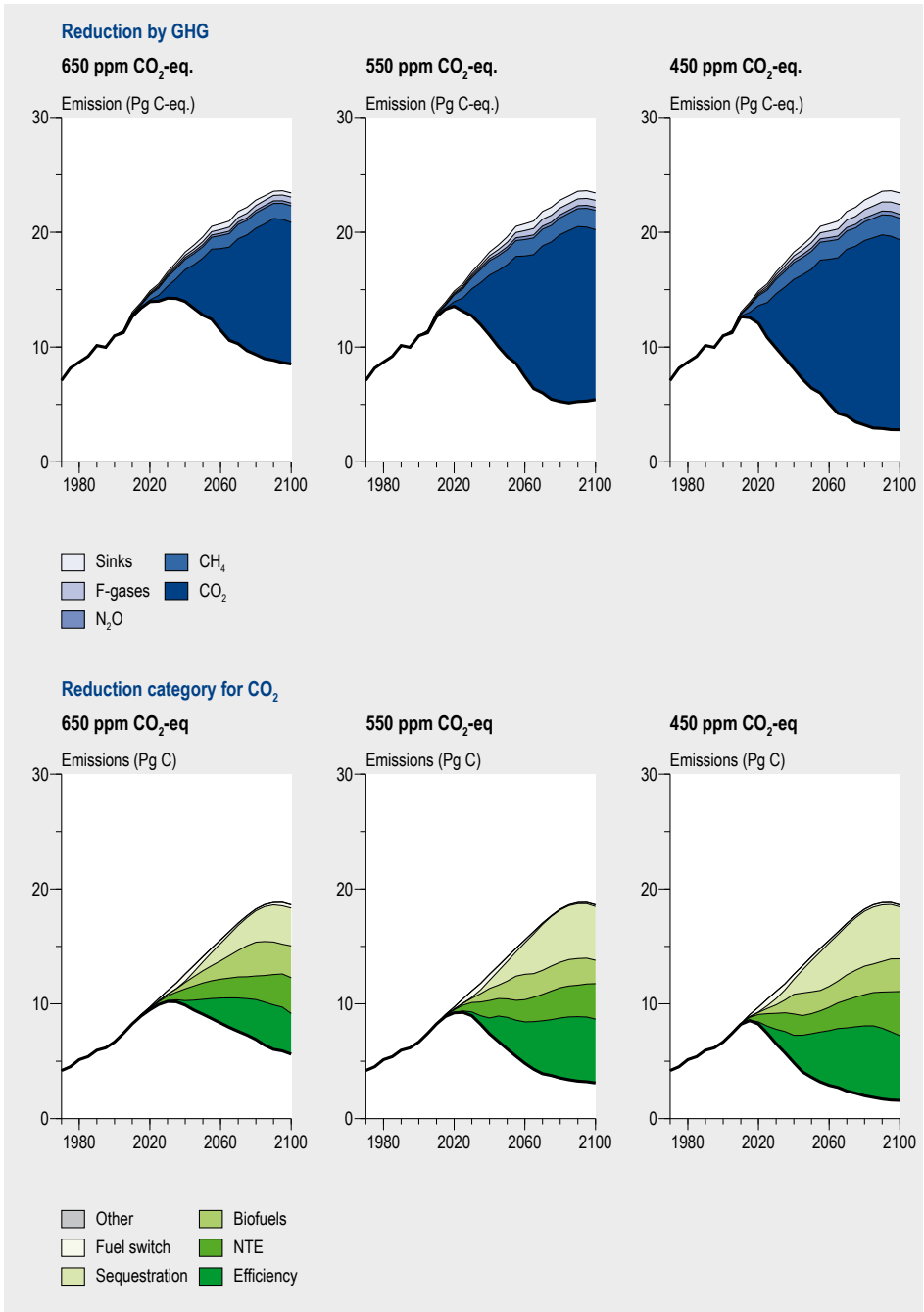


Figure 3.9. Emission reductions for total GHG emissions for different gases (top) and for energy CO<sub>2</sub> emissions contributed by reduction measure category (bottom) applied to stabilization scenarios at 650, 550 and 450 ppm CO<sub>2</sub>-eq (Van Vuuren et al., 2006). Calculations are based on the B2 baseline.

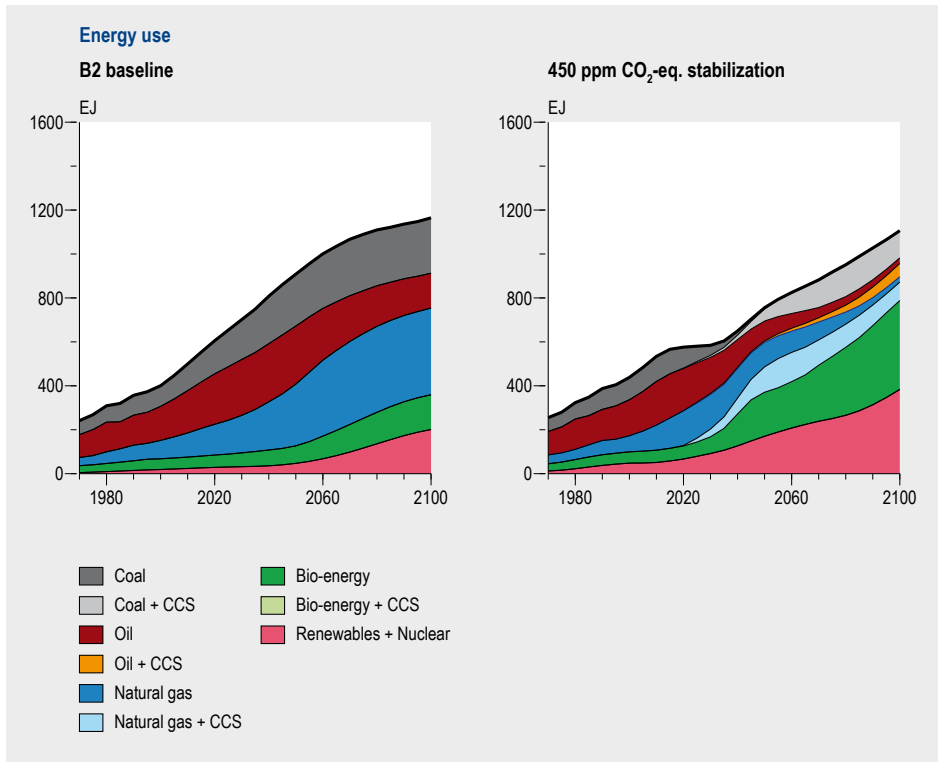


Figure 3.10. Primary energy use in the B2 baseline (left) and the 450 ppm CO<sub>2</sub>-eq stabilization scenario (right). Nuclear, solar, wind and hydro power have been reported at a virtual efficiency of 40%; bioenergy includes traditional biomass; renewables include hydro, solar and wind power (Van Vuuren et al., 2006).

ppm CO<sub>2</sub>-eq. In the most stringent scenario, global primary energy use is reduced by around 20%. Clearly, the reductions are not similar for the different energy carriers. The largest reductions occur for coal, in which the remaining coal consumption is primarily in electric power stations that use carbon capture and storage. There is also a substantial reduction for oil. Reductions for natural gas are smaller, while other energy carriers, in particular solar, wind and nuclear-based electricity and modern biomass, gain in market share.

The largest reduction in the energy sector results from changes in energy supply (Figure 3.9). Some changes stand out. First of all, under our default assumptions carbon capture and storage, mainly in the power sector, accounts for up to one-third of the reductions in energy-related CO<sub>2</sub> emissions. Energy efficiency represents a relatively important part of the portfolio of reduction options early in the century. Bioenergy use also accounts for a large proportion of the emission reductions. In the baseline scenario, about 200 EJ yr<sup>-1</sup> of bioenergy is used. In the most stringent stabilization scenario, bioenergy use increases to 350 EJ yr<sup>-1</sup>. The use of bioenergy requires land in places where in the baseline there would be natural vegetation sequestering carbon.

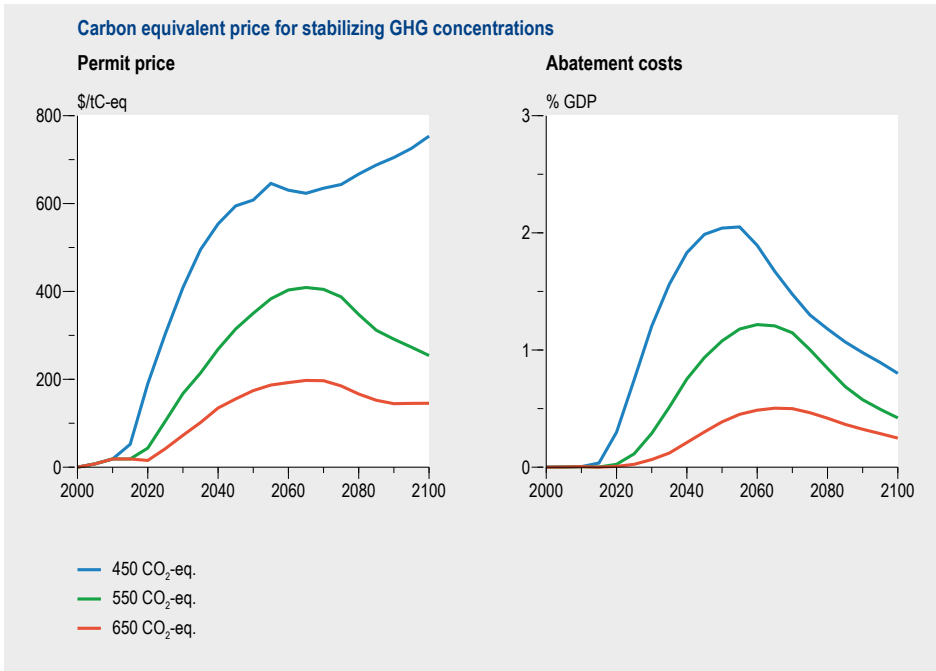


Figure 3.11. Carbon-equivalent price for stabilizing greenhouse gas concentrations at 650, 550 and 450 ppm CO<sub>2</sub>-eq from the B2 baseline (left); abatement costs as a percentage of GDP for these scenarios (Van Vuuren et al., 2006) (right).

Solar, wind and nuclear power also account for a considerable proportion of the required reductions. Due to their intermittent character, the contribution of solar and wind power is somewhat limited by a declining ability to contribute to a sufficiently reliable electric power system at high penetration rates. Therefore, the increase in nuclear power compared to the baseline is larger in the model results than the increase of renewables (see also MIT, 2003; Sims et al., 2003). However, more flexible power systems, different assumptions on the consequences of intermittency for renewables, the development of storage systems, technological breakthroughs or taking into account public acceptance of nuclear power could easily lead to a different mix of zero-emission power technologies.

Figure 3.11 shows the permit prices and abatement costs. The latter are calculated on the basis of the marginal permit prices and represent the direct additional costs due to climate policy. Scenarios involving stabilization at 650 and 550 ppm CO<sub>2</sub>-eq ppm are characterized by a fairly smooth increase in the marginal price followed by a drop by the end of the century. The drop is caused by a fall in emissions in the baseline and further cost reductions in mitigation technologies (in particular, hydrogen fuel cells start entering the market by this time, allowing for reductions in the transport sector at much lower costs). In the 450 ppm stabilization scenario, the marginal price rises rapidly during the first part of the century and reaches a marginal price of over 600 US\$ per ton C-eq by 2050, and stabilizes at 800 US\$ per ton C-eq by the end of the cen-

*Table 3.2. Overview of several key parameters for the stabilization scenarios explored.*

	2100 Concentration (ppm)		Reduction of Cumulative Emissions in 2000–2100 (%)	Temperature change (°C)	
	CO <sub>2</sub> -eq	CO <sub>2</sub>		2100	Equilibrium
B2	947	708	0	3.0	-
B2 650 ppm CO <sub>2</sub> -eq	625	524	36	2.3	2.9
B2 550 ppm CO <sub>2</sub> -eq	538	463	50	2.0	2.5
B2 450 ppm CO <sub>2</sub> -eq	479	424	61	1.7	2.0

ture. The high marginal price is necessary to reduce emissions from the less responsive sources such as CO<sub>2</sub> emissions from transport or some of the non-CO<sub>2</sub> emissions from agricultural sources. Other sources, such as electric power, already have their emission reduced to virtually zero at permit prices of 200–300 US\$ per ton C-eq.

The three multi-gas stabilization scenarios analyzed here lead to clearly different temperature increases. Table 3.2 shows some of the scenario parameters for a medium estimate of climate sensitivity of 2.5°C. The table shows that in 2100 the 650 and 550 ppm CO<sub>2</sub>-eq stabilization scenarios are still approaching the stabilization levels, while the 450 ppm CO<sub>2</sub>-eq scenario has in fact exceeded its target (as designed) and is approaching its target from a higher concentration level. Temperature increases (as calculated by IMAGE) range from 2.3 to 1.7°C in 2100.

In summary, we find that stabilizing greenhouse concentrations at 650, 550, 450 ppm and, under specific assumptions, at 400 ppm CO<sub>2</sub>-eq, is technically feasible from median baseline scenarios on the basis of technologies currently available. Our calculations show that the first decades of the 21<sup>st</sup> century represent the most difficult period for climate change policy, even assuming the full participation of all countries under a climate regime, with a rapidly rising costs level. The net present value of abatement costs increases from 0.2% to 1.2% of the net present value of GDP (5% discount rate) when moving from 650 to 450 ppm. On the other hand, the probability of meeting a 2°C target increases from 0–18% to 22–73%. In addition to direct abatement costs, stabilization also involves indirect costs and benefits (for example, the changes in the fuel trade). Strategies are also shown to consist of a portfolio of measures. The reductions in our stabilization scenarios are achieved through a set of measures rather than a single measure. The reasons for this result include: (i) limitations in the potential of individual options; (ii) regional and sub-regional differentiation; (iii) increasing costs for penetration rates as a result of depletion and (iv) differentiation between sectors. At the same time, carbon capture and storage represent a very attractive technology to reduce greenhouse gas emissions under our default assumptions.

### 3.6. Concluding remarks

The Timer 2 model has been developed to explore different pathways of the global energy system in the context of climate change or long-term depletion of fossil-fuel resources. Several applications of the model, mostly coupled to other elements of IMAGE, such as the land-use model and the FAIR model, have shown its capacity to fulfil this aim. However, the model can be improved further. Issues that merit future research include the following: (i) the implication of the energy transition in developing countries and (ii) modelling physical drivers of energy demand. With reference to (i), increasing energy demand in most scenarios, in developing countries represents the main driving force behind increasing global energy consumption. Nevertheless, representation of developing-country energy issues in global energy models like TIMER is limited. We will explore whether improvements can be made. Referring to (ii), in the current version of TIMER primarily monetary indicators are used to determine energy demand. By modelling the underlying physical drivers (passenger kilometres or steel production), a deeper insight can be obtained in opportunities to change the energy system.



## 4 MODELLING AGRICULTURAL TRADE AND FOOD PRODUCTION UNDER DIFFERENT TRADE POLICIES

- As an alternative to the agricultural demand model of earlier IMAGE versions, the IMAGE 2.4 framework now includes a linkage to the global agricultural trade model GTAP, which determines the regional food production on the basis of dietary preferences, agricultural trade regimes and food prices.
- An iterative linkage of GTAP and IMAGE allows an assessment of the economic and environmental consequences of specific trade policies. GTAP calculates consumption and trade of agricultural products by taking into account regional and world market prices, which result from production functions explicitly including capital, labour and land prices. In return, IMAGE 2.4 provides yield and yield changes due to climate change and expansion of agriculture to less productive areas; it also simulates the geographically explicit environmental impacts.
- Results from recent studies using the coupled GTAP-IMAGE model framework show that trade liberalization will lead to an increase in trade of agricultural products with positive economic consequences for almost all regions (growth in GDP), but with higher environmental pressure on developing exporting regions like Latin America and Southern Africa. In total, trade liberalization will lead to a larger expansion of arable land and therefore to higher pressure on ecosystems.

### 4.1 Introduction

For many decades, food supply and food distribution have been among the most important issues in the global political arena. At the first World Food Summit in 1974, political leaders from around the world set themselves a goal to eradicate hunger in the world within 10 years. As history has proven, this ambitious goal was not met, leading to new goals at the second World Food Summit in 1996. There, the world leaders committed themselves to reducing the number of chronically undernourished by 50% by the year 2015. This target has been endorsed at many other meetings since then and is now known as one of the eight Millennium Development Goals (MDGs) of the United Nations (United Nations, 2001). The MDGs commit the international community to adopting an extended view on development and recognizing the importance of creating a global partnership for achieving sustainable economic growth.

The term ‘sustainable economic growth’ embraces the marriage of economy and ecology introduced by Brundtland (1987) in ‘Our Common Future’. This report emphasizes the importance of development of poor countries as a prerequisite for peace, security and protection of the environment. At the 1992 Earth Summit in Rio de Janeiro, world leaders agreed to make sustainable development the prime objective for environmental policy. Agriculture is the world’s largest subsidized sector. In 2002, the World Summit on Sustainable Development at Johannesburg called for an international approach towards phasing out ‘harmful subsidies’, unfortunately failing to specify what these

were. Negotiations on lowering subsidies linked with trade regimes are the mandate of the World Trade Organization (WTO). Given the debated beneficiary effects of liberalization of trade, agriculture has been one of the major causes of discontent between developed and developing countries within the WTO. After a period of nearly 20 years of preparing, negotiating and implementing the Uruguay Round Agreement on Agriculture, subsidies and protection have remained high, in particular in industrialized countries. Therefore, developing countries have started to indicate that any new trade round or multilateral trade agreement should particularly benefit the developing world for it to be meaningful. In Doha consensus was reached in November 2001 on a mandate to dedicate the new round of trade liberalization to serve development and the environment and produce an outcome that specifically would benefit the developing world (the Doha Development Agenda).

In contrast to the intensive media attention on this subject, there are relatively few scientific studies that deal with the complex relation between trade liberalization and environmental resources. Studies of trade and the environment often come to widely varying conclusions depending on the scientific background of their authors (Huang and Labys, 2001; Eickhout et al., 2004). Environmentalists often stress the negative environmental impacts of large-scale, intensive production following trade liberalization (CBD, 2002), whereas economists argue that the right response in the case of negative effects is to address the underlying problem through domestic regulation or environmental treaties and not to restrict trade (see Bulte and Barbier, 2004). A key question is whether the political climate is such that institutions can be created to deal with possible negative impacts on the environment.

The adjusted version of the Global Trade Analysis Project (GTAP) model (Hertel, 1997; Van Meijl et al., 2006) model included in the IMAGE 2.4 framework offers a viable approach to assess the impact of non-agricultural sectors on agriculture and contains a full treatment of factor markets with special land modelling features. Although the IMAGE 2.2 model claimed to ‘assess the global environment’, its simple agricultural demand model (Strengers, 2001) was not appropriate for dealing with the issues of agricultural trade and policies, mainly due to the lack of an economic trade model with explicit policy options. The combination of IMAGE and GTAP offers a modelling framework to analyze both the economic and environmental conditions that determine the global future food market.

## 4.2 Methodology

### *Standard GTAP model*

The GTAP model is a multi-regional, static, general equilibrium model based on neo-classical micro-economic theory (Hertel, 1997). The standard model is based on regional and national input-output tables. GTAP distinguishes 12 sectors (grains, oils, sugar, horticulture, other crops, cattle, other animal products, raw milk, dairy products, other agricultural food products, industry and services). It explicitly links industries in a value

added chain from primary goods, over continuously higher stages of intermediate processing, to the final assembling of goods and services for consumption.

In the model, the objective of the producers in each sector within a country or region is to maximize profit by choosing a combination of inputs of labour, capital and intermediates to produce a single sectoral output. Perfect competition is assumed in all sectors. In the case of crop and livestock production, farmers also take decisions on land allocation. Intermediate inputs are either produced domestically or imported, while primary factors cannot move across borders. Markets are typically assumed to be competitive.

When taking decisions on inputs for production, prices of inputs and outputs are exogenous input to the model. Primary production factors, land, labour and capital are fully employed within each economy, and hence returns to land and capital are endogenously determined at equilibrium, i.e. the aggregate supply of each factor equals its demand. Each region is equipped with one regional household which distributes income over savings and consumption expenditures according to fixed budget shares.

In contrast to most Partial Equilibrium (PE) models, GTAP assumes that land is heterogeneous. The heterogeneity is introduced by specifying a transformation function, which takes total land as an input and distributes it among various sectors in response to relative rental rates. A Constant Elasticity of Transformation (CET) function is used, where the elasticity of transformation is a synthetic measure of land heterogeneity. Prices of goods and factors are adjusted until all markets are simultaneously in (general) equilibrium. Only changes in gross trade flows are modelled. Hence, factor markets are competitive, and labour, capital and land are mobile between sectors but not between regions.

GTAP assumes that products are differentiated by country. This is modelled using the Armington approach (Hertel, 1997). In this approach imports and domestic commodities are assumed to be imperfect substitutes in demand; the CET function describes the substitution possibilities between these commodities. The bilateral commodity trade is modelled then in this manner. Taxes and other policy measures are included in the theory of the model at several levels. All policy instruments are represented as ad valorem tax equivalents which create differences between the undistorted prices and the policy-inclusive prices.

Below we discuss a number of modifications to the standard GTAP model, including approaches for an improved land allocation, factor market segmentation and feed demand. In addition, we present the implementation of land supply curves in GTAP on the basis of IMAGE and the update of land productivity while iterating GTAP and IMAGE.

### ***An extended land allocation tree***

The standard version of GTAP represents land allocation in a CET structure (Figure 4.1) assuming that the various types of land use are imperfectly substitutable, but with equal substitutability among all land-use types. For our purposes, the land-use

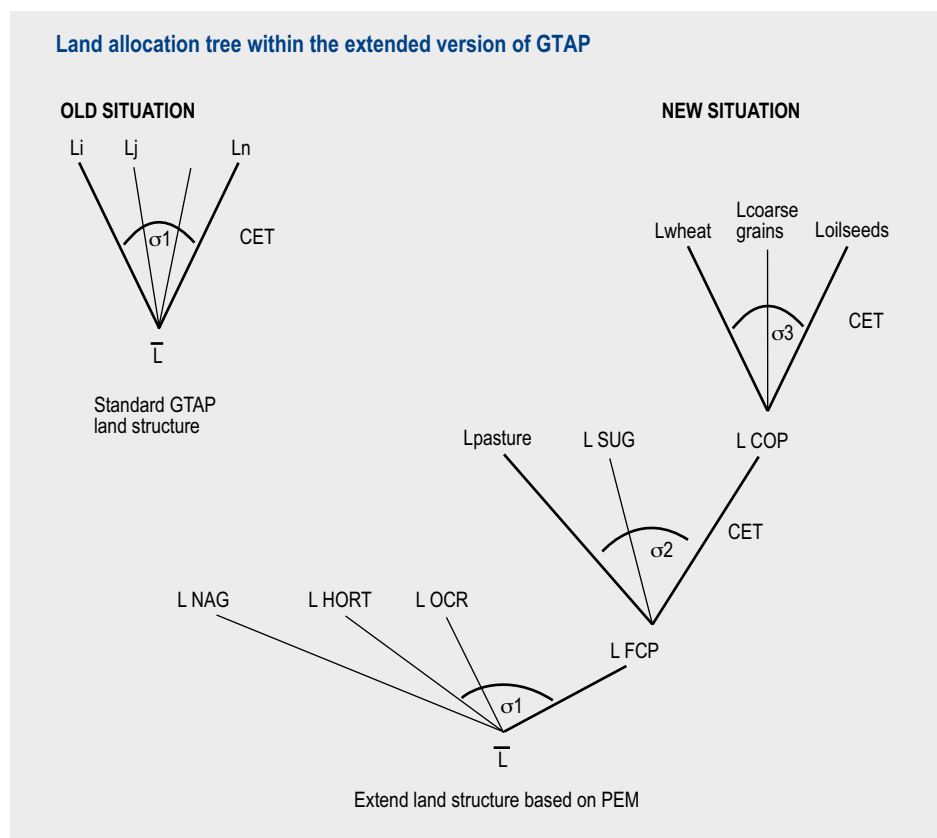


Figure 4.1. Land allocation tree within the standard and extended version of GTAP.

allocation structure is extended by taking into account that the degree of substitutability differs between types of land (Huang et al., 2004) using the more detailed OECD Policy Evaluation Model (PEM) structure (OECD, 2003) (Figure 4.1). It distinguishes different types of land in a nested 3-level CET structure. The model covers several types of land use with different suitability levels for various crops (i.e. cereal grains, oilseeds, sugar cane/sugar beet and other agricultural products).

The lower nest assumes a constant elasticity of transformation between ‘vegetables, fruit and nuts’ (HORT), ‘other crops’ (e.g. rice, plant-based fibres; OCR), the group of ‘Field Crops and Pastures’ (FCP) and non-agricultural land (NAG). The transformation is governed by the elasticity of transformation  $\sigma_1$ . The FCP-group is itself a CET aggregate of Cattle and Raw Milk (both Pasture), ‘Sugarcane and Beet’ (SUG), and the group of ‘Cereal, Oilseed and Protein crops’ (COP). Here, the elasticity of transformation is  $\sigma_2$ . Finally, the transformation of land within the upper nest, the COP group, is modelled with an elasticity  $\sigma_3$ . In this way the degree of substitutability of types of land can be varied between the nests. Agronomic features are captured to some extent. In general it is assumed that  $\sigma_3 > \sigma_2 > \sigma_1$ , which implies that it is easier to change the allocation of land within the COP group, while it is more difficult to move land out of

COP production into, say, vegetables. The values of the elasticities are taken from PEM (OECD, 2003).

### ***Factor market segmentation***

Wage differentials between agriculture and non-agriculture can be sustained in many countries (especially in developing countries) through limited off-farm labour migration (De Janvry et al., 1991). Returns to assets invested in agriculture also tend to diverge from returns of investment in other activities.

To capture these stylized facts, we incorporate segmented factor markets for labour and capital by specifying a CET structure that transforms agricultural labour (and capital) into non-agricultural labour (and capital) (Hertel and Keening, 2003). This specification has the advantage that it can be calibrated to available estimates of agricultural labour supply response. In order to have separate market-clearing conditions for agriculture and non-agriculture, we need to segment these factor markets with a finite elasticity of transformation. We also have separate market prices for each of these sets of endowments. The economy-wide endowment of labour (and capital) remains fixed, so that any increase in supply of labour (capital) to manufacturing labour (capital) has to be withdrawn from agriculture, and the economy-wide resources constraint remains satisfied. The elasticities of transformation can be calibrated to fit estimates of the elasticity of labour supply from OECD (2003).

### ***Feed conversion in livestock***

The intensification of livestock production systems also influences the composition of the animal feed required by livestock production systems (chapter 5). In general, intensification is accompanied by decreasing dependence on open range feeding and increasing use of concentrate feeds, mainly feed grains, to supplement other fodder. At the same time, improved and balanced feeding practices and improved breeds in ruminant systems enable more of the feed to go to meat and milk production rather than to maintenance of the animals. IMAGE simulates the production of livestock products, the animal stocks, productivity per animal, feed conversion and the use of different feedstuffs (crops, residues and fodder crops, animal products, grass and scavenging, see chapter 5).

In the extended GTAP model, future shifts in feed composition are taken from the IMAGE implementation of the FAO projection up to 2030 (Bruinsma, 2003) as described in Bouwman et al. (2005) (see also chapter 5). The grazing intensity is assumed to change in addition on the basis of GTAP results for intensification or extensification (see below).

### ***Land supply curves***

Regional differences in land quality and changes in land quality due to land degradation, water stress and climate change are not considered in the standard GTAP model. From an economic point of view, the agricultural land supply is a function of the price of land as expressed by land rent. We implemented land supply curves in GTAP to cap-

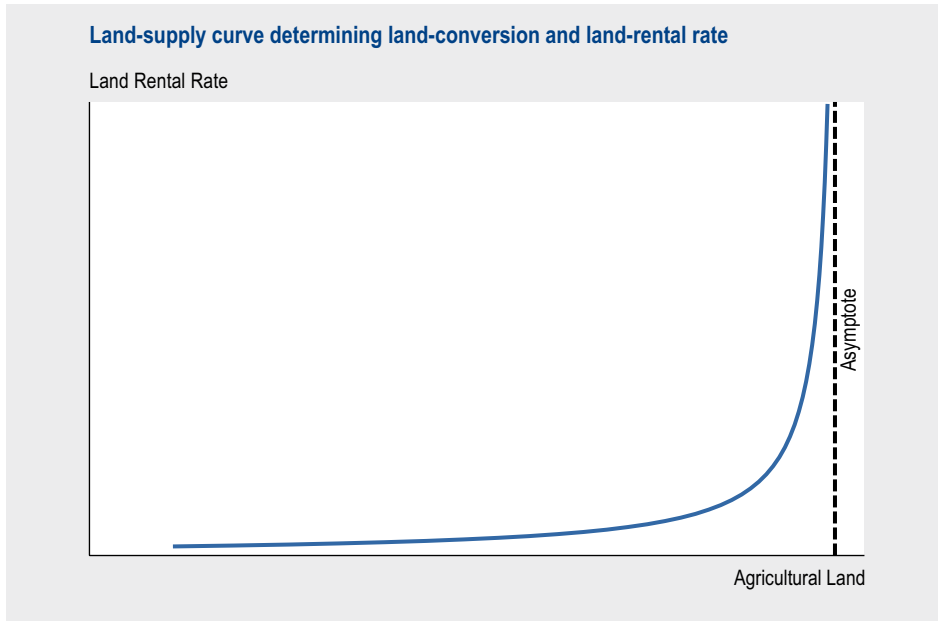


Figure 4.2. Land-supply curve determining land-conversion and land-rental rate.

ture the (changes in) land quality and describe regional variations in land rent. These curves serve to translate the biophysical information on land productivity (based on soil and climatic conditions, see chapter 5) generated by IMAGE to land rent. The first concept of using land-supply curves was derived from Abler (2003). We calibrated the curves using FAO land-use projections and IMAGE results (Van Meijl et al., 2006; Tabeau et al., 2006).

The supply of agricultural land depends on its biophysical availability (potential area of suitable land), institutional factors (agricultural and urban policy, policy towards nature) and land price. The assumption that the most productive land is taken into production first leads to the shape of the agricultural land-supply curve presented in Figure 4.2. If the gap between agricultural land potentially available and land actually used in the agricultural sector is large, any increase in demand for agricultural land will lead to land conversion for agricultural use and will be accompanied by a modest increase in land price. Such a situation occurs in the flat part of the land supply curve (Figure 4.2). In contrast, when the agricultural land that is in use is close to the potential area, an increase in demand for agricultural land will lead to an increasing land price (land becomes scarce). In such a situation, land conversion is difficult to achieve, and therefore the elasticity of land supply with respect to land price is also low. Points situated on the steep part of the land-supply curve in Figure 4.2 describe this situation.

In IMAGE, the productivity for seven food crops is calculated for each 0.5 by 0.5 degree grid cell using the crop growth model of IMAGE (Leemans and Van den Born, 1994).

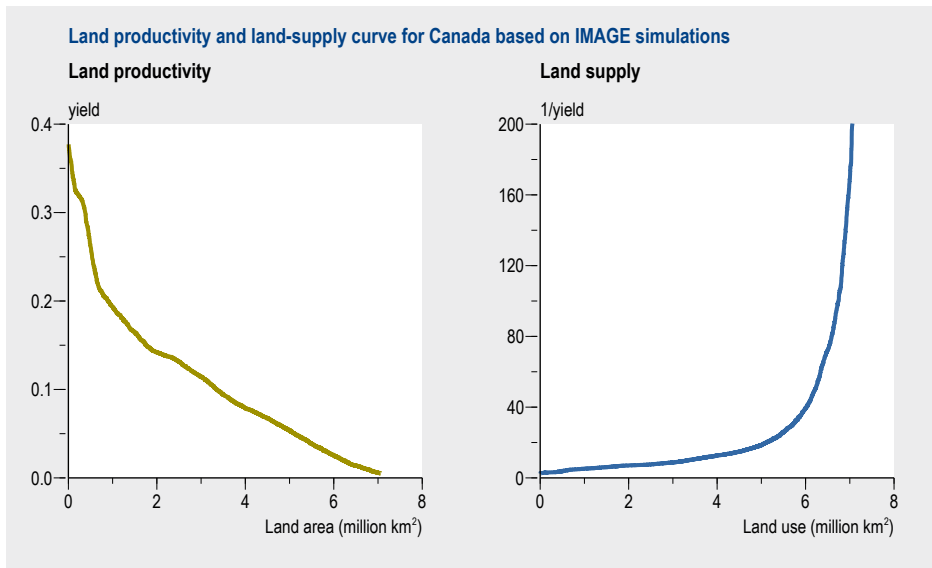


Figure 4.3. Land productivity and land-supply curve for Canada on the basis of IMAGE simulations.

For GTAP this information is aggregated to an estimate of the overall productivity for each grid cell. This overall crop productivity is expressed on a relative scale between 0 and 1 on the basis of the potential crop productivity. Land productivity curves are obtained by ordering all grid cells in each of the 24 world regions from high to low productivity, and summing the total area (Figure 4.3). The land productivity curve can be translated to a land-supply curve assuming that the land price is a function of the inverse of the land productivity (Figure 4.3). By using different mathematical functions that approach the inverse of the productivity curve, a land-supply curve is thus implemented in GTAP for each region (Tabeau et al., 2006).

We estimated the land supply function for 24 countries and regions. The curves are fitted to the data using the non-linear least square estimation method. Since the inverse of yield is not a good proxy of real land price if land is scarce or when only a small fraction of the potentially available area is actually used, we allowed a lower fit to the data at the beginning and ending of the curves. The asymptote of the land-supply curve is an estimate of the availability of land in each region. All grid cells with yield values of zero (mainly ice and desert) as well as urban area and protected bioreserves are excluded.

In the case of EU and Japan, the conversion of non-agricultural land to agriculture is severely restricted by nature policy. Therefore, we assumed that only set-aside and abandoned agricultural land can be transformed to agricultural land in the EU and Japan: we excluded the forested areas in the land-supply curves in these regions by setting yields to zero.

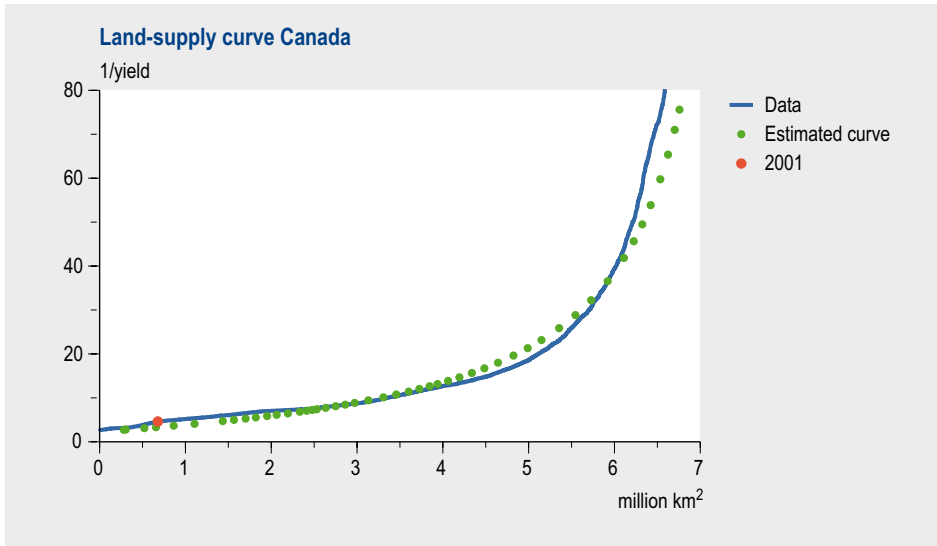


Figure 4.4. Land-supply curve for Canada.

The results indicate scarcity of agricultural land in North Africa, EU, the Rest of Western Europe, Former Soviet Union, Middle East, China, Japan and Oceania. This means that these regions are currently on the steep part of their land-supply curve and the associated land-supply elasticity with respect to the land price is lower than 1. Agricultural land is not scarce in Canada, and here, expansion of agriculture can take place without a fast increase in the land price (Figure 4.4). The opposite situation can be seen in China. A small expansion of agricultural land here will lead to a high increase in the land price, and this stimulates the intensification processes in the agricultural production systems (Figure 4.5).

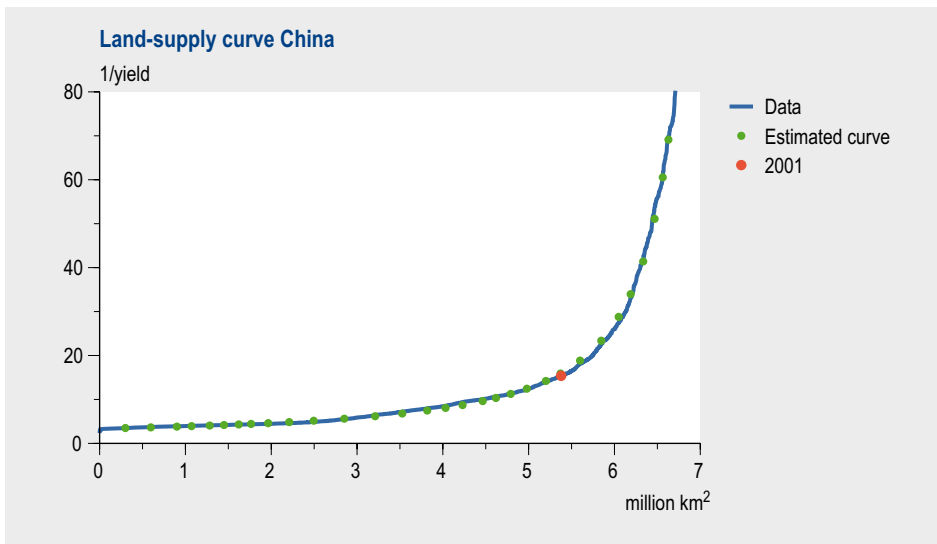


Figure 4.5. Land-supply curve for China.

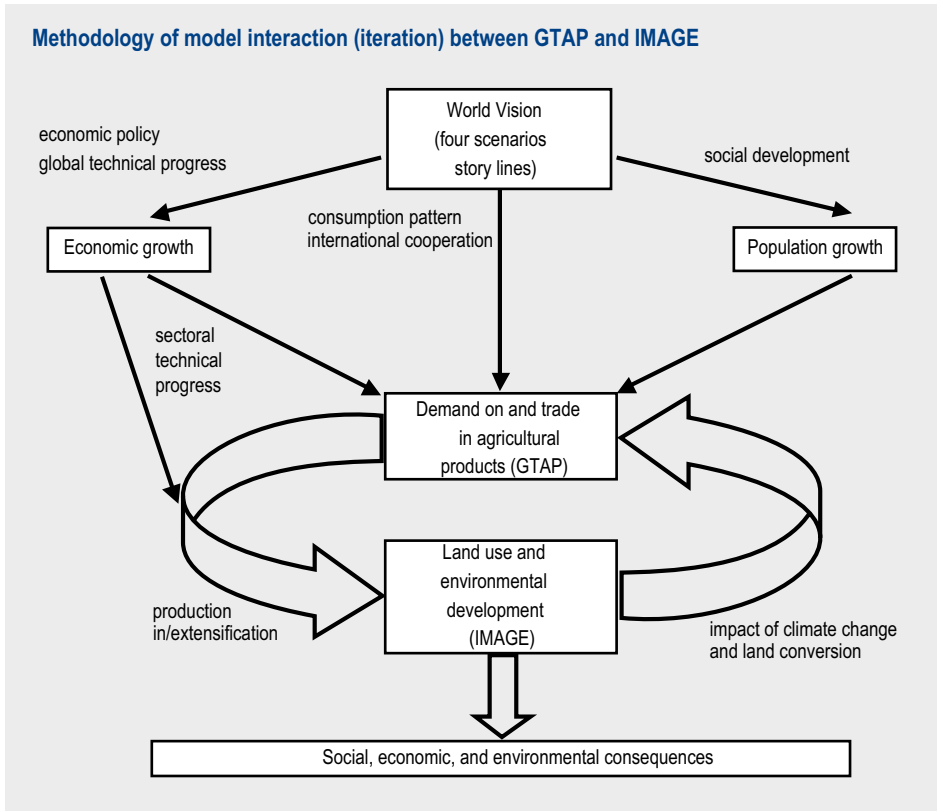


Figure 4.6. Scheme showing the methodology of model interaction (iteration) between GTAP and IMAGE.

### ***Exchanging land productivities between GTAP and IMAGE***

Figure 4.6 shows the methodology of iterating the extended version of GTAP with IMAGE. Yields in GTAP depend on an exogenous part (the trend component) and an endogenous part with relative factor prices (the management component). The production structure used in GTAP implies that substitution is possible among the different production factors. If land prices rise, the producer will substitute land for other production factors such as capital and, as a consequence, land productivity (yields) will increase.

The exogenous trend of the yield is taken from Bruinsma (2003) where macro-economic prospects are combined with local expert knowledge to produce best-guesses of the technological change for each country for the coming 30 years. The FAO data were therefore used as exogenous input for a first model run with the adjusted GTAP model. However, many studies indicated this change in productivity is enhanced or reduced primarily by climate change (Rosenzweig et al., 1995; Parry et al., 2001; Fischer et al., 2002). Climate change may have a negative impact on global mean crop yields when temperature increases above 3 to 4°C compared to pre-industrial levels. Moreover, the amount of land expansion or land abandonment will have an additional impact on productivity changes, since land productivity is not homogeneously distributed over each region.

The output of GTAP used for the iteration with IMAGE comprises sectoral production growth rates and the endogenous determined intensification or extensification (Figure 4.6). The exogenous assumptions based on FAO (Bruinsma, 2003) are translated to IMAGE parameters beforehand (see chapter 5). For crops, the endogenous GTAP values are added to the management factor within IMAGE. For pigs and poultry, the additional intensification is added to the animal productivity of these commodities. For dairy and non-dairy cattle and sheep and goats the additional value is added to the grazing intensity.

Subsequently, the IMAGE model calculates the yields, the demand for land and the environmental consequences on crop productivity. IMAGE simulates global land-use and land-cover changes by reconciling the land-use demand with the land potential. Agricultural land is allocated to 0.5 by 0.5 degree grid cells within each world region until the total demand for this region is satisfied. The results depend on changes in the demand for food and feed and a management factor as computed by GTAP. The allocation of land-use types at grid cell level is determined by specific land allocation rules like crop productivity, distance to existing agricultural land, distance to water bodies and a random factor (Alcamo et al., 1998). This procedure yields the area of agricultural land needed for each world region and the corresponding changes in yields related to the extent and productivity of the land and climate change. These additional changes in crop productivity are returned to GTAP (Figure 4.6). A general feature is that yields decline if significant land expansion occurs, as the productivity of land last taken into production is by definition lower than that of the existing agricultural area. When the agricultural land area is close to the potential area, even marginal land may be taken into production. In the short term, these factors may even be more important than the effects of climate change.

The iteration between GTAP and IMAGE is ended when land-use projections in both models are similar. Since GTAP bases its calculations on land-supply curves from IMAGE, the amount of iteration needed is limited.

### 4.3 Scenario analysis

#### *General*

The GTAP-IMAGE modelling framework can be used to assess the economic and environmental consequences of different scenarios. Recent applications of the modelling framework are published in Eickhout et al. (2004; 2006a,b) and in Van Meijl et al. (2006). Here, we discuss a 'business as usual' scenario and a variant of this baseline with full trade liberalization, which could be one of the outcomes of future trade policies agreed upon in the WTO.

The baseline scenario is based on projections for land-use changes from FAO (Bruinsma, 2003) and for world energy from IEA (IEA, 2004). The scenario includes autonomous developments in demography, economics and technology, and current policies agreed

upon in international treaties. The scenario assumes moderate population growth and economic development. The global population growth is from 6.1 billion in the year 2000 to 9 billion in 2050, but with a gradually declining growth rate. Over the same period, the global average annual income increases from US\$ 5300 to US\$ 16,000 per capita. The combined effect of population and economic growth represents more than a fourfold increase in global GDP in the next half century. Due to structural shifts of economies to less energy-intensive sectors and technological improvements leading to energy savings, total primary energy consumption increases by just over a factor of 2 (from 400 to 900 EJ yr<sup>-1</sup> in 2050) (EJ, exajoule; 1 EJ = 10<sup>18</sup> J). In the baseline, energy supply continues to rely on fossil resources (coal, oil and gas) leading to continued increase of emissions of greenhouse gases from combustion. Together with emissions from land use and other sources, this leads to a rise in global temperature of 1.8°C over pre-industrial levels in 2050, which is faster than the observed increase in the last 130 years. After implementation of the Kyoto Protocol for 2008-2012, no further climate mitigation measures are included in the baseline scenario.

In the liberalization variant of the baseline, full trade liberalization is assumed to be implemented immediately in 2015. Liberalization of the agricultural market is accompanied by high rates of technology transfer; it has an additional effect on economic drivers and influences changes of food production, land use, agricultural intensification, habitat loss and atmospheric nitrogen deposition. Multilateral cooperation on economic issues and successful WTO negotiations are assumed, leading to substantial improvements in market access of all countries, a phasing out of all forms of export subsidies and substantial reductions in trade-distorting domestic support. Hence, a successful agreement on the Doha Development Agenda is assumed, comprising the implementation of binding commitments to: (i) substantial improvements in market access; (ii) reductions and eventually phasing out of all forms of export subsidies; and (iii) substantial reductions of trade-distorting domestic support.

The baseline and its trade liberalization variant are implemented for the period 2000-2030. The environmental consequences are focused on land-use change and impacts on biodiversity, using the relative mean species abundance (RSA) as a proxy for this (Alkemade et al., 2006; Eickhout et al., 2006b). The RSA is determined by an undisturbed RSA value for each land use type minus different pressures, causing a decrease of this initial RSA. Examples of pressures taken into account are climate change and nitrogen deposition. The decrease of the initial RSA due to different pressures is based on literature translated into dose-response relationships for each land-use type in each region (chapter 10).

## **Results**

**Baseline.** Consumption of agricultural products lags behind overall economic growth, but the combined effect of increasing population and improving diets with higher caloric intake, particularly for those in currently undernourished regions, and the shift towards more animal products in the diet at higher income levels cause a fast increase in agricultural production (Figures 4.7 and 4.8). The agricultural crop production in

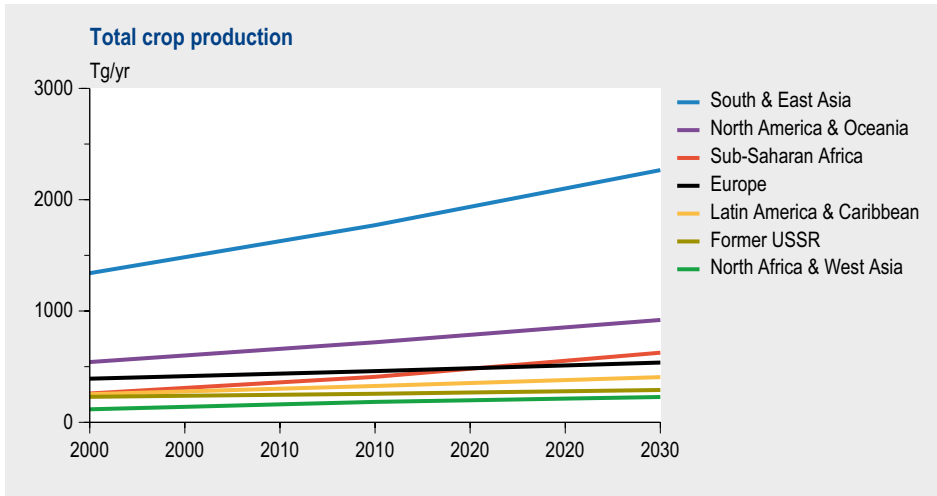


Figure 4.7. Total crop production in the baseline scenario up to 2030.

South and East Asia increases by 70% and livestock production by 65%. The increase in livestock products substantially increases the agricultural area, especially in feed exporting regions like Sub-Saharan Africa (total crop production increase of 140%) and Latin America and Caribbean (increase of 70%). Industrialized regions like Europe and North America and Oceania experience a lower increase of production, especially Europe (only 10% increase of livestock production; Figure 4.8).

The increase in production is not always reflected directly in the size of agricultural land, mainly due to expected increases in agricultural productivity (Figures 4.9 and 4.10). The increase of both crop and animal production mainly affects the increase of arable land at the cost of grassland. For example, in North America and Oceania about

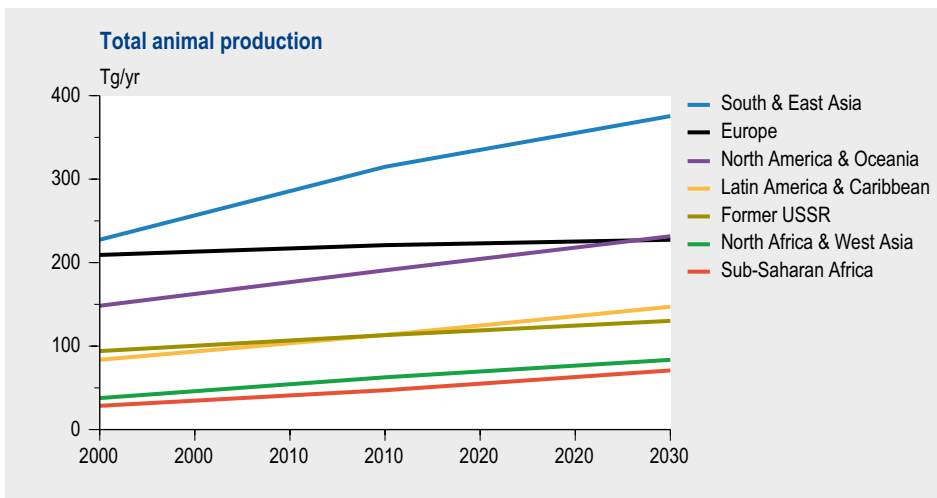


Figure 4.8. Total animal production in the baseline scenario up to 2030.

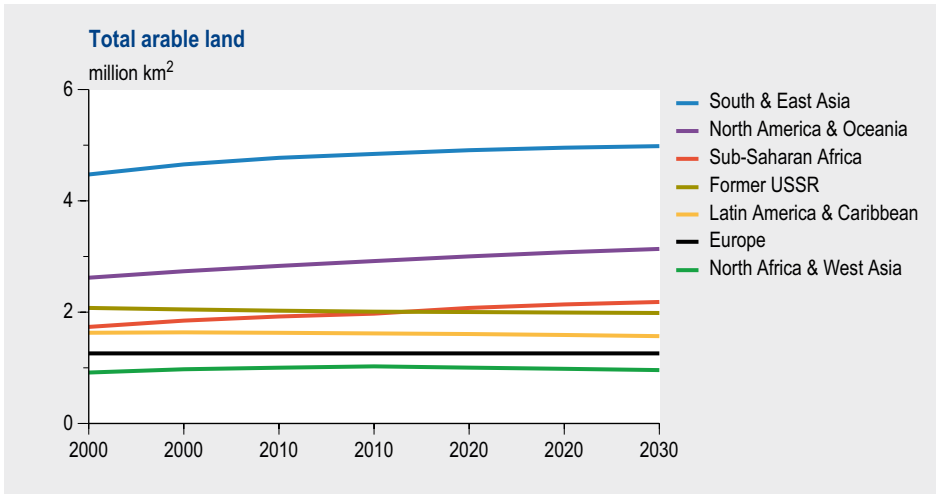


Figure 4.9. Arable land area in the business as usual scenario up to 2030.

450,000 km<sup>2</sup> of pastureland is converted to 500,000 km<sup>2</sup> of arable land. Only Sub-Saharan Africa shows a clear increase of the arable land area (of 25%), while grassland shows only slight changes. The expansion of arable land takes place mainly in a dry climate zone (Alkemade et al., 2006), which is in line with findings of the Millennium Ecosystem Assessment (2005). Hence, in most regions where agricultural area is projected to increase, there is a trade-off between the environment and economic growth. Sub-Saharan Africa is a special case, however. With its low economic growth hampering technological improvement in the agricultural sector, the population growth rate is high. This combination causes a poor outcome for sustainable development indicators, with slow economic growth and a fast increase in environmental pressure.

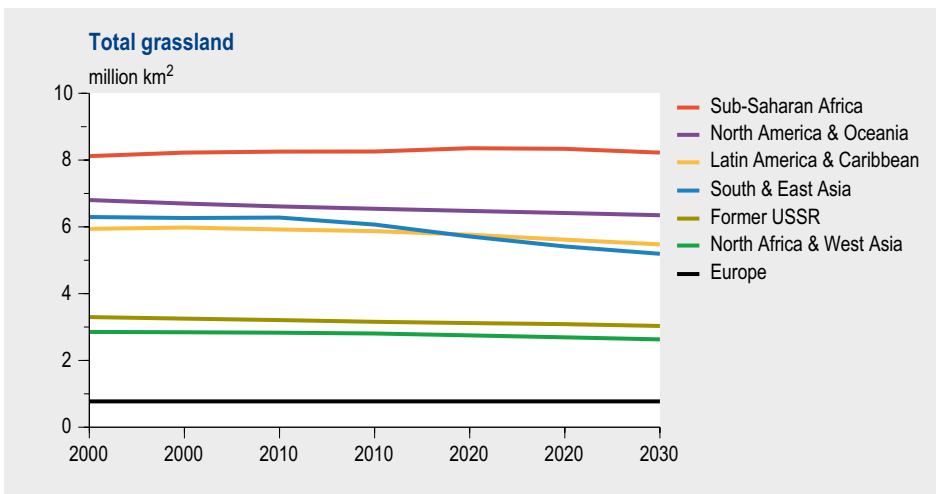


Figure 4.10. Grassland area in the business as usual scenario up to 2030.

*Table 4.1. Impact of trade liberalization on GDP and biodiversity as proxies for economic and environmental consequences, respectively. Relative change in 2030 compared to 2000.*

Region	Change of RSA <sup>a</sup> (%)	GDP <sup>b</sup> (%)
Sub-Saharan Africa	-3.7	5.0
North Africa	-0.2	17.0
South & East Asia	-0.3	2.0
West Asia	-0.7	0.2
Latin America & Caribbean	-5.4	2.0
North America	1.4	0.0
Europe	4.2	0.2
Former USSR	-0.1	0.4
Oceania	-0.1	0.6

<sup>a</sup> RSA, relative mean species abundance in total area compared to potential mean species abundance of the total area in pristine or undisturbed state.

<sup>b</sup> Cumulative percentage changes from the baseline in 2030.

**Trade liberalization variant.** Trade liberalization is beneficial for economic growth (Table 4.1). Developing regions benefit especially from free trade in agricultural products. According to our analysis, the world economy will experience a growth of 1% yr<sup>-1</sup> in 2030, with a faster growth in industrialized countries. Liberalization of the agricultural market has by far the strongest effect in Latin America. Liberalization induces a boost in ‘south-south-trade’ in agricultural products, driven by low production costs and an ample supply of productive land. In Latin America there is a strong expansion of agriculture, and the area of arable land and grassland combined grows by 10% in 2030 compared to 2000, in contrast to the decrease of 7% in the baseline scenario (Figure 4.11). The main habitats affected by land conversion are tropical dry and rain forest (inducing deforestation), and grassland and savannah areas.

In Sub-Saharan Africa, liberalization leads to a significant further reduction of the remaining biodiversity (species abundance decreases by 3.7%; Table 4.1), mainly in tropical forest, grassland and savanna regions. The negative biodiversity effect of liberalization is smaller than in Latin America. In absolute terms, shifts in global agricultural production are small, given the modest role that Africa plays in world trade. In relative terms the region highly benefits from trade liberalization, with a GDP increase of 5% yr<sup>-1</sup> above the baseline values in 2030.

The largest positive effect on biodiversity is in Europe (species abundance increases by 4.2%, Table 4.1). Lifting trade regulations implies that other players on the international market can improve their position at the expense of Europe. North America and Oceania can benefit more from trade liberalization due to lower land prices and more potentially available land (mainly in Oceania through its intensification of livestock production systems). The abandoned land in Europe is slowly returning to a natural state with a higher biodiversity value (Table 4.1), particularly in Mediterranean forests, woodland, shrub and temperate forest areas. The global decrease in agricultural land use seen in the baseline is now reversed, as the opening up of global markets induces a

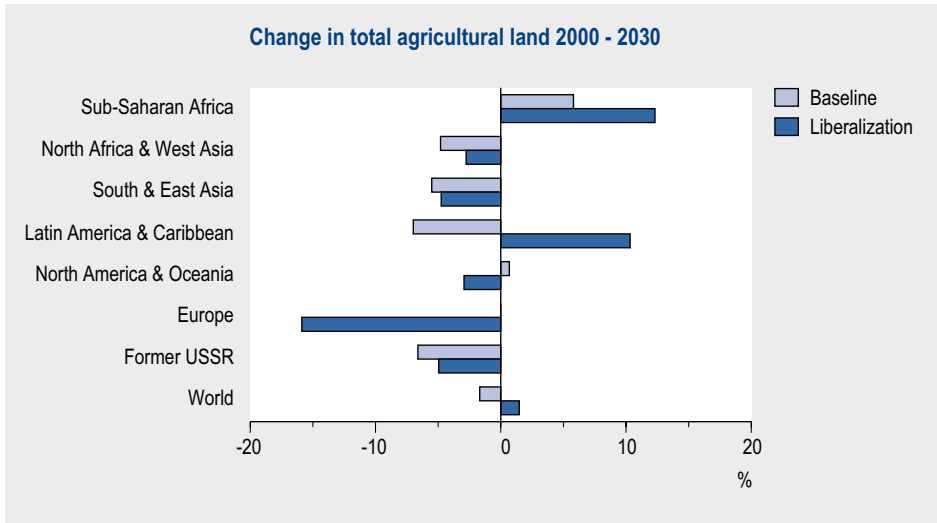


Figure 4.11. Change in agricultural land area between 2000 and 2030 in the baseline scenario and the liberalization variant (in %).

shift of agricultural production to low-production regions like Latin America and Sub-Saharan Africa. Lifting trade regulations allows these regions to capture a larger share of the world market, capitalizing on lower production cost structures and availability of productive land. However, the total agricultural area is increasing due to lower yields in these new producing regions compared to the high yields in regions where agricultural production diminishes due to trade liberalization, like Europe. Summarizing, our liberalization scenario suggests that the environment pays the price for the economic growth due to trade liberalization.

The liberalization option is rather extreme in assuming that all barriers of agricultural products to free trade are abolished simultaneously. In reality, such agreements are introduced with delays, exemptions and special conditions, leading to more gradual and partial shifts. Differences in wages and land rents that drive the observed shift from North to South tend to decrease as time elapses. The effects will therefore never materialize to the full extent reported here. Moreover, the WTO rules allow for interventions in trade under certain conditions, including environmental impacts and regulations. Altogether, this means that the negative effects of liberalization are probably smaller, as the process will take place along smoother paths. This will result in a less dramatic effect on land use, production shifts and biodiversity decline.

#### 4.4 Concluding remarks

The model coupling of the economic model GTAP with the IMAGE model for the global environment allows analysis of the consequences of specific trade policies both on the economic and the environmental side. Moreover, by combining GTAP and IMAGE

we use the strengths of both models: the economic model determines the amount of goods traded between regions and the total change in food supply and demand; the environmental model allocates the desired land using detailed information on soil quality and atmospheric conditions, resulting in spatially explicit environmental consequences which are communicated to the economic model on an aggregated level.

However, the coupling of models which differ so widely in their basic concepts (economic land value in dollars versus the biophysical model with production in tons per unit of land area in square kilometres) is not a trivial matter. A thorough analysis and testing period is needed before detailed conclusions on the effectiveness of proposed trade policies can be drawn. However, the new IMAGE 2.4 approach presented in this chapter is a major improvement to the simple model for demand and trade in IMAGE 2.2 (Strengers, 2001).

It is clear that in many parts of the world there is a trade-off between biodiversity and economic growth. In the case of trade liberalization, higher economic growth comes at the expense of global biodiversity. However, on the regional, national and local scale the outcome may be different. Trade liberalization has a negative impact on the environment in the short term, mainly for land-use changes as shown here, but also on other environmental aspects like emissions of reactive nitrogen (see chapter 8). To what extent the economic growth will lead to a transition in demographics (chapter 2) and therefore in both economic and environmental consequences remains an area for further research.

## 5 MODELLING LIVESTOCK-CROP-LAND USE INTERACTIONS IN GLOBAL AGRICULTURAL PRODUCTION SYSTEMS

- Livestock production systems in earlier versions of IMAGE were described by an aggregated, region-specific ‘management factor’ for grassland, representing the mean animal density for all grassland. In large world regions, however, ‘grassland’ ranges from arid and semi-arid marginal lands to highly productive grassland. A more detailed description of animal production systems was needed to include this spatial variability in grazing systems, and to address the rapid development of intensive ruminant production on managed grassland and the rapidly increasing use of various feedstuffs.
- IMAGE 2.4 includes a model for describing pastoral and mixed/landless (industrial) livestock production systems. Pastoral systems rely mainly on grazing by ruminants, whereas mixed/landless systems have integrated crop and livestock production in which animal diets consist of a mix of several feedstuffs. In these mixed/landless systems the by-products of one activity (crop by-products, crop residues and manure) serve as inputs for another.
- Total feed requirement and its composition are, in the new approach, calculated separately for both types of production systems. The IMAGE 2.4 model allows for a geographically explicit calculation of the land areas, including grassland and arable land, needed for the production of the various feed resources, and the calculation of animal densities on the basis of changing demand and transformations in the livestock production systems.

### 5.1 Introduction

The world population can increase from about 6 billion inhabitants to 8.2 to 9.3 billion between now and 2030 (Nakicenovic et al., 2000). Food production will have to increase to meet the increasing population-induced demand, while increasing prosperity and falling production costs may see dietary patterns shifting towards a higher share of meat and milk. The decrease in costs of animal products is related to the increasing share of production of particularly white meat in efficient mixed and landless production systems, and the decreasing importance of traditional pastoral systems (Delgado et al., 1999).

There is major concern about the potential of the global agricultural system to expand its production and the environmental consequences of such expansion for many reasons. One of these is that increasing livestock production may lead to expansion of grazing land and particularly arable land for the production of crops for feeding animals; this may occur at the cost of natural vegetation. Most of the current arable land expansion is needed for increasing the production of animal feedstuffs (Bouwman et al., 2006). The second is that ruminants release large amounts of methane formed

during enteric fermentation; the animal excreta are sources of ammonia, methane, nitrous oxide and nitric oxide. Thirdly, on a more local scale the production of odour and leaching of nitrate to groundwater are major problems. Fourthly, a significant part of grazing land used for ruminants may consist of marginal unproductive grassland with low carrying capacity and a high risk of land degradation due to overgrazing, especially in the arid and semi-arid tropics and sub-tropics (Seré and Steinfeld, 1996; Delgado et al., 1999). Loss of productivity in such areas may be compensated for by expansion of the agricultural area by forest clearing.

Livestock production systems differ in their ability to respond to increasing demand for livestock products. Generally, poultry and pork (white meat) production systems respond quickly to increasing demand, since they are commonly industrial with fast reproduction cycles and adaptable feeding systems, with higher conversion efficiency than in ruminant production. The production of red meat (beef, mutton and goat meat) has longer reproduction cycles, a relatively low feed conversion efficiency and generally a lower degree of specialization than white meat production. Therefore, transformations in red meat production systems are slower than in pork and poultry production systems (Seré and Steinfeld, 1996).

The response of traditional mixed livestock production systems to increasing demand is slower than that of modern poultry and pork production systems. This is mainly because livestock has other economic and cultural functions within the traditional farm system than meat and milk production alone. Traditional mixed systems have therefore been unable to increase their production sufficiently in the past decades. As a consequence, the supply of modern livestock production systems is increasing with larger shares of poultry and pork, particularly in developing countries (Bruinsma, 2003).

For developing scenarios it is therefore necessary to consider the interactions between crop and livestock production and to understand the consequences of changing livestock production for food crop production and arable land use. IMAGE 2.4 includes a model for describing two aggregated livestock production systems, pastoral systems, and mixed and landless (industrial) systems. Pastoral systems rely mainly on grazing by ruminants, whereas mixed and landless systems have integrated crop and livestock production in which animal rations consist of a mix of several feedstuffs, including food crops, crop by-products, grass, fodder crops and crop residues. In these mixed (and landless) systems the by-products of one activity (crop by-products, crop residues, and manure) serve as inputs for another.

The two-system approach was an improvement on IMAGE 2.2 (IMAGE-team, 2001), which was considered as one aggregated livestock production system. The main problem in IMAGE 2.2 was the aggregated 'management factor' for grassland, representing the mean animal density for large world regions for a wide range of grasslands ranging from marginal ones in semi-deserts to highly productive grassland. With this aggregated management factor it was difficult to describe the fast

development of landless and intensive mixed ruminant production on managed grassland. Scenarios for agriculture often yielded unrealistic expansion of grazing areas in different parts of the world.

By taking into account different feed efficiencies, both the total feed requirement and its composition are calculated in the new approach for both production systems. The IMAGE 2.4 model allows for geographically explicit calculation of the land areas, including grassland and arable land needed for the production of the various feed resources, and animal densities on the basis of changing demand and transformations in the livestock production systems. The new livestock production model is described in detail elsewhere (Bouwman et al., 2005; Bouwman et al., 2006; Eickhout et al., 2006).

In this chapter we will briefly describe the new approach for simulating livestock production systems and illustrate the model with results for one scenario. Model components for assessing environmental impacts of the livestock-crop-land use interactions are presented in chapter 8.

## 5.2. Data and methods

### *General*

In contrast to IMAGE 2.2, where the livestock production sector was treated as one aggregated system, IMAGE 2.4 distinguishes two livestock production systems, i.e. pastoral systems, and mixed and landless systems. Landless production is included in mixed and landless systems, because it has the same interrelations (food crops, fodder, manure, etc.) with crop and grass production systems as mixed livestock production.

For the period 1970-2000 we used the standard IMAGE 2.4 historical calculations for agricultural production. To illustrate the model, we present scenario calculations after 2000 up to 2030 based on the IPCC Special Report on Emission Scenarios (Nakicenovic et al., 2000) and the B2 scenario for GDP as implemented in the IMAGE 2.2 model (IMAGE-team, 2001). This is combined with projections for food demand and production from Bruinsma (2003). The B2-GDP scenario, similar to that of Bruinsma (2003), was used to achieve consistency with simulations of the energy and industry sectors and climate change.

### *Livestock production*

Livestock production data for the 1970-2000 historical period in IMAGE are based on data on production, use and trade of meat, milk, eggs and other products. This applies to the various animal categories for individual countries from FAO, 2005, hereafter referred to as FAOSTAT data.

We use FAOSTAT country data on production for the complete stock of animals in each category, including productive and non-productive animals in different age classes. To simplify matters, the IMAGE model considers small ruminants (sheep and goats) as one

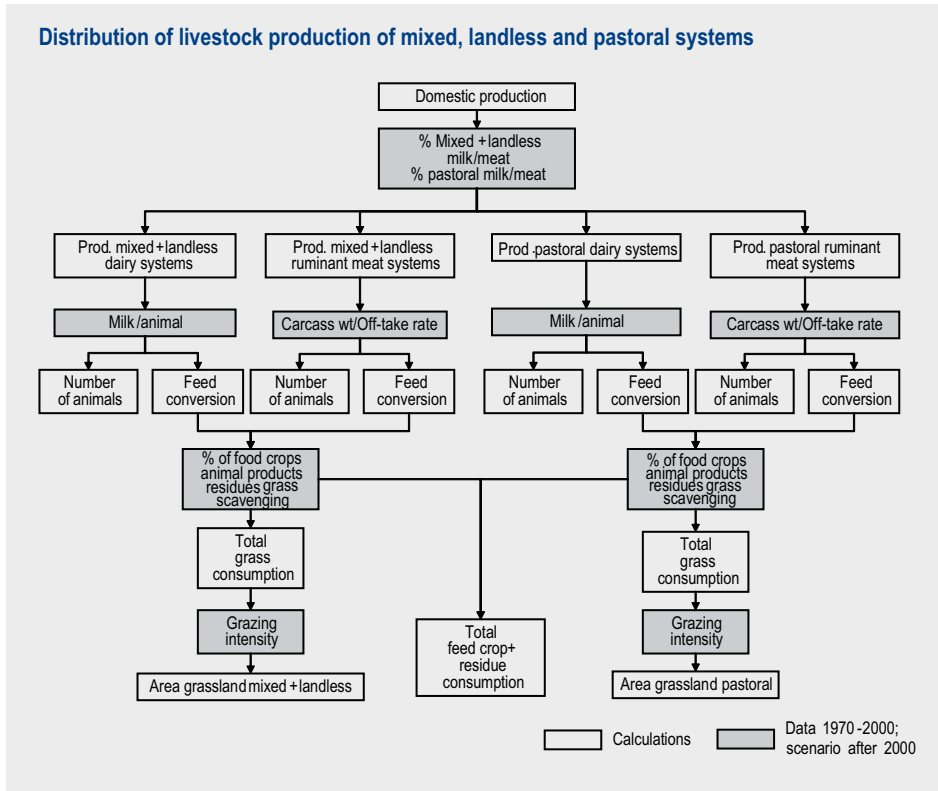


Figure 5.1. Scheme showing the distribution of livestock production over mixed landless and pastoral systems, the calculation of the number of animals from the milk production per animal for dairy cattle, and carcass weight and off-take rate for beef cattle, and sheep and goats, feed conversion efficiency, composition of feed, and finally total feed crop, residue consumption and area of grassland via the grazing intensity.

group of animals, while meat from buffaloes is included in the beef cattle category, and milk from buffalo is included in dairy cattle. Poultry production includes meat and eggs. The FAOSTAT country data are aggregated to the level of 24 world regions used in IMAGE 2.4. The distribution of the animals and production of meat and milk in different production systems for the 1970-2000 period was based on Seré and Steinfeld (1996) as described in Bouwman et al. (2005).

Projections for livestock production for individual countries were taken from Bruinsma (2003); these comprised total production of meat for beef cattle and buffaloes, and milk for dairy cattle and buffaloes, along with meat production for small ruminants, pigs and poultry, as well as milk production per animal and off-take rates for meat production. For crop production we used country data on yields, harvested areas and cropping intensities from Bruinsma (2003). All these data were aggregated from the country scale to the level of 24 world regions to be used in the IMAGE 2.4 model. For the development of the distribution of the production over the two production systems we assumed a continuation of trends in the development of mixed and pastoral systems observed in the past three decades by Seré and Steinfeld (1996).

The number of animals is calculated from milk production per animal for dairy cattle and carcass weight and off-take rate for beef cattle and small ruminants (Figure 5.1).

### *Feed requirements*

The net energy requirements for dairy cattle are divided into maintenance, grazing, lactation and pregnancy. The energy requirement for feeding of cattle is obtained from the fraction of grass in the diet, assuming that this corresponds to the time spent in pastures, and the fraction of the maintenance requirement. The energy required for lactation is calculated from the milk production and fat content of the milk. The energy required during pregnancy depends on the weight of the calf and the gestation period. In livestock production systems with a low productivity, the share of maintenance is dominant, while in high-production systems the energy requirement for lactation is generally about equal to the maintenance. The feed requirements for the year 2000 for small ruminants was based on estimates presented by de Haan (1999) for different production systems and agro-ecosystems. We assumed that their feed requirement in pastoral, and mixed and landless, systems for the historical period was proportional to that of non-dairy cattle in the corresponding systems. Feed intake for pigs and poultry is similar to that used in IMAGE 2.2 (IMAGE-team, 2001). More details can be found in Bouwman et al. (2005).

In scenarios the feed conversion efficiency for cattle also depends on animal productivity, which, in turn, is related to GDP. For the other animal categories the feed conversion rates (kg feed per kg of product) depend directly on the economic development as expressed by the per capita GDP with minimum values equal to the current Western European value for pigs and poultry and the value for North Africa for the small ruminants in mixed and landless systems. The feed conversion of small ruminants in pastoral systems is assumed not to change. The general idea is that rising incomes induce rapidly increasing demand for meat and milk, motivating livestock holders to produce more at lower cost, mainly in modern mixed and intensive livestock production systems.

Five feed categories are distinguished (Figure 5.1): (i) grass, including hay and silage grass; (ii) food crops and by-products (such as cakes remaining after vegetable oil extraction); (iii) crop residues and fodder crops such as fodder maize, and beet and alfalfa (fodder crops can not be distinguished as a separate group, because FAOSTAT provides no data on their production and harvested areas); (iv) animal products (mainly milk); and (v) scavenging, including road-side grazing, household wastes, feedstuffs from backyard farming, etc. For the period 1970-2000 we used the FAOSTAT data on feed use of crops, crop by-products and animal products (mainly milk products).

Pigs and poultry feed purely on food crops, crop by-products, and residues and fodder crops. We assumed that in developing countries pigs and poultry consume 40-60% crop residues and fodder crops, the complement being food crops and crop by-products. In developed countries with a higher proportion of industrial production and less backyard monogastric production, pigs and poultry consume 60-75% food crops and crop by-products, with the complement consisting of crop residues and fodder crops.

A number of assumptions were made on the other types of feed used for ruminants. In pastoral ruminant production systems grass makes up close to 100% of the feed, except for most developing regions where scavenging is assumed to contribute 5%, and South and Southeast Asia where scavenging is a large fraction of total feed. In pastoral mutton and goat-meat production systems grass also makes up 100% of the feed, except for most developing countries where scavenging is assumed to contribute 5-10%, and India, where scavenging constitutes 50% of the feed resource. For mixed and landless production systems the contribution of food crops, and residues and fodder is much higher than in the pastoral systems.

The production for each animal category and the feed efficiency are used to calculate total feed demand (Figure 5.1). Based on the ration for each animal category including the five feed categories listed above, IMAGE 2.4 computes the total demand for food crops, which is added to human demand yielding total demand (Figure 5.1). Demand for crop residues is compared with the availability of crop residues based on the crop yields and the harvest index (ratio straw : harvested product) to prevent overestimation of this feed resource. The demand for grass is translated into the required area of grassland using the grazing intensity (see section 2.4).

For the years after 2000 we use the same feed composition for each animal category and production system. This is so that changes in total production, feed efficiency of the different animal categories and the gradual trend to more production in mixed and landless systems will lead to changes in the total demand for the five feed categories.

### ***Land use***

IMAGE 2.4 distinguishes three agricultural land-cover types: (i) agricultural land, including cropland and grassland with a potential productivity of more than 10% of global maximum productivity under crop-specific optimal climate and soil conditions; (ii) marginal grassland with a potential productivity of less than 10% of the theoretical world maximum and (iii) land for bioenergy (new in IMAGE 2.4; see chapter 7). IMAGE 2.4 uses a new base map based on satellite data and statistical information for the distribution of agricultural land as discussed in chapter 6.

IMAGE 2.4 allocates grassland and seven different crops (rainfed and irrigated) on the land-cover type agricultural land, and four energy crop types on the land for bioenergy using data on the domestic production, yields and cropping intensity for the 24 world regions. The allocation procedure for grassland and crops is presented in detail in Alcamo et al. (1998). Here a brief outline is given. Expansion and abandonment of agricultural land is based on a number of rules founded on the land's suitability, distance to existing agricultural areas, urban areas, rivers and a random factor. Land suitability is based on climate and soil characteristics using the Agro-Ecological Zones (FAO, 1978-1981) approach for modelling productivity of crops and grass (IMAGE-team, 2001). The allocation of energy crops on the land-cover type land for bioenergy is performed according a comparable approach. The demand for energy crops comes from the energy model TIMER (see chapter 3). TIMER simulates the energy mix on the basis

*Table 5.1. Percentage of grid cells covered by arable land in mixed and landless ruminant livestock production systems for different world regions in IMAGE 2.4.*

World region	Arable land (%)
Southern Africa	>25
Canada	>35
USA, Central America, West Africa, Eastern Europe <sup>1</sup> , former USSR <sup>1</sup> , Middle East, Oceania	>50
South America, Northern + Eastern Africa, South, East, Southeast Asia, Japan	>65
Western Europe <sup>2</sup>	-

<sup>1</sup> Pastoral grassland in Eastern Europe and the former USSR are assumed to be semi-natural.

<sup>2</sup> In Western Europe all grassland is assumed to be in mixed and landless systems.

of energy prices, which, for bioenergy, is based on potential crop productivities from IMAGE (Hoogwijk et al., 2004). Further details on the energy model and the choice of energy carriers, including energy crops, is given in chapter 3 and Van Vuuren et al. (2006). The areas of arable land (including permanent crops) and grassland are calibrated with FAOSTAT information using data on actual crop yields at the level of world regions.

In IMAGE 2.4 the areas of grassland are further subdivided into mixed and landless systems, and pastoral systems (including the marginal grassland). Mixed and landless systems are assumed to occur in mosaics with arable land, while grid cells with pastoral systems have less arable land (arable land is absent in the grid cells covered by marginal grassland). This is to ensure that the production of crops for feeding animals and possibilities for disposal of animal waste as manure, required in mixed and landless systems, are available at a short distance. The fraction of arable land in cells with mixed and landless production systems varies from one world region to another (Table 5.1). The rest of all the grassland, including the low-production grassland, is assigned to the pastoral systems (Figure 5.2). In spite of the loss of spatial information noted above, the new land-cover map offers a number of advantages in comparison with the land-cover map in previous IMAGE versions (IMAGE-team, 2001), especially with regard to the allocation of low-production grassland in arid and semi-arid climates, for example, in China, Australia and the U.S.A.

Seré and Steinfeld (1996) assigned grassland for countries as a whole to mixed livestock production systems where arable land (on country scale) comprises more than 15% of the total agricultural area. On the global scale this approach yields 1241 Mha of grassland in mixed systems.

With our definition based on grid cells (Table 5.1) the global area of grassland in mixed systems of 522 Mha is much smaller than the area estimated by Seré and Steinfeld (1996). In the IMAGE model grid cells dominated by arable land generally have a higher net primary productivity than grassland-dominated cells. With our approach we obtain higher, but not unrealistic, animal densities and grass consumption in mixed

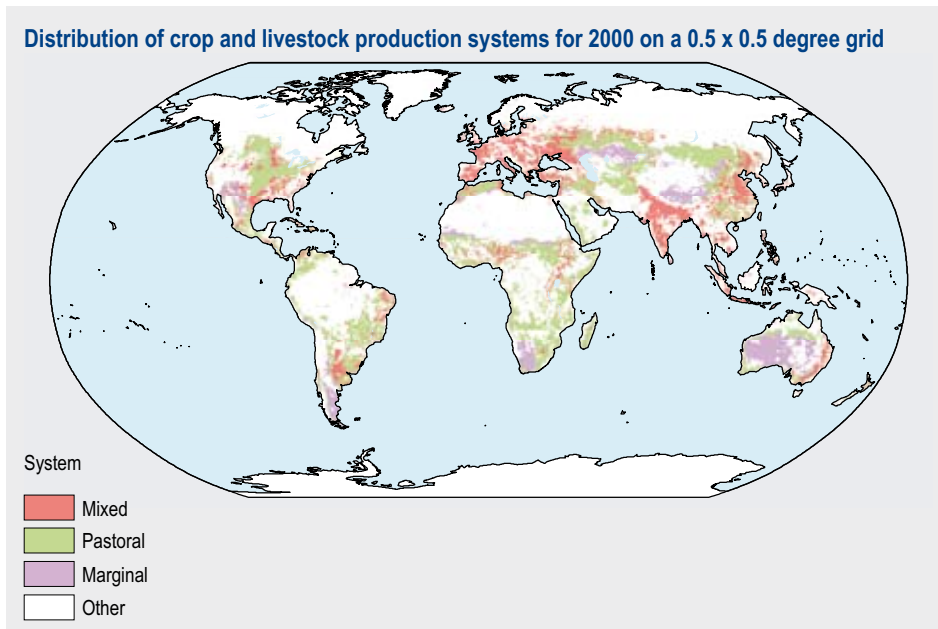


*Figure 5.2. Distribution with 0.5 by 0.5 degree resolution of crop and livestock production systems for 2000.*

and landless systems than in pastoral systems. On the basis of larger grassland areas for the mixed and landless systems, the animal densities would have been too low compared to those for the pastoral grassland.

We use the grazing intensity for each production system (Figure 5.1), defined as the ratio between the calculated grass consumption and the net primary production (NPP), to obtain the estimates of grassland areas and their spatial distribution for scenarios. NPP is generated by the IMAGE model on the basis of climate and soil conditions for each year. By comparing the grazing intensity and the stocking rates, the number of animals in each system, as well as the feeding rations, can be attuned to come to realistic distributions.

In general the grazing intensity and animal density of ruminants is lower in pastoral systems than in mixed grazing systems (Figure 5.3). For future projections the grazing intensity in pastoral systems is assumed not to change much, except where the pressure induced by population growth leads to higher stocking rates and possibly land degradation. In mixed and landless systems the grazing intensity can increase to high values based on more favourable climatic and soil conditions. Increasing stocking rates in mixed systems is accompanied by improved management, use of grass-clover mixtures for improving the nitrogen supply, and fertilizer inputs (see chapter 8).

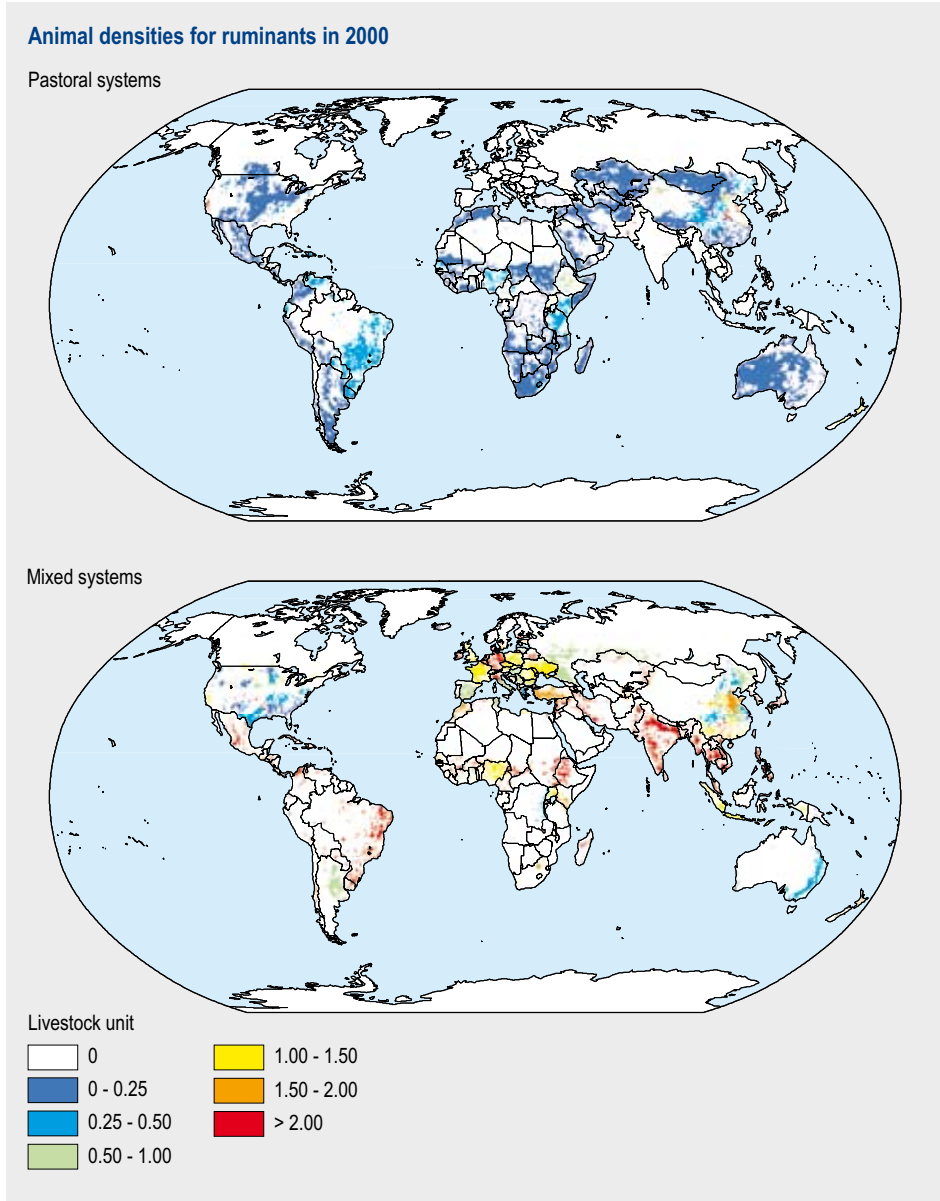


Figure 5.3. Animal density for ruminants in livestock units for pastoral (top panel) and mixed systems (bottom panel) for the year 2000. A livestock unit is defined here on the basis of N excretion rates, whereby a dairy cow is 1 livestock unit, a non-dairy cow 0.5 to 0.67, and a goat 0.08 to 0.17 livestock units.

## 5.3 Results and discussion

### *Changes in demand and production*

Changes in the demand for agricultural products is largely determined by population growth and changing human diets. According to the population projection used in this

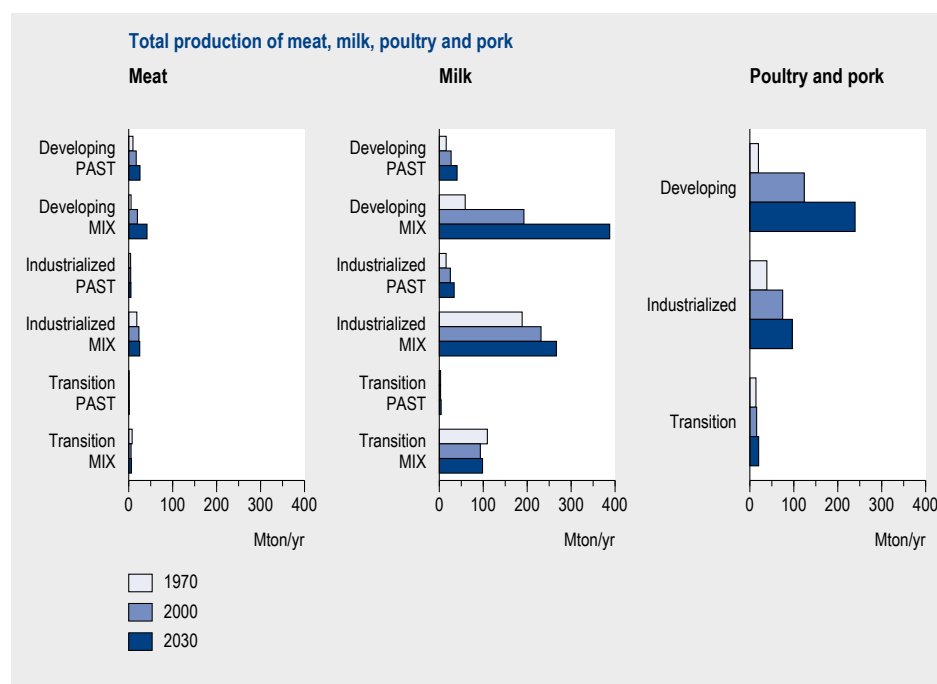


Figure 5.4. Total production of ruminant meat (cattle, sheep and goats) (left panel), milk (middle panel) for pastoral (PAST), mixed, and landless production systems (MIX), and production of poultry and pork (right panel) for developing, industrialized and transition countries for 1970, 2000 and 2030.

chapter, the world population growth will gradually slow down from  $1.5\text{ yr}^{-1}$  during the late 1990s to  $1.2\text{ yr}^{-1}$  up to 2015 and  $0.9\text{ yr}^{-1}$  between 2015 and 2030, reaching a world total of 8270 million inhabitants in 2030. However, in developing countries the population growth will slow down from the  $1.7\text{ yr}^{-1}$  during the late 1990s to  $1.1\text{ yr}^{-1}$  between 2015 and 2030. In industrialized countries the growth rate will decrease from the current  $0.7\text{ yr}^{-1}$  to  $0.2\text{ yr}^{-1}$ , while the projected growth in transition countries (Eastern Europe and the former USSR) will be negative in the coming three decades (between  $-0.2$  and  $-0.3\text{ yr}^{-1}$ ). The projected growth of per capita gross domestic product (GDP) is particularly high in developing and transition countries ( $4$  and  $4.1\text{ yr}^{-1}$  for the coming three decades, respectively), and somewhat lower for industrial countries ( $2.7\text{ yr}^{-1}$ ).

Per capita meat consumption will show a strong world-wide increase (25% between the late 1990s and 2030), with very fast growth in developing and transition countries (42 and 33%, respectively). Although the annual meat consumption of 88 kg of meat per person in industrialized countries is much higher than in developed countries, a further increase of 14% is projected.

As a result of the changing demand, the production of all livestock products strongly increased between 1970 and 2000, with a higher growth of pork and poultry meat

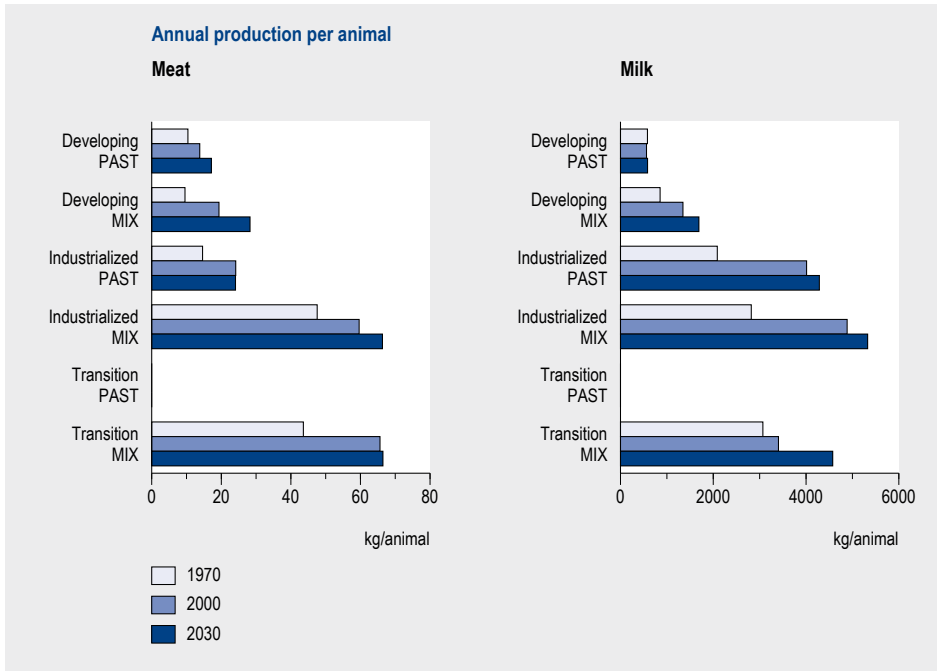


Figure 5.5. Annual meat (left panel) and milk (right panel) production per animal for pastoral (PAST), and mixed and landless, production (MIX) systems for all ruminants in developing, industrialized and transition countries for 1970, 2000 and 2030.

than of beef, sheep and goat meat (Figure 5.4). Between 1970 and 2000 the global annual beef production increased by 20 Tg yr<sup>-1</sup>. About 70% of this gain was achieved in the mixed and landless systems. For milk, 88% of the total increase of 182 Tg yr<sup>-1</sup> was achieved in mixed and landless systems, while for mutton and goat meat this was 64% of the 4 Tg yr<sup>-1</sup> production growth.

In the same period, the productivity of all animal categories increased, most strongly in mixed and landless systems (Figure 5.5). Farmers not only increased the productivity per animal, but also achieved important increases in the productivity per hectare of grassland (Figure 5.6), particularly in the mixed and landless systems.

In the coming three decades the production of pork and poultry is likely to increase more strongly than that of ruminant meat. White meat production in the developing countries is projected to grow from 124 to 251 Tg yr<sup>-1</sup>, while ruminant meat production increases from 17 to 27 Tg yr<sup>-1</sup> in pastoral systems, and from 20 to 43 Tg yr<sup>-1</sup> in mixed and landless systems (Figure 5.4). The growth of white meat production in the industrialized countries (75 to 98 Tg yr<sup>-1</sup>) will slow down somewhat compared to the 1970-2000 period, while the ruminant meat production in pastoral systems will not change substantially, while the production in mixed and landless systems will increase only slightly from 23 to 25 Tg yr<sup>-1</sup> between 2000 and 2030. In the transition countries the ruminant meat production will increase from 5 to 6 Tg yr<sup>-1</sup> and that of white meat from 16 to 20 Tg yr<sup>-1</sup> in mixed and landless systems (Figure 5.4).

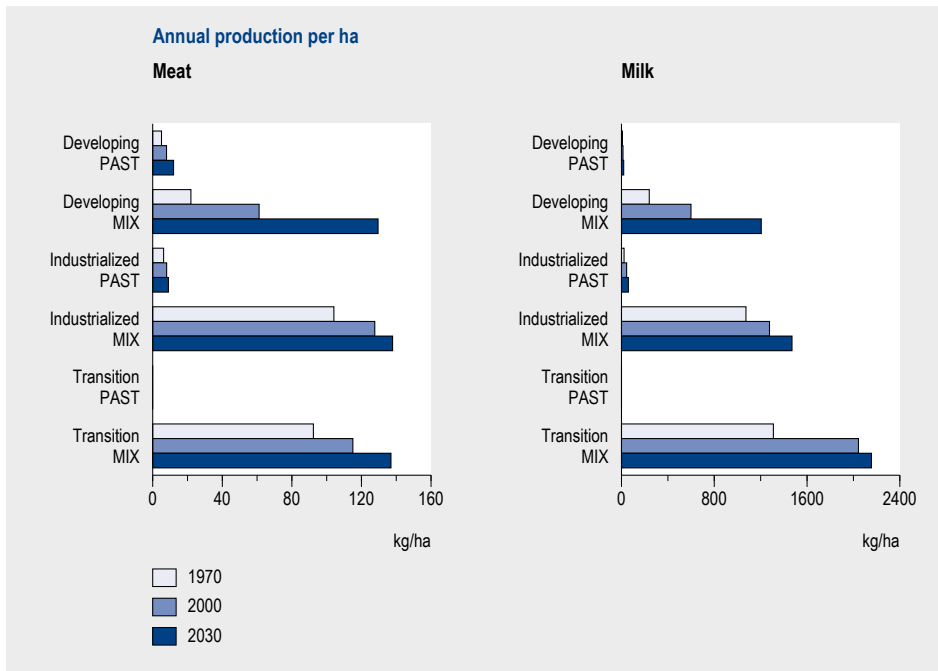


Figure 5.6. Annual meat (left panel) and milk (right panel) production per hectare of grassland for pastoral (PAST), and mixed and landless (MIX), production systems for all ruminants in developing, industrialized and transition countries for 1970, 2000 and 2030.

The growth in the production of milk shows similar changes. As in the 1970-2000 period in the developing countries, milk production will slowly increase in pastoral systems in the coming three decades (27 to 42 Tg yr<sup>-1</sup>). The increase in mixed and landless systems will increase much faster in the coming three decades (193 to 406 Tg yr<sup>-1</sup>) than in the period 1970-2000 (59 to 193 Tg yr<sup>-1</sup>). In the industrialized countries the milk production in pastoral systems is insignificant compared to that in the mixed and landless systems, where the production increased from 189 Tg yr<sup>-1</sup> (1970) to 231 (2000) and will increase further to 269 Tg yr<sup>-1</sup> in the coming three decades. The changes in milk production over the whole period 1970-2030 in the transition countries are only minor. The development of the productivity of animals and the production per hectare in the coming three decades shows a continuation of the development in the period 1970-2000 (Figures 5.5 and 5.6).

#### Changes in feed use

Ruminant production (cattle, buffaloes, sheep and goats) takes place under very diverse conditions. There is, however, a general tendency towards intensification to meet the increasing demand for livestock products. In general, this intensification is accompanied by decreasing dependence on open-range feeding and increasing use of concentrate feeds, mainly feed grains, to supplement other fodder.

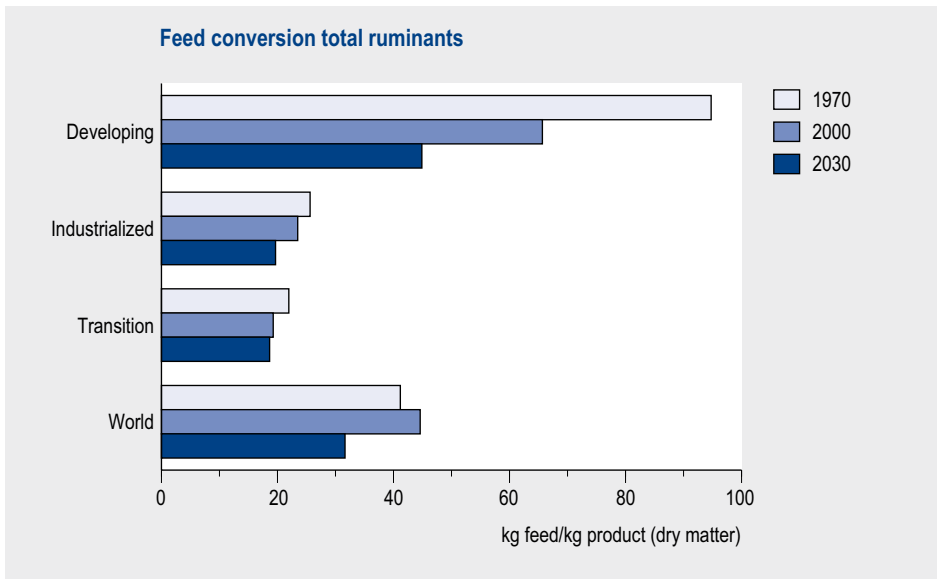


Figure 5.7. Feed conversion for total ruminant production in developing, transition and industrialized countries for 1970, 2000 and 2030.

The calculated total feed intake shows large differences between regions. In both monogastric and ruminant systems increasing overall feed conversion efficiencies have been achieved (Figure 5.7) by improved and balanced feeding practices and increased production per animal as a result of increasing carcass weight, off-take rates and milk production per animal (Bouwman et al., 2005). In addition, the use of animal traction, providing draft power for about 28% of the world's arable land (Delgado et al., 1999), has decreased in recent decades (Bruinsma, 2003), leading to important decreases in the feed energy requirements, for example, in East Asia.

The current use of feed for the different categories was compared and calibrated as far as possible by Bouwman et al. (2005) with estimates from the literature for various countries and world regions. These include the U.S.A., Canada, Western Europe, former U.S.S.R. and Eastern Europe, China, India, North Africa and the Middle East, along with the global feed crop use by animal category. Our results indicate an increase in the feed use for ruminants, and pigs and poultry, of 44% for all feed categories between 1970 and 2000, and another 41% between 2000 and 2030. Total use of food crops for pigs and poultry will increase by 51%, while the increase for cattle is 27%. Total grass consumption will increase by about 30% between 2000 and 2030 (Figure 5.8).

### ***Changes in land use***

Most of the world's ruminant production comes from only one-sixth of the global area of grassland (~3400 Mha in the year 2000), while pastoral systems cover 85% Mha, while including ~978 Mha of semi-natural or marginal land used for nomadic grazing (Figure 5.2 and Table 5.2).

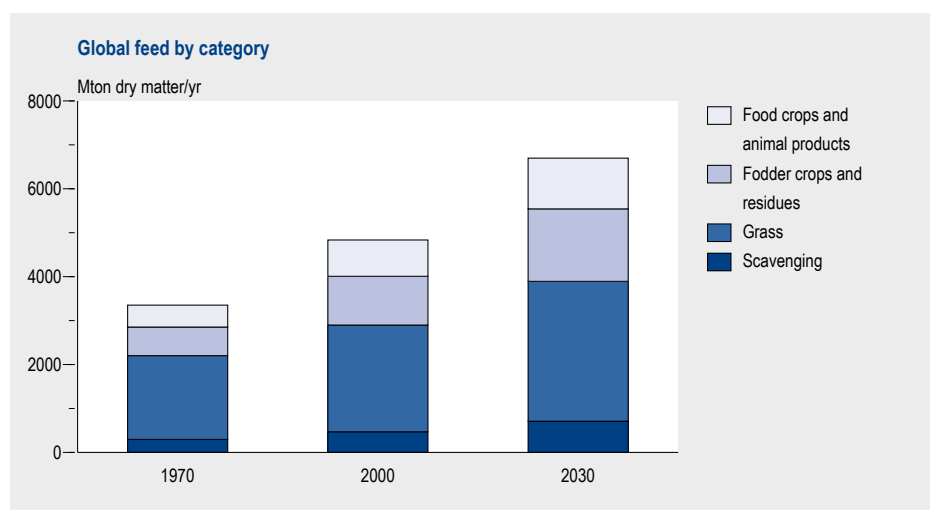


Figure 5.8. Global feed use by category for total livestock production (including monogastric production) for 1970, 2000 and 2030.

Changes in the distribution of ruminant production in pastoral, and mixed, and landless production systems have led to small changes in the grassland area between 1970 and 2000 (Table 5.2). This is because the increase in ruminant meat and milk production during the past three decades has primarily been achieved by increasing the production in mixed and landless production systems and much less so in pastoral

Table 5.2. Distribution of grassland in mixed and pastoral systems, total grassland, and arable land for 1970, 2000 and 2030 for the developing, industrialized and transition countries (former Soviet Union and Eastern Europe).

Type	Developing	Industrialized	Transition	World
(Mha)				
1970				
Mixed grassland	214	101	225	540
Pastoral grassland <sup>a</sup>	576	255	1839	2670
Total grassland	790	356	2064	3210
Arable	389	289	712	1390
2000				
Mixed grassland	202	59	240	501
Pastoral grassland <sup>a</sup>	514	300	1969	2783
Total grassland	716	359	2209	3284
Arable	370	250	889	1510
2030				
Mixed grassland	186	69	268	523
Pastoral grassland <sup>a</sup>	526	275	1968	2769
Total grassland	712	343	2236	3292
Arable	363	247	983	1593

<sup>a</sup> Including marginal grassland

systems. Despite the fast increase of 40% in ruminant production in the period 1970-2000, the global area of grassland increased by only 2% in the same period.

Only slight changes in the global extent of grassland in mixed, and landless and pastoral, systems are projected for the period 2000 to 2030, which is consistent with the trends in recent decades. In many industrialized regions, the extent of grassland in the mixed and landless systems shows a slight decrease, while grassland is expanding in some developing regions. This implies that increased grass consumption will come from intensification, as illustrated by increasing production per hectare (Figure 5.6). The considerable increase of about 30% in grassland production can only be achieved by increasing inputs of fertilizers, use of grass-clover mixtures and improved management (Bouwman et al., 2005).

The global arable land area increased by 9% (1410 to 1532 Mha) between 1970 and 2000 (FAO, 2005). Since the arable land areas slightly decreased during this period in the industrialized and transition countries, there has been a considerable expansion in the developing countries. According to the projection used, the global arable land area will increase by 8% between 2000 and 2030 (Table 5.2). While in industrialized countries the arable land area increases only slightly during this period, there will be a major expansion by 12% in the developing countries.

The global increase in food production between 1998 and 2030 calculated from data provided by Bruinsma (2003) is about 1600 Tg yr<sup>-1</sup> (in dry matter). The contribution of yield increase to the total growth of production is about 70% (Bruinsma, 2003). Hence, crop yield increase alone would be sufficient to produce the extra amount of 1200 Tg yr<sup>-1</sup> (in dry matter) of crops for direct human consumption. The remaining production increase of 300-400 Tg yr<sup>-1</sup> (in dry matter) equals the increase in production of food crops used to feed animals. This implies that most of the projected arable land expansion is needed for increasing the production of animal feedstuffs.

## 5.4 Concluding remarks

The IMAGE 2.4 approach to describing two livestock production systems represents an improvement of the aggregated description of one single production system in several ways. One is the disaggregation of livestock production into two broad systems, which enables us to estimate the use of different feedstuffs and the livestock-crop-land use interactions better. Secondly, we are now better able to describe the production parameters and processes in each system, which enables the model to simulate future areas of grassland that are in line with historical data and expectations. The extensively used pastoral grassland, forming the major part of global grassland areas, shows slight and only gradual changes. The area of intensively used grassland in mixed and landless systems also shows only gradual changes in area. However, the production characteristics change, with trends towards intensification, and integration of a growing part of ruminant production in mixed crop and livestock production systems. Thirdly, the

different feedstuffs have different methane conversion rates in enteric fermentation and thus allow for better estimations of methane emissions. Finally, our approach allows for estimating the amounts of animal manure produced in both systems based on the production characteristics and for spatially distributing the amounts of animal manure excreted during grazing. Furthermore, it allows for stored manure available for spreading in crop systems, as well as the resulting gas emissions to air and leaching losses of nitrate (see chapter 8).

However, a number of links between IMAGE model parts still need to be established. One is a consistent approach for crop residues to prevent conflicts between the different uses of residues (feed, fuel, incorporation, burning). A second is the use of fodder crops for which no consistent global data are available, and the link with the crop growth modelling and land allocation in IMAGE. These crops are important feed resources in many countries, and also need to be included for establishing surface nutrient balances, as discussed in chapter 8. A third is the production of a large number of crops including many fruits and vegetables, stimulants, sugar, fibre crops, cocoa, rubber and cotton. These crops are not included in the seven broad crop groups distinguished in the current IMAGE components for crop growth modelling and land allocation. About 20% of the animal feed comes from these crops and they play an important role in nutrient cycling in agro-ecosystems (see chapter 8).

A further improvement is the explicit description of landless livestock production systems. In these systems the characteristics of the production may differ significantly from those in land-based mixed systems.

We assumed that only small changes in the global grassland area will occur in the coming three decades, which is a continuation of trends in the past decades. This assumption is based on a decreasing dependence of ruminant production on grassland resources, and an increasing importance of food crops and other feedstuffs. If grassland areas do not expand in the near future, the required increase in grassland productivity of about 30% for the scenario analyzed will have to come from increasing inputs of fertilizers, grass-clover mixtures and improved management. Further in-depth research and model development on this issue is needed when combining local production characteristics with environmental and socio-economic information to evaluate the biophysical and economic viability of intensification of grassland use.

## 6 HYDE 3: CURRENT AND HISTORICAL POPULATION AND LAND COVER

- As a result of the dramatic increase in world population during the last three centuries, global areas of cropland and grassland have expanded rapidly; this has contributed significantly to cumulative carbon dioxide increase in the atmosphere and loss of vast areas of natural ecosystems and biodiversity. However, the few existing historical, gridded land-cover inventories disagree about the areas of grassland and cropland, as well as their spatial distribution.
- HYDE version 3 includes updated historical land-use data, more spatial detail and new time-dependent allocation procedures based on the land's attractiveness for agricultural production. For the allocation of cropland we use newly developed time-dependent weighting maps based on population density, the land's suitability for crop production and the distance to rivers. For allocating grassland we use weighting maps based on population density and the natural vegetation type (to mimic the use of natural grassland types). In comparison with HYDE 2, this resulted in a more realistic distribution of agricultural land in many parts of the world.
- The HYDE 3 database and grid-based inventory of historical land use can be used as a tool to analyze historical population and land-use changes, and their consequences for the global carbon cycle and the Earth system.

### 6.1 Introduction

People have been altering the global landscape for a long time. Historical changes in land use, primarily deforestation, have contributed considerably to the cumulative carbon dioxide (CO<sub>2</sub>) increase in the atmosphere. However, estimates of historical CO<sub>2</sub> emissions from deforestation are uncertain (Ruddiman, 2003). Several recent studies (e.g. DeFries et al., 1999; McGuire et al., 2001; Pacala, 2001; Houghton, 1999; 2003) indicate that land-use change is an important source of CO<sub>2</sub> causing global emissions of  $2 \pm 0.8 \text{ Pg yr}^{-1}$  (Pg, petagram;  $1 \text{ Pg} = 10^{15} \text{ g}$ ) of carbon (C) for the 1980s and  $2.2 \pm 0.8 \text{ Pg yr}^{-1}$  for the 1990s, which is roughly one-fifth of the total anthropogenic CO<sub>2</sub> emission (IPCC, 2001). IPCC (2001) concluded that in order to close the global carbon budget there must be a 'missing' biospheric sink of carbon, but it is still uncertain in which ecosystems this C uptake occurs.

There are many ways in which land-cover change can affect climate. For example, albedo (Hansen et al., 1998; Betts, 2001) and evapotranspiration may be altered when natural vegetation is converted to cropland or grassland (see chapter 9). One of the first studies showing the importance of incorporating land use in global climate models was that of Wilson and Henderson-Sellers (1985), who had developed a global archive of soil and land-cover data for use in Global Circulation Models (GCM).

Recently, a new generation of dynamic, simplified GCMs has emerged; these GCMs were used to study the historical C cycle as affected by land cover (Betts, 2001; Chase et al., 2000; Pitman and Zhao, 2000; Bertrand et al., 2002; Pitman, 2003; Matthews et al., 2003; 2004; Feddema et al., 2005; Brovkin et al., 2006). Brovkin et al. (2006) compared six earth system models of intermediate complexity for simulating the bio-geophysical effects of historical land-cover changes. Such models allow for evaluating the transient response of the climate system to different climate forcings on a much longer time-scale than GCMs. Most studies indicated global biogeophysical cooling as a result of a land-cover change of 0.13-0.25 °C compared to pre-industrial times. One of the major uncertainties in these results turned out to be the historical land-cover distribution.

The original HYDE database (version 2) (Klein Goldewijk, 2001) was developed to make consistent historical land-use and land-cover data available to the research community on a spatially explicit basis and with a satisfactory resolution for global climate change modellers. HYDE includes both general topics such as land use and land cover, population, livestock, gross domestic product (along with value added generated in industry and the service sector), and specific data on energy, the economy, atmosphere, oceans and the terrestrial environment. Most data are organized on the national scale for the period 1890-2000, and, where available, for 1700-2000. The HYDE-IMAGE combination offers a unique combination of comprehensive historical land cover based on statistical information, and integrated modelling of global change, including regional land-use related emissions, feedback mechanisms and global effects (chapters 7 and 9).

We decided to update the HYDE historical land-cover data for several reasons. First, new data are now available, including sub-national population and land-cover data, and population and land-cover/land-use maps with a 5 by 5 minute resolution. Second, more data are now available to improve our historical land-cover allocation procedure. Section 3 describes a number of existing historical land-cover inventories, including HYDE 2. The methods for developing HYDE 3 are discussed in section 6.3, and section 6.4 describes some results. These and other results of the work described in this chapter are available from <http://www.mnp.nl/hyde>.

## 6.2. Existing historical land-cover inventories

There are two approaches for developing global historical land-cover inventories. The first is modelling of land cover with Dynamic Global Vegetation Models (DGVM), which explicitly represents the interaction between ecosystem C and water exchange and vegetation dynamics to compute long historical transient time series of land cover. Cramer et al. (2001) compared six DGVMs and demonstrated that simulated historical land-cover distribution varied greatly among the models. Most DGVMs are based on biomes representing an envelope of plant functional types. These biomes are generalized ecosystem representations and lack fragmentation or human influences. Secondly, are the historical land-cover datasets based on statistical information. A number of historical land-use datasets were prepared on the basis of statistics at the sub-national and

*Table 6.1. Estimates of historical global cropland and grassland areas from various reports from the literature compared with results from HYDE 3 for 1700-2000.*

Reference	1700	1850	1860	1980	1990	2000
Cropland area (Mha)						
Matthews (1983)	n.d.	n.d.	n.d.	1760	n.d.	n.d.
Richards (1990)	270	540	n.d.	1500	n.d.	n.d.
Williams (1990)	n.d.	n.d.	570	n.d.	1420	n.d.
Klein Goldewijk and Battjes (1997)	270	540	n.d.	1500	n.d.	n.d.
Ramankutty and Foley (1999)	400	820	n.d.	n.d.	2030	n.d.
HYDE 2.0	270	540	n.d.	n.d.	1430	n.d.
FAO (2006)	n.d.	n.d.	n.d.	1429	1489	1475
HYDE 3.0	262	530	573	1429	1489	1475
Grassland area (Mha)						
Klein Goldewijk and Battjes (1997)	530	780	n.d.	3340	n.d.	n.d.
HYDE 2.0	520	1280	n.d.	n.d.	3100	n.d.
FAO (2006)	n.d.	n.d.	n.d.	3268	3364	3440
HYDE 3.0	410	1020	1095	3268	3364	3440

n.d. = no data

national scale, for example for Burgundy in France (Crumley, 2000), the Ardennes in Belgium (Petit and Lambin, 2002), Colombia (Etter and Van Wynngaarden, 2000) and the U.S.A. (Maizel et al., 1998). Other historical land-cover inventories were made on the regional and continental scale, for example, for Australia (AUSLIG, 1997), Southeast Asia (Richards and Flint, 1994) and Central Europe (Williams, 2000).

Estimates of the global historical areas of cropland and grassland are uncertain (Table 6.1). Different approaches were used in the available global estimates. Houghton et al. (1983), Houghton (1991) and Houghton and Hackler (2005) used a bookkeeping model with conversion rates of different land-cover types to estimate C fluxes. Ramankutty and Foley (1998) calibrated the IGBP 1 km-resolution Global Land Cover Classification (GLCC) dataset against cropland inventory data for 1992 to create a global map of cultivated land for 1992. Subsequently, Ramankutty and Foley (1999) (hereafter referred to as RF) used a 'hindcast' modelling technique to extrapolate these data, using a compilation of historical cropland inventory data to create a dataset of croplands for the period 1700 to 1992. Unfortunately, Ramankutty and Foley (1998; 1999) did not consider grassland, which is the major global agricultural land use (Table 6.1).

Klein Goldewijk (2001) developed the History Database for the global Environment (HYDE, version 2), with a 0.5 by 0.5 degree resolution. He used a Boolean approach to generate distributions for global cropland, grassland and natural vegetation for the period 1700-1990, based on a combination of statistical information with natural potential land-cover results of the IMAGE model. In this Boolean approach, complete 0.5 by 0.5 degree grid cells are assigned one unique land-cover type; in this approach there is no fractional distribution within grid cells.

The RF and HYDE 2 datasets are generally consistent in representing cropland change over the last 300 years. In 1700, both the RF and HYDE databases show little cropland in the New World (e.g. the Americas, Australia) and most of the cropland is found in the Indus valley, scattered parts of Europe and Africa, and Eastern China. By 1850, croplands are found in the eastern part of North America, and the area of cropland has expanded further in Europe and China. Between 1850 and 2000, croplands of North America have migrated to the West, while abandonment has occurred in the eastern seaboard. In the same period, in South America crop cultivation has developed in the Pampas region of Argentina and in southeast Brazil, mainly in the 19th and 20th centuries. By the beginning of the 20th century croplands are also found in central East Africa (the Lake District), the Sahel, the eastern part of South Africa, and Southwest and East Australia, thus capturing the major agricultural areas of the world. Between 1850 and 2000, croplands have also expanded further in Europe and the Former U.S.S.R.

Although Klein Goldewijk and Ramankutty (2004) found agreement in the overall global distribution of the two datasets, there are significant differences between RF and HYDE 2 in many parts of the world. Croplands in the RF dataset extend further east in the Former U.S.S.R. than in HYDE 2. In contrast to RF, HYDE 2 shows no cropland in Manchuria. In South America, the cropland areas in RF are scattered, while in HYDE 2 they are located in southeast Brazil and the Pampas of Argentina. Croplands in eastern Australia extend further north in HYDE 2 than in RF. Obviously, the RF scaling approach can only lead to realistic distributions if detailed, sub-national information is available in combination with a reliable base map. Regarding the base map, Klein Goldewijk et al. (2006) showed that the RF data for 1992 do not match with the statistics of FAO (2006). Where no sub-national data on cropland and grassland are available, for example, in the former U.S.S.R., scaling can easily lead to widespread scattered agriculture with very low areas. The disagreement between the two approaches indicates that there is a need for improving the allocation procedures (the simple scaling method of RF and the Boolean approach of HYDE 2) and for better data on historical land cover (Klein Goldewijk, 2001).

## 6.3 Methods

### *General*

The update of HYDE described here includes several improvements compared to its predecessor: (i) the HYDE 2 version used a Boolean approach with a 30 minute degree resolution, while HYDE 3 uses fractional land use on a 5 minute resolution; (ii) more and better sub-national (population) data (Klein Goldewijk, 2005) to improve the historical (urban and rural) population maps as a basis for allocation of land cover; (iii) updated historical land-cover data for the period 1700-2000 (Tables 6.2 and 6.3); (iv) implementation of different allocation algorithms with time-dependent weighting maps for cropland and grassland.

Table 6.2. Historical regional estimates of cropland area for the period 1700-2000.

World region	1700	1750	1800	1850	1900	1950	2000
Mha							
Canada	0	0	0	2	25	43	46
U.S.A.	2	5	11	41	145	193	179
C. America	5	6	8	10	14	27	44
S. America	1	2	2	4	12	51	89
N. Africa	5	5	5	6	8	19	28
W. Africa	16	16	16	17	23	51	84
E. Africa	8	9	9	9	13	28	46
S. Africa	1	1	2	3	6	25	42
W. Europe	53	62	72	85	94	101	87
E. Europe	13	16	21	27	35	49	46
Former U.S.S.R.	34	48	67	94	148	216	222
M. East	13	14	14	14	20	44	64
S. Asia	50	67	92	128	140	176	213
E. Asia	52	57	68	77	78	105	140
S.E. Asia	8	9	10	11	25	53	90
Oceania	0	0	0	0	5	28	51
Japan	1	1	2	2	2	5	5
Greenland	0	0	0	0	0	0	0
World	262	319	400	530	794	1214	1475
Country data aggregated to the level of world regions							

Table 6.3. Historical regional estimates of grassland area for the period 1700-2000.

World region	1700	1750	1800	1850	1900	1950	2000
Mha							
Canada	0	0	0	1	4	18	29
U.S.A.	3	5	9	22	139	254	239
C. America	10	15	21	30	48	80	99
S. America	21	31	47	80	149	333	460
N. Africa	9	13	17	23	38	65	75
W. Africa	32	44	59	79	133	226	251
E. Africa	29	39	53	71	120	203	246
S. Africa	39	52	68	90	149	328	333
W. Europe	64	66	71	75	75	69	60
E. Europe	13	15	18	22	22	20	20
Former U.S.S.R.	77	103	137	183	236	305	359
M. East	22	30	40	54	91	154	257
S. Asia	7	9	12	16	27	46	49
E. Asia	80	120	180	269	318	388	529
S.E. Asia	2	3	4	6	9	14	18
Oceania	0	0	0	0	27	404	419
Japan	0	0	0	0	0	0	0
Greenland	0	0	0	0	0	0	0
World	410	543	735	1019	1588	2909	3444
Country data aggregated to the level of world regions							

The HYDE 3 historical land-cover inventory is based on a number of general concepts for allocating land cover. We argue that early settlers or pioneers in large parts of the world (e.g. U.S.A. in early 18<sup>th</sup> century, South America, South Africa and Australia) were quite limited in their decisions on where to settle and start agricultural activity. Accessibility was limited in many regions, either by the nature of the surrounding landscape (swamps, mountains, dense forests, poor soils, unfavourable climate) or the hostile indigenous population. In addition, large parts of the world were not accessible due to lack of infrastructure. This limited the early spreading of agriculture considerably.

Hence, for allocating historical land use we made three major assumptions: (i) coastal areas and river plains with fertile soils are most favourable for early settlement and land with the highest suitability is colonized first; (ii) historical (rural) population densities and the agricultural activity are strongly correlated; (iii) historical agricultural activity is started first near freshwater resources (rivers); and (iv) old growth forests are less prone to conversion to agriculture than other land-cover types.

The first assumption (i) is based on the history of North America, where prospectors were sent into the 'wilderness' to inventory the vast inland forests and soils. We assume that cropland is more strongly determined by land suitability than grassland, because areas with natural grassland or savanna are easy to use for pastoral grazing. According to assumption (ii) historical (rural) population densities and the agricultural activity are strongly correlated. In this respect it is not clear whether small settlements or villages developed first. This assumption was followed by agricultural activity close to settlements, or in the case of pioneer farmers, by development of small urban settlements. Under the third assumption (iii) historical agricultural activity is started first near freshwater resources (rivers). The pioneers and colonists were limited in their choice of settlement, because it was not feasible in those days to explore far inland territory (e.g. the Americas) due to the unknown terrain conditions, lack of maps, hostile environments and lack of means of transport (roads, railways). The only natural transport ways were coastal shorelines, large navigable rivers, and lakes. Therefore, we assume that river shorelines were more attractive for settlement than the surrounding uplands. Fourth assumption (iv) is that many old-growth forests were already present in 1700. We assume these forests to be less prone to clearing than other land-cover types, e.g. in Europe. This is less relevant in many parts of the New World, where other determinants of forest clearing are dominant.

The situation changed when new technologies enabled farmers to exploit land areas for agricultural purposes further away from towns and villages. With technological development, mechanization, irrigation and widespread use of synthetic fertilizers, people became gradually less dependent on natural factors for agricultural activity such as the natural soil fertility. Thus areas with less favourable soil conditions could be increasingly cultivated.

### *Current distribution of grassland and arable land*

The starting point for all historical hindcasting procedures is the present situation. Here we use the 5 by 5 minute resolution contemporary global cropland and grassland maps developed by Klein Goldewijk et al. (2006). These maps were based on satellite data and national land-use statistics (FAO, 2006) and sub-national land-use data for U.S.A. (USDA, 2006) and China (China National Bureau of Statistics, 2006a,b). Klein Goldewijk et al. (2006) used two satellite maps: (i) the International Geosphere-Biosphere Programme (IGBP) map based on DISCover version 2 data using the IGBP classification map (Loveland et al., 2000) and (ii) the Global Land Cover (GLC) based on the Global Land Cover 2000 VEGA2000 data (Bartholome et al., 2002).

Using the classes in the IGBP map with dominant cropland and grassland did not yield a satisfactory match with FAOSTAT land-use data (FAO, 2006). Therefore, the underlying DISCover data from the seasonal land-cover regions were used to determine fractions of cropland and grassland within the various classes, with mosaics of natural vegetation and cropland and grassland from the IGBP map. No such data were available for the GLC map, so a trial and error approach was used. While neither of the two base maps produced in this manner completely matched the FAO country data, a combination of the IGBP and GLC maps resulted in a satisfactory match with FAO data for all countries. Apart from noise in the data, interpretation problems and uncertainties in the ancillary data used in interpretation, a major problem in allocating grassland is the broad definition used for grassland by FAOSTAT, allowing for important differences between countries in the type of grassland included in the statistics. A large area (~40%) of global grassland occurs in semi-deserts, deserts and sub-polar tundra, regions with unfavourable climates with low productivity and low carrying capacity (Klein Goldewijk et al., 2006). Cropland occurs in more favourable climates. Figure 6.1 shows the global 5 by 5 minute resolution distributions of cropland and grassland for 1970, which form the basis for the historical land-cover allocation.

It should be noted that for applying the base map in IMAGE land-cover simulations (chapter 5), the fractional 5 by 5 minute land-cover map was aggregated to the larger 0.5 by 0.5 degree grid cells. This was done in three steps, reserving the fractions of grid cells covered by built-up areas (urban and infrastructure) and protected areas. Step 1 involved a simple aggregation to the 0.5 by 0.5 degree cells. This aggregation implies a loss of spatial detail in regions where agricultural land occurs in mosaics with natural vegetation. In step 2, cropland and grassland were grouped into one class of agricultural land. The IMAGE model has no fractional land use, i.e. a grid cell is either covered by agricultural land or natural vegetation. Therefore, in step 3 agricultural land was allocated (concentrated) to 0.5 by 0.5 degree grid cells with 100% agricultural coverage. This allocation was done by ranking in which grid cells with the largest fraction agricultural land after step 2 were first classified as agricultural land, until a complete match with FAO land-use data was achieved. Hence, although the general land-use patterns are the same in the 5 by 5 minute maps of Klein Goldewijk et al. (2006) and in IMAGE, the details on the spatial distribution of grassland and cropland are partly lost in steps 2 and 3.

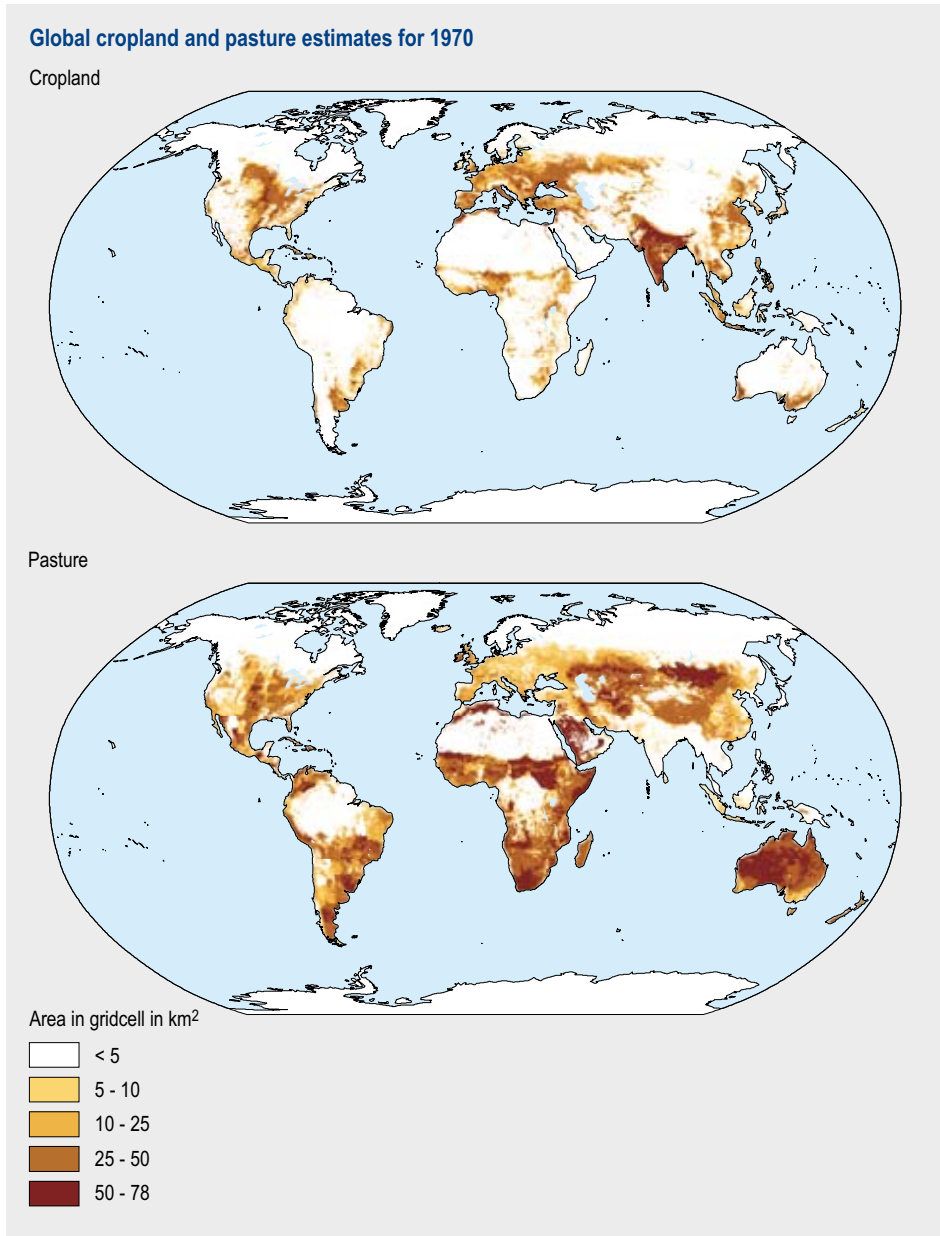


Figure 6.1. Global cropland and grassland area per 5 by 5 minute gridcell for 1970.

#### ***Allocation of historical urban area and population density***

Since the proximity of human settlements is one of the main criteria for early settlement, we first need to know where people live and where urban areas are. For this purpose, historical population maps were computed by downscaling the historical population numbers on a sub-national basis to the 5 minute Landscan population counts map (Landscan, 2006) using statistics and the literature, as presented by Klein Goldewijk (2005) and shown in Figure 6.2. Thus we made a population density map on a 5 by 5

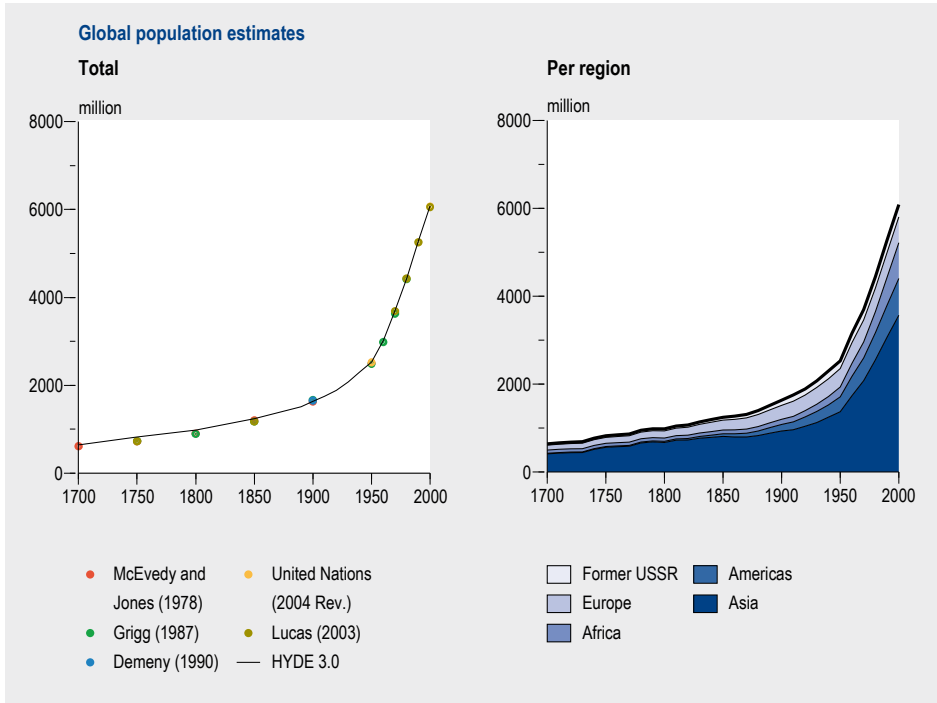


Figure 6.2. Comparison of HYDE 3 with other global population estimates (left) and the HYDE 3 regional historical population estimates for the period 1700-2000.

minute resolution for each time step of 10 years for the period 1700-1970; Figure 6.3 presents the computed population density map for the year 1800.

Maps for current urban area were created by first combining 'Urban and Built-up' from the DISCover map with the areas of 'Artificial surfaces and associated areas' from GLC2000. Subsequently, an overlay of this urban area map was made with the Landscan population counts map to calculate the average population density within urban areas for each country (UPD). We corrected the UPD table by using data from Demographia (2006) to avoid unrealistic (i.e. too high) values for urban population density.

The total number of urban dwellers per country was allocated with the URD for each year, as taken up by the United Nations (UN, 2004) for the time period 1950-2000 and HYDE for 1700-1950. The resulting historical urban areas were excluded from allocation of cropland and grassland.

#### ***Allocation of historical cropland***

On the basis of our general concepts, we use the distributions of population density, land suitability, distance to major rivers and natural land cover as weighting maps to allocate historical cropland. This weighting is similar to the allocation rules in IMAGE, based on the land's suitability and distance to existing agricultural areas, urban areas and rivers (chapter 5).

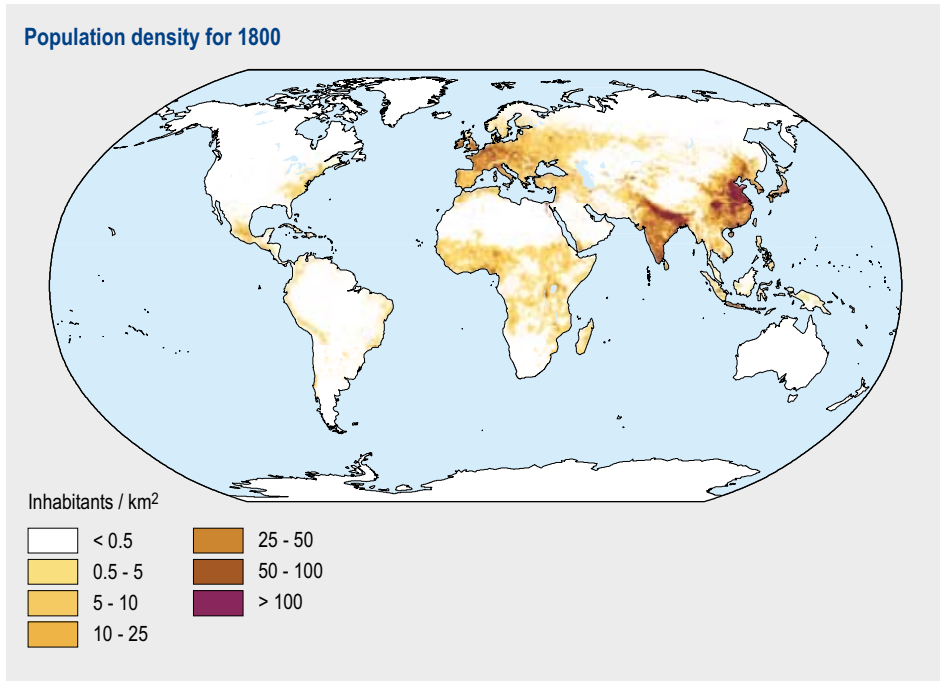


Figure 6.3. Computed global distribution of population density for 1800.

First, a weighting map ( $W_{\text{popd}, t}$ ) was produced by taking the  $^{10}\log$  of the historical population density, multiplied by 10, to dampen the effect of extreme high densities (cities, towns). With the use of this weighting map, those areas with population densities lower than 0.1 inhabitants  $\text{km}^{-2}$  were excluded in the allocation of cropland area (too few people to sustain permanent agriculture), while population densities exceeding 2000 inhabitants  $\text{km}^{-2}$  were excluded, assuming that there is no space available for agriculture.

Cropland was allocated on the basis of the suitability or attractiveness of the land for crop growing. We used the Global Agro-Ecological Zones map (GAEZ) of FAO-IIASA (GAEZ, 2000) to create a second weighting map ( $W_{\text{suit}}$ ). GAEZ (2000) distinguishes seven classes, ranging from 'severe climate constraints' to 'no constraints' on the basis of climate, and soil and terrain conditions. We inverted this classification to create a suitability ranking (Table 6.4).

A weighting map for the distance to major rivers was created ( $W_{\text{river}}$ ) by performing a cost-distance analysis with the World Major Rivers map of DCW (1993), and with a simplified high resolution Digital Elevation Map (DEM) (GLOBE, 1999) as cost raster. The 30-arc-seconds ( $\sim 1$  km) DEM map was reclassified into 10 classes (0 to 1000 metre into 200 metre classes, then 500 metre classes up to 2500 metre classes; the last class is  $> 2500$  metre). Thus, a weighting map was generated with arbitrary scaling between 1 and 10 to describe the attractiveness of the landscape for allocating cropland. Thus,

Table 6.4. Ranking GAEZ climate, soil and terrain constraints for rainfed crops.

GAEZ class	Rank
No constraints	8
Very few constraints	7
Few constraints	6
Partial constraints	5
Frequently severe constraints	4
Very frequently severe constraints	3
Unsuitable	2
Severe climate constraints	1

flat river plains are relatively more attractive for agriculture than sloping areas in the river valley, and the attractiveness decreases with increasing distance from the river.

All classes of the IGBP and GLC2000 satellite-derived maps containing tree cover were used for producing a weighting map  $W_{forest,i}$ . We use the inverse of tree cover to assign less weight to the forested areas than other land-cover classes. This procedure results in less clearing of old growth forests in Europe than, for example, in the U.S.A., where other driving factors such as population are dominant.

Cropland is then allocated by combining historical cropland areas from HYDE (Table 6.2) with inverted tree cover, population density, land suitability and the distance to rivers:

$$W_{crop,i,t} = GAREA_{i,t} W_{forest,i} W_{pop,i,t} W_{suit,i} W_{river,i} \quad (1)$$

Where  $GAREA_{i,t}$  is the total land area (no ice and snow) minus the urban area per 5 minute grid cell  $i$  and historical year  $t$ . Figure 6.4 presents  $W_{crop}$  for the year 1800.

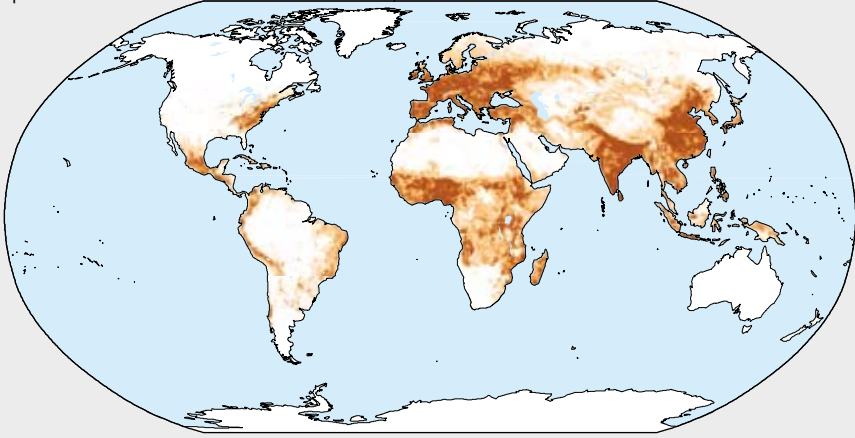
#### **Allocation of historical grassland**

The historical population density maps were also used to allocate more grassland in the neighbourhood of grid cells with a high population density. We excluded areas with values of less than 0.01 inhabitants per km (too few people to maintain livestock) and 2000 inhabitants per km (no space left for agriculture). Please note that the lower threshold is lower than that for the cropland to allow for the occurrence of pastoral grazing in areas with low population density. Thus, population weighting was computed for each year for the allocation of grassland ( $W_{pop,i,t}$ ).

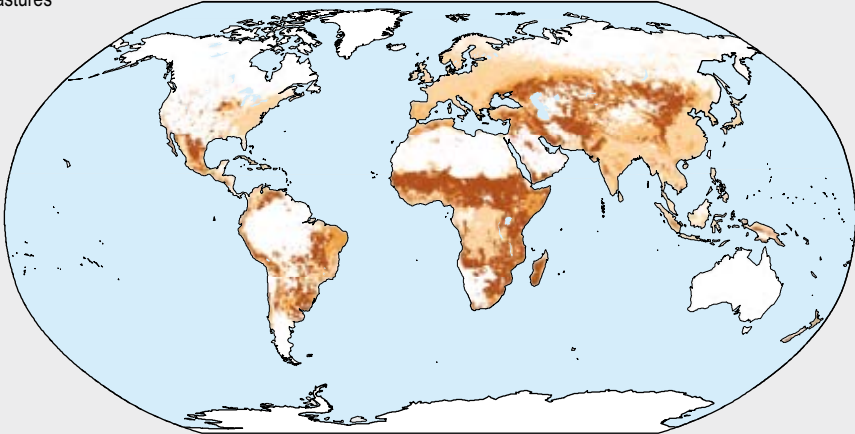
The definition of permanent grassland used by FAO (2006) includes natural and semi-natural types of grassland. We therefore included these natural grasslands in our allocation procedure by ranking the categories of the BIOME map of natural potential vegetation (Prentice et al., 1992) to generate a weighting map ( $W_{biome,i}$ ). In this map, ecosystems with a relatively high proportion of herbaceous vegetation were assigned a high value (Table 6.5).

### Weighting maps for allocation of cropland and pasture for 1800

Croplands



Pastures



Relative weighting factor

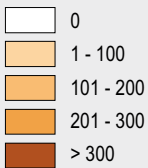


Figure 6.4. Weighting maps for cropland and grassland for the year 1800.

Grassland areas were allocated after the allocation of cropland, implying that area already occupied by cropland is not available for grassland. In the available space, grassland is allocated by combining historical grassland areas from HYDE with the weighting maps for the inverse of tree cover, natural vegetation, crop distribution and population density:

Table 6.5. Ranking BIOME types for weighting in the allocation of grassland.

BIOME type	Rank
Grassland/steppe	6
Open shrubland	5
Savanna	4
Dense shrubland	3
Tundra	2
Evergreen/deciduous mixed forest/woodland	1
Temperate broadleaved evergreen forest/woodland	1
Temperate deciduous forest/woodland	1
Temperate needle leaf evergreen forest/woodland	1
Tropical deciduous forest/woodland	1
Polar desert/rock/ice	0
Boreal deciduous forest/woodland	0
Boreal evergreen forest/woodland	0
Tropical evergreen forest/woodland	0
Hot desert	0

$$W_{grassland_{i,t}} = [GAREA_{i,t} - cropland_{i,t}]W_{forest_i} W_{biome_i} W_{pop_{i,t}} \quad (2)$$

Figure 6.4 presents  $W_{grassland}$  for the year 1800. Subsequently, the satellite-based maps for cropland and grassland were downscaled with historical land-use data (Tables 6.2 and 6.3) for each time step between 1700 and 1970.

Population density turned out to be an unsuitable proxy for the allocation of cropland and grassland in the 20<sup>th</sup> century. With ongoing technological development (mechanization, fertilizer use, etc.), agricultural production gradually became less dependent on natural factors such as soil fertility. Therefore, we consider the years between 1900 and 1970 as a transition period with a diminishing influence of population density in the allocation scheme, and an increasing influence of the satellite-based weighting maps (Figure 6.1). In this manner, a smooth convergence is achieved of the modelled land-cover maps for 1900 to the 1970 situation based on satellite imagery.

## 6.4 Results

### *Eighteenth century*

The 18th century is characterized by dramatic changes in European landscapes by the development of the transportation infrastructure. The emergence of a global economy at the end of the fifteenth century boosted the migration of people into the ‘new world’. Vast virgin forest areas in the Asian part of Russia and North America were cleared and exploited by European settlers (Williams, 2000). This process was driven by various factors, including new politics (imperialism) and religion, new technology (new types of ships and navigation skills, advanced weaponry) and the discovery of natural environments similar to (or even more favourable than) those found in the

Table 6.6. Absolute change and annual growth of the cropland area in various world regions for the period 1700-2000.

World region	Absolute change				Annual growth			
	18th century Mha	19th century Mha	20th century Mha	1950-2000 Mha	18th century % yr <sup>1</sup>	19th century % yr <sup>1</sup>	20th century % yr <sup>1</sup>	1950-2000 % yr <sup>1</sup>
Canada	0	25	21	3	3.4	5.7	0.6	0.1
U.S.A.	9	133	34	-14	1.5	2.6	0.2	-0.1
C. America	3	6	29	16	0.5	0.6	1.1	0.9
S. America	1	10	77	37	0.8	1.7	2.0	1.1
N. Africa	0	3	20	9	0.1	0.4	1.2	0.8
W. Africa	1	7	61	32	0.0	0.4	1.3	1.0
E. Africa	0	4	33	18	0.0	0.4	1.3	1.0
S. Africa	1	5	35	17	0.4	1.4	1.9	1.0
W. Europe	19	23	-7	-14	0.3	0.3	-0.1	-0.3
E. Europe	8	14	11	-2	0.5	0.5	0.3	-0.1
Former U.S.S.R.	33	81	74	6	0.7	0.8	0.4	0.1
M. East	1	6	44	20	0.0	0.4	1.2	0.7
S. Asia	43	47	73	37	0.6	0.4	0.4	0.4
E. Asia	16	10	62	35	0.3	0.1	0.6	0.6
S.E. Asia	2	15	65	37	0.2	0.9	1.3	1.1
Oceania	0	5	46	23	1.2	4.4	2.3	1.2
Japan	0	1	3	0	0.0	0.4	0.9	0.1
Greenland	0	0	0	0	n.a.	n.a.	n.a.	n.a.
World	137	394	681	261	0.4	0.7	0.6	0.4

country of origin. The first European settlers arrived in the beginning of the 17<sup>th</sup> century, initially along North America's eastern coast, and pioneers settled in other parts of the world too (Australia, South America). Extensive areas of forest were cleared for timber, crop growing and grazing. The indigenous population was decimated by diseases introduced by the settlers, and much of the land was thus depopulated and constituted agricultural frontier zones.

These developments are reflected in the data, which indicate that the rate of change is not the same in all world regions. During the 18th century, North America already experienced a yearly increase between 1.5 and 3.5% per year in croplands (Table 6.6). The area of cropland in the former U.S.S.R., South Asia and East Asia grew by 0.6-0.8% per year, while the expansion in Europe and Africa was much slower.

The global cropland area increased from roughly 260 Mha in 1700 to 400 Mha in 1800 (Tables 6.1 and 6.2). The estimate for 1700 is close to that of Richards (1990), but lower than Ramankutty and Foley (1999), who presented much higher historical areas of cropland than other studies for most world regions. Natural grassland and savanna were converted into managed grassland and the global grassland area increased from 410 to 735 Mha in 1800 (Table 6.3). It should be noted that the estimates for grassland areas are more uncertain than those for cropland (Table 6.1).

Table 6.7. Absolute change and annual growth of the grassland area in various world regions for the period 1700-2000.

World region	Absolute change				Annual change			
	18th century Mha	19th century Mha	20th century Mha	1950 - 1990 Mha	18th century % yr <sup>-1</sup>	19th century % yr <sup>-1</sup>	20th century % yr <sup>-1</sup>	1950-2000 % yr <sup>-1</sup>
Canada	0	4	25	11	3.0	4.5	1.9	1.0
U.S.A.	6	130	100	-15	1.0	2.8	0.5	-0.1
C. America	11	27	51	19	0.7	0.8	0.7	0.4
S. America	26	102	310	126	0.8	1.2	1.1	0.6
N. Africa	8	22	36	10	0.6	0.8	0.7	0.3
W. Africa	26	75	118	25	0.6	0.8	0.6	0.2
E. Africa	24	67	126	43	0.6	0.8	0.7	0.4
S. Africa	28	81	184	5	0.5	0.8	0.8	0.0
W. Europe	7	4	-15	-9	0.1	0.0	-0.2	-0.3
E. Europe	5	4	-3	0	0.4	0.2	-0.1	0.0
Former U.S.S.R.	60	99	123	54	0.6	0.5	0.4	0.3
M. East	18	51	166	103	0.6	0.8	1.0	1.0
S. Asia	5	15	22	3	0.6	0.8	0.6	0.1
E. Asia	99	139	211	141	0.8	0.6	0.5	0.6
S.E. Asia	2	5	9	4	0.7	0.9	0.7	0.5
Oceania	0	27	392	14	17.5	15.0	2.8	0.1
Japan	0	0	0	0	0.6	0.8	2.0	2.9
Greenland	0	0	0	0	7.2	7.2	1.8	0.2
World	325	852	1856	535	0.6	0.8	0.8	0.4

### Nineteenth century

The 19<sup>th</sup> and the early 20<sup>th</sup> century were periods with rapid expansion of large-scale agricultural plantations in Asia and Latin America. After early successes with sugar cane in the Caribbean and cotton cultivation in North America, financial resources were made increasingly available to penetrate further into the New World and cultivate a wider variety of crops. European owners mobilized local labour to clear jungle lands in order to grow, for example, rubber in Malaysia, cacao in Africa, tea in India, coffee in Brazil and bananas in Central America.

The strong increase of croplands in North America continued at a rate of more than 5% yr<sup>-1</sup> in Canada and 2.6% yr<sup>-1</sup> in the U.S.A. during the 19<sup>th</sup> century, followed by South America and South Africa with rates of around 1.5% yr<sup>-1</sup> (Table 6.6). Central America and Australia experienced an expansion of cropland areas of about 1% per year. Large areas in the Russian continent (0.8% yr<sup>-1</sup>) and Southeast Asia (0.9% yr<sup>-1</sup>) were also colonized and brought under cultivation. Global cropland area increased in this period from 400 Mha in 1800 to approximately 530 Mha in 1850 and 800 Mha in 1900. The estimate for 1850 is very close to the estimates for the same year of Richards (1990) and Williams (1990), who indicated 540 Mha and 570 Mha, respectively (Tables 6.1 and 6.2). The area of grassland increased from 940 Mha to roughly 1020 Mha in 1850 and expanded further to 1590 Mha in 1900, with rapid expansion in North America (Tables 6.3 and 6.7).

### *Twentieth century*

The process of colonization and transformation of natural vegetation to cropland continued in the first half of the 20th century. However, the rate of expansion of cropland decreased considerably. The annual increase of the cropland area in Canada went down from a staggering 5% yr<sup>-1</sup> in the 19th century to 0.6% yr<sup>-1</sup> in the 20th century (especially after 1950 the rate slowed down to 0.13% yr<sup>-1</sup>), while the expansion rate in the U.S.A. fell from 2.6% yr<sup>-1</sup> in the 19th century to 0.2% yr<sup>-1</sup> in the 20th century. After 1950, the expansion of cropland even reversed in some temperate regions. U.S.A. (-0.15% yr<sup>-1</sup>) and Western (-0.30% yr<sup>-1</sup>) and Eastern Europe (-0.10% yr<sup>-1</sup>) show negative rates, indicating that agricultural land was abandoned (Table 6.6).

After the Second World War, the conversion of undisturbed ecosystems to agriculture dramatically increased worldwide, but now shifted towards the tropical regions. The global cropland area increased from roughly 800 Mha in 1900 to 1475 Mha in 2000, while in this time period the global area of grassland grew from 1590 Mha to 3430 Mha (Table 6.1). The expansion of grassland for cattle grazing (Latin America), logging (Africa and Asia) and expansion for agriculture (Asia) were the main driving forces (FAO, 2005). Many African countries show cropland expansion rates between 1 and 2% per year in the 20th century. The same applies to Southeast Asia, Oceania and Central and South America (Table 6.6 and Figure 6.5).

The area of permanent grassland increased by more than 500 Mha from 2909 Mha to 3444 Mha in the 1950-2000 period, while the total increase over the 20th century was 1856 Mha (Table 6.7). Oceania (2.8% yr<sup>-1</sup>) and Canada (1.9% yr<sup>-1</sup>) witnessed rapidly increasing grassland areas. Expansion of grassland was also fast in South America and Oceania (more than 1% yr<sup>-1</sup>) and Central America and Africa (~0.7% yr<sup>-1</sup>). In contrast, Western and Eastern Europe showed shrinking grassland areas (Table 6.7). The grassland area also decreased in the U.S.A., but only after 1950.

It is remarkable that China witnessed an accelerated expansion of cropland in the 1970s and 1980s, compared to the slow pace in the first half of the 20th century. This led to considerable forest losses, but this trend came to a halt and was followed by large forest planting campaigns during the 1990s. In South America, Brazil continued to show considerable deforestation rates throughout the 1970-2000 period. However, recent satellite-based estimates indicate that deforestation rates may have been overestimated (FAO, 2005; DeFries et al., 1999). As mentioned before, parts of Europe and North America experienced a modest decrease in agricultural area, probably as a result of intensification and improved technology, many agricultural areas were taken out of production and often reforested (often referred to as the 'forest transition').

During the last three centuries, agricultural areas have expanded in almost all parts of the world with favourable conditions for crop cultivation. No expansion occurred in regions with extreme climatic conditions, such as the hot desert areas of the Sahara, Middle East and Australia, the cold high latitudinal regions of Canada and Russia, and the remote tropical rainforest areas of the Amazon Basin, central Africa and Asia. The

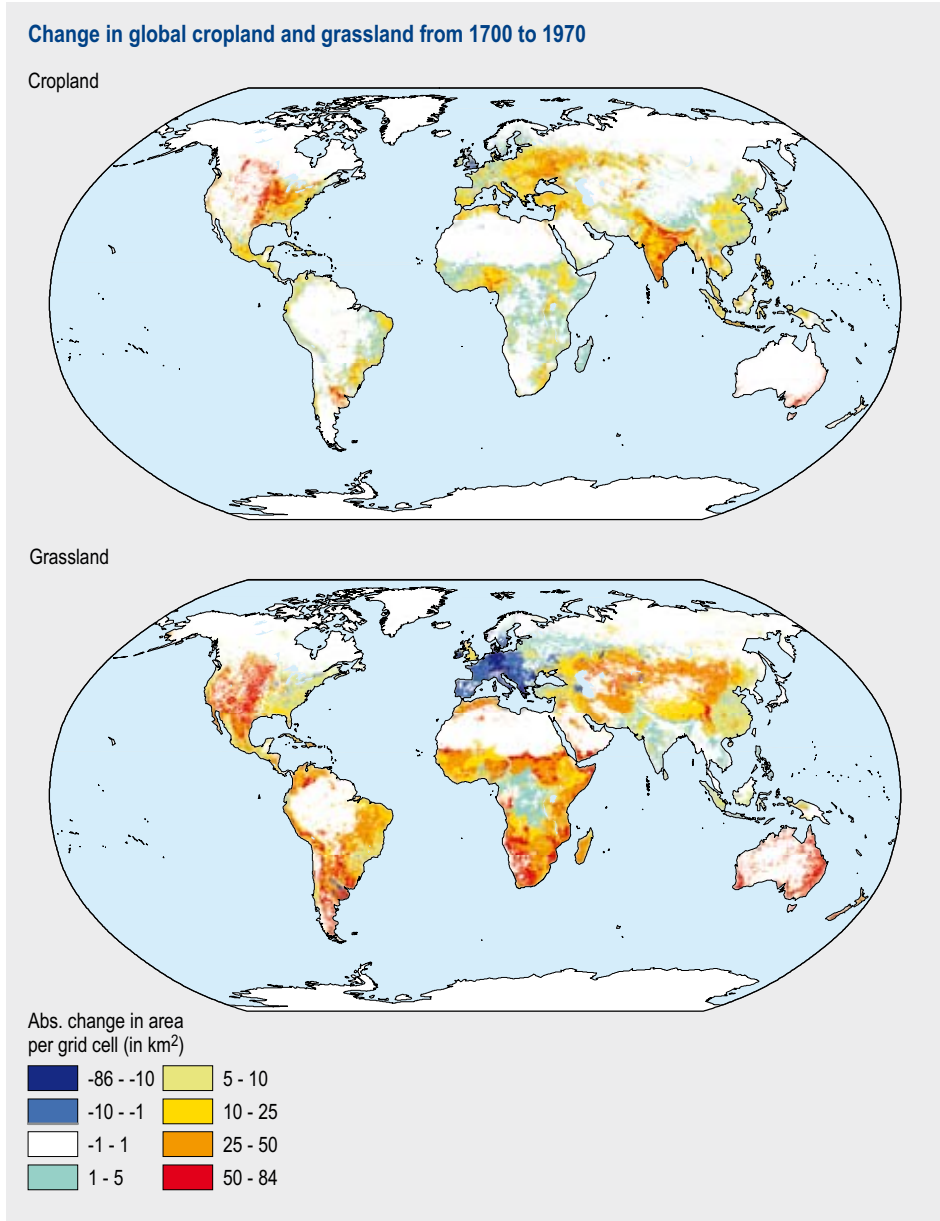


Figure 6.5. Absolute change in cropland and grassland area for each 5 by 5 minute grid cell during the period 1700-1970.

area of cropland, and even more so the grassland area, expanded rapidly in many parts of the world, except for Europe where a decline in the area of grassland occurred between 1700 and 1970 (Figure 6.5).

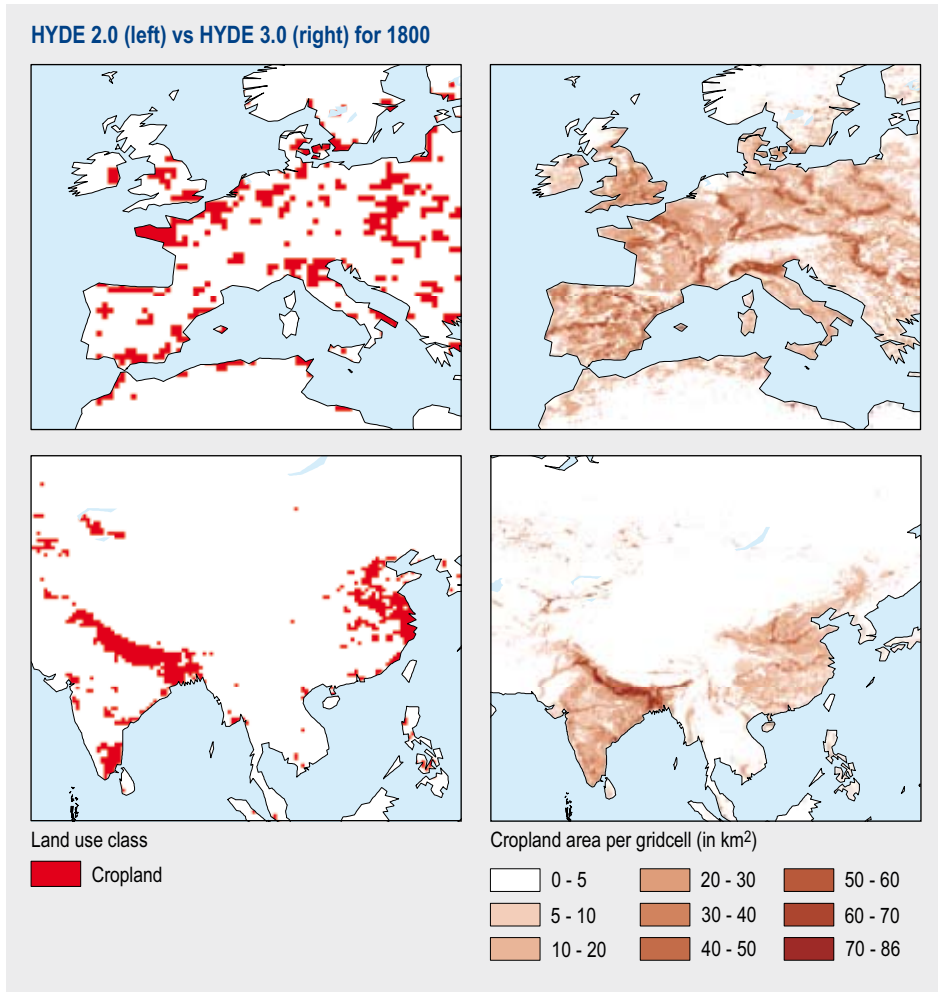


Figure 6.6. Difference in the distribution of cropland areas, HYDE 2.0 and HYDE 3.0, for Europe and South and East Asia for the year 1800.

### Comparison with HYDE 2

It is interesting to compare the spatial historical distributions for agricultural land cover of HYDE 2 and HYDE 3. Differences may stem from the combination of the resolution and the allocation procedure. The change from a Boolean approach in HYDE 2.0 for a 0.5 by 0.5 degree resolution (Figure 6.6, left panel) towards a fractional approach for 5 by 5 minute resolution in HYDE 3.0 (right panel), resulted in much less concentration of agricultural land cover. The higher resolution of HYDE 3 allows for a better and more flexible allocation of agricultural land cover, without losing spatial information. In addition, the use of sub-national data resulted in improved spatial distributions within each country. This is illustrated in Figure 6.6, which shows that cropland in Europe is much less concentrated in HYDE 3 (right panel). In the year 1800, Europe was in the process of rapid structural change, and several countries increased

their agricultural productivity substantially (Allen, 1998). European agriculture was a widespread and dynamic activity, and not confined to limited areas.

The high resolution weighting maps used for HYDE 3 also allow for investigating different approaches for allocating historical land cover, resulting in more plausible historical land-use reconstructions. In Asia the agricultural cropland areas are spatially distributed in HYDE 3, with occurrences in nearly all grid cells with suitable land, and concentrations in major river floodplains (right panel). This distribution is the result of using the population density and other weighting maps, and directly reflects the sub-national data for states in India and provinces in China. In contrast, in HYDE 2 there are croplands in some confined parts of India and China only, which is not realistic.

## 6.5 Concluding remarks

A good understanding of development processes in the past is essential for our understanding of the future. Historical databases such as HYDE can serve as an important tool for evaluating and improving the historical land-cover changes based on regional and national data. Unfortunately, there are only a few global-scale studies available for comparing our historical land-cover inventory.

HYDE 3 now includes better historical data and new allocation procedures based on attractiveness of the land for agricultural activities. The attractiveness of the land for crop cultivation is based on weighting maps for population density, the land's suitability for crop production, forest occurrence and the distance to transport corridors such as rivers. For allocating grassland areas we use weighting maps based on the type of natural vegetation and population density. Furthermore, a transition period between the historical population weighted allocation and the contemporary satellite-based allocation algorithms is used, where the historical allocation scheme phases into modern times, and thus a smooth change is guaranteed between the modelled and actual land-cover maps over time.

In comparison with HYDE 2 (using the Boolean method with no fractional land cover) and Ramankutty and Foley (1999) (scaling with historical national and sub-national data on satellite-derived cropland patterns), HYDE 3 is representative of a more transparent approach, resulting in more realistic distributions of agricultural land in many parts of the world.

Gridded time series of global cropland and grassland are useful for evaluating global environmental change for the historical period using integrated Earth system models. The unique combination of HYDE and IMAGE offers a good basis for examining the effect of historical land-use changes over the past three centuries; the first study planned will focus on the global historical carbon cycle.



## 7 SIMULATING CARBON EXCHANGE BETWEEN THE TERRESTRIAL BIOSPHERE AND THE ATMOSPHERE

- The carbon cycle model implemented in the IMAGE framework has been subjected to a thorough evaluation, which has shown it to be suitable for simulating global and regional carbon pools and fluxes. The model also accounts for important feedback mechanisms related to changing climate, carbon dioxide concentrations and land use. In addition, it allows the potential for carbon sequestration in the terrestrial biosphere to be evaluated.
- Sensitivity analysis shows that uncertainties in the response of the biosphere to climate and land-use change are crucial to understanding the global carbon cycle. A dominant factor at both the global and regional scales is the reaction of the biosphere to increasing concentrations of carbon dioxide. Since this reaction is beset with considerable uncertainties, more research is needed to improve our understanding of carbon dioxide fertilization under changing environmental conditions.
- Results from scenario studies show that the terrestrial biosphere will probably continue to be a net sink for carbon in the coming decades, thus reducing the increase of the atmospheric carbon dioxide concentration. It is, however, uncertain whether this carbon sequestration will continue after this period. In some scenarios the terrestrial biosphere may even turn into a net source of carbon during the course of this century.

### 7.1 Introduction

The carbon dioxide ( $\text{CO}_2$ ) concentration in the atmosphere has increased by about 100 ppm (parts per million) since the 1880s, leading to a concentration of about 380 ppm in 2005. This increase in atmospheric  $\text{CO}_2$  and other greenhouse gases (GHG) leads to anthropogenic greenhouse warming (Mitchell et al., 2001). The contribution of  $\text{CO}_2$  to greenhouse warming is about 50%, since it is the most abundant GHG and because it has a long atmospheric residence time.  $\text{CO}_2$  emissions from fossil fuel combustion and cement production have been the dominant  $\text{CO}_2$  source in the past decades.

The terrestrial carbon (C) cycle plays an important role too. Historical changes in land use have contributed considerably to the cumulative  $\text{CO}_2$  increase. Current land-use change (loss of forest area) is responsible for a  $\text{CO}_2$  emission of 1-2 Pg C yr<sup>-1</sup> (Pg = petagram; 1 Pg = 10<sup>15</sup> g) (Achard et al., 2002; Houghton, 2003), which is considerable compared to the global  $\text{CO}_2$  emission from fossil fuels of 7.3 Pg yr<sup>-1</sup> (CDIAC, 2006).

While deforestation is a source of  $\text{CO}_2$ , the remaining natural land cover sequesters C and thus slows down the atmospheric  $\text{CO}_2$  increase. The sink strength is, however, uncertain with present-day estimates, ranging between 1.6 and 4.8 Pg C yr<sup>-1</sup> (Houghton, 2003). This is because global terrestrial soil and vegetation C pools change rapidly

(Prentice et al., 2001), as they are determined by multiple physiological and ecological processes that vary in time and space as a result of changing environmental conditions (e.g. CO<sub>2</sub> concentration, climate, atmospheric nitrogen deposition inputs, tropospheric ozone, soil and terrain properties), and land use (Zaehle et al., 2005). Knowledge of the interaction between the various processes and mechanisms is also essential for assessing policy options for reducing climate change, such as cultivation of energy crops or establishment of C plantations.

Model exercises have been performed to analyze the consequences of uncertainties in land-use, climate and vegetation response to changing environmental conditions on the terrestrial C cycle. Most studies, however, did not integrate all aspects but concentrated mainly on one or a few elements. For example, Cramer et al. (2001), Joos et al. (2001) and Friedlingstein et al. (2003) all focused on the effect of changing CO<sub>2</sub> concentrations and climate on the terrestrial C cycle; Sitch et al. (2005) evaluated the role of land-cover changes; Davidson et al. (2006) analyzed the consequences of different parameterizations of soil responses to climate change; while Guisan and Thuiller (2005) stressed the importance of the migration capability of ecosystems as they respond to climate change. It is difficult to compare and synthesize the results of these studies because of differences in assumptions, models and scales. Furthermore, the studies seldom allow for a comparison of the consequences of different parameterizations of the C cycle with the consequences of land use and socio-economic development.

In this chapter we present the current C cycle model of IMAGE, focusing on the processes that affect the terrestrial C cycle. Furthermore, we discuss results of a sensitivity analysis on the consequences of uncertainties in land-use, climate change and vegetation response for the simulated global and regional C cycle. Although the C cycle model has hardly changed since IMAGE 2.0, it is here referred to as the C cycle model of IMAGE 2.3, as all experiments were carried out with version 2.3. The main difference between IMAGE 2.2 (IMAGE-team, 2001) and IMAGE 2.3 is the addition of energy crops and carbon plantations (see chapter 1). Through this analysis we assess the importance of the different factors and processes in the global C cycle on different geographical scales and evaluate if our modelling approach is appropriate for describing the most relevant aspects of the terrestrial C cycle on the global and continental scale. In section 7.2 we present the current C cycle model of IMAGE, including the description of energy crops and carbon plantations that have been added as a separate land-cover type in IMAGE 2.3. The results of the sensitivity analysis are discussed in sections 7.3 and 7.4 and concluding remarks in section 7.5.

## 7.2 The IMAGE C cycle model

### *Model description*

The terrestrial C cycle modelling in IMAGE as affected by changes in land cover and climate is described in detail in Klein Goldewijk et al. (1994) and Van Minnen et al. (2000). Here we only give a brief overview. Although IMAGE is global in application, all land-

related calculations (including the C exchange between terrestrial ecosystems and the atmosphere) are performed for a terrestrial resolution of 0.5 by 0.5 degrees. Each cell is characterized by its climate (temperature, precipitation and resulting soil moisture and cloudiness), soil and land cover (natural ecosystems or agriculture). The distribution of 14 natural land-cover types is computed with the BIOME model (Prentice et al., 1992) on the basis of climate, soil and atmospheric CO<sub>2</sub> concentration. When climate changes vegetation patterns may shift. Time lags in these shifts due to limiting migration capabilities of species are considered explicitly elsewhere (Van Minnen et al., 2000).

Anthropogenic land-cover types include agriculture (arable land and grassland), marginal grassland, land for bioenergy and carbon plantations. Carbon plantations and energy crops were added as two separate land-cover categories to deal with their effects on the terrestrial C cycle. We refer to chapter 5 for the anthropogenic land-cover types and the drivers of land-use change.

The terrestrial C model of IMAGE 2.3 is driven by net primary productivity (NPP, plant photosynthesis minus plant respiration), which is a function of climate, soil, atmospheric CO<sub>2</sub> concentration, altitude, land-cover type and land-cover history (equations 1 and 2):

$$NPP_j(t) = NPPI_{l,i} \sum_{m=1}^{12} \left( [CF_{j,m}(t)] \frac{f_1(T_{j,m}(t), l_j) f_2(SWS_{j,m}(t))}{AF_{l_j}} \right) \quad (1)$$

$$AF_{l_j} = \frac{\sum_{i \wedge i \in l} (f_1(T_{i,m}(1970), l_i) f_2(SM_{i,m}(1970))) area_i}{\sum_{i \wedge i \in l} area_i} \quad (2)$$

where *NPP* is net primary production (Mg C km<sup>-2</sup>), *NPPI*, the mean NPP of one land-cover type in 1970 (Mg C km<sup>-2</sup>), *CF*, the CO<sub>2</sub> fertilization factor (-) (see equations 3 and 4), *T*, the monthly temperature (°C) and *SWS*, the monthly soil-water status (%); *f*<sub>1</sub> and *f*<sub>2</sub> are multipliers (-) for direct temperature effect on plant growth and for water availability effect on plant growth, respectively, *AF*, a normalization factor to 1970 average (-) and *area*, the grid cell area (km<sup>2</sup>). Indices include *t*, the year (1970-2100); *j*, the grid-cell number (1-66,663); *m*, month (1-12); *l*, land-cover type (1-20) and *i*, the index of all grid cells covered by one land-cover type in 1970 (*i* is a subset of *j*).

NPP is allocated over the living biomass compartments (i.e. leaves, branches, stems and roots). From the living biomass, C either shifts to the non-living biomass compartments (litter, soil humus and charcoal), where it (slowly) decomposes and returns as CO<sub>2</sub> to the atmosphere, or it is harvested and stored in pulpwood and particles (with a turnover of 10 years), sawlogs, veneer or industrial roundwood (with a turnover of 100 years). The allocation fractions and turnover times are defined for each land-cover type and C compartment (Table 7.1).

Table 7.1. Parameter settings in the Terrestrial C cycle model of IMAGE 2.3, where regrowth forests and carbon plantations use settings of underlying or corresponding land cover types; values for ice are zero.

Agricultural land-cover type/biome	NPPI <sup>a</sup> (g m <sup>-2</sup> yr <sup>-1</sup> )	Allocation fraction (-)				Lifetime (yr)				HF <sup>b</sup> (-)			
		Leaves	Branches	Stems	Roots	Leaves	Branches	Stems	Roots	Litter	Humus	Charcoal	
<b>Agriculture</b>													
Agricultural land	400 (350)	0.8	0	0	0.2	1	n.a.	n.a.	1	1	*	500	0.35
Marginal grassland	400 (350)	0.8	0	0	0.2	1	n.a.	n.a.	1	1	*	500	0.3
Sugarcane (bioenergy)	1700	0.5	0.3	0	0.2	1	1	n.a.	1	1	*	500	0.3
Maize (bioenergy)	450	0.7	0.1	0	0.2	1	1	n.a.	1	1	*	500	0.3
Wood (bioenergy)	1100	0.3	0.2	0.3	0.2	1	1	1	1	1	*	500	0.3
<b>Biomes</b>													
Tundra	100	0.5	0.1	0.1	0.3	1	10	50	3	2	50	500	0.5
Wooded tundra	300	0.3	0.2	0.3	0.2	2	10	50	10	3	50	500	0.5
Boreal forest	500 (350)	0.3	0.2	0.3	0.2	2	10	50	10	3	50	500	0.6
Cool conifer forest	550	0.3	0.2	0.3	0.2	3	10	50	10	3	40	500	0.5
Temp. mixed forest	600 (650)	0.3	0.2	0.3	0.2	2	10	50	10	2	40	500	0.5
Temp. decid. forest	650 (700)	0.3	0.2	0.3	0.2	1	10	50	10	2	40	500	0.4
Warm mixed forest	650 (700)	0.3	0.2	0.3	0.2	1	10	50	10	2	40	500	0.4
Steppe	450	0.6	0	0	0.4	1	10	50	2	1	30	500	0.4
Hot desert	50	0.6	0	0	0.4	1	10	50	2	1	50	500	0.4
Scrubland	400	0.3	0.2	0.2	0.3	1	10	30	5	2	30	500	0.4
Savanna	500	0.3	0.2	0.2	0.3	1	10	30	5	2	20	500	0.4
Tropical woodland	900 (950)	0.3	0.2	0.3	0.2	1	10	30	10	2	20	500	0.4
Tropical forest	1200 (1250)	0.3	0.2	0.3	0.2	1	10	30	10	2	20	500	0.4

<sup>a</sup> The sensitivity analysis and comparison of IMAGE 2.3 results with other studies and observations have resulted in a modification in IMAGE 2.4 of the  $\beta_{\text{in}}$  value from 0.7 to 0.35 and a modification of NPPI estimates.

<sup>b</sup> HF, humification fraction, which is the fraction of the litter that enters the humus pool; the remainder is oxidized to CO<sub>2</sub>.

<sup>c</sup> Values of underlying natural vegetation type are used.

Soil respiration is the C flux to the atmosphere resulting from the oxidation of soil C (litter, humus and charcoal). This flux depends on the C stocks in the different soil compartments, their turnover rates, and environmental conditions (i.e. soil water availability and temperature). During decay of litter and dead roots, a part is transformed into soil humus (using the humification factor HF in Table 7.1), while the remainder is oxidized to CO<sub>2</sub> and lost to the atmosphere. The soil humus pool changes as a result of the above additions and oxidation to CO<sub>2</sub> by decomposition, while a small fraction is transformed into charcoal. Charcoal is a major C pool in many land-cover types. Its respiration flux is therefore significant, despite its long lifetime of 500 years.

Net ecosystem productivity (NEP) represents the net C flux between the atmosphere and biosphere, and is equal to the NPP minus soil respiration. Negative values indicate a net release of CO<sub>2</sub>, while positive values indicate a net uptake by the biosphere.

The C cycle model includes different climate feedback processes that modify NPP and soil decomposition (and thus NEP) in each grid cell (Klein Goldewijk et al., 1994; Van Minnen et al., 1995). Some processes increase NEP (negative feedback), while others cause a decrease (positive feedback). These feedback processes include the effect of CO<sub>2</sub> (equations 3 and 4), moisture and temperature on plant growth and soil respiration, using different response functions depending on temperature, soil water and species characteristics.

$$CF_{i,m} = 1 + \beta_{i,m} \ln\left(\frac{[CO_2]_t}{[CO_2]_{1970}}\right) \quad (3)$$

$$\beta_{i,m} = \beta_{ini} f_3(T_{i,m}, SWS_{i,m}) f_4(nut_i, sp_i, alt_i) \quad (4)$$

where  $\beta_{ini}$  is the initial CO<sub>2</sub> fertilization factor,  $[CO_2]_t$  and  $[CO_2]_{1970}$ , the atmospheric CO<sub>2</sub> concentration in year  $t$  and 1970, respectively (ppmv),  $f_3(T_{i,m}, SWS_{i,m})$ , a multiplier (-) for temperature ( $T$ ) and soil moisture ( $SWS$ );  $f_4(nut_i, sp_i, alt_i)$ , a multiplier (-) for nutrient availability ( $nut$ ), species characteristics ( $sp$ ) and altitude ( $alt$ ) in grid cell  $i$  (all constant over time).

It should be noted that all C fluxes within the terrestrial C cycle are calculated using a monthly time step, aggregated to annual totals for use in C balance calculations. With the monthly resolution we can take into account the plant responses in different seasons. This temporal resolution is also consistent with the downscaling of monthly climate-change patterns in the atmosphere-ocean system.

The atmosphere-ocean model of IMAGE (Eickhout et al., 2004) computes changes in the atmospheric concentration of CO<sub>2</sub> and other greenhouse gases from land use and energy-related sources, while accounting for oceanic and terrestrial C uptake and atmospheric chemistry. The atmospheric changes control climate change, which are subsequently calculated and linked to scenarios of advanced climate models (i.e. GCMs) to obtain regional changes in monthly temperature and precipitation (chapter 9).

IMAGE explicitly distinguishes four major land-cover conversions: (i) natural vegetation to agricultural land (either cropland or pasture); (ii) agricultural land to natural land-cover types; (iii) forests to regrowth forests; and (iv) one type of natural vegetation into another. The terrestrial C cycle model consistently, both in time and space, handles the effects of these land-cover conversions on the global C pools and fluxes. These effects may be considerable. For example, different transformations occur after conversion of natural vegetation to agricultural land or regrowth forest: (i) emission of part of the living biomass into the atmosphere via biomass burning during tropical deforestation; (ii) use of living biomass for wood products (stems and branches may be

harvested); (iii) use of living biomass for fuel (fuelwood is used as a traditional energy source); (iv) decomposition and transformation to non-living biomass and (v) decomposition of non-living biomass (litter, soil organic matter).

The conversion from one natural land-cover type to another also alters NPP and NEP. The processes involved are influenced by the rate of climate change and the possibility of natural land-cover types adapting to new conditions. The procedure for calculating this transient response for each grid cell starts with the BIOME model's computation of the potential natural land-cover type for each grid cell. The potential land cover within a grid cell may change from what it was in earlier time steps; if this land cover is located within the potential migration zone, the transformation to the new land-cover type can begin. If not, the old type remains, and it is assumed that its NPP cannot increase to mimic the process of degradation. If transformation from one natural land-cover type to another begins, NPP also changes over the assigned transition period. These periods are assumed to be short if plant types disappear from a grid cell, but long if new plant types are introduced.

The assumed migration distances and rates are based on plant species occurring in each land-cover class (Van Minnen et al., 2000). For example, grasses grow fast and are assumed to be widely dispersed, therefore migrating rapidly over long distances. Tree species grow and disperse more slowly, and have smaller migration potentials. The resulting vegetation shifts are therefore a function of distance and growth rates of vegetation types.

### **Carbon plantations**

Carbon plantations were introduced as a new land-cover class in IMAGE 2.3 for assessing land-use related activities as options for achieving stabilization of the atmospheric CO<sub>2</sub> concentration, the ultimate objective of Article 2 of the United Framework Convention on Climate Change (UNFCCC, 1993). The net C sequestration potential is used to quantify the additional C sequestration by C plantations compared to the natural land cover that would otherwise grow at the same location, and the C losses associated with the conversion from natural land cover into a plantation. This sequestration potential is calculated according to Van Minnen et al. (2006b):

$$C_{seq} = bE + \sum_{t=t_0}^{t=2100} [NEP_t - NEP_{CP,t}] \quad (5)$$

where  $C_{seq}$  is the net C sequestration in a grid cell in the period  $t_0$  to 2100 (Mg C km<sup>-2</sup>),  $t$ , the year (2000-2100),  $t_0$ , the start-year of C plantations in a grid cell,  $NEP_{CP,t}$ , the NEP for the tree species with fastest growth in a grid cell (Mg C km<sup>-2</sup> yr<sup>-1</sup>),  $NEP_t$ , the NEP of the original vegetation according the baseline scenario (Mg C km<sup>-2</sup> yr<sup>-1</sup>),  $E$ , the above-ground C of the original vegetation (Mg C km<sup>-2</sup>), and  $b$ , the burning of the original vegetation ( $b$  is either 0 or 1). When a natural forest or woodland is converted to a C plantation, it is assumed that the original vegetation is burnt entirely ( $b = 1$ ), resulting in instantaneous CO<sub>2</sub> emission ( $E$ ).

Table 7.2. Tree species selected for carbon plantations in IMAGE 2.3 and their climatic requirements.

	Tree species	Corresponding natural land-cover type	$T_{\text{cold}}^{\text{a}}$ ( $^{\circ}\text{C}$ )	Moisture <sup>b</sup> (-)	$\text{GDD5}_{\text{min}}^{\text{c}}$ ( $^{\circ}\text{C}$ )
1	Eucalyptus camadulensis (river red gum)	Tropical deciduous	>15.5	0.45-0.8	
2	Eucalyptus grandis (rose gum)	Tropical evergreen	>15.5	0.8-1.0	
3	Pinus radiata (radiata pine)	Temperate evergreen	>5	0.55-0.95	
4	Populus nigra (black poplar)	Temperate deciduous	-15 to 15.5	0.65-1.0	1200
5	Picea abies (Norway spruce)	Boreal evergreen	-35 to -2	0.75-1.0	350
6	Larix kaempferi (Japanese larch)	Boreal deciduous	< 5	0.65-1.0	350

<sup>a</sup>  $T_{\text{cold}}$  is the average temperature of the coldest month.

<sup>b</sup> Moisture is expressed as the Priestley Taylor index, i.e. AET/PET (Cramer and Solomon, 1993). The lower end of the range can decrease due to increasing Water Use Efficiency (WUE) as a result of increasing atmospheric  $\text{CO}_2$  levels.

<sup>c</sup>  $\text{GDD5}_{\text{min}}$  is the minimum growing degree days for establishment (considering a  $5^{\circ}\text{C}$  base).

Hence, all C fluxes and pools in vegetation and soil are considered, including the C losses due to the establishment of the plantations. Alternative land-use options are considered in the allocation of plantations in order to avoid conflicts with, for example, food production.

Six plantation types have been selected on the basis of the ‘Top 14 Most Planted World’s Trees’ (FAO, 2001; Del Lungo, 2003) to represent the most suitable species in different geo-climatic regions around the world (Table 7.2). NPP and NEP for each plantation type are determined by multiplying the NPP of the natural land-cover type that best matches the tree species considered by an additional growth factor (AGF, Table 7.3). The AGF values for each plantation type are based on an extensive literature review as described in Van Minnen et al. (2006b).

Two types of management practices can be considered: (i) harvesting, in which a plantation is harvested at the moment of maximum C sequestration followed by regrowth; (ii) non-harvesting, in which a plantation is not harvested but grows to a stable level of C storage after which additional C sequestration is limited. One application of modeling carbon plantations with IMAGE is discussed in chapter 9.

In addition to the biophysical model for C plantations, costs are included, enabling a comparison with other options to mitigate the build-up of  $\text{CO}_2$  in the atmosphere. Costs in this respect refer only to land and establishment costs. Other types of costs are excluded for different reasons (e.g. compensation by revenues from timber). We refer to Strengers et al. (2006) and Van Vuuren et al. (2006) for details on the cost aspects of C plantations.

Table 7.3. Growth characteristics of carbon plantations listed in Table 7.2.

	Tree Species	Yield (m <sup>3</sup> ha <sup>-1</sup> yr <sup>-1</sup> )	Recovery period (yr)	LRL <sup>a</sup> (yr)	HI <sup>b</sup> (-)	WD <sup>c</sup> (Mg DM m <sup>-3</sup> )	FNPP <sub>CP</sub> <sup>d</sup> (Mg C ha <sup>-1</sup> yr <sup>-1</sup> )	AGF <sup>e</sup> (-)
1	<i>E. camadulensis</i>	12 (3-20)	8	15	0.65	0.550	18.9	2.02
2	<i>E. grandis</i>	20 (10-35)	8	15	0.70	0.425	22.2	1.77
3	<i>P. radiata</i>	14 (10-30)	15	28	0.87	0.450	11.0	1.62
4	<i>P. nigra</i>	16 (8-28)	18	25	0.83	0.350	11.8	1.77
5	<i>P. abies</i>	11 (4-20)	30	60	0.87	0.400	8.2	1.49
6	<i>L. kaempferi</i>	7 (4-12)	25	60	0.87	0.490	5.6	1.11

<sup>a</sup> Likely Rotation Length (LRL) for *E. camadulensis* (eucalyptus) was obtained from FAO (2001), for *P. radiata* (pine) LRL was based on the average of Nabuurs and Mohren (1993), Nilsson and Schopfhauser (1995) and Del Lungo (2003), for *P. nigra* (black poplar) on Nabuurs and Mohren (1993) and Del Lungo (2003); for *P. abies* (Norway spruce) on the upper limit given by Nilsson and Schopfhauser (1995), and for *L. kaempferi* (Japanese larch) LRL was obtained from different yield tables (e.g. Cannell, 1982; Schober, 1975).

<sup>b</sup> Harvest Index (HI) data are based on information from IPCC (2004).

<sup>c</sup> Wood density (WD) in Mg Dry Matter (DM) m<sup>-3</sup> oven-dry wood. Data stem from IPCC (2004), Nabuurs and Mohren (1993), Ilic et al. (2000), and Gracia and Sabate (2002).

<sup>d</sup> FNPP<sub>CP</sub> is the average NPP of full grown plantations around 1995. It is a function of yield, recovery period, LRL, HI and WD (Van Minnen et al., 2006b).

<sup>e</sup> AGF is the growth rate of a plantation (i.e. FNPP<sub>CP</sub>) compared to the average growth (i.e. NPP) of the natural land-cover type that best matches the tree species considered (see Van Minnen et al., 2006b for more details).

### Energy crops

As in IMAGE 2.3, a separate land-cover type is assigned to energy crops. Three energy crops are distinguished: sugarcane, maize and 'wood' (i.e. fast growing tree species like poplar and willow in short rotation cycles) (see also chapter 5). This allows us to model (i) the interaction or even competition between agricultural land for growing either energy or food and feed crops and (ii) the consequences for the C cycle to use abandoned agricultural land to grow either energy crops, carbon plantations or let it recover to a (more or less) natural state (Van Vuuren et al., 2006). The parameters in the carbon cycle model are set to focus on growing energy crops capturing 'energy' (and thus carbon) instead of maximizing the size of the 'edible' parts. This is also shown in Table 7.1, where the NPPI values of energy crops (i.e., the main parameter determining the outcome of the NPP simulation) are much higher than the average values for agricultural land. These NPPI values were obtained by matching the energy crop results of the C cycle model as much as possible with the agricultural model (in terms of C). In order to match the energy crop yields in different latitudinal belts, the temperature/ photosynthesis response curves also had to be adapted for energy crops.

## 7.3 Sensitivity analysis

A number of experiments have been performed with IMAGE 2.3 to analyze the consequences of uncertainties in various biogeochemical and migration processes for the C cycle. The experiments use the IPCC-SRES A1b scenario (Nakicenovic et al., 2000)

as baseline. A1b represents an intermediate scenario in terms of anthropogenic drivers and, consequently, emissions of greenhouse gases and deforestation. For example, the global CO<sub>2</sub> emission in 2100 for A1b is 17.6 Pg C yr<sup>-1</sup>, which is in the range of 6.2 (B1 scenario) to 30.9 Pg C yr<sup>-1</sup> (A2). The effect of greenhouse gas emissions on global climate change is based on a medium-climate sensitivity of 2.5°C for a doubling of the CO<sub>2</sub> concentration relative to the pre-industrial era. Regional temperature and precipitation changes are derived from downscaling global values using the output of the HadCM2 model (GCM of the Hadley Centre). The effects of using alternative climate models and climate sensitivities can be found in Leemans et al. (2002).

All experiments except the baseline assume a constant land-use pattern. Although the IMAGE model is explicitly designed to deal with land-use change, such changes are excluded here in order to focus on the effects of vegetation response for the terrestrial C cycle per se. Furthermore, without land-use change our results can be compared more easily with other studies which seldom consider land-use changes. As an illustration, we show the A1b baseline results with and without considering land-use change (Table 7.4). This allows for comparing the importance of biophysical and biogeographical processes for the C cycle with that of land-use change.

The experiments vary in terms of the assumptions made regarding biogeochemical processes and migration of plants as they respond to climate change. They are grouped in five sets of experiments (Table 7.4), focusing on CO<sub>2</sub> fertilization, NPP response to climate, migration and soil respiration. A final set comprises combined experiments to investigate interactions between processes.

In the first set of experiments we vary parameters that determine the CO<sub>2</sub> fertilization effect in IMAGE 2.3. The initial CO<sub>2</sub> fertilization factor  $\beta_{ini}$  (equation 4) is assumed to be 0.7. This implies a maximum of 70% NPP increase at a doubled CO<sub>2</sub> concentration, assuming that other factors are not limiting. Because of the two multipliers, the actual fertilization factor  $\beta_{i,m}$  is lower (globally 0.43 over the year) with a considerable variation in biomes and time. For example, the value is 0.2 for boreal forest in winter and 0.51 for tropical forest (Brinkman et al., 2005). The value of the fertilization factor is uncertain. Harvey (1989) and Alexandrov et al. (2003) proposed a value of between 0.3 and 0.6, whereas Cao and Woodward (1998) expected a saturation of the effect on the longer term, and Heath et al. (2005) and Körner et al. (2005) even questioned the existence of long-term and large-scale CO<sub>2</sub> fertilization. For analyzing the sensitivity of the C cycle model, we modified  $\beta_{ini}$  in three experiments (Table 7.4).

In the second set we vary the NPP response to changing temperature (Table 7.4). The NPP response was implemented in IMAGE by an optimum curve proposed by Woodward et al. (1995) and Larcher (2003). The effect of temperature on NPP is assumed constant after 2000 in experiment ConstTempNPP.

The third set focuses on soil respiration (Table 7.4). Uncertainties in this process may have considerable consequences for the C cycle because of the large amounts of C

Table 7.4. Experiments on the sensitivity analysis of the IMAGE 2.3 C cycle model.

Experimenta	Summary
<b>Baseline</b>	
Base_A1b	A1b SRES baseline scenario, including changes in land use.
NoLUC	A1b Baseline scenario based on HadCM2 climate model and excluding land-use changes.
<b>Set 1. CO<sub>2</sub> fertilization</b>	
(-) 0Fert	No CO <sub>2</sub> fertilization ( $\beta_{ini} = 0$ ).
(-) 50Fert	CO <sub>2</sub> fertilization is 50% of the original response ( $\beta_{ini} = 0.35$ ).
(-) ConstFert	Maintenance of the CO <sub>2</sub> fertilization effect in each grid cell at its 1995 value.
<b>Set 2. NPP response to climate</b>	
(-) ConstTempNPP	Maintenance of the NPP response to changing temperature in each grid cell at its 1995 value.
<b>Set 3. Soil respiration</b>	
(-) NewSoilresp	Soil respiration response curve of IMAGE 2.3 is replaced by the Arrhenius equation (Lloyd and Taylor, 1994) as used in the LPJ model (Sitch et al., 2003).
(+) ConstResp	Maintenance of the soil respiration response to changing climate (i.e. moisture and temperature) at its 1995 value in each grid cell.
<b>Set 4. Migration</b>	
(-) NoMigration	Migration as a response to climate change is excluded.
(+) FastMigration	Instantaneous migration in response to climate change.
<b>Set 5. Combined experiments</b>	
NoFeedbacks	All feedbacks (No CO <sub>2</sub> fertilization, temperature and moisture responses, migration) are excluded.
NoNegFb	All negative feedbacks (i.e. experiments indicated by '-', i.e. no CO <sub>2</sub> fertilization, constant temperature effect on NPP, no migration and with an Arrhenius response curve for soil respiration) are excluded.
NoPosFb	All positive feedbacks (i.e. experiments indicated by '+', i.e. constant effect of temperature and moisture on soil respiration, instantaneous migration) are excluded.
OnlyTempNPP	All feedbacks except the temperature effect on NPP are excluded.
OnlyCResp	All feedbacks except temperature and moisture effect on soil decomposition are excluded.
OnlyTempNPP_Resp	All feedbacks except the temperature effect on NPP and the temperature and moisture effect on soil decomposition are excluded.
ConstClim	Maintenance of all temperature and moisture sensitivities at 1995 values in each grid cell.

Note that not all experiments consider changes in land use, except base (A1b).

<sup>a</sup> Negative feedbacks are indicated by '(-)', positive feedbacks by '(+)'.

stored in the soil, with a mixture of decomposition rates (Davidson and Janssens, 2006). Main drivers of soil decomposition are temperature and moisture availability (Jenny et al., 1949; Knorr et al., 2005; Davidson and Janssens, 2006). In one experiment we kept soil respiration rates constant from the year 2000 onwards, ignoring changes in temperature or moisture availability (experiment ConstRes). In experiment NewSoilResp we replaced the default optimum curve of temperature on soil decomposition by the Arrhenius equation of the LPJ model (Sitch et al., 2003) (Table 7.4). The Arrhenius equation describes an exponential response of soil respiration to increasing temperatures:

particularly beyond the optimal temperature range; this leads to higher soil respiration rates compared to the standard IMAGE 2.3 approach.

In the fourth set of experiments we assume alternative migration rates of the natural land-cover types (Table 7.4). Migration of species as a response to climate change is poorly understood (Araujo et al., 2004). Higher migration rates than those derived from historical records (Davis, 1981; Huntley and Webb, 1989) may be needed to cope with climate change as anticipated in different scenarios (Leemans and Eickhout, 2004). The rates will, however, not be infinite and will differ between species, as the geographical reorganization of ecosystems is a slow process (Huntley and Webb, 1989). To assess the consequences of the uncertainty in migration rates for the terrestrial C cycle we use two alternatives (Table 7.4) that are compared to the IMAGE approach of Van Minnen et al. (2000). Ignoring the possibility of species migration (experiment NoMigration) leads to less-than-optimum or even degraded ecosystems. In the FastMigration experiment migration is assumed to occur instantaneously. This results, for example, in immediate pole-wards shifts of forests under global warming.

Finally, in the fifth set several combined experiments are included to assess interactions between processes: the overall role of climate change, on the one hand, and CO<sub>2</sub> response on the other, and the full sensitivity range of the experiments (Table 7.4). The results of the combined experiments allow comparison with other studies (e.g. Cramer et al., 2001; Joos et al., 2001; Friedlingstein et al., 2003) that focus on 'climate only' and 'CO<sub>2</sub> only'.

## 7.4 Results and discussion

In this section we summarize the main findings of the consequences for the global and regional C cycle of uncertainties in the response of the terrestrial biosphere to climate change. More details can be found in Leemans et al. (2002) and Van Minnen et al. (2006a).

Despite identical fossil-fuel related CO<sub>2</sub> emissions in the different scenarios, terrestrial C fluxes and pools differ considerably between the experiments (Table 7.5). By ignoring land-use changes since 2000 (experiment NoLUC) the NEP increases from about 2.5 Pg C yr<sup>-1</sup> in the late 1990s to about 6.8 Pg C yr<sup>-1</sup> around 2060, followed by a decline to 5.9 Pg C yr<sup>-1</sup> in 2100. If we include changes in land use (Base\_A1b), the NEP is projected to increase continuously up to 2100 due to increasing abandonment of agricultural land (Table 7.5).

Global NEP reaches 7.4 Pg C yr<sup>-1</sup> in 2100 when ignoring all positive feedbacks (experiment NoPosFb), whereas it remains approximately constant at 0.7 Pg C yr<sup>-1</sup> if all feedbacks (CO<sub>2</sub> and climate) are ignored, while the terrestrial biosphere turns into a source of C if all negative feedbacks are excluded (NoNegFb) or if only the climate effect on soil decomposition is considered (OnlyCResp).

Table 7.5. Global terrestrial C pools and fluxes for the different experiments.

	NPP <sup>a</sup> (Pg C yr <sup>-1</sup> )		NEP <sup>b</sup> (Pg C yr <sup>-1</sup> )		Living biomass <sup>c</sup> (Pg C)		Soil carbon <sup>d</sup> (Pg C)	
	2050	2100	2050	2100	2050	2050	2050	2100
<b>Baseline</b>								
Base_A1b	77	86	6.3	6.6	535	613	1675	1801
NoLUC	77	89	6.4	5.9	641	779	1684	1842
<b>Set 1. CO<sub>2</sub> fertilization</b>								
0Fert	62	64	1.4	1.3	562	602	1583	1585
50Fert	70	78	4.1	3.9	606	701	1639	1729
ConstFert	65	67	1.7	1.4	582	627	1616	1627
<b>Set 2. NPP response to climate</b>								
ConstTempNPP	75	85	5.2	4.6	629	743	1669	1787
<b>Set 3. Soil respiration</b>								
NewSoilresp	77	90	5.7	5	642	784	1699	1813
ConstResp	76	87	7.4	7.2	639	768	1710	1934
<b>Set 4. Migration</b>								
NoMigration	76	86	5.5	4.4	632	738	1676	1800
FastMigration	77	89	6.8	6.3	650	793	1690	1880
<b>Set 5. Combined experiments</b>								
NoFeedbacks	58	57	0.8	0.9	531	533	1585	1602
NoNegFb	58	57	-1.6	-1.9	531	529	1562	1445
NoPosFb	77	88	7.6	7.4	647	781	1715	1944
OnlyTempNPP	60	62	2.2	2.4	547	573	1603	1666
OnlyCResp	58	57	-0.4	-0.5	531	533	1555	1502
OnlyTempNPP_Resp	60	62	0.9	0.8	547	574	1573	1563
ConstClim	74	84	5.9	5.4	623	726	1692	1860

Note that positive fluxes represent a carbon uptake by the biosphere.

<sup>a</sup> 1970-1980 average NPP is 58 Pg C yr<sup>-1</sup>; NPP for 2000 ranges from 58 to 62 Pg C yr<sup>-1</sup>.

<sup>b</sup> 1970-1980 average NEP is 0.6 Pg C yr<sup>-1</sup>; NEP for 2000 ranges from 0.5 to 2.7 Pg C yr<sup>-1</sup>.

<sup>c</sup> 1970-1980 average living biomass is 537 Pg C; biomass for 2000 ranges from 450 to 550 Pg C.

<sup>d</sup> 1970-1980 average value for the global soil carbon pool is 1572 Pg C and 1598 Pg C for the NewSoilResp experiment; the global soil carbon pool for 2000 ranges from 1493 to 1600 Pg C.

The differences in terrestrial C fluxes and pools cause large differences in atmospheric composition and global climate (Table 7.6). For example, the CO<sub>2</sub> concentration in 2100 varies, respectively, from 749 to 696 ppm in the baseline with and without changes in land use, and from 658 to 946 ppm in the experiments (see also Van Minnen et al., 2006a).

The analysis of the importance of individual biogeochemical feedbacks for the global C pools and fluxes (Table 7.5, set 1) shows the dominant role of CO<sub>2</sub> fertilization. If we ignore CO<sub>2</sub> fertilization (0Fert), the global NPP and NEP are projected to increase by only 5.4 and 0.7 Pg C yr<sup>-1</sup>, respectively, between 2000 and 2100, compared to 31.5 Pg C and 5.3 Pg C in the baseline. It should be noted that the parameter setting of the CO<sub>2</sub> fertilization in IMAGE is at the high end of the scale in the literature. But even if we assume a 50% lower CO<sub>2</sub> fertilization effect (50Fert), the C pools and fluxes are projected

Table 7.6. Atmospheric CO<sub>2</sub> concentration, global mean temperature change and global mean precipitation change for 2050 and 2100 for the different experiments.

	Atmospheric CO <sub>2</sub> concentration (ppmv)		Global mean temperature change <sup>a</sup> (°C)		Global mean precipitation change <sup>a</sup> (mm yr <sup>-1</sup> )	
	2050	2100	2050	2100	2050	2100
<b>Baseline</b>						
Base_A1b	560	749	2.0	3.4	29	58
NoLUC	527	696	1.9	3.2	26	55
<b>Set 1. CO<sub>2</sub> fertilization</b>						
0Fert	590	854	2.1	3.7	29	62
50Fert	555	765	2.0	3.4	29	58
ConstFert	572	831	2.0	3.6	29	62
<b>Set 2. NPP response to climate</b>						
ConstTempNPP	537	729	1.9	3.3	26	51
<b>Set 3. Soil respiration</b>						
NewSoilresp	532	714	1.9	3.3	26	55
ConstResp	519	666	1.9	3.1	26	55
<b>Set 4. Migration</b>						
NoMigration	533	726	1.9	3.3	26	55
FastMigration	523	685	1.9	3.2	26	51
<b>Set 5. Combined experiments</b>						
NoFeedbacks	600	873	2.2	3.7	33	62
NoNegFb.	619	946	2.2	3.9	33	69
NoPosFfb	515	658	1.8	3.1	26	51
OnlyTempNPP	588	833	2.1	3.6	29	62
OnlyCResp	611	911	2.2	3.8	33	66
OnlyTempNPP_Resp	599	872	2.2	3.7	29	62
ConstClim	531	708	Constant climate			

<sup>a</sup> Compared to the 1961-1990 average.

to change more than with climate-induced feedback processes. The dominance of the CO<sub>2</sub> fertilization effect is in line with other modelling studies that have compared the role of CO<sub>2</sub> with the effect of climate change (Cramer et al., 2001; Joos et al., 2001; Friedlingstein et al., 2003).

Despite the projected prominent role of CO<sub>2</sub> fertilization, the climate-driven feedbacks also have considerable effects on the global land cover, and C pools and fluxes (Table 7.5). If all climate feedbacks are ignored (experiment ConstClim), the C storage in vegetation is projected to increase by 7% less than in the baseline, whereas soil C storage exceeds the baseline by 1%. This 1% exceedance is caused by the response of soil decomposition to changing temperatures and soil moisture availability. The relevance of this response for the terrestrial C cycle can be illustrated by comparing the baseline with the experiment with a constant response (experiment ConstSoilResp) and the experiment that excludes all feedbacks except this respiration response (experiment OnlyCresp). In the case of a constant response, soil decomposition is projected to decrease and more C is stored in the soil (despite the smaller input from the vegetation), resulting in a 22%

Table 7.7. Global mean NEP in  $g\ m^{-2}\ yr^{-1}$  for different ecosystem types.

	Boreal forest		Tropical rainforest		Savanna		Scrubland		Grassland	
	2050	2100	2050	2100	2050	2100	2050	2100	2050	2100
<b>Baseline</b>										
Base_A1b	93	101	157	171	74	46	64	30	44	30
NoLUC	87	92	130	103	49	27	44	44	40	33
<b>Set 1. CO<sub>2</sub> fertilization</b>										
0Fert	29	33	15	11	3	-3	0	5	12	10
50Fert	61	66	78	64	28	14	25	27	28	23
ConstFert	35	36	19	13	6	-3	5	8	13	11
<b>Set 2. NPP response to climate</b>										
ConstTempNPP	53	53	128	110	43	26	36	36	27	21
<b>Set 3. Soil respiration</b>										
NewSoilresp	82	86	112	83	42	20	42	41	40	31
ConstResp	112	126	132	101	52	29	51	50	54	52
<b>Set 4. Migration</b>										
NoMigration	82	70	128	103	36	23	24	20	25	15
FastMigration	108	126	132	106	39	28	47	45	42	35
<b>Set 5. Combined experiments</b>										
NoFeedbacks	21	28	14	16	-9	-13	3	3	6	4
NoNegfb	-26	-41	-15	-10	-14	-11	-15	-12	-17	-20
NoPosfb	129	153	133	103	43	30	51	51	54	53
OnlyTempNPP	57	69	19	15	-4	-10	10	8	20	21
OnlyCResp	-9	-8	8	12	-14	-17	-6	-3	-8	-11
OnlyTempNPP_Resp	28	31	13	10	-8	-14	3	2	6	3
ConstClim	76	73	127	103	47	28	42	37	37	37

Initial value is the average NEP for the period 1970-1980; for boreal forest this is  $17\ g\ C\ m^{-2}\ yr^{-1}$ ; for tropical rainforest 14, for savanna -2, for scrubland 7 and for grassland  $10\ g\ C\ m^{-2}\ yr^{-1}$ .

increased NEP by 2100. If we only include the temperature effect on soil decomposition, the terrestrial biosphere is projected to turn into a C source around 2050.

Likewise, if we change the NPP response to changing temperatures (ConstTempNPP) or exclude migration (NoMigration), the global NEP in 2100 is projected to be about 25% lower than in the baseline. This lower projection results from a degradation of ecosystems under the changing climate conditions when migration is not allowed in IMAGE. In contrast, allowing instantaneous migration (FastMigration) the global forest area, in particular, is projected to increase (Van Minnen et al, 2006a), resulting in a 7% higher NEP compared to the baseline.

Regionally, the differences between the experiments are even larger than at the global scale (Table 7.7; Figure 7.1). Without any feedback process (NoFeedbacks), NPP and NEP of most land-cover types remain constant, while savanna biomes even become a small C source. If we ignore negative feedback processes (NoNegFb), all biomes turn into a source of C.

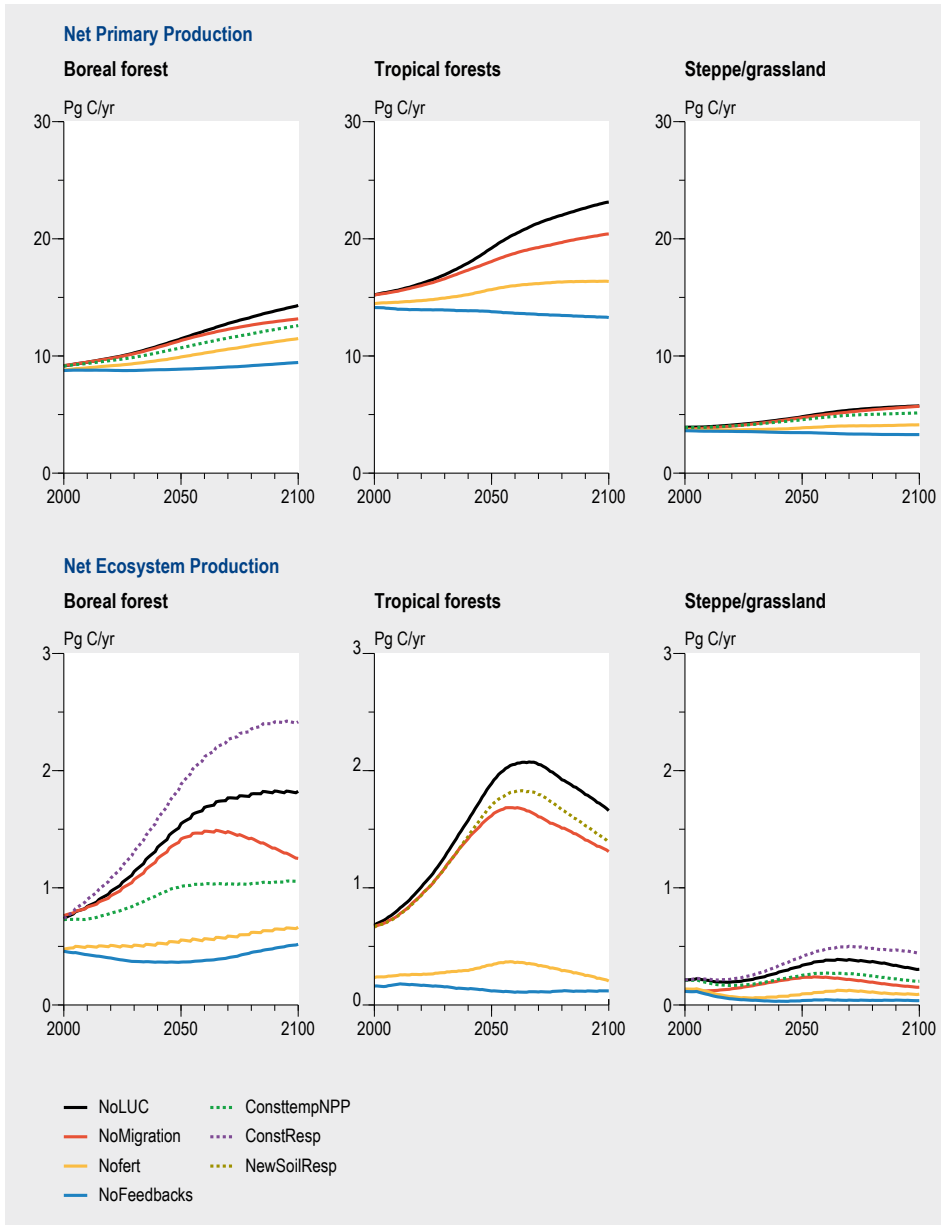


Figure 7.1. NPP (left panel) and NEP (right panel) for important biomes in different model experiments dealing with the C cycle.

CO<sub>2</sub> fertilization is also the dominating process for the C pools and fluxes on the regional scale (Table 7.7; Figure 7.1). Without CO<sub>2</sub> fertilization (NoFert), tropical forests in South America and Asia turn from a sink into a (small) C source, whereas African tropical forests remain a C sink. The most important climate feedback for the terrestrial C cycle in tropical regions is soil decomposition. Outside the tropical regions other

feedback processes are more relevant. The projected 60% increase of the NPP in boreal forests in 2100, for example, is the result of a combination of all processes.

Temperature has a considerable impact on soil decomposition at high latitudes. Boreal forests are projected to change into a source of C if we consider only the temperature effect on soil decomposition (OnlyCresp). Alternative migration assumptions lead to considerable differences in projected C pools and fluxes in boreal forests, savanna and grassland around the world. The boreal forest extent shows a particularly large variation in the experiments, ranging from a reduction of 12% assuming a fast migration in some experiments to a 15% increase in many others. Due to this considerable reduction in area, alternative migration assumptions have an even larger effect on total NPP of boreal forests than CO<sub>2</sub> fertilization.

The experiments in sets 1-4 suggest a larger sum of individual responses than the effect of combined experiments due to non-linearities (NoFeedbacks, NoNegFb, NoPosFb). This shows the importance of considering the biospheric responses to various drivers, both simultaneously and in a geographically explicit manner. Furthermore, the differences between the experiments, in terms of assumptions on the migration capabilities of ecosystems, show the need for a better understanding of the spatial dynamics of the response of the biosphere to climate change.

In our baseline A1b scenario we did not see a shift from a global terrestrial sink into a source of C for the period 2050-2100, as shown by other model exercises (e.g. Cox et al, 2004; Sitch et al., 2003). In these studies, the tropics turn into a major source of C due to declining NPP, while soil respiration in the rest of the world increases more rapidly than NPP as a result of climate warming.

We also project a declining NEP in tropical regions without CO<sub>2</sub> fertilization (i.e. under climate change only). NPP is projected to decrease due to beyond-optimal temperatures and increasing moisture stress, whereas soil respiration is projected to increase (especially in the NewSoilResp experiment). However, the decline in the tropics is smaller than in other studies (e.g. due to less drought stress) and is counterbalanced by increased NEP in other parts of the world (especially boreal forests, showing a large response to increasing CO<sub>2</sub> levels).

Some results can be used to compare with observations and results of more complex Dynamic Global Vegetation Models (DGVM). A few examples will be discussed here; more details are given by Van Minnen et al. (2006a). The NPP in the 1990s, calculated by IMAGE (61 Pg C yr<sup>-1</sup>), is within the ranges of observations (54-63) and other model applications (55-65 Pg C yr<sup>-1</sup>) (Cramer et al., 2001; Zaehle et al., 2005). Li et al. (2003) and Krankina et al. (2004) reported a contemporaneous NEP of 0.4 Mg C ha<sup>-1</sup> yr<sup>-1</sup> and 0.36 Mg C ha<sup>-1</sup> yr<sup>-1</sup> for Canadian and Russian boreal forest, respectively, whereas IMAGE predicts 0.4-0.5 Mg C ha<sup>-1</sup> yr<sup>-1</sup> and 0.3-0.4 Mg C ha<sup>-1</sup> yr<sup>-1</sup> for boreal forest in the corresponding countries. We may slightly underestimate the C fluxes in tropical forest,

having a NEP of  $0.5 \text{ Mg C ha}^{-1} \text{ yr}^{-1}$  compared to  $0.6\text{-}0.9 \text{ Mg C ha}^{-1} \text{ yr}^{-1}$  (Prentice et al., 2001) and  $0.7 \text{ Mg C ha}^{-1} \text{ yr}^{-1}$  (Baker et al., 2004).

With respect to the simulated C cycle up to the year 2100, the global soil respiration flux and vegetation C pools are comparable to outcomes of various DGVMs. The projected NPP and the resulting NEP for 2050 and 2100 are also within the range of other studies (albeit at the high end), while the projected soil biomass pools exceed the range. The maximum projected NEP, for example, is  $6.8 \text{ Pg C yr}^{-1}$  (around 2050) compared to  $5.0 \pm 2.5 \text{ Pg C yr}^{-1}$  for the average across a range of DGVMs (Cramer et al., 2001) and  $5.4 \pm 2.7 \text{ Pg C yr}^{-1}$  for LPJ in combination with a number of climate models (Schaphoff et al., 2006). Many model studies including IMAGE show a decrease in NEP during the second half of the 21<sup>st</sup> century (White et al., 2000; Cramer et al., 2001; Friedlingstein et al., 2003).

## 7.5 Concluding remarks

Based on the agreement with observations and similar trends with other modelling studies, we conclude IMAGE to be an appropriate model for describing the global and continental dynamics of the terrestrial C cycle. We have shown that the terrestrial biosphere will probably store an increasing amount of C in the decades to come, although there are large regional differences. This will slow down the build-up of atmospheric  $\text{CO}_2$  concentrations caused by human emissions. The enhanced sink function will decrease towards the end of the 21<sup>st</sup> century and the terrestrial biosphere may even turn into a net C source. This would imply stringent mitigation measures to achieve stabilization of GHG in the atmosphere.

We recognize that there are large uncertainties, especially in terms of  $\text{CO}_2$  fertilization. The sensitivity analysis showed a considerable variation among the experiments in C fluxes and pools, indicating the uncertainty of the response of the terrestrial biosphere to climate change. The relevance of the different feedback mechanisms depends on the scale considered. On the global scale, the most important process for the terrestrial C cycle is the  $\text{CO}_2$  fertilization effect. Even when halving the NPP response to increasing  $\text{CO}_2$  levels,  $\text{CO}_2$  fertilization remains the dominant process. Other feedback processes are mainly relevant at the regional scale.

The dominant role of  $\text{CO}_2$  fertilization in the global and regional C cycle is in agreement with other modelling studies (Sitch et al., 2003). However, our understanding of the large-scale and long-term  $\text{CO}_2$  fertilization effect is still poor (Heath et al., 2005). The feasibility of the large increase in terrestrial C uptake (globally up to  $6 \text{ Pg C yr}^{-1}$ -regionally a doubling or even tripling of the current-day growth in boreal forests) is questionable, because other environmental constraints (e.g. nutrient availability) may limit growth and thus the  $\text{CO}_2$  fertilization effect (Alexandrov et al., 2003; Körner et al., 2005).

The series of model experiments with the C cycle model had a number of problems which we hope to solve in future updates of the model. Firstly, some of the projections are high compared to other modelling studies, mainly due to the strong NPP response to changes in atmospheric CO<sub>2</sub>. Furthermore, not all relevant processes are included in the IMAGE 2.4 model. For example, disturbances such as forest fires and pests are not included, whereas they may have considerable impacts, for example, in the tropics (Cramer et al., 2004) and boreal regions (Li et al., 2003), particularly if disturbances change in extent or frequency. Furthermore, the IMAGE 2.4 model does not account for biophysical effects such as changes in albedo caused by land-cover changes. In chapter 9 these biophysical responses are shown relevant for climate change.

The analysis and comparison with other studies and observations, as described in this chapter, has resulted in an adaptation of the C cycle parameters in IMAGE 2.4, in particular, the 50% reduction of the CO<sub>2</sub> fertilization factor. Other limitations, such as the omission of fires and albedo, will be captured when the IMAGE framework is extended by a Dynamic Global Vegetation Model (DGVM) coupled to a General Circulation Model for use in detailed climate-change studies (see chapter 9). Nevertheless, a realistic representation of all C cycle processes at every temporal and spatial scale will remain a major challenge for researchers for many years to come. The C cycle model described in this chapter will continue to be part of IMAGE for scenario studies focusing on global environmental studies on sustainable development.

## 8 MODELLING THE FATE OF NUTRIENTS THROUGH THE SOIL AND HYDROLOGICAL SYSTEM

- IMAGE 2.4 includes a new module to assess the consequences of changing population, the economy and technological development for surface nutrient balances, and reactive nitrogen emissions from point sources and non-point sources. The calculations are spatially explicit to demonstrate the large-scale and trans-boundary effects of local emissions released into the environment.
- Processes accounted for in this module are human emissions, wastewater treatment, surface nitrogen and phosphorous balances for terrestrial systems, ammonia emissions, denitrification and  $N_2O$  and  $NO$  emissions from soils, leaching of nitrate, and transport and retention of N in groundwater and surface water. In order to derive spatially explicit scenarios, tools were developed to translate regional or country-specific information into grid-specific input parameters.
- The new module allows for assessing N and P surface balances and the consequences of surpluses for emissions of reactive N to air, groundwater and surface water. In addition, policy options can be assessed by modifying various technical coefficients and effects of the N cascade.

### 8.1 Introduction

Human activities have accelerated the Earth's nitrogen (N) cycle by increasing the natural rate of N fixation (Galloway et al., 2004). Nitrogen fixation is the transformation of the highly abundant but biologically unavailable atmospheric dinitrogen ( $N_2$ ) to 'reactive' reduced and oxidized N forms such as ammonia ( $NH_3$ ), nitrate ( $NO_3$ ), nitrous oxide ( $N_2O$ ) and nitric oxide ( $NO$ ).

Specialized algae and bacteria, either free-living or in a symbiotic relationship with higher plants, especially legumes cause biological N fixation. Estimates of biological N fixation in marine systems range from  $<30$  Tg to  $>300$  Tg  $yr^{-1}$  (Tg, teragram; 1 Tg =  $10^{12}$ g) (Vitousek et al., 1997). Biological N fixation in natural terrestrial ecosystems accounts for 100-290 Tg  $yr^{-1}$  (Cleveland et al., 1999). Lightning causes further natural N fixation ( $<10$  Tg  $yr^{-1}$ ) (Galloway et al., 2004). Anthropogenic N fixation occurs in N fertilizer (80 Tg  $yr^{-1}$ ) and energy ( $\sim 30$  Tg  $yr^{-1}$ ) production as well as in the cultivation of leguminous crops in agricultural systems (40 Tg  $yr^{-1}$ ) (Galloway et al., 2004). The resultant total human-induced increase of global N fixation is about 150 Tg  $yr^{-1}$ .

While most of the reactive N emissions occur locally in the terrestrial system, the influence of these emissions spreads regionally and globally as they move through water and air across political and geographic boundaries causing eutrophication. The process of eutrophication is the biogeochemical response to enrichment with plant nutrients, primarily N and P (phosphorus).

Atmospheric N deposition rates onto the Earth's surface have increased from threefold to more than tenfold since pre-industrial times (Galloway et al., 2004). In terrestrial ecosystems eutrophication caused by increased N deposition has a number of important negative impacts, including loss of biodiversity (Bobbink et al., 1998).

The problem of eutrophication of aquatic ecosystems has continued in all densely populated countries, particularly since the 1950s, and is affecting lakes, reservoirs, estuaries and coastal seas (Vollenweider, 1992). Harmful effects of eutrophication in coastal marine systems have been spreading rapidly, with large-scale implications for biodiversity, water quality, fisheries and recreation in both industrialized and developing regions (UNEP, 2002). In freshwater and coastal marine systems it is not only the inputs of N but also the alteration of the stoichiometric balance of N, P and silica (Si) (Rabalais, 2002) that affect both the total production and quality. In combination with increased N fluxes during the past decades, similar changes have occurred with P (Smith et al., 2003), while the Si loads have remained constant or even decreased in many rivers, primarily as a result of dam construction (Conley, 2002). When diatom growth is compromised by Si limitation, non-diatoms may be competitively enabled, with a dominance of flagellated algae, including noxious bloom-forming communities (Turner et al., 2003). Thus food web dynamics leading to fishery harvests are affected by shifts in the relative availability of N, P and Si.

IMAGE 2.4 now includes approaches to assess the consequences of changing population, the economy and technological development for nutrient (N and P) emissions from both point and non-point (diffuse) sources. Such approaches were absent in earlier versions of IMAGE. In addition, scenarios for fertilizer use were based on economic development only, without considering agricultural production and efficiency of nutrient use.

The IMAGE 2.4 calculations discussed in this chapter are spatially explicit to allow demonstration of the large-scale and trans-boundary effects of local emissions that are spread in the environment. The new approach consists of a number of elements such as: (i) sewage effluents from point sources, including wastewater from households and industrial activities; (ii) surface N and P balances for non-point sources; (iii) NH<sub>3</sub> emissions for non-point sources; (iv) denitrification in soils; (v) nitrous oxide and nitric oxide emissions to air; (vi) leaching of nitrate from the subsoil to groundwater; (vii) transport and retention of N in groundwater and surface water; and (viii) tools for construction of scenarios. These new elements will be briefly discussed in the subsequent sections 8.2-8.4. Although the method for calculating the river export of particulate P was presented by Beusen et al. (2005), handling the surplus of P (soil P fixation, erosion and re-deposition within river basins, and P leaching) has yet to be worked out. Section 8.5 provides an example of the kind of results that can now be generated by IMAGE 2.4.

## 8.2 Point sources

The basis of the calculation of emissions from point sources is the conceptual relationship from Van Drecht et al. (2003) between per capita human N emission from human excreta and other household and industrial wastes, and per capita income:

$$N_{em} = 8 + 11(GDP / 43,639)^{0.5} \quad (1)$$

where  $N_{em}$  is the per capita daily human N emission (g per person per day) and  $GDP$  the per capita gross domestic product (1995 US\$ per capita per year). The  $GDP$  for each country is divided by 43,639, the world's highest per capita  $GDP$  in 1995 (Switzerland). Low-income countries have human per capita N emissions of about 10 g per day; for industrialized countries these emissions amount to between 15 and 18 g per day. Data for a number of industrialized countries show good agreement with equation (1) (Van Drecht et al., 2003).

The amount of N that is actually discharged to surface water is estimated as follows:

$$N_{sw} = (1 - R) D N_{em} \quad (2)$$

where  $N_{sw}$  is the net N emission to surface water (g per person per day),  $R$ , the removal of N in wastewater treatment expressed as a fraction of the N influent to treatment plants, and  $D$  the fraction of the population connected to sewerage systems.  $D$  is known for most OECD countries from the literature for at least one year in the period of 1970 to 1995. For years where no data are available,  $D$  is calculated from the trend, in the product of the urban population fraction and the fraction of the urban population with access to improved sanitation.

This implies an exclusion of human N emissions from the rural population in these cases (mainly developing countries) (Figure 8.1). Access to improved sanitation differs between rural and urban areas. For industrialized countries access is generally 100% for both rural and urban populations, while outside Europe, sewerage systems in rural areas are rare. Particularly in the rural areas of many developing countries, human waste is commonly collected in latrines or septic tanks; we assume that this waste does not enter the surface water (Figure 8.1).

The removal of nitrogen ( $R$ ) is calculated as the weighted average of no treatment, and mechanical, biological and advanced treatment. Data on the distribution over the different types of treatment are known for most European countries (EEA, 1998; Eurostat, 2000). Data for other countries rely on various sources. For countries where no data were found to estimate  $R$  we use regional estimates on the basis of primarily WHO/UNICEF (2000). In most developing countries the overall N removal rate is low, because advanced and biological treatment systems are not widespread. Errors in the estimated effluent from sewerage systems in developing countries are therefore small.

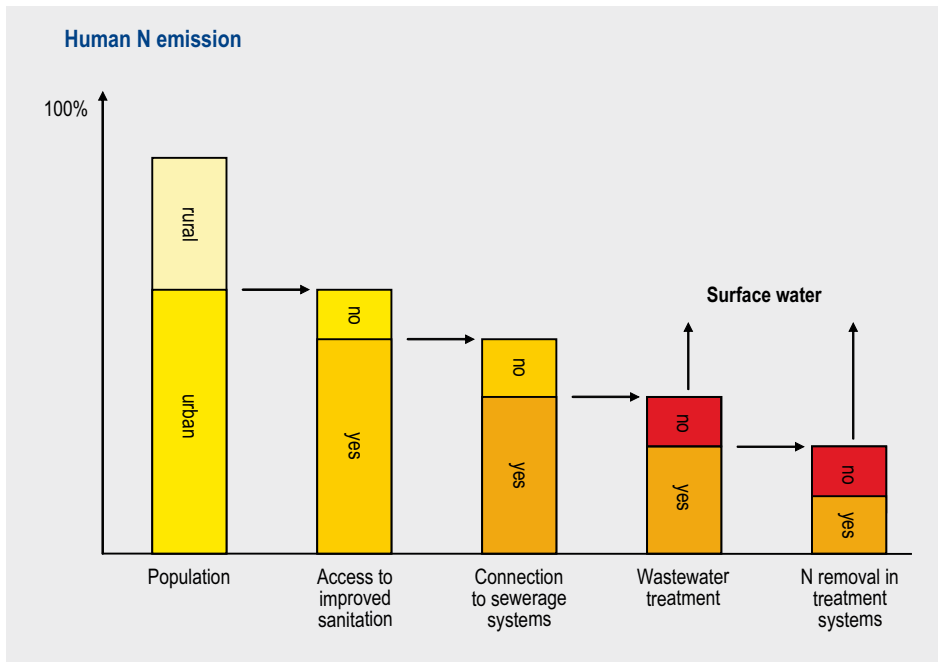


Figure 8.1. Scheme showing estimation of sewage N effluent to surface water.

To obtain spatially distributed estimates for the total N emission from point sources, we use 0.5 by 0.5 degree spatial data on population density for urban and rural areas (Van Drecht et al., 2003) and projections for population and per capita GDP.

### 8.3 Non-point sources

#### *Surface balance approach*

Since we focus on the geographic distribution of the fate of N and P in the environment, the surface balance approach considering all relevant input and output terms for a given land area is more appropriate than farm-gate or system balances. Farm-gate or whole system budgets or balances consider the N and P input, output and total loss to the farm or system considered without specifying where and in which form losses occur (Van der Hoek and Bouwman, 1999).

The annual surface N balance (Figure 8.2) includes the N inputs and outputs for a given area of land, here 0.5 by 0.5 degree grid cells. N inputs include biological N fixation ( $N_{\text{fix}}$ ), atmospheric N deposition ( $N_{\text{dep}}$ ), application of synthetic N fertilizer ( $N_{\text{fert}}$ ) and animal manure ( $N_{\text{man}}$ ). Outputs in the surface N balance include N removal from the field by crop harvesting, hay- and grass-cutting, and grass consumption by grazing animals ( $N_{\text{exp}}$ ). The surplus of the surface N balance ( $N_{\text{sur}}$ ) is calculated as follows:

$$N_{\text{sur}} = N_{\text{fix}} + N_{\text{dep}} + N_{\text{fert}} + N_{\text{man}} - N_{\text{exp}} \quad (3)$$

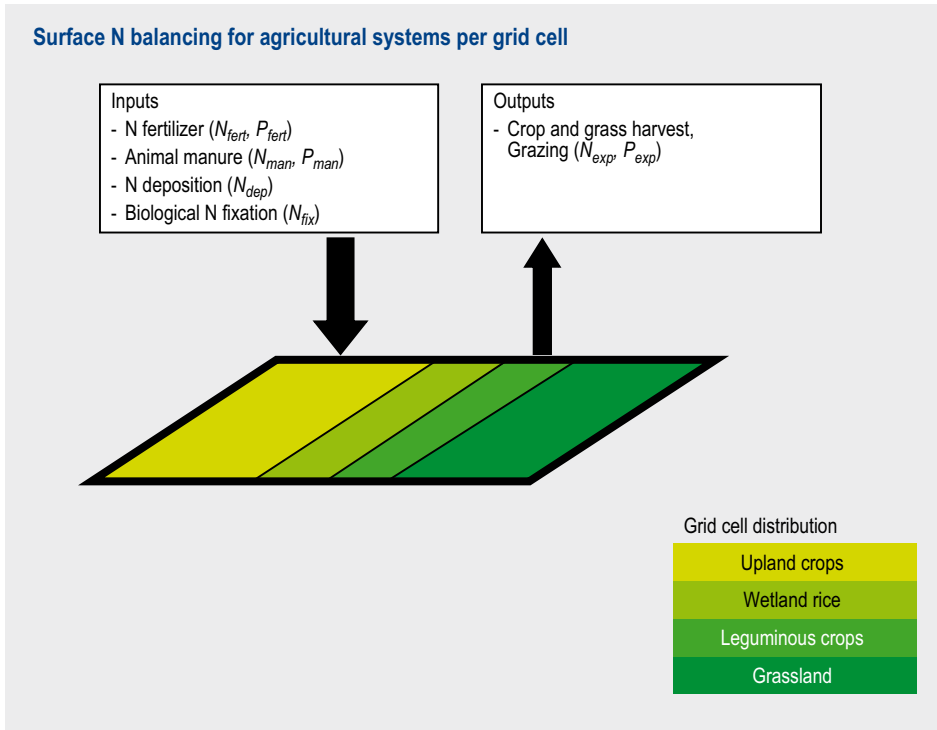


Figure 8.2. Surface N balancing for agricultural systems within each 0.5 by 0.5 degree grid cell in IMAGE 2.4.  $N_{sur}$  is defined as the difference between N inputs and outputs according to equation (1).  $N_{sur}$  is subject to  $NH_3$  volatilization, denitrification or leaching. The steady-state N surface balance approach does not account for changes in soil N.

The surface N balancing is a steady state approach, not taking into account change of N in soil organic matter.  $N_{sur}$  is subject to  $NH_3$  volatilization, denitrification and leaching (see below).

For P the same method is used, with the exception that the surplus of P is primarily fixed in soils. Although the method for calculating river export of particulate P has been presented by Beusen et al. (2005), the handling of the P surplus, erosion and re-deposition within river basins, and P leaching of P, has yet to be worked out.

Each IMAGE agricultural 0.5 by 0.5 degree grid cell consists of fractions of grassland, rice, temperate cereals, maize, tropical cereals, pulses, root and tuber crops, oilcrops and other crops. These categories are aggregated into four broad groups, including grassland (which is further divided into pastoral grassland and grassland in mixed systems, see chapter 5), wetland rice, leguminous crops (pulses, soybeans) and other upland crops (Figure 8.2). Leguminous crops are considered as a separate group because they can fix atmospheric N, while wetland rice is a special case for N cycling because of the hydrological conditions promoting denitrification and leaching,  $NH_3$  volatilization and N fixation. The different input and output terms of the surface balance are discussed briefly below.

$N_{\text{fix}}$  N fixation by pulses and soybeans is calculated from the crop production data (FAO, 2005) and N content for these crops. Total biological N fixation in biomass during the growing season of pulses and soybeans is calculated by multiplying the N in the harvested product by a factor of 2 to account for all above- and below-ground plant parts (i.e. according to Mosier et al., 1998). Furthermore, we use a rate of non-symbiotic N fixation of  $5 \text{ kg ha}^{-1}\text{yr}^{-1}$  for non-leguminous upland crops and grassland, and  $25 \text{ kg ha}^{-1}\text{yr}^{-1}$  for wetland rice as proposed by Smil (1999).

Biological N fixation of atmospheric N in natural ecosystems was estimated on the basis of N fixation rates taken from the inventory of Cleveland et al. (1999). The biological N fixation rates were combined with the spatial distribution of 17 types of natural ecosystems and areas of crops and grassland.

$N_{\text{dep}}$  In the current IMAGE 2.4 model there is no chemistry-transport model to compute atmospheric deposition rates from the emission fields for  $\text{NO}_x$  and  $\text{NH}_3$ . Therefore, in the work published by Bouwman et al. (2005b) and Bouwman et al. (2005d) the atmospheric N deposition rates for the current situation were calculated with the STOCHEM model (Collins et al., 1997), and deposition rates for historical and future years were obtained by scaling the current deposition fields for the mid-1990s using emission inventories for N gases for the corresponding years (IMAGE-team, 2001; Olivier et al., 2001). In more recent studies (and in this chapter) we used deposition estimates from Dentener et al. (2006).

$N_{\text{fert}}$  and  $P_{\text{fert}}$  We use country data from IFA/FAO/IFDC (2003) on N and P fertilizer application rates by crop for the mid-1990s, and subnational data for the U.S.A. (AAPFCO/TFI, 2006), and China (China National Bureau of Statistics, 2006a; China National Bureau of Statistics, 2006b; USDA, 2006). These data were aggregated to obtain application rates for grassland, wetland rice, leguminous crops and other upland crops. For years prior to 2000 the application rates are multiplied by the change in crop yield obtained from FAO (2005), ignoring changes in efficiency of N and P uptake by crops.

$N_{\text{man}}$  and  $P_{\text{man}}$  For animal manure inputs we use constant N and P excretion rates per head for large ruminants (dairy and nondairy cattle, buffaloes), small ruminants (sheep and goats), pigs, poultry, horses, asses, mules and camels obtained from Van der Hoek (1998). This implies that the N and P excretion per unit of product depends on the animal productivity, i.e. the manure production decreases with increasing milk and meat production per animal. Animal stocks are obtained from FAO (2005) and subnational data for the U.S.A. from AAPFCO/TFI (2006); for China from the China National Bureau of Statistics (2006a, b) and USDA (2006). The livestock production for each animal category is divided into mixed and landless and pastoral systems using data from Bouwman et al. (2005c) and US-EPA (2006) (see chapter 5). Within each system the manure is distributed over grazing, housing and storage systems, and other uses (Figure 8.3). The fraction grazing is derived from the ratio of grass to total feed in the ration of each animal category, as discussed in chapter 5. The data for other uses, and stored but unused manure, is primarily based on data presented by Mosier et al. (1998).

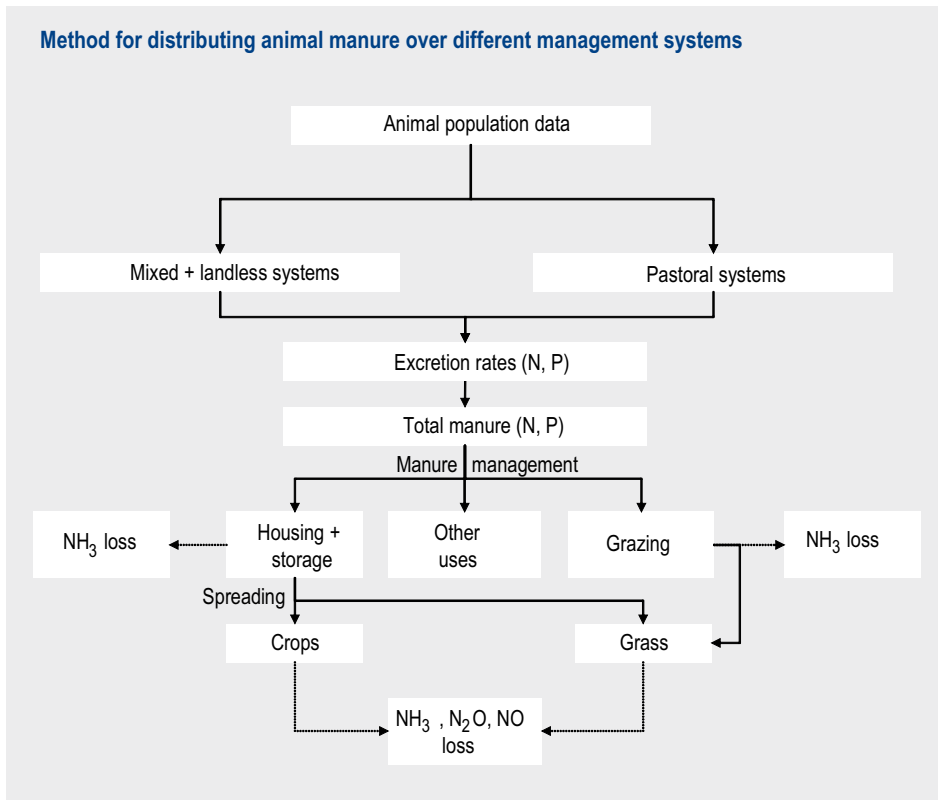


Figure 8.3. Method for distributing animal manure over different management systems.

Animal manure N and P available for application to crops and grassland is all manure in animal houses or stored manure, excluding  $\text{NH}_3$  volatilization from animal houses and storage systems, and other uses (Figure 8.3). Other uses include: (i) manure excreted outside the agricultural system, for example, in urban areas, forests and roadsides; (ii) stored manure that is not used, and (iii) manure used as a fuel or for other purposes.

In a number of countries the a priori estimates of the distribution over pastoral and mixed and landless systems, and within each system over grazing and stables and storage, and other uses, lead to unrealistic annual input rates. In such cases, the manure is redistributed until annual input rates are less than or close to pre-defined maximum rates, which are  $250 \text{ kg ha}^{-1} \text{ yr}^{-1}$  of N in mixed and landless systems and  $125 \text{ kg ha}^{-1} \text{ yr}^{-1}$  in pastoral systems. Maximum application rates reflect, for example, regulations within specific countries or regions, such as the maximum application rate for manure within the EU countries of  $170\text{--}250 \text{ kg N ha yr}^{-1}$ .

$N_{\text{exp}}$  and  $P_{\text{exp}}$ . Crop N and P export is based on crop production data from FAO (2005) for the historical period 1970–2000 with reference to 34 different crop groups, including cereals, pulses, soybeans, oilcrops, root and tuber crops, sugar, fibre and industrial

crops, fruits and vegetables, and stimulants such as coffee and tea. For the U.S.A. (AAPFCO/TFI, 2006) and China (China National Bureau of Statistics, 2006a,b; USDA, 2006) subnational data are used. The N and P removal in the harvested product is calculated from the crop production and N and P content for each crop (Bouwman et al., 2005d) and then aggregated to the broad categories wetland rice, leguminous crops and other upland crops (Figure 8.2).

To account for the production of fodder crops such as alfalfa, fodder maize and beet, which are not reported in international agricultural statistics (FAO, 2005), we use estimates for the removal of N in harvested fodder crops from the Organization for Economic Co-operation and Development (OECD, 2001) for OECD countries (Bouwman et al., 2005c). The production of fodder crops is assumed to take place on arable land, and the N removal was added to the crop N and P export for upland crops. For other countries the contribution of fodder crops to total crop N and P export is assumed to be negligible (Bouwman et al., 2005d) based on data from Bruinsma (2003). For years prior to 2000 we assume that the N and P removal in harvested fodder crops in each country was proportional to total meat production. Grass-N and P consumption was assumed to be 60% of all N inputs (manure, fertilizer, deposition, N fixation) excluding  $\text{NH}_3$  volatilization (Bouwman et al., 2005d).

We ignored N uptake in natural ecosystems, assuming that these systems would not have a net accumulation of biomass. This would be incorrect for many managed, semi-natural, or disturbed natural ecosystems, where net uptake of N occurs. However, we find this error acceptable, considering the low N inputs when compared to agricultural systems.

$N_{\text{sur}}$  and  $P_{\text{sur}}$ . The surface balance for N and P is calculated for each grid cell (Figure 8.4). Comparison with independent estimates has to be done on a nationwide scale. Bouwman et al. (2005b) compared data from OECD (2001) and Hansen (2000) and found a fair agreement between the global approach in IMAGE 2.4 and the country estimates involving very detailed analysis of the various inputs and outputs in agriculture.

### ***Ammonia volatilization***

Ammonia volatilization rates for the 10 animal categories for stables and grazing systems were taken from Bouwman et al. (1997) (Figure 8.5). Volatilization from the spreading of animal manure is calculated with the empirical model based on crop type, fertilizer type, manure or fertilizer application mode, soil CEC, soil pH, and climate, as presented by Bouwman et al. (2002a). As a default we assume that all manure applied to crops is incorporated, and manure applied in grassland is broadcast. In the model, incorporation leads to considerable reductions of  $\text{NH}_3$  loss of up to 50% compared to broadcasting (Bouwman et al., 2002a).

### ***Denitrification and leaching***

We developed a model for soils under rainfed crops that combines the effect of temperature, crop type, soil properties and hydrological conditions on annual mean

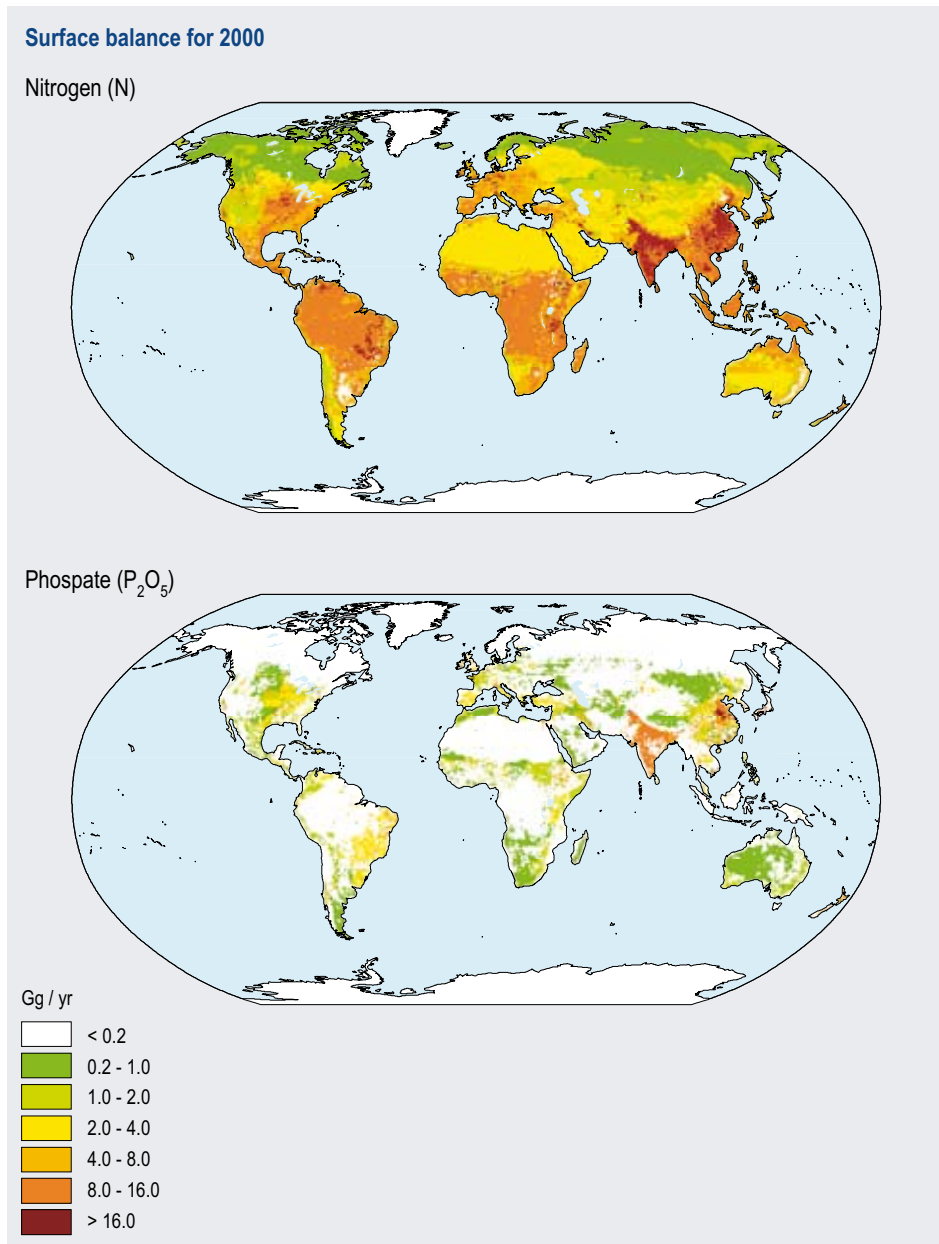


Figure 8.4. Surface balance for nitrogen (top panel) and phosphate (bottom panel) for 2000 calculated according to the scheme in Figure 8.2. Note that the P balance is calculated only for areas with known P inputs and outputs, i.e. for agricultural systems.

nitrate leaching and denitrification rates, relying on simplifications of empirical models from the literature (e.g. Kolenbrander (1981), Kragt et al. (1990) and Simmelsgaard et al. (2000)).

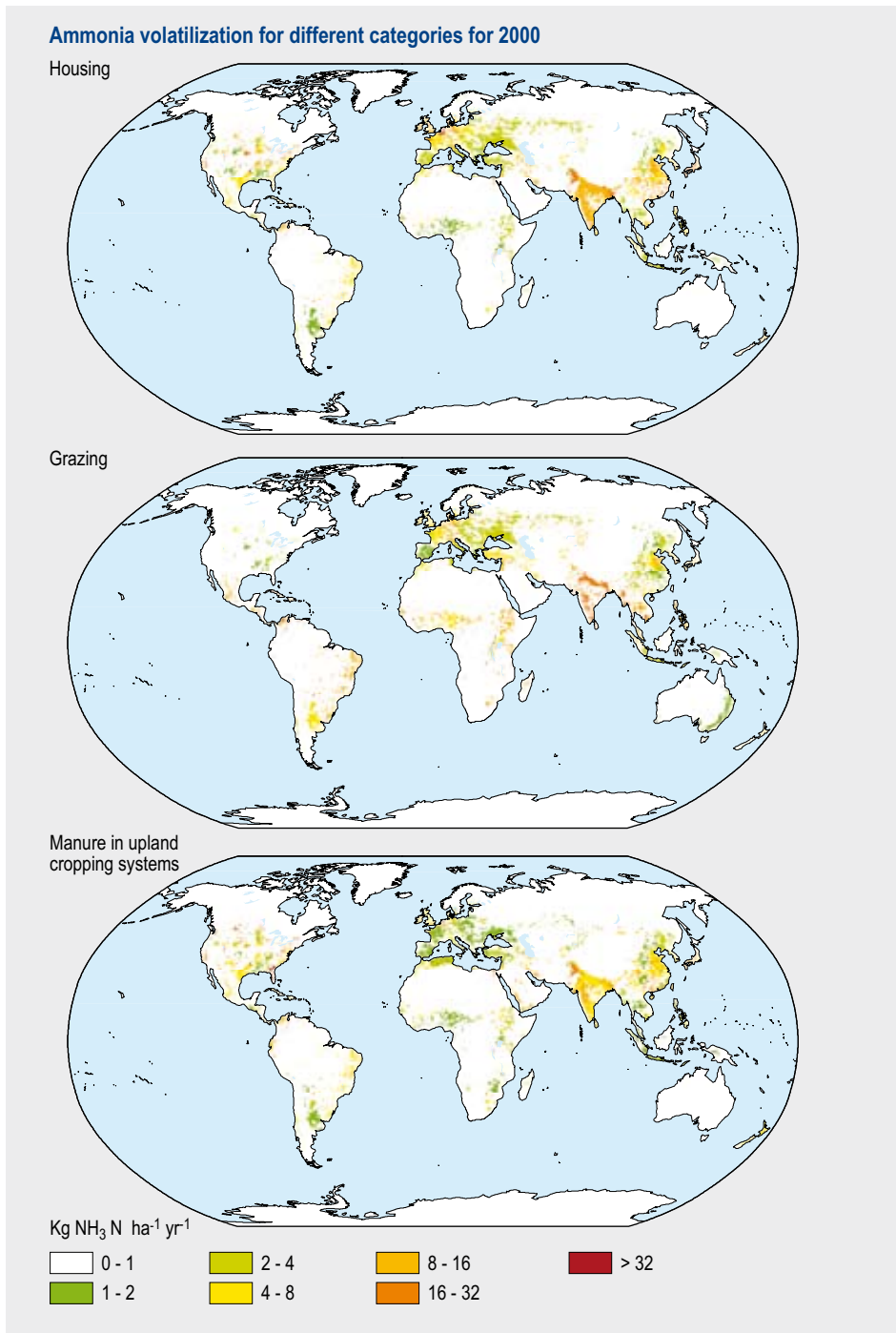


Figure 8.5.  $\text{NH}_3$  emission from housing + storage (top panel) and grazing (middle panel) in mixed and landless systems and from spreading of manure in upland cropping systems (bottom panel) for the year 2000. The tool for scenario construction (section 8.4) allows us to assess the consequences of a change, for example, in the proportion of the production in pastoral versus mixed and landless systems, the  $\text{NH}_3$  emission factor for animal houses and manure storage systems, and for the reactive N emissions from the agricultural system as a whole.

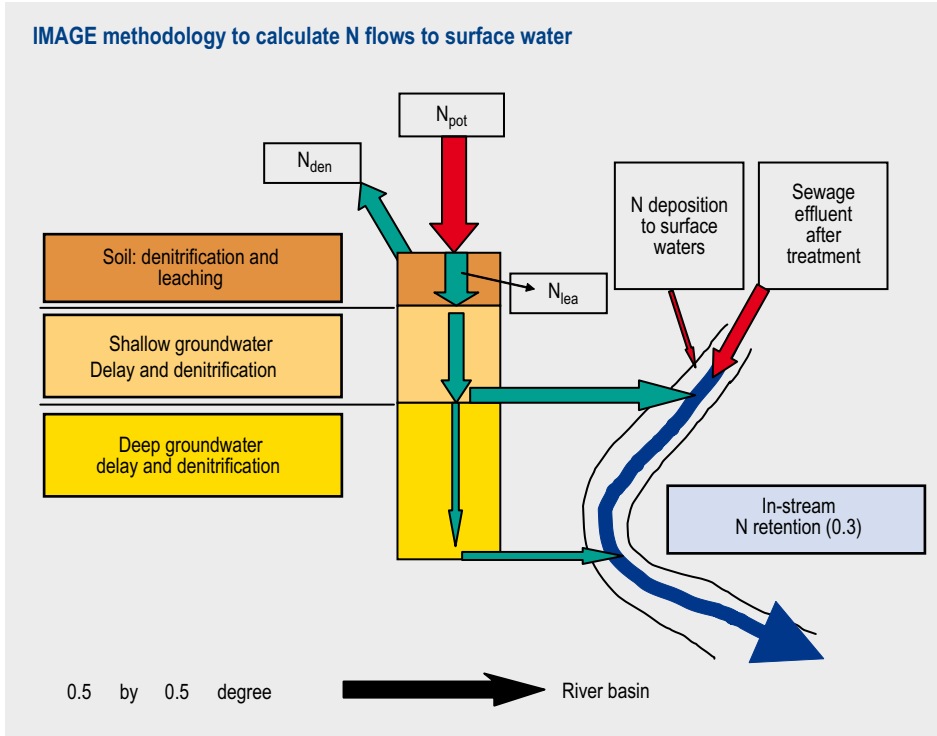


Figure 8.6. IMAGE 2.4 calculation of N leaching from root zone to subsoil, shallow groundwater and deep groundwater (base flow) to surface water, direct N inputs to surface water from atmospheric N deposition and sewage N effluent (based on Van Drecht et al. (2003)).

The potential loss from the plant-soil system,  $N_{pot}$  (Figure 8.6) is calculated as the difference between  $N_{sur}$  and the  $NH_3$  volatilization ( $N_{vol}$ ):

$$N_{pot} = N_{sur} - N_{vol} \quad (4)$$

Denitrification in soil is calculated as an empirical fraction  $f_{den}$  of  $N_{pot}$ :

$$N_{den} = f_{den} N_{pot} \quad (5)$$

The denitrification fraction  $f_{den}$  is composed empirically of four factors, each ranging individually from 0 to 1, with their sum having a maximum value of 1:

$$f_{den} = \text{MIN}[(f_{climate} + f_{text} + f_{drain} + f_{soc}), 1] \quad (6)$$

where  $f_{climate}$  (-) represents the effect of climate on denitrification rates, combining the effects of temperature and residence time of water and nitrate in the root zone;  $f_{text}$ ,  $f_{drain}$  and  $f_{soc}$  (-) are factors representing effects of soil texture, soil drainage and soil organic carbon content, respectively.

Nitrate leaching ( $N_{\text{lea}}$ ) – the nitrate in percolating water from the root zone to the sub-soil where it is no longer available to plant roots – is calculated as follows:

$$N_{\text{lea}} = N_{\text{pot}} - N_{\text{den}} = (1 - f_{\text{den}}) N_{\text{pot}} \quad (7)$$

The concentration of nitrate in the percolating water can be calculated for each grid cell from the excess of precipitation over evapotranspiration and  $N_{\text{lea}}$ . It should be noted that  $N_{\text{lea}}$  includes surface runoff and water drained by drainage systems which are not treated explicitly in our simplified approach (Van Drecht et al., 2003).

In the IMAGE 2.4 approach, climates with a large annual precipitation excess have high leaching rates and short residence times of nitrate in the soil solution. In dry climates the annual water flow through the soil is small and the residence time of nitrate is longer than in humid climates. N transformation rates are higher in tropical climates than in temperate ones. In arid climates the precipitation excess is small and soil water percolation rates are low. As a consequence, the residence time of nitrate in the soil solution is long and nitrate leaching limited. This implies that gaseous N loss processes dominate in dry climates as discussed elsewhere (Seitzinger et al., 2006). In temperate and humid climates, precipitation excess generally exceeds the available soil moisture capacity and, as a consequence, soil water percolation and nitrate leaching rates are high.

The factors  $f_{\text{text}}$ ,  $f_{\text{drain}}$  and  $f_{\text{soc}}$  account for soil properties that influence denitrification through the soil's water and oxygen status. Fine-textured soils have more capillary pores and hold water more tightly than sandy soils do. As a result, anaerobic conditions favouring denitrification may be more easily reached and maintained for longer periods in fine-textured soils than in coarse-textured ones. Soil drainage conditions also influence soil aeration, and denitrification rates are generally higher in poorly drained soils than in well-drained soils. Finally, the soil oxygen status is influenced by root respiration and microbial activity. Oxygen consumption by micro-organisms is driven by temperature, supply of carbon and water availability. Since temperature and soil water are already represented in  $f_{\text{climate}}$ , we use soil organic carbon content as a proxy for the carbon supply. We use 0.5 by 0.5 degree resolution information on derived soil properties taken from the WISE database (Batjes, 1997; Batjes, 2002).

Since data on irrigation water use, its efficiency and leaching requirements are not available on the scale of our calculations, we ignored irrigation in all crops except wetland rice. At present wetland rice production systems cover about 120 Mha or 45% of the global total irrigated area (FAO, 2005). Since N fertilizer application rates and leaching rates are generally higher in irrigated systems than in rainfed ones (Singh et al., 1995), ignoring the remainder of irrigated crops may lead to underestimation of nitrate leaching rates in about 10% of the global arable area of ~1400 Mha.

In wetland rice systems the efficiency of fertilizer use is generally low due to high  $\text{NH}_3$  volatilization and denitrification rates (Bouwman et al., 2002a). The effects of soil

texture, soil organic carbon, drainage and precipitation surplus for these systems are ignored, because they are assumed to be predominantly anaerobic. Since rice is primarily produced in subtropical and tropical climates, we assumed denitrification to always be 75% of the surface N balance surplus, so that  $f_{\text{den}} = 0.75$ . This value was selected on the basis of measurements, indicating that about 30% of the total N input or 75% of the surface balance N surplus is lost through denitrification (Van Drecht et al., 2003).

### *Emission of N<sub>2</sub>O and NO*

The IMAGE 2.4 calculation of emissions of N<sub>2</sub>O and NO from agricultural and natural ecosystems are presented in various papers. The method for N<sub>2</sub>O from soils under natural vegetation is from Bouwman et al. (1993) and that for NO from Davidson and Kinglerlee (1997); Mossier et al (1998) was the source for the calculation of N<sub>2</sub>O emission from animal manure storage and grazing systems, along with indirect emissions of N<sub>2</sub>O from groundwater and surface water stemming from N leached from soils.

Finally, direct N<sub>2</sub>O and NO emission from fertilizer application and spreading of animal manure is calculated according to Bouwman et al. (2002b) using residual maximum likelihood (REML) models. For N<sub>2</sub>O the REML model, based on 846 series of measurements in agricultural fields, is used and for NO, based on 99 measurements (Bouwman et al., 2002b). The calculations are almost identical to the original results (Bouwman et al., 2002b). Slight differences may occur since we use updates for the spatial datasets for soil organic carbon content, soil drainage and soil pH (Batjes, 1997; Batjes, 2002) in IMAGE 2.4 for both 0.5 by 0.5 degrees and 5 by 5 minute resolution. For N<sub>2</sub>O the model is based on: (i) environmental factors (climate, soil organic C content, soil texture, drainage and soil pH); (ii) management-related factors (N application rate per fertilizer type and type of crop, with major differences between grass, legumes and other annual crops) and (iii) factors related to the measurements (length of measurement period and frequency of measurements). The factors used for calculating NO emissions include the N application rate per fertilizer type, soil organic-C content and soil drainage. The above models for direct N<sub>2</sub>O and NO emission and a more recent update of the approach for agricultural systems using an extended data set (Stehfest and Bouwman, 2006) have been used to compute the so-called fertilizer-induced emissions of N<sub>2</sub>O and NO, which are used in the IPCC methodology for national greenhouse gas inventories to represent the anthropogenic emission. These results were used in the update of the IPCC default emission factor (IPCC, 2006). The leaching of nitrate from the subsoil (Figure 8.6) is used to compute the 'indirect' emissions of N<sub>2</sub>O, i.e. emission from groundwater and surface water.

The calculation of NH<sub>3</sub> volatilization, denitrification, N<sub>2</sub>O and NO emissions, and leaching are done on a grid basis from which aggregations for countries or world regions can be made (Figure 8.7).

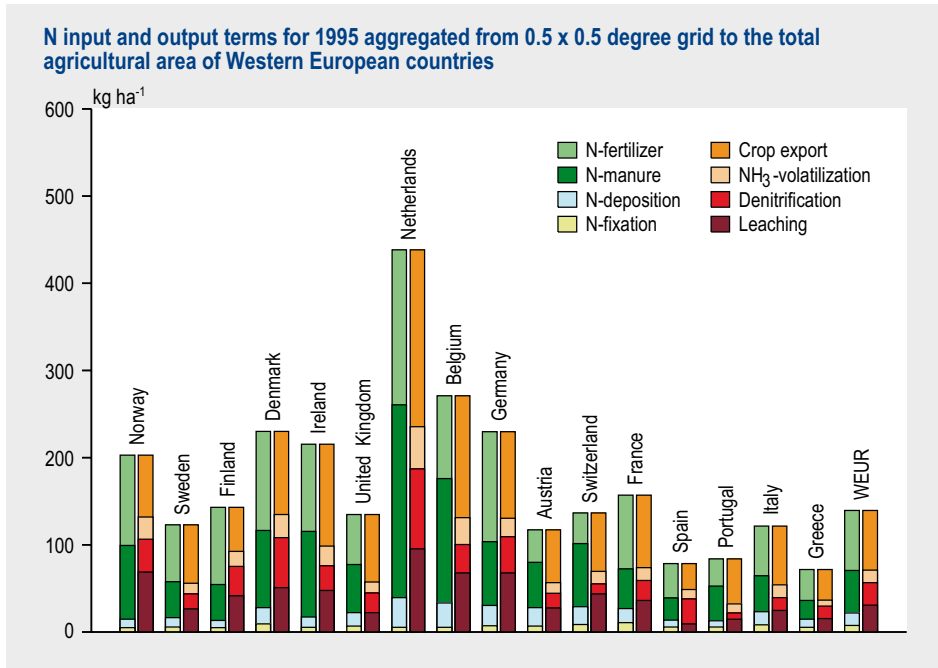


Figure 8.7. N input and output terms for 1995 aggregated from 0.5 by 0.5 degree grid cells to the total agricultural area (arable land and grassland) for Western European countries (Modified from Bouwman et al. (2005d)).

### Transport and retention in groundwater and surface water

The groundwater flowing into draining surface water is generally a mixture of water with varying residence times in the groundwater system. The nitrate concentration in groundwater depends on the historical year of water infiltration into the saturated zone and on the denitrification loss during its transport.

In many parts of the world the use of N fertilizers was much less 3 to 4 decades ago than it is at present (FAO, 2005). Groundwater that infiltrated in the 1960s or 1970s will therefore contribute less nitrate to the surface water than more recently infiltrated groundwater, with concentrations corresponding to current fertilization rates (Meinardi, 1994). Hence, for simulating the outflow concentration of nitrate from the groundwater system, we need to consider the distribution of residence times of water leaving the groundwater system and the historical fertilizer N inputs. We therefore applied the flowpath approach for a typical homogenous groundwater system described in detail in Van Drecht et al. (2003).

Two subsystems are distinguished: (i) those with rapid transport of nitrate in surface runoff and flow through shallow groundwater to local water courses and (ii) those with slow transport through deep groundwater towards larger streams and rivers (base flow) (Figure 8.6). The rapid flow responds with a varying but, generally, short delay to variation in the precipitation surplus during the year, while the base flow shows only

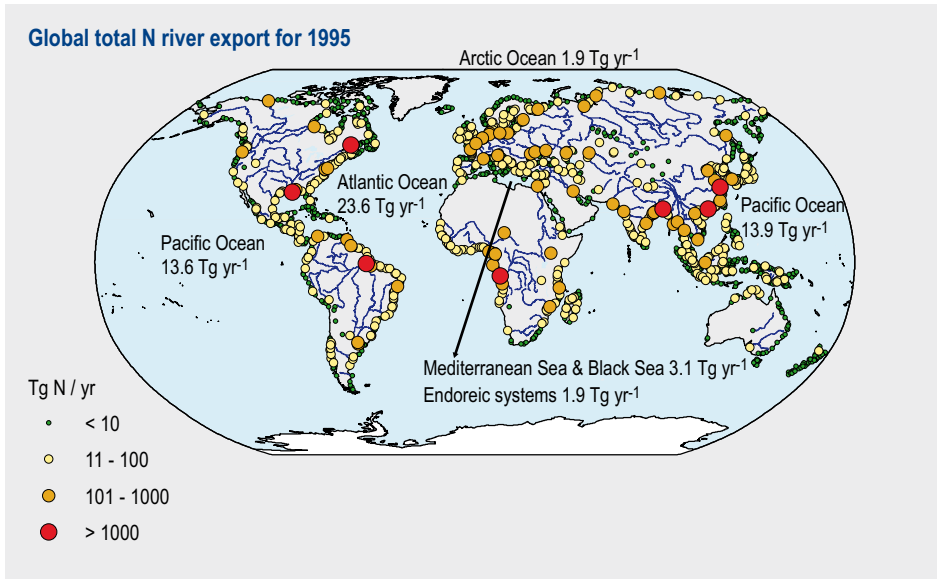


Figure 8.8. Global total N river export for 1995 (Modified from Van Drecht et al. (2003)).

slight variation throughout the year. We assumed that shallow groundwater recharges the deep groundwater layer as well as discharging into local water courses. Hence, the concentration in the upper part of the deep groundwater will equal that of the outflow from the shallow groundwater.

The partitioning of water entering each groundwater layer and surface water is estimated according to Klepper and Van Drecht (1998) from characteristics such as soil texture, thickness of aquifers, geology, slope and other factors. The nitrate concentration of the outflow for each groundwater layer is calculated by combining the effects of historical N inputs from fertilizer, manure and atmospheric N deposition, residence time and denitrification. Historical N inputs are obtained from the above-surface N balance calculations. The residence time is obtained from the effective porosity and aquifer thickness, which depend on the characteristics of the aquifer considered. Values for effective porosity and aquifer thickness were applied to the geological map of the world taken from Klepper and Van Drecht (1998).

The nitrate concentration of the outflow from shallow aquifers is reduced by using a half-life of two years. We assumed most of the dissolved organic carbon compounds required by denitrifiers as electron donors to be decomposed in the shallow groundwater layer; hence denitrification rates gradually decrease with depth, and are assumed to be zero in the deep groundwater layer (see references in Van Drecht et al., 2003).

The total N from point sources, direct atmospheric deposition and nitrate flows from shallow and deep groundwater form input to the surface water within each grid cell. Once N enters the aquatic system, in-stream N transformations will occur which are

primarily concerned with metabolic processes removing N from the stream water by transferring it to the biota, atmosphere or stream sediments. Various factors influence N loss and retention, including temperature, availability of organic matter, nitrate concentration in stream water overlying stream sediments and the stream-flow regime and residence time. Lumped catchment models generally apply export coefficients, which are useful for obtaining rough estimates of annual nutrient loads (Heathwaite, 1993). Because we lacked a globally applicable model and input data for simulating in-stream processes, a global river-export coefficient of 0.7 (implying retention and loss of 30% of the N discharged to streams and rivers) was adopted. This represents a mean of a wide variety of river basins in Europe and the U.S.A. used by Van Drecht et al. (2003) (Figure 8.8).

While the P balances for the non-point sources are included in the current IMAGE 2.4 framework, and a model has been developed for river export of N and P in particulate matter (Beusen et al., 2005), work on P emissions from point sources is still ongoing. We also plan to work on modelling the river Si export in order to predict changing N:P:Si ratios and the risk of algal blooms in coastal seas.

## 8.4 Scenario construction

The new elements for point (section 8.2) and non-point sources (8.3) require spatially explicit distributions of population, agricultural production and management, etc. For constructing spatially explicit scenarios, we have therefore developed tools that allow for downscaling IMAGE output for world regions to the scale of countries (or states and provinces for the U.S.A. and China, respectively) and grid cells.

Various papers have used country-scale data on crop production for the 34 crops distinguished above, fertilizer use, fertilizer-use efficiency, livestock production and land use from the FAO projection Agriculture Towards 2030 (Bruinsma, 2003). These data were used directly as a base for generating spatial distributions of livestock production and land use (Bouwman et al., 2005c), nutrient inputs and outputs (Bouwman et al., 2005d), emissions of reactive N gaseous compounds and nitrate leaching (Bouwman et al., 2005a).

When constructing other scenarios (for example, IPCC SRES, Millennium Assessment, OECD, GEO) the regional output for changes in animal stocks, crop production, crop nutrient export and fertilizer inputs is downscaled to the country level (Figure 8.9). In this approach the number of animals for one of the 24 IMAGE regions, for example, is distributed over the countries within that region on the basis of the distribution in the FAO projection for 2030. The same approach is used for crop uptake.

The downscaling of fertilizer use from world regions to the country level also occurs in a similar manner. IMAGE 2.4 uses the scenario called Variable fertilizer use efficiency (FUE) (Table 8.1). In the projection of Bruinsma (2003) for 2030, the FUE increases con-

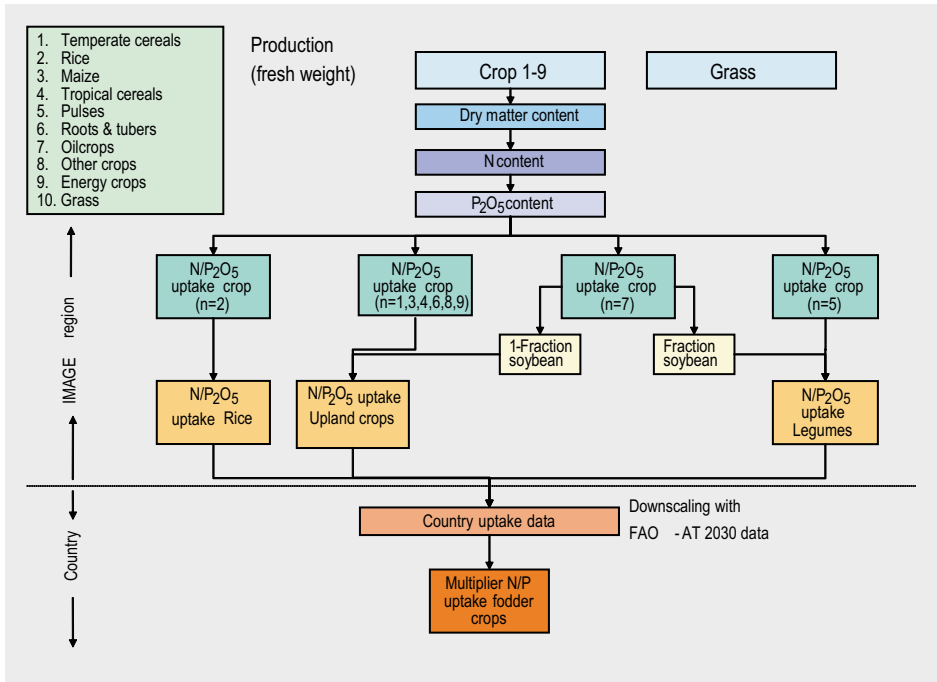


Figure 8.9. The IMAGE 2.4 approach for downscaling IMAGE regional data to countries using the country-scale data from the FAO Agriculture Towards 2030 projection for crop nutrient uptake.

Table 8.1. System N recovery and fertilizer use efficiency (FUE) for mixed systems (excluding pastoral systems) for various world regions for 1970, 1995 and 2030.

	System N recovery (%) <sup>a</sup>			FUE (%) <sup>b</sup>		
	1970	1995	2030	1970	1995	2030
North America	42	43	51	49	48	63
Western Europe	44	49	58	44	54	68
Transition countries	38	46	55	43	67	83
Latin America	51	43	49	82	49	66
Middle East + North Africa	54	47	50	85	58	63
Sub-Saharan Africa	48	51	58	139	108	131
South Asia	42	31	38	99	41	58
East Asia	61	43	39	108	48	42
Southeast Asia	58	55	61	135	78	90
World	46	43	47	67	52	61
Developing	52	42	45	103	51	58
Industrialized	44	45	52	48	49	62

<sup>a</sup> System N recovery is calculated as the N in all harvested crops, grass cut and N consumed by animals, expressed as % of total inputs from N deposition, N fixation, N fertilizer and animal manure.

<sup>b</sup> FUE is calculated as the N recovery in upland crops and wetland rice (excluding leguminous crops) as % of N input from fertilizers and manure.

siderably in the period 2000-2030. For subsequent years the data from FAO (2006) will form a good basis for a similar baseline scenario. The approach also explicitly considers the use of fertilizers in energy crop production. Formulating a relationship between crop production and fertilizer inputs is an important improvement on the previous IMAGE versions, where total fertilizer use was simply a function of GDP only, and a relationship between crop production and fertilizer inputs was absent. In future versions the approach for constructing scenarios for fertilizer use will be improved further by establishing relationships between crop yield and nutrient inputs in the new crop growth model that is under development (chapter 1).

Further variables that can be used to modify a scenario or to analyze the effects of policy options include the  $\text{NH}_3$  losses from animal houses and manure storage systems, mode of application of animal manure and fertilizers, maximum application rates of fertilizers and animal manure. Figure 8.5 shows the global distribution of  $\text{NH}_3$  emissions from animal houses and storage systems, grazing and spreading of animal manure. A change in the  $\text{NH}_3$  emission factor for animal houses and manure storage systems affects the quantity of N in the manure available for spreading, and thus  $\text{NH}_3$  volatilization from manure spreading. An example of an analysis of the sensitivity of the model to variation of input data was presented by Bouwman et al. (2006), showing, for example, how  $\text{NH}_3$  emissions from animal housing and manure storage systems can influence the reactive emissions from the agricultural system as a whole.

Since land cover and soil data are now available at finer resolutions than the 0.5 by 0.5 degree grid cells of IMAGE, the system is independent of the resolution and can be applied to the standard 0.5 by 0.5 degree resolution of the IMAGE model, as well as to a finer resolution of 5 by 5 minutes, as demonstrated by Bouwman et al. (2006).

For the point sources, target values for 2030 are used for the connection of households to sewerage systems and wastewater treatment taken from WHO/UNICEF (2000), with adjustments for many countries on the basis of past developments or trends observed in other countries and the scenario for GDP.

## 8.5 Results

### *Surface N balance*

We will now briefly discuss the results for the surface N balance approach presented by Bouwman et al. (2005a,b,d) on the basis of the FAO Agriculture Towards 2030 study (Bruinsma, 2003). The surface N balance, aggregated from the 0.5 by 0.5 degree estimates to the total agricultural area (arable land and grassland) for large world regions, shows the N input per hectare in the developing countries to have increased rapidly between 1970 and 1995. This increase will continue at a lower rate up to 2030 (Figure 8.10) due to a rapid increase in all N input terms. The total N input per hectare in developing countries is expected to exceed input in industrialized countries in 2030, reflecting high cropping intensities (two or more crops per year) that prevail in many

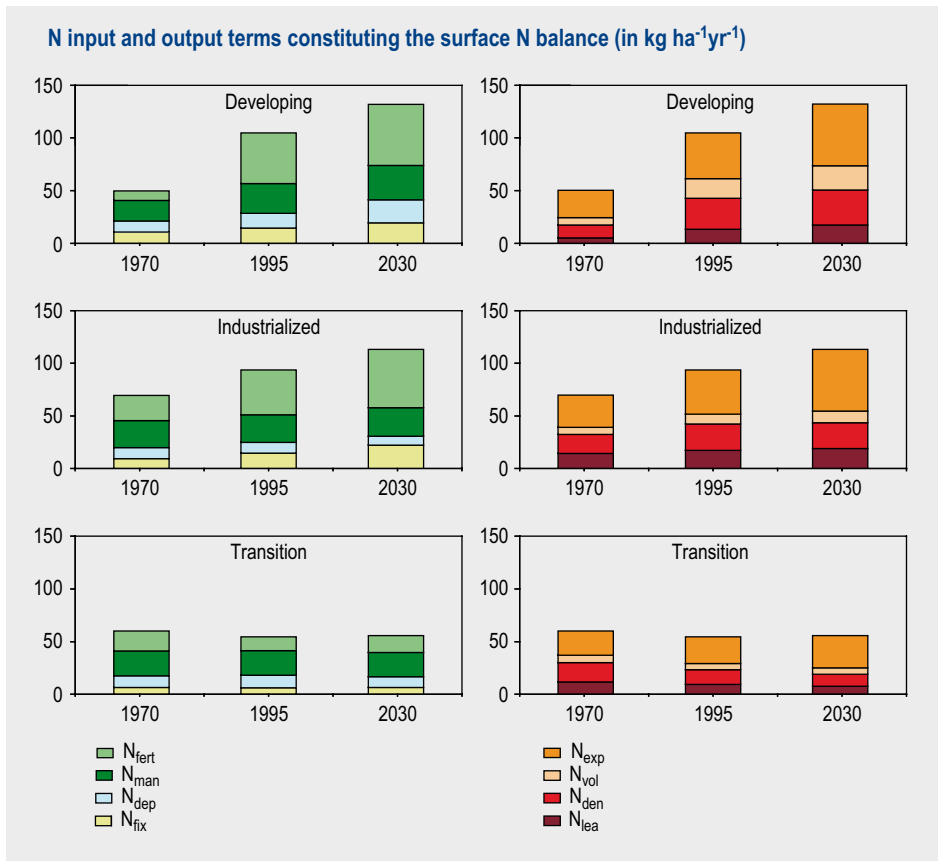


Figure 8.10. N input and output terms constituting the surface N balance for 1970, 1995 and 2030, aggregated from 0.5 by 0.5 degree grid cells to the total agricultural area (arable land and grassland) for developing, industrialized and transition countries (Modified from Bouwman *et al.* (2005b)).

tropical countries where irrigated agriculture is dominant. The N input per hectare in industrialized countries will increase slightly in the coming decades (Bruinsma, 2003) as a result of increasing inputs from biological N fixation and fertilizers. These inputs are partly offset by slightly decreasing N inputs from animal manure and atmospheric deposition (Figure 8.10). In the transition countries there are only minor changes after 1995.

### Fertilizer use efficiency

We estimated the crop uptake and the overall system N recovery based on estimated fertilizer use efficiency (FUE). According to our results there has been a steady decrease of the overall system N recovery in the developing countries between 1970 (52%) and 1995 (42%) (Table 8.1). In industrialized countries the overall system N recovery slowly increased from 44 to 45%. Further increases are projected for 2030; these will amount to 45% in developing regions in the period 1995-2030, with an improved efficiency in industrialized countries of up to 52%.

There are also important differences between regions for the FUE for upland crops and wetland rice. The industrialized countries show a slow increase of FUE from close to 48% in 1970 to 49% in 1995 (Table 8.1). In the period up to 2030, FUE values will increase further (depending on the projection used) to values in the order of 62% in the industrialized countries. In 1970 the transition countries showed FUE values of 43%, which are similar to those in Western Europe. However, after 1990 fertilizer use strongly decreased, and the FUE increased to 67%. For 2030 we project a decrease in the transition countries down to about 80%.

Turning to the developing countries, we see high values of FUE for 1970. For example, in Sub-Saharan Africa, and Southeast and East Asia the FUE for 1970 exceeds 100%, while in other developing regions the FUE exceeds 80%. Between 1970 and 1995 the FUE values for developing countries decreased. While in Sub-Saharan Africa the FUE for 1995 still exceeds 100% and in Southeast Asia it is close to 80%; in other developing regions it dropped sharply between 1970 and 1995 to values comparable to those in industrialized countries in 1970.

For the coming three decades the average FUE value for the developing countries as a whole is projected to increase to 58%. However, there are large differences between regions and countries. The FUE for 2030 for Sub-Saharan Africa will exceed 100%, while the FUE for Southeast Asia will be 90%, which is comparable to the 1970 values of many other developing regions. The FUE for South Asia, Middle East and North Africa and Latin America will increase to reach the 1995 values for industrialized countries of 50-60% or higher.

In Asia and Africa soil N depletion is probably the main cause of the high overall system N recovery and FUE. The low N input systems in these world regions have been able to sustain a low total production volume at low levels of crop yields (see FAO, 2005) but at the cost of soil fertility. In fact, crop yields have not increased substantially in many, primarily African, countries (FAO, 2005).

### ***Reactive N emissions***

The N surface balance is a good overall indicator of environmental problems associated with agricultural production. The surplus N is lost from the agricultural system via various pathways, including  $\text{NH}_3$  volatilization, denitrification,  $\text{N}_2\text{O}$  and NO emissions, and nitrate leaching from the root zone. Global  $\text{NH}_3$ -N emissions from fertilizer and animal manure application and stored manure increased from 18 to 34 Tg  $\text{yr}^{-1}$  between 1970 and 1995, and will further increase to 44 Tg  $\text{yr}^{-1}$  in 2030 (Bouwman et al. 2005a). Similar developments are seen for  $\text{N}_2\text{O}$ -N (2.0 Tg  $\text{yr}^{-1}$  in 1970, 2.7 in 1995 and 3.5 in 2030) and NO-N emissions (1.1 Tg  $\text{yr}^{-1}$  in 1970, 1.5 in 1995 and 2.0 in 2030) from mixed intensive agricultural systems. Consequences of such increases in  $\text{NH}_3$  and NO emissions from agriculture and other sources after re-deposition for global biodiversity are discussed in chapter 10.

Global nitrate-N leaching increased from 18 to 29 Tg yr<sup>-1</sup> between 1970 and 1995, and will further increase to 35 Tg yr<sup>-1</sup> in 2030. Increased concentrations of nitrate have been observed in groundwater in many agricultural regions and have given cause for concern in some industrialized regions; the European Union, for example, adopted standards for acceptable concentrations in water intended for human consumption. Recently, nitrate concentrations in groundwater have also been shown to increase in developing countries with intensive agricultural production (Singh et al., 1995).

### *River N export*

As a result of leaching and runoff, river N loads will strongly increase in large parts of the world in the coming decades. The projected increase of river N export to oceans in the period 1995-2030 is 13% globally, about 10% in North America and Oceania and 27% in developing countries. This is a consequence of increasing N inputs to surface water associated with urbanization, sanitation, development of sewerage systems and lagging wastewater treatment, as well as increasing food production. Only in Europe is a decrease of 20% projected for the 1995-2030 period, which is a consequence of the projected decrease in fertilizer inputs and animal manure production, and continued improvement of wastewater treatment. Our results for the period 1970-2030 indicate rapid increases in river N export for the Indian (46%) and Pacific (38%) oceans, and a slower increase (6%) for the Atlantic Ocean. A slow decrease in river N export is estimated for the Mediterranean and Black Seas (-9%).

The contribution of agriculture to the human-induced river N export is dominant on global scale (78% in 1970 and 80% in both 1995 and 2030). When aggregated to large world regions the point sources make a relatively minor contribution to the total N load. However, in many river basins, point sources may dominate the total N load, particularly in densely populated river basins or in basins where large population centres are located near the river mouth (Bouwman et al., 2005b).

Anthropogenic disturbance of river nutrient loads and export to coastal marine systems is a major global problem affecting water quality and biodiversity. Nitrogen is the major nutrient in rivers. Growing river N loads are expected to be accompanied by increasing P loads, and together this will lead to increased incidence of problems associated with eutrophication in coastal seas.

## 8.6 Concluding remarks

The model for simulating the fate of nutrients through the soil and hydrological system described in this chapter offers a wide variety of possibilities for analyzing scenarios. Examples are agronomic analyses of efficiencies in agriculture, studies on reactive N emissions (emissions of N<sub>2</sub>O, NO, NH<sub>3</sub> to air and nitrate to water), atmospheric N deposition and impacts on biodiversity, and analyses of effects of changing N and P river export on freshwater biodiversity and impacts on coastal marine environments. The IMAGE work on nutrients has been used in the Millennium Assessment (Carpenter

et al., 2006) and plays a pronounced role in the Global Nutrient Export from Watersheds (NEWS) project of UNESCO International Oceanographic Committee (IOC) (Seitzinger et al., 2005; American Geophysical Union, 2006).

IMAGE 2.4 uses sub-national data for China and the USA. For other large countries, such as Brazil and India, sub-national data are available and will be included in future versions to improve the spatial distributions of animals, animal manure, fertilizer, and fluxes of N and P compounds.

## 9 CLIMATE: VARIABILITY, PREDICTABILITY AND INTERACTIONS WITH LAND COVER

- Limitations of the current climate model and the natural vegetation module inhibit the study of important non-linear interactions with IMAGE 2.4 between land, the atmosphere and the ocean. For this reason the atmosphere/ocean/cryosphere model ECBilt was linked to IMAGE. ECBilt was forced by greenhouse gas and land-cover scenarios from IMAGE in various studies using both a one-way and an iterative approach.
- Major findings from the research in this ECBilt model's application: (i) climate variability causes diminished predictability of climate-change projections when abrupt climate changes are involved; (ii) establishing carbon plantations on abandoned agricultural land in northern extra-tropical regions leads to a lower albedo than planting energy crops, the effect of which – in terms of climate change – is comparable to the amount of carbon fixed by these options, and (iii) a fully coupled climate-vegetation system is necessary to assess the impacts of changes in extremes and interannual/interdecadal climate variability on a regional scale.
- However, since ECBilt performed rather poorly with respect to the simulation of variability and changes in atmospheric circulation in the tropics, it has been decided to incorporate instead the General Circulation Model SPEEDY. To address the necessary climate-vegetation interaction, SPEEDY was coupled to the Dynamic Global Vegetation Model LPJ. Initial results indicate that the climate and vegetation patterns generated by the coupled SPEEDY/LPJ framework show general agreement with the observations in most regions.

### 9.1 Introduction

Although many uncertainties are still unresolved, it is generally accepted by both policy makers and scientists that our climate is changing and will continue to do so in the decades or even centuries that lie ahead of us. Consequently, policy questions are increasingly focusing on climate impacts, for example, on land use, food security, water availability and management, biodiversity and adaptation to climate change on a regional scale. To address such questions it is no longer sufficient to know the change in average climate. Increasingly, attention shifts to changes in climate variability and frequency of extreme events, as motivated by research on impacts and statistics. Changing climate variability may be manifested, for example, by more frequent droughts, periods of high rainfall, cyclones and hurricanes, or extreme temperatures, posing threats to food security and human health.

Exploratory studies on possible impacts indicate larger repercussions for societies confronted with extreme events than is suggested by changes in mean climate. An important example of a system that is highly sensitive to changes in extremes is an agricultural system functioning under conditions away from optimal mean climate

indicated by maximum mean climate-driven biomass accumulation of the crops in question (Riha et al., 1996). Infrastructure, human health and energy systems are other examples of human systems sensitive to changes, for example, in the temperature and flooding regime. Natural systems (biodiversity) can also be sensitive to changes in extremes (Parmesan et al., 2000). Within the climate debate, the impact of extremes on natural systems is perhaps best known in the case of coral reefs responding to the frequency of high water temperature events (Hughes et al., 2003).

Turning to statistical analysis, we have shown in recent studies that the frequency of extreme events changes non-linearly with the change in mean climate, in which case a small change in the mean can result in a large change in the frequency of extremes (Easterling et al., 2000). Moreover, this frequency is more sensitive to changes in variability than to shifts in the mean (Katz and Brown, 1992). Thus, knowledge on changes in the mean climate have little value when one is concerned with changes in extreme events (Schaeffer et al., 2005).

The increasing focus of policy makers on climate impacts also poses challenges to our knowledge on the climate-terrestrial interlinkages. Traditionally, studies on climate variability have focused on the interactions between atmosphere and ocean. The focus in research is gradually shifting towards exploring how patterns of variability are affected by the interaction with natural vegetation and by large-scale changes in land use. Changes in land use and the consequent changes in land-cover properties modify the interactions between land surface and atmosphere, both locally and regionally (Kabat et al., 2004). Important factors in these interactions are the biochemical fluxes of carbon dioxide (CO<sub>2</sub>) and other trace gases, and the biophysical fluxes of energy and water vapour. Modelling studies, well-validated with detailed observations, show that changing land use in the past centuries have influenced local, regional and – more likely than not – also global climate patterns (e.g. Houghton et al., 2001). Historically, land-use-mediated climate change appears to be an important factor (Brovkin et al., 2005). In medium to high latitudes, for example, land-use changes influence surface-air temperature because of the large difference in surface albedo between different land covers, such as cropland and forest in snow-covered conditions (Robinson and Kukla, 1985; Bonan et al., 1995; Harding and Pomeroy, 1996; Sharrat, 1998). The feedback on changes in land cover on climate with respect to long time scales (from centuries to millennia) has already been suggested (e.g. Claussen et al., 2003). The impact of land-cover changes on climate and extreme events on the decadal time scale (Pielke Sr. et al., 2002) has recently been demonstrated in observations presented by Chapin et al. (2005) and climate projections based on IMAGE 2.2 land-use scenarios from Feddema et al. (2005).

The current climate model of the IMAGE versions 2.2 to 2.4 captures global mean climate change by means of an energy-balance, upwelling-diffusion climate model (Eickhout et al., 2004). This current climate model lacks the capacity to address climate variability and the land-use feedbacks to the climate system (separate from climate impacts of land-use-related greenhouse gas (GHG) emissions). In the past few years

these limitations have been addressed. In this chapter then, we will present analyses where the simple IMAGE climate model is replaced by a General Circulation Model (GCM) of intermediate complexity, coupled with a Dynamic Global Vegetation Model (DGVM). In the first (exploratory) track we used the coupled atmosphere/ocean/cryosphere model ECBilt-CLIO (hereafter simply referred to as ECBilt; see Opsteegh et al., 1998 and Schaeffer et al., 2006) from the Royal Netherlands Meteorological Institute (KNMI). Studies discussed in sections 9.2 and 9.3 using ECBilt point to the crucial behaviour of the climate system in shaping projections of future climate change that are not covered in IMAGE 2.4. In section 9.4 we discuss results of exploratory studies that show the importance of future land-use change on the climate system and vice versa, employing soft linkages between IMAGE and ECBilt. After concluding that ECBilt did not meet our current model requirements, further work concentrated on another GCM of intermediate complexity, called SPEEDY, which is coupled with a DGVM called Lund-Potsdam-Jena (LPJ) (section 9.4). All experiments were carried out with IMAGE 2.3, which differs from IMAGE 2.2 (IMAGE-team, 2001), mainly through the addition of energy crops and carbon plantations (see chapters 1 and 7).

## 9.2 Predictability of abrupt regional climate change

The climate system occasionally undergoes substantial and rapid variations (Bond et al., 2001). Observed variations have been linked to (sudden) transitions – to which the north Atlantic Ocean may be particularly prone (Manabe and Stouffer, 1988) – between different quasi-stable states, and to such transitions, which may also occur under future global warming (Manabe and Stouffer, 1993; Rahmstorf and Ganopolski, 1999). In the past, deep ocean convection in the north Atlantic was modified under the influence of external forcings (Bond et al., 2001). Such a reorganization of deep convection affects the thermohaline circulation (THC) and could possibly lead to local cooling under global warming (Russell and Rind, 1999).

Here we summarize the work of Schaeffer et al. (2002), who examined the consequences of a sudden reorganization of convection in the North Atlantic for predictability in 21<sup>st</sup> century scenario projections using the EC-Bilt model. The scenarios used to drive ECBilt are the IPCC SRES A1b and B1 scenarios implemented through the use of the IMAGE 2.2 model (IMAGE-team, 2001). In 2100 this results in CO<sub>2</sub>-equivalent concentrations of 1050 ppmv and 680 ppmv, respectively. The third scenario was the B1stab-450 scenario, an intervention scenario designed to stabilize the CO<sub>2</sub> concentration at 450 ppmv and total CO<sub>2</sub>-equivalent concentration of 580 ppmv in 2100 (Van Vuuren and de Vries, 2001). The climate sensitivity assumed in ECBilt is 1.7 °C for a doubling of the CO<sub>2</sub> concentration relative to the pre-industrial era, which is on the low end of the estimated range (Houghton et al., 2001).

For each scenario, ten ensemble members were generated by applying insignificantly small random distortions in the atmospheric state in 1960. Because of the chaotic nature of atmosphere dynamics, the atmospheric circulation patterns of members

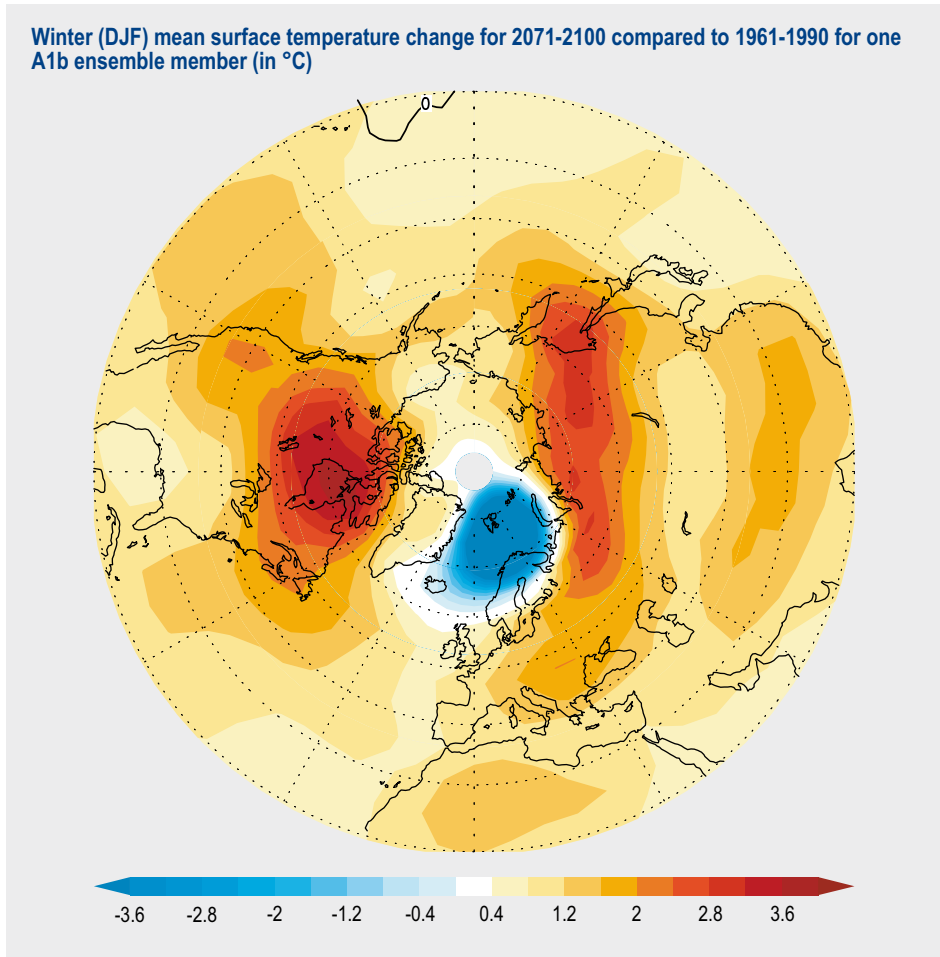


Figure 9.1. December-January-February mean surface-air temperature change (°C) for 2071-2100 compared to 1961-1990 for one A1b ensemble member.

within an ensemble were completely uncorrelated in a few simulation weeks, except for the small influence of the oceans. The various members within one ensemble represent different evolutions of the climate system with the same probability of occurrence. Hence, the spread in the results of the individual members provides an indication of the limits to predictability in scenario projections arising from natural, or internal, climate variability.

In the A1b and B1 scenarios, ECBilt simulates a sudden transition to a regionally colder climate in the course of the 21<sup>st</sup> century (Figure 9.1). The thinning of Arctic Sea ice drives this transition, which leads to increased export of fresh water from the Arctic to the sea around Greenland, Iceland and Norway. Eventually, the water column here becomes stable and convection stops. Maximum north Atlantic overturning is reduced by about 27%, or 6 Sv ( $\text{Sv} = 10^6 \text{ m}^3\text{s}^{-1}$ ), close to the mean for the range of most GCMs

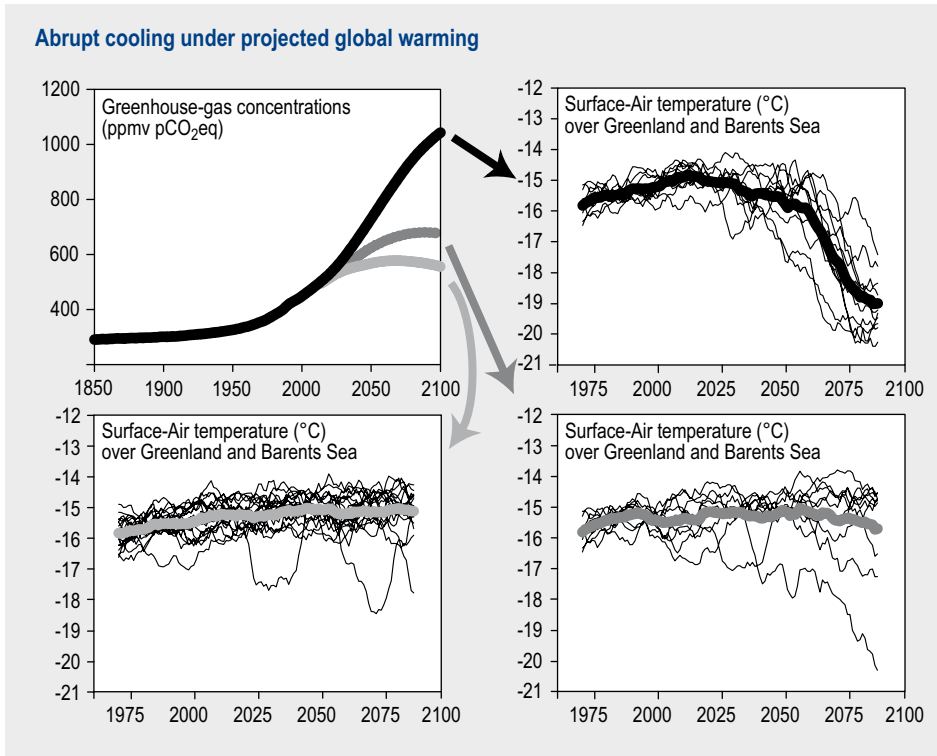


Figure 9.2. Abrupt cooling under projected global warming. The top-left panel shows greenhouse gas concentrations for the A1 (top), B1 (middle) and B1stab (bottom) scenarios. The other panels show the surface-air temperature response for each scenario over the northern north Atlantic Ocean. In each of these panels, the thin lines show 10 individual model simulations that represent a different evolution of the climate system for the same scenario, with equal probability of occurrence. The spread among the individual ensemble members within each scenario is caused by internal climate variability. The heavy temperature lines represent the 10-member ensemble means for each scenario. Note the different horizontal time axis in the top-left panel.

compared by Houghton et al. (2001). The cooling resulting from the collapse of convection near Spitzbergen extends over Scandinavia and Iceland, and tempers the global warming signal over Siberia, northern Canada and Greenland (Figure 9.1).

The probability of the climate transition appears to depend strongly on the scenario under consideration. The changes in the THC in our model occur between 2040 and 2080 for the A1b scenario and from 2040 to beyond 2100 in the B1 scenario (Figure 9.2). Thus, the transition is much less predictable in B1 than in the A1b scenario. In B1stab the transitions have not yet occurred by 2100. Extending the B1stab ensemble with another ten members indicates that temporary instabilities occur in 10% of the cases, but do not lead to the transitions seen in A1b and B1.

The analysis shows that if the external forcing is relatively gradual (as in B1), it is the internal variability that will 'determine' when exactly the system crosses the threshold

(for a more elaborate analysis, see Schaeffer et al., 2002). In other words, the timing of the onset of the transition becomes uncertain. In a scenario where GHGs increase relatively fast, as in A1b, the timing is linked to the forcing and varies over only a few decades, comparable to the time scale of the transition itself (Figure 9.2). In other scenarios, for example B1, where GHG concentrations increase more slowly, the uncertainty in the timing is extended to the centennial time scale. The timing is essentially decoupled from the forcing.

This illustrates that the limited predictability of an abrupt climate change involving the THC may be an issue on decadal time scales within the 21<sup>st</sup> century, and not just on centenary to millennium time scales, as found by Knutti and Stocker (2002). The implication of the limited predictability of crossing a threshold to a different semi-equilibrium state is that even if we knew the current state of the oceans in great detail and a model was available with high predictive capacity, the internal climate variability would still limit the predictability of the timing of a non-linear transition.

The exact transition dates and time scales are model-dependent, because of model uncertainties (Schaeffer et al., 2004). However, in more general terms the scenario experiment explores conditional behaviour: ‘if multiple semi-equilibrium states exist in a system with internal variability then the predictability of the timing of a transition from one state to another is intrinsically limited’. Interpreted in this way, the experiments illustrate the system behaviour in threshold situations with implications beyond THC changes alone. Analogous behaviour can be expected regarding the predictability of the timing of other potential abrupt changes within the 21<sup>st</sup> century, like accelerated dieback of the Amazon forests under global warming (Cox et al., 2000; 2004), ice-sheet collapse (Oppenheimer and Alley, 2004) or transitions in freshwater ecosystems (Scheffer, 2001).

### 9.3 Climate impacts of large-scale extra-tropical plantations

Future land-use change does not only include deforestation and afforestation as a consequence of expanding or contracting agricultural area (leading to changes in the carbon (C) cycle), but other land uses, such as plantations for C sequestration or bioenergy production (to substitute fossil fuels), are likely to become important in future decades. Energy crops and C plantations may not only influence climate change by reducing global GHG concentrations, but also have an impact on the energy fluxes between land surface and the atmosphere. Forested areas have a lower albedo than agricultural areas, especially at medium to high latitudes in winter due to snow-masking (Robinson and Kukla, 1985; Harding and Pomeroy, 1996). The global warming by albedo changes associated with high-latitude C plantations may even outweigh global cooling by C sequestration (Betts, 2000).

Here, the importance of the biophysical (non-CO<sub>2</sub>) climate impact of future land-use changes is compared for two major mitigation options: (i) production of energy crops and (ii) permanent C plantations, focusing on the impact of surface-albedo changes due to effect of land-use change on climate in the extra-tropics. For this purpose we constructed three scenario variants based on the A1b scenario implemented with IMAGE, i.e. the non-mitigation IM-nat (no energy crops) and IM-C (C plantations), and the mitigation variant IM-bio (energy crops with a five year rotation). We updated the albedo model in ECBilt (Schaeffer et al., 2006), including albedo for snow-free and snow-covered conditions, drawing from field and satellite observations.

In the baseline A1b scenario large areas of agricultural land are abandoned in the course of the 21<sup>st</sup> century as a result of further increases in agricultural yields and stabilizing or even declining global population. We assume that abandoned agricultural areas in temperate zones provide the most interesting locations to use for either biomass or C plantations, in line with Hoogwijk et al. (2005).

Since energy crops are planted on all abandoned cropland in IM-bio, the total area of biofuel plantations is larger than that of C plantations in the IM-C experiment with the additional NPP constraint (Figure 9.3a). In all regions the largest area increase of biofuel plantations occurs in the first half of the 21<sup>st</sup> century, except in Eastern Asia (Figure 9.3b).

ECBilt (denoted with EC) was run twice for each of the three modified IMAGE-2.2 A1b experiments: one with only GHG changes (denoted with GHG) and a second with both GHG and land-cover changes (denoted with TOT). Since we expected that the difference in climate impact between the scenarios would be small, an ensemble of 20 experiments was performed for each scenario. Compared to a single climate model run, the mean of the ensembles provides a better estimate of the mean climate response by reducing the sampling error (caused by internal climate variability).

In the scenarios IM-nat and IM-C, the global use of modern biomass in 2100 is reduced from 250 EJ to 150 EJ per year (EJ, exajoule; 1 EJ=10<sup>18</sup> J) compared to the original A1b scenario. Here, energy crops are produced only in the tropical NH and the Southern Hemisphere, yielding higher CO<sub>2</sub> emissions. In the IM-bio scenario the worldwide use of modern biomass is 440 EJ yr<sup>-1</sup> and oil use is reduced by 140 EJ yr<sup>-1</sup> in 2100. Smaller reductions occur for natural gas (65 EJ yr<sup>-1</sup>), coal and nuclear/solar/wind. CO<sub>2</sub> emissions from fossil fuels are reduced from 17 Pg C yr<sup>-1</sup> (Pg, petagram; 1 Pg=10<sup>15</sup> g) in 2100 for the IM-nat and IM-C scenarios to 12 Pg C yr<sup>-1</sup> for IM-bio (Figure 9.4a). The gross CO<sub>2</sub> emission (not accounting for the C uptake in the plantations) from bioenergy in IM-bio reaches 7 Pg C yr<sup>-1</sup> in 2100. Because we assumed that efficiency of energy production from combustion of energy crops is lower than for gas or oil, this emission more than offsets the 5 Pg C yr<sup>-1</sup> reduction of fossil fuel use.

The terrestrial uptake is highest in the IM-bio case where the biofuel plantations are harvested every five years. This implies a fast rate of C uptake in the initial years

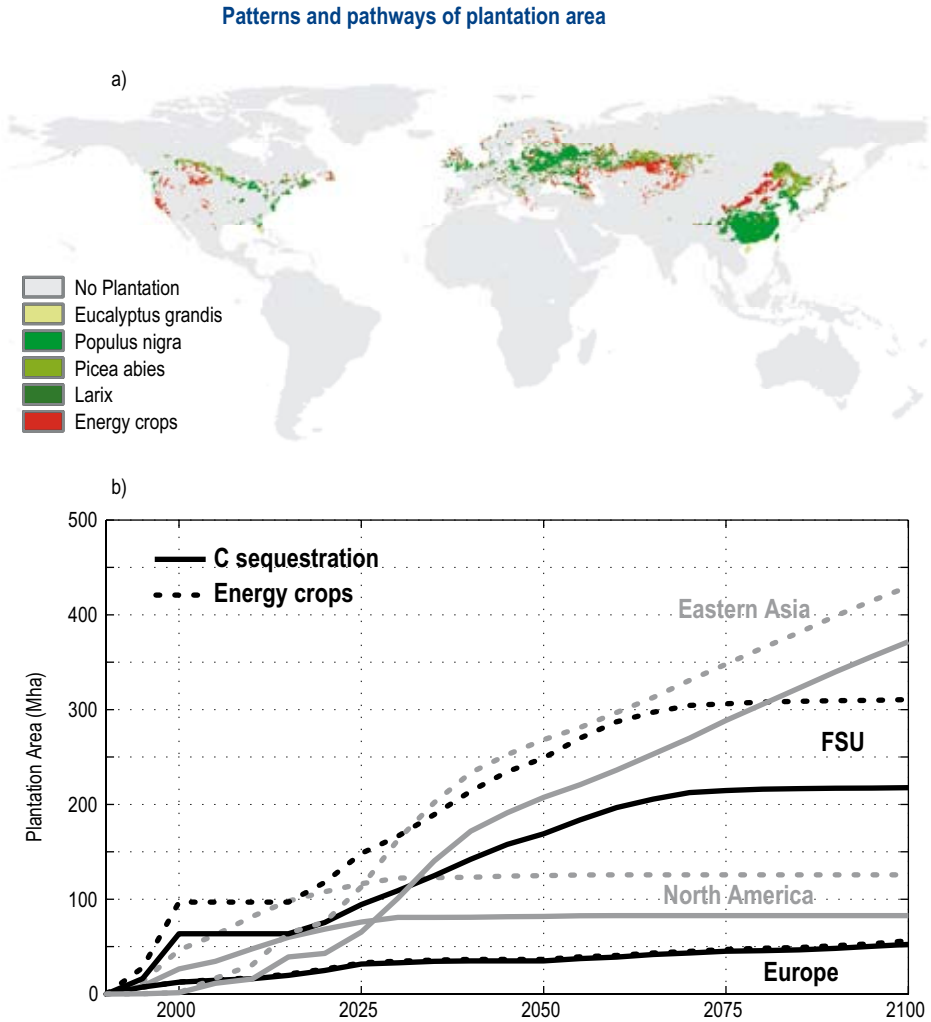


Figure 9.3. Pattern and pathways of plantation area. The top panel (a) supplies IMAGE grid cells in the year 2050, with C plantations (green) of different tree types and additional cells (red) with energy crop plantations. The lower panel (b) shows the evolution in time of total plantation area per region for each of the two plantation scenarios.

of each rotation period for these fast-growing crops. The net effect of the high C uptake in biofuel plantations is more reduced by higher soil respiration fluxes than in natural vegetation or C plantations. Logically, the IM-nat scenario yields the lowest terrestrial C uptake, since no management is applied to the abandoned agricultural land and the vegetation types are not primarily selected on the basis of optimal C sequestration. The terrestrial uptake in IM-C is higher than for IM-nat due to the management of C plantations, but lower than for IM-bio, since we assumed no harvest of the C plantations. The differences in the resulting atmospheric CO<sub>2</sub> concentrations between IM-C and IM-bio are minor (Figure 9.4b), both reaching about 700 ppmv or 70-80 ppmv less than in IM-nat.

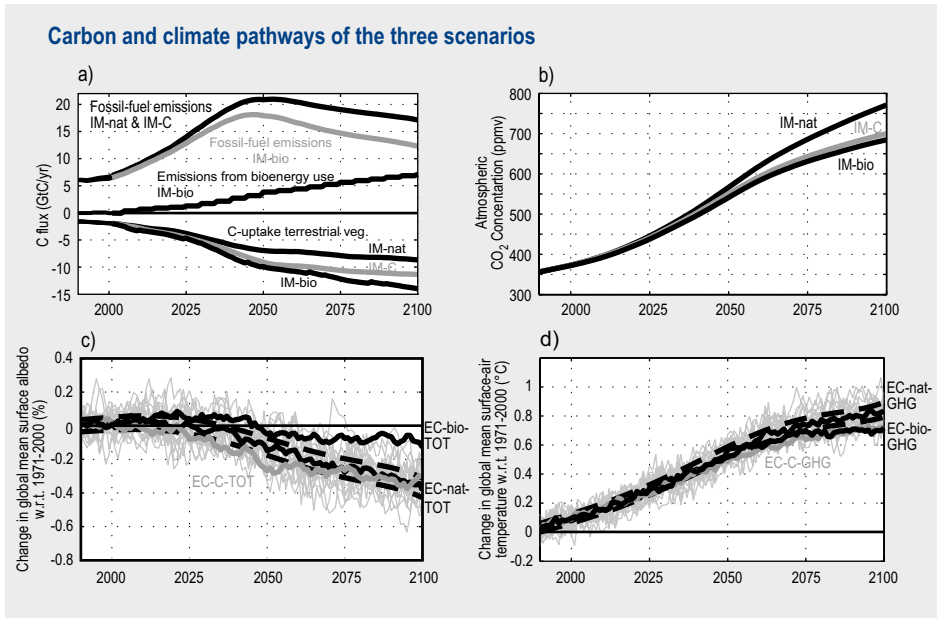


Figure 9.4. C and climate pathways of the three scenarios. The two top panels give IMAGE results for C fluxes (a) and CO<sub>2</sub> concentration (b). The lower panels show ECBilt results (denoted with EC) for global-mean albedo change (c) and near-surface air temperature (d). Dashed lines indicate uncertainty limits given by internal climate variability, indicating when results in the mitigation scenarios deviate from the baseline with less than 5% uncertainty. Heavy lines indicate ensemble means, while thin grey lines show the individual ensemble members in the EC-nat experiments.

IM-nat and IM-C scenarios result in a lower global mean surface albedo than the biomass plantation scenario IM-bio (Figure 9.4c). In all experiments, global warming gradually reduces the snow cover, resulting in a gradual decline of surface albedo which has a considerable impact. About 300 W m<sup>-2</sup> of the global mean solar radiation reaching the atmosphere (342 W m<sup>-2</sup>) actually reaches the earth surface (Kiehl and Trenberth, 1997). If we assume no climate feedbacks and a present-day surface albedo of 15%, the total decline of albedo of 0.4% by 2100 in IM-C corresponds to a global mean 0.8 W m<sup>-2</sup> increase of absorbed solar radiation. The total radiative forcing by GHGs will increase by 1.3 W m<sup>-2</sup> (from 2.6 to 3.9 W m<sup>-2</sup>) between the mid-1990s and 2100.

The increase in CO<sub>2</sub> concentration to 770 ppmv in the IM-nat scenario leads to a rise in global mean surface-air temperature (SAT) of 0.8°C by the year 2100 compared to the 1971-2000 average (Figure 9.4d). This relatively modest increase is due to the low climate sensitivity assumed in EC-Bilt and because only changes in GHGs are included in the ECBilt experiments, not the expected decrease in sulphur emissions that would lead to further global warming. The reduction in CO<sub>2</sub> concentrations in the two mitigation scenarios (IM-C and IM-bio) moderates global mean temperature increase by about 0.1°C in 2100, thus mitigating global warming over the 21<sup>st</sup> century by more than 10%.

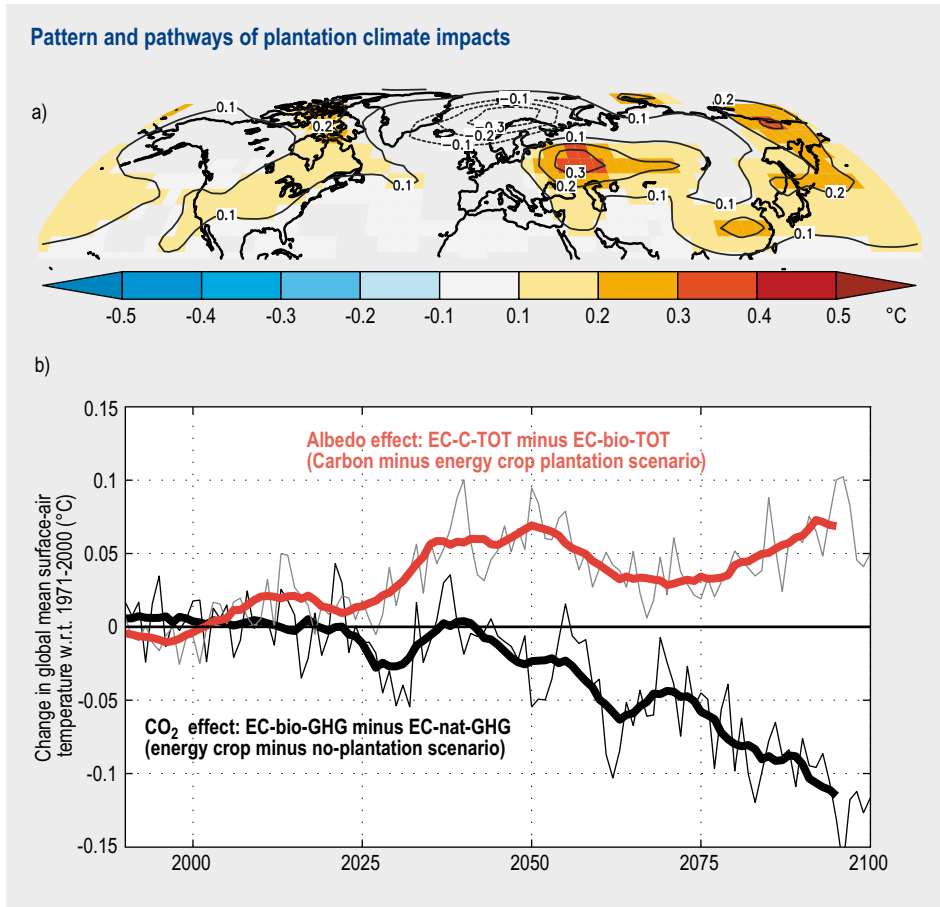


Figure 9.5. Pattern and pathways of plantation climate impacts. The top panel (a) gives the ensemble-mean difference in annual-mean surface-air temperature of EC-C-TOT compared to EC-bio-TOT (EC refers to ECbilt). The lower panel (b) shows evolution in time of the difference in the same variable comparing the impact of CO<sub>2</sub> with land-cover changes. The thin lines indicate annual ensemble mean values, while the heavy lines show 10-year running means.

Although the CO<sub>2</sub> pathways of the two mitigation scenarios are comparable, the albedo difference causes different climate impacts (Figure 9.5a). In the regions of major land-use changes (Figure 9.3) surface-air temperature is higher in the C plantation scenario IM-C. The difference reaches 0.3°C in some regions, which is about 25% of the full climate change signal over the 21<sup>st</sup> century in those regions. In central and western Eurasia, heating in the spring increases evaporation, thereby reducing the soil moisture content. The less intensive hydrological cycle in summer reduces latent heat fluxes, amplifying the albedo-induced summer heating and extending this heating far outside the area of land-use change itself. A further indication of a complex response of the climate system outside the area of albedo changes (teleconnections) is given by a reduction of up to 10% in annual mean rainfall over North Africa (Schaeffer et al., 2006).

The changes in climate due to albedo changes accelerate rapidly in the short to medium term while the impact of the difference in CO<sub>2</sub> concentrations gradually increases up to the end of the 21<sup>st</sup> century (Figure 9.5b). By that time, the CO<sub>2</sub> effect on climate has become somewhat larger than that of albedo change. Relative to the impact of changes in CO<sub>2</sub>, albedo change thus gradually becomes less important, but remains the dominant forcing in these scenarios over the major part of the 21<sup>st</sup> century. C plantations are often considered as an option to allow for a delay of transformations in the energy sector. Since we found that the albedo effect in the short-to-medium term is unfavourable for the C-plantations case, it is questionable whether C plantations in the Northern Hemisphere could actually be effective mitigation options in the medium term. On the centennial time scale, over which the albedo effect becomes relatively less important, the permanency of C plantations is also questionable (e.g. Barford et al., 2001).

The (regional) climate feedbacks and teleconnections illustrated above confirm the conclusion that climate effects other than just the impact of changes in CO<sub>2</sub> concentrations need to be taken into account when assessing mitigation options that involve land-use changes. When the effects of changing albedo are ignored, the large-scale use of C or biofuel plantations in the Northern Hemisphere has similar benefits in avoiding climate change. Including the impact of changes in albedo, however, almost completely erodes the climate-change mitigation impact that C plantations might have via the C cycle.

## 9.4 The interaction between climate and land-cover change

The two previous sections dealt with a one-way coupling, in which ECBilt was forced by greenhouse gas (9.2 and 9.3) and land-cover (9.3) scenarios from IMAGE 2.2. To explore interactions between climate and land cover, we performed a series of experiments with IMAGE and ECBilt using an iterative approach. For this purpose ECBilt was updated with a simple Planetary Boundary Layer (PBL) scheme and a Surface-Vegetation-Atmosphere Transfer (SVAT) scheme (Hutjes et al., 2001; Ronda et al., 2003). The latter includes a C3 and C4 photosynthesis model that couples CO<sub>2</sub> fluxes to evapotranspiration and includes albedo, rooting depth and surface roughness parameters that depend on vegetation type. C3 plants thrive best in cool and moist conditions, and under normal light, because they require less machinery (fewer enzymes and no specialized anatomy). C4 plants photosynthesize faster than C3 plants under high light intensity and high temperatures, and are more efficient in use of water..

In running the model, GHG concentrations and land-cover changes were simulated by IMAGE 2.3 for the SRES A1b scenario. Subsequently, ECBilt was run twice to calculate climate changes up to the year 2050. In the first run (A1b-GL), both GHG concentrations and land-cover changes were used as input for ECBilt, while in a second run (A1-G), only GHG concentration changes were taken into account. This set-up is comparable to the analysis presented in section 9.3.

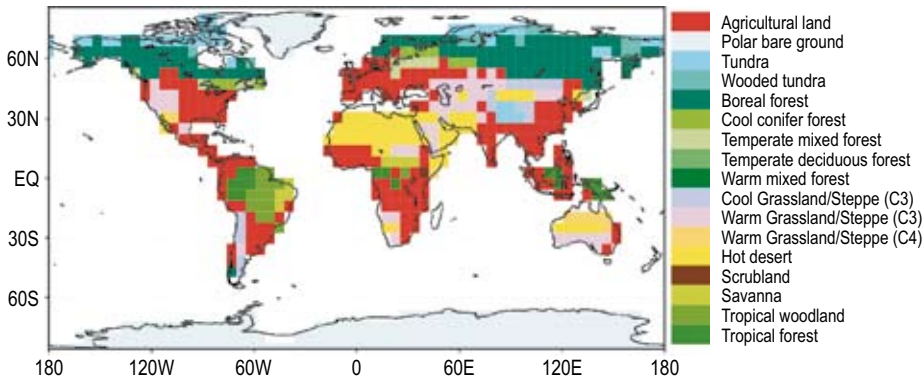


Figure 9.6. Dominant land-cover types for A1b in 2050.

In the IMAGE SRES A1b scenario, agricultural area in North and South America, Eurasia and Africa in the year 2050 is larger compared to the year 2000 (Figure 9.6). On grasslands, the C4 grasses are increasingly being replaced by C3 grass species, as the latter benefit more from increasing atmospheric  $\text{CO}_2$  concentrations than C4 grasses (Collatz et al., 1998).

In the GHG-only experiment of ECBilt (A1-G) the strongest change in climate is the increase in temperature at high latitudes, which is amplified by the ice-albedo feedback (see section 9.3). In mid-latitude continental regions, higher springtime temperatures lead to a drying-out of soils earlier on in the year. This results in summer drought.

When the effects of land-cover change are also included (A1-GL), even stronger temperature responses are seen in the higher latitudes, mainly through the northward shift of the forest/tundra boundary (affecting albedo, as discussed in section 9.3). The increase of agricultural area in eastern North America and southern Scandinavia lowers temperatures somewhat due to higher albedo values. In western North America and Mongolia, cool C3 grasses and C4 grasses are replaced by sparser warm C3 grassland. This effectively decreases soil moisture in the climate model, resulting in summer drought and temperature increases.

To explore possible feedbacks in the complete linked system, we used the climate change patterns of ECBilt as input for new simulations with IMAGE. Using the common GCM-pattern scaling approach (Eickhout et al., 2004), we scaled the global mean temperature of the A1b scenario for the year 2100. Here, the climate pattern of ECBilt for the year 2050 was applied to visualize the differences between the runs better.

Different climate patterns result in specific terrestrial responses and thus affect the C cycle. The ECBilt pattern results in a somewhat lower  $\text{CO}_2$  concentration than seen in the ECHAM4 and HadCM2 patterns (Table 9.1). However, these differences are smaller than those caused by soil respiration or  $\text{CO}_2$  fertilization feedbacks, which could lead to differences of up to 150 ppmv over a 100 year period (see chapter 7). The reason

Table 9.1. CO<sub>2</sub> concentrations in IMAGE using different GCM patterns for the A1b scenario.

GCM pattern	CO <sub>2</sub> concentration in 2100 (ppmv)
ECHAM4	774.1
HadCM2	771.4
ECBilt (A1b-G)	755.4
ECBilt including Land cover (A1b-GL)	765.9

for this relatively small effect is that the influence of land cover on climate is strongly variable on the world regional scale, while on the global scale the regional differences tend to balance out.

The ECBilt-G pattern within IMAGE leads to less warming in high latitudes compared to the ECBilt-GL. The additional warming for the GL-pattern occurs mainly in western Siberia on the border of boreal forest and tundra through the albedo mechanism, as explained above. In the G-run, the temperature changes in Europe lead to a shift in forest boundaries in southwest Europe, Scandinavia (Figure 9.7), northwestern Siberia and southern Russia, where the vegetation patterns and changes for Europe are indicative, because agricultural expansion is not accounted for. The latter generally occurs at the expense of forests, while the climate-induced warming in the high latitudes leads to additional shifts in forested areas.

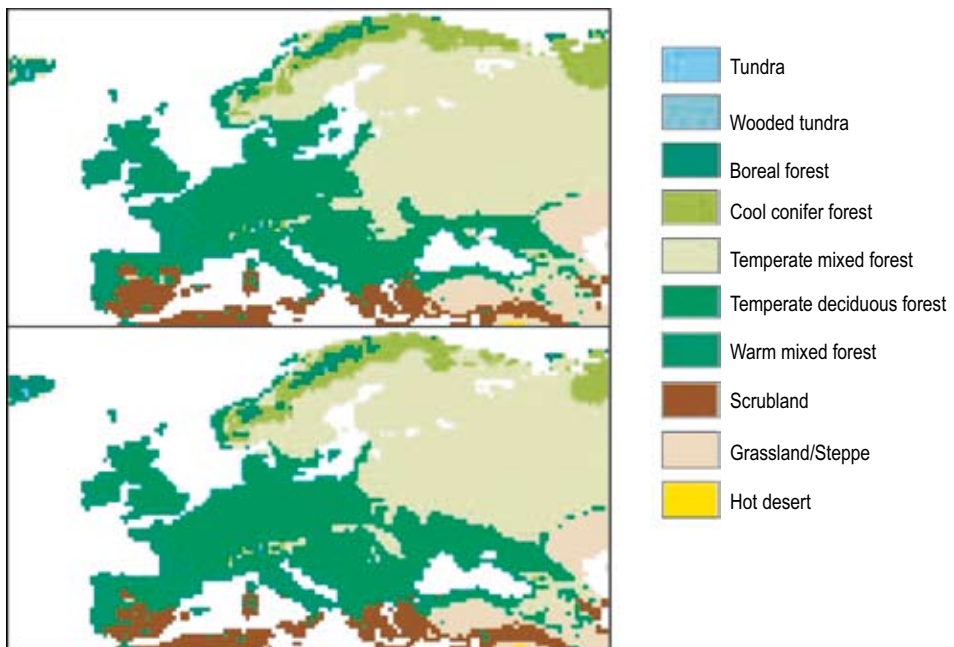


Figure 9.7. Potential vegetation in Europe in the year 2100 using the two ECBilt patterns A1-G (up) and A1-GL (down).

In the world's drylands the increased drying in the ECBilt-G scenarios causes a transformation of the potential vegetation from grassland to desert, which in turn leads to additional drying in the GL scenario (positive feedback). This process occurs in all regions with increasing aridity, but especially in the southwest of North America and in Mongolia.

This first attempt to assess interactions between the terrestrial system and climate indicates the importance of a fully coupled climate-vegetation system in studies on climate impacts. However, the combination of a simple climate model and a static vegetation model in the current IMAGE 2.4 model does not allow for incorporating these climate impacts.

## 9.5 From ECBilt to SPEEDY

The original purpose of ECBilt was to study interdecadal climate variability in the extra-tropics. For computational efficiency, quasi-geostrophical dynamics were implemented at the core of ECBilt, instead of the full primitive equations of atmospheric motion. As a result, ECBilt performed rather poorly on the simulation of variability and changes in atmospheric circulation in the tropics.

Because of the large land-cover and land-use changes that occurred in tropical countries and that are expected to continue in the coming decades (chapter 5), as well as the societal impact of (changes in) tropical climate variability, a climate model is needed that performs equally well in the tropics as in the extra-tropics.

Therefore, ECBilt has been replaced by the Simplified Parameterizations primitive Equation DYNamics model (SPEEDY), a General Circulation Model (GCM) of intermediate complexity. This involved a number of steps that are discussed in the following sections. First, the coupling of SPEEDY to the simple Land Bucket Model (LBM) is briefly described, as well as the modifications needed for coupling the model to IMAGE. Subsequently, we discuss the coupling of SPEEDY and the Lund Potsdam Jena (LPJ) DGVM and, finally, we present our plans for incorporation of SPEEDY/LPJ in the IMAGE framework.

### *Atmosphere/Land model SPEEDY*

SPEEDY is an atmospheric GCM of intermediate complexity developed at the International Centre for Theoretical Physics (ICTP) in Trieste (Italy) by Molteni (2003). The model has seven layers in the vertical and a spectral truncation at total wave number 30 (T30), corresponding to 4 degrees latitude and longitude. The model contains parameterization schemes for large-scale condensation, convection, clouds, radiative fluxes, surface fluxes and vertical diffusion, and is based on the same physical principles adopted in the schemes of state-of-the-art GCMs. The basic time step is 40 minutes. Computationally, SPEEDY is one order of magnitude faster than a state-of-the-art GCM at the same horizontal resolution, whereas the quality of the simulated

climate in the free atmosphere compares well with those models and with observations (Molteni, 2003). It is therefore suitable for studies on inter-decadal or inter-centennial variability.

The original SPEEDY model was coupled to a simple LBM. This model consists of grid cells with temperature, soil moisture, soil ice, snow cover and run-off as state variables. There is no horizontal or vertical transport in the model, and the heat and moisture budgets are closed, i.e. energy is conserved. The data exchange between SPEEDY and LBM took place once per simulated day. More details can be found in Haarsma et al. (1996).

The focus of the original SPEEDY model was to investigate processes in the free atmosphere and the interaction with the ocean, using a state of everlasting half-light. It was not developed to produce reliable estimates of near-surface temperature in a cycle of day and night over land. To improve surface fluxes and surface climate, we included a day-night cycle and a relatively simple boundary layer scheme, based on Ronda et al. (2003). Furthermore, LBM only contained a one-layer soil temperature simulation, which is not suitable for computing the temperature in the upper layer and the skin layer. Therefore, a two-layer snow temperature calculation based on Van Den Hurk (2000) and a three-layer bottom temperature calculation was included (taken from the land module of EC-Bilt).

The data exchange between SPEEDY and LBM took place once a day, but to simulate the highly non-linear process of boundary layer build-up during daytime, the SPEEDY temperature should correspond to the temperature of the skin of the upper soil layer and evaporation on a sub-daily time scale. To obtain the highest precision possible, the information is exchanged between SPEEDY and LBM every SPEEDY time step of 40 minutes.

Adding a boundary layer scheme in SPEEDY and a bottom layer scheme in LBM was not a trivial exercise. Although the surface climate of the model has improved enormously, air temperature at 2 metres above the surface and precipitation patterns should be more realistic for obtaining realistic vegetation patterns when coupling with LPJ. Compared to results from state-of-the-art GCMs, northern hemispheric summer climatology is reproduced reasonably well by SPEEDY, but predicted temperatures in winter for middle Asia, northeast Siberia and northern Canada are too high. Deviations from observed climate in the latter two regions also occur in many state-of-the-art GCMs because of strong inversions in winter; such phenomena can only be described in highly detailed boundary layer schemes that would, however, require too much computation time (Van Ulden and Van Oldenborgh, 2006).

### ***The Dynamic Global Vegetation Model LPJ***

The Lund-Potsdam-Jena Model (LPJ) is described in detail by Sitch et al. (2003). It has many features of the BIOME family of models. In LPJ, ten Plant Functional Types (PFT, derived from traits based on species morphology, physiology and/or life history) are defined,

eight being woody (two tropical, three temperate, three boreal) and two herbaceous. In addition to the attributes controlling physiology and dynamics, each PFT is assigned bioclimatic limits, which determine whether it can survive or regenerate under the climatic conditions prevailing in a particular grid cell at a particular point in time. Unlike previous models in the BIOME family, LPJ also includes explicit representations of vegetation structure, dynamics, competition between PFT populations and soil biogeochemistry. This consideration of sub-grid landscape variability is important for determining surface fluxes when coupling to climate models.

The fundamental entity simulated in LPJ is the average individual within a PFT using leaf-level parameters. A savanna, for example, does not have an inherent photosynthetic and stomatal response to light, but rather consists of grasses and trees that do have measurable leaf physiology. The grid cell is treated as a mosaic divided into fractional coverage of PFTs and bare ground. This concept provides a simple way for scaling up processes acting at the level of the plant individual to the 'population' over a grid cell, instead of aggregation of properties to those of generalized biomes.

For survival and regeneration, bioclimatic limits are applied to 20-year running means. Each PFT population is characterized by a set of variables describing the state of the average individual, and by the population density. Fire is the most important natural disturbance on the global scale, and is the only form of disturbance explicitly represented in LPJ.

Four scaling rules define individual physiognomy and constrain biomass allocation among the three pools of living tissue (leaves, fine roots and sapwood) in woody plants. The scaling rules consider the relationship between: (i) leaf area and sapwood cross-sectional area; (ii) investment in roots versus that in leaves based on water stress; (iii) vegetation height and stem diameter; and (iv) crown area and stem diameter.

Each pool of living tissue is assigned a PFT-specific tissue turnover rate, which is transferred either to litter or from living sapwood to heartwood. Above and below-ground litter pools are updated for every year. It is assumed that the physical environment of the plants is well mixed, meaning that the PFTs do not occupy discrete blocks, but compete locally for resources. The number of new individuals established annually is the product of the PFT-specific potential establishment rate and the fraction of the grid cell currently devoid of woody vegetation, i.e. areas sufficiently illuminated to allow sapling growth. Additional mortality can result from depressed growth efficiency, heat stress and negative net primary production (NPP). Whether a particular PFT can be established also depends on the available soil moisture and bioclimatic limits.

### ***Coupling the Dynamic Global Vegetation Model LPJ to SPEEDY***

Coupling the intermediate complexity model SPEEDY to LPJ allows for investigating ensemble runs for vegetation-climate interactions and feedbacks for different scenarios, assessing biome changes as function of climate change, and analyzing the types of dependencies (linear, discontinuities, thresholds or 'tipping points'). Since such analyses

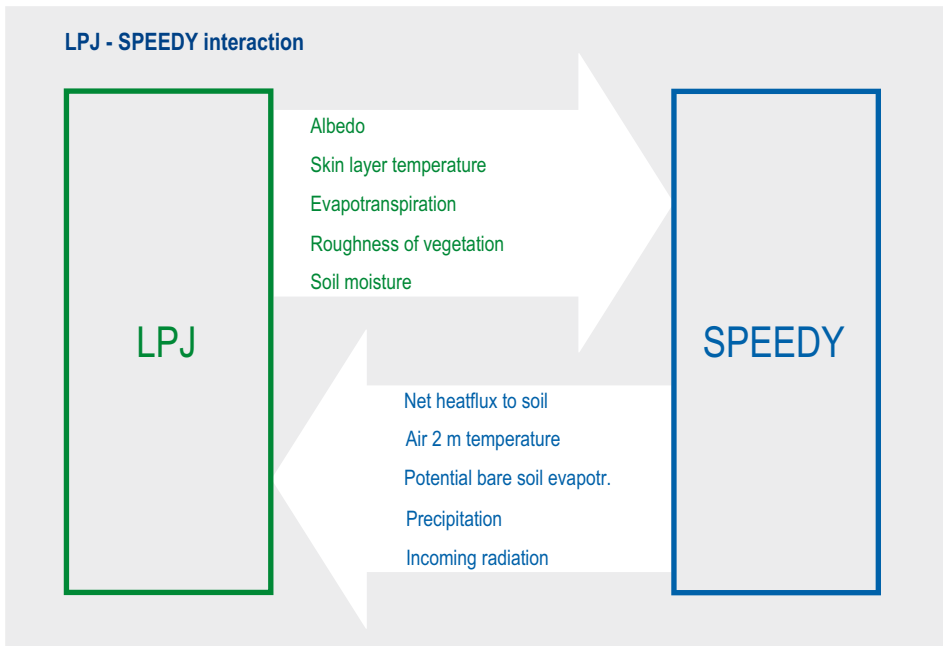


Figure 9.8. Exchange of information between LPJ and SPEEDY.

are not possible with complex GCMs at present because of computational limitations, there have been few attempts to couple DGMVs to GCMs (Foley, 2005).

For computing the surface heat fluxes, SPEEDY needs information on evapotranspiration and the skin temperature from LPJ every time step of 40 minutes (Figure 9.8). Therefore, several other variables in LPJ must be computed every 40 minutes, including the non-water stressed canopy conductance, the water demand of vegetation and the wetness of the leaves. Since LPJ only contained a simple bottom temperature computation, we included a two-layer snow temperature calculation and the three-layer bottom temperature calculation.

As the time step of 40 minutes in LPJ causes a large increase in computation time, an option was built in to run LPJ at lower spatial resolutions (multiples of a half degree). As described by Müller and Lucht (2006), coarser resolution levels hardly affect global outcomes. However, in specific areas with strong environmental gradients, spatial aggregation will cause loss of information. Another option to decrease run time is to exchange data between LPJ and SPEEDY every other time step or even less frequently. We want, firstly, to implement a link between LPJ/SPEEDY and IMAGE, in which the IMAGE output of a complete scenario run in terms of land-use change will be used to drive SPEEDY/LPJ. A full coupling, including the climate-vegetation feedbacks, will be established later.

Initial results indicate that the vegetation patterns generated by the coupled SPEEDY/LPJ framework agree reasonably well with observed vegetation patterns such as the IGBP DisCover and GLC 2000 maps (see chapter 6, incl. references); in some cases, vegetation patterns are even more realistic than the patterns generated with LPJ using prescribed climate data. In summer SPEEDY/LPJ generate temperature patterns that are in reasonable agreement with observations, also considering the performance of state-of-the-art GCMs of the same resolution. In winter, however, there are large deviations between predicted and observed temperature in northern hemisphere climates (Central Asia and eastern Canada).

## 9.6 Discussion and conclusions

The first part of this chapter dealt with coupling IMAGE 2.3 to ECBilt. The applications focused on future climate changes resulting from human-induced increases in GHG concentrations and large-scale changes in land cover. We highlighted the interactions within the climate system that lead to non-linear behaviour, i.e. there is no simple proportional relation between cause (average climate change) and effect (sudden changes in the THC). Further exploration of such non-linear behaviour of the climate system may yield new insights that are potentially surprising within the current policy debate on anthropogenic climate change.

Climate effects other than just the impact of changes in CO<sub>2</sub> concentrations need to be taken into account when assessing mitigation options that involve land-use changes. When the effects of changing albedo are ignored, the large-scale use of C or bio-fuel plantations in the Northern Hemisphere has similar benefits in avoiding climate change. Including the impact of changes in albedo, however, almost completely erodes the climate-change mitigation impact that extra-tropical C plantations may have via the C cycle relative to the bioenergy scenario.

This chapter has illustrated the importance of accounting for climate variability and land transformations, which will be essential in future policy-oriented assessments with the IMAGE model. This will only be possible by including a climate model, such as ECBilt or SPEEDY, which is capable of exploring non-linear behaviour resulting from (regional) climate feedbacks. A new coupled climate-vegetation model SPEEDY/LPJ, developed in close co-operation between MNP, PIK and KNMI has been tested and the first results are promising. This model is planned to be coupled to IMAGE for such purposes as: (i) simulating non-linear feedbacks and decadal climate variability; (ii) providing a two-dimensional surface interaction between the atmosphere and the (changing) land surface and (iii) calculating and comparing multiple scenarios and ensembles.

## 10 GLOBIO 3: FRAMEWORK FOR THE ASSESSMENT OF GLOBAL TERRESTRIAL BIODIVERSITY

- The GLOBIO 3 framework was developed to assess past, present and future biodiversity. It consists of clear and transparent relationships between pressure factors and biodiversity, based on state-of-the-art knowledge.
- The pressure factors or driving forces of biodiversity loss considered are land-cover change, land-use intensity, fragmentation, climate change, atmospheric N deposition and infrastructure development. The model is linked to the IMAGE 2.4 framework through changes in land use, shifts in vegetation zones and climate change.
- Issues that can be addressed with GLOBIO 3 on a regional, continental and global scale include: (i) impacts of human pressures on biodiversity and ecosystems, and their relative importance; (ii) expected trends in mean species abundance (under various future scenarios) and (iii) likely effects of various policy options.

### 10.1 Introduction

During the sixth meeting of the Conference of Parties on the Convention on Biological Diversity (CBD), the parties committed themselves to achieving a significant reduction of the current rate of biodiversity loss at the global, regional and national level by 2010 (UNEP, 2002a). The governments adopted a plan of implementation at the 2002 World Summit on Sustainable Development (WSSD) in Johannesburg which recognizes the same target; this plan endorsed the CBD as the key instrument in realizing the conservation and sustainable use of biological diversity.

Among the several studies on global biodiversity loss carried out the last few years are those describing the contemporaneous situation (Hannah et al., 1994; Sanderson et al., 2002; Wackernagel et al., 2002; McKee et al., 2003; Cardillo et al., 2004) or expert opinions used for estimating impacts (Sala et al., 2000). In the Global Environmental Outlook 3 (UNEP, 2002b) the consequences of four socio-economic scenarios on biodiversity were assessed using both the Natural Capital Index (NCI) approach of IMAGE and the GLOBIO 2 approach (UNEP/RIVM, 2004). In the IMAGE-NCI approach, energy use, land-use change, forestry and climate change were considered as pressure factors and biodiversity loss defined as a deviation from the undisturbed pristine situation due to these pressure factors. In GLOBIO 2 (UNEP, 2001) the human influence on biodiversity is based on relationships between species diversity and the distance to roads.

To meet the challenge of evaluating the targets set by CBD and WSSD, an international consortium of UNEP-World Conservation and Monitoring Centre (WCMC), UNEP-GRID-Arendal and the Netherlands Environmental Assessment Agency (MNP) has combined the GLOBIO 2 and the IMAGE-NCI approach into a new Global Biodiversity Model framework (GLOBIO 3). The outcomes of this model framework are in line with the indicators decided on by the Conference of Parties of the CBD in Kuala Lumpur

(UNEP, 2004), particularly with regard to the extent of ecosystems and habitats, and the abundance and distribution of species. The GLOBIO 3 framework, designed to support policy makers in a supra-national setting (e.g. CBD, United Nations Environmental Programme, Organization for Economic Co-operation and Development and European Union), can be used to evaluate the consequences of possible socio-economic scenarios and policy options for biodiversity at global and regional level. It may also help to formulate strategies for biodiversity conservation and sustainable development.

The GLOBIO 3 framework is based on transparent relationships between pressure factors and biodiversity, derived from state-of-the-art knowledge from available literature and data. The model can be used to assess (i) biodiversity in the past, present and future in relation to the impacts of human pressures on species diversity and abundance; (ii) the relative importance of these pressures and (iii) likely effects of various policy options. The model is designed to make a quantitative comparison of biodiversity patterns and changes in these on the world-region scale.

In this chapter we will briefly describe the modelling approach and the relationships between the pressure factors and species diversity that are included in the GLOBIO 3 model framework. Subsequently, we will present results of the model applied to the current situation and for different scenarios for the year 2030.

## 10.2 Modelling approach

### *General*

The GLOBIO 3 model framework describes biodiversity through estimation of the remaining mean species abundance of the original species of each ecosystem, relative to their abundance in primary vegetation. This indicator of mean species abundance (MSA) is conceptually similar to the Biodiversity Integrity Index (Majer and Beeston, 1996), the Living Planet Index (Loh et al., 2005) and the Biodiversity Intactness Index (Scholes and Biggs, 2005). MSA can be considered as a measure for the CBD indicator on trends in abundance of selected species (UNEP, 2004).

The core of GLOBIO 3 is a set of regression equations describing the impact on biodiversity of the degree of pressure using dose–response relationships. These dose–response relationships are derived from a database of observations of species response to change. The database includes separate measures of MSA, each in relation to different degrees of pressure exerted by various pressure factors or driving forces. The entries in the database are all derived from studies in the peer-reviewed literature, reporting either on change through time in a single plot, or on response in parallel plots undergoing different pressures. Each contributing study considers one pressure.

The current version of the database includes data from about 500 reports: about 140 reports on the relationship between species abundance and land cover or land use, 50 on atmospheric N deposition (Bobbink, 2004), over 300 on impacts of infrastructure

*Table 10.1. Major driving forces used in large-scale studies of human impacts on natural systems.*

Driving force	Type <sup>a</sup>	Reference
Land-use change (including forestry)	D	Hannah et al. (1994); Sala et al. (2000); Sanderson et al. (2002); Wackernagel et al. (2002); Petit et al. (2001); UNEP/RIVM (2004); UNEP (2001)
Climate change	D	Sala et al. (2000); Petit et al. (2001); UNEP/RIVM (2004)
Atmospheric N deposition	D	Sala et al. (2000); Petit et al. (2001)
Biotic exchange	D	Sala et al. (2000)
Atmospheric CO <sub>2</sub> concentration	D	Sala et al. (2000)
Fragmentation	D	Wackernagel et al. (2002); Sanderson et al. (2002)
Infrastructure	D	Wackernagel et al. (2002); Sanderson et al. (2002); UNEP (2001)
Harvesting (including fisheries)	D	Wackernagel et al. (2002)
Human population density	I	McKee et al. (2003); Cardillo et al. (2004); UNEP/RIVM (2004)
Energy use	I	UNEP/RIVM (2004)

<sup>a</sup> Direct (D) and indirect (I) according to the definition of the conceptual framework of the Millennium Ecosystem Assessment (Millennium Assessment, 2003).

(UNEP, 2001) and several literature reports on minimal area requirements of species. Dose–response relationships for climate change are based on model studies (Bakkenes et al., 2002; Leemans and Eickhout, 2004).

Many studies address the effects of human pressure on global biodiversity and distinguish various indirect and direct drivers or pressure factors (Table 10.1). A direct driver unequivocally influences ecosystem processes and can therefore be identified and measured with varying degrees of accuracy. Main categories of direct drivers are changes in land cover and land use, species introduction and removal, and external inputs such as fertilizer use, pest control or irrigation water (Millennium Assessment, 2003). An indirect driver operates more diffusely, often by altering one or more direct drivers. Major indirect drivers include demographic, economic and socio-political circumstances; science and technology and cultural factors.

The driving forces (pressures) considered by GLOBIO 3 include land-cover change (taken from IMAGE), land-use intensity (partly taken from IMAGE), atmospheric nitrogen (N) deposition (see chapter 8), infrastructure development (as applied in GLOBIO 2), fragmentation and climate change (both taken from IMAGE).

Indirect drivers, such as human population density and energy use, are not used explicitly in the GLOBIO 3 framework, but have an impact on biodiversity through their influence on other – direct – drivers. For example, changes in the direct drivers (land use, climate, atmospheric N deposition and forestry) due to changing demography and socio-economic developments are calculated with IMAGE. Changes in infrastructure are calculated with the GLOBIO 2 model (UNEP, 2001).

Table 10.2. Relationship between GLC 2000 classes and land-use categories used in GLOBIO 3, including corresponding relative mean species abundance (MSA).

Main GLC 2000 class (GLC 2000 class <sup>a</sup> )	Sub-category	Description	MSA <sub>LU</sub>
Snow and ice (20)	Primary vegetation	Areas permanently covered with snow or ice considered as undisturbed areas	1.0
Bare areas (19)	Primary vegetation	Areas permanently without vegetation (e.g. deserts, high alpine areas)	1.0
Forest (1, 2, 3, 4, 5, 6, 7, 8, 9, 10)	Primary vegetation (forest)	Minimal disturbance, where flora and fauna species abundance are near pristine	1.0
	Slightly disturbed or managed forest	Forests with extractive use and associated disturbance like hunting and selective logging, where timber extraction is followed by a long period of regrowth with naturally occurring tree species	0.7
	Secondary forest	Areas originally covered with forest or woodlands where vegetation has been removed, forest regrowing or areas with a different cover and no longer in use	0.5
Shrubs and grassland (11, 12, 13, 14, 15)	Forest plantation	Planted forest, often with exotic species	0.2
	Primary vegetation (grass or shrubland)	Grassland or shrub-dominated vegetation (e.g. steppe, tundra or savanna)	1.0
	Livestock grazing	Grasslands where wildlife is replaced by grazing livestock	0.7
Mosaic: cropland /forest (17)	Man-made pasture	Forests and woodlands that have been converted to grasslands for livestock grazing	0.1
	Agroforestry	Agricultural production intercropped with (native) trees; trees kept for shade or as wind shelter	0.5
Cultivated and managed areas (16, 18)	Low input agriculture	Subsistence and traditional farming; extensive farming and low external-input agriculture	0.3
	Intensive agriculture	High external-input agriculture, conventional agriculture, mostly with a degree of regional specialization, irrigation-based and drainage-based agriculture	0.1
Artificial surfaces (21)	Built-up areas	Areas more than 80% built-up	0.05

<sup>a</sup> 1, Broadleaved evergreen forest; 2, Closed broadleaved deciduous forest; 3, Open broadleaved deciduous forest; 4, Evergreen needle-leaf forest; 5, Deciduous needle-leaf forest; 6, Mixed forest; 7, Swamp forest; 8, Mangrove and other saline swamps; 9, Mosaic: forest/other natural vegetation; 10, Burnt forest; 11, Evergreen shrub; 12, Deciduous shrub; 13, Grassland; 14, Sparse shrub and grassland; 15, Flooded grassland and shrub; 16, Cultivated and managed areas; 17, Mosaic: cropland/forest; 18, Mosaic: cropland/other natural vegetation; 19, Bare areas; 20, Snow and ice; 21, Artificial surfaces.

### Drivers of biodiversity loss

**Land use and land-use intensity.** We found about 140 published datasets comparing the species diversity and abundance between different land-cover/land-use types. Some of these studies include pristine, undisturbed ecosystems (e.g. primary forest).

*Table 10.3. Percentage of low-input and intensively used agricultural land for selected world regions based on farming system descriptions (Dixon et al., 2001) and GLC 2000.*

Region	Intensive agriculture	Extensive agriculture	Total
	(%)	(%)	(1000 km <sup>2</sup> )
Middle East and North Africa	64	36	852
Sub-Saharan Africa	24	76	1632
Eastern Europe and Central Asia	42	58	2738
South and Central America	73	27	1576
South Asia	57	43	2141
East Asia and Pacific	93	7	2356

The different land-use types from these studies were grouped in ten globally consistent categories: primary vegetation, including naturally non-vegetated areas like deserts and ice cover; slightly disturbed or managed primary forests; secondary forests; forest plantations; agroforestry; livestock grazing; man-made pastures; low input agriculture; intensive agriculture and built-up areas (Table 10.2). Most studies describe plant or animal species in the tropical forest biome, but the small number of available studies in other biomes confirms the general picture.

We calculated the value of MSA as the mean of all studies covering each land-cover/land-use category (Table 10.2). The MSA estimates obtained are thus in line with the results of Scholes and Biggs (2005), who estimated fractions of original species populations to be found in a range of land-use types based on expert knowledge.

The data for land cover/land use and changes in these, in which the resolution is 0.5 by 0.5 degrees, originate in the IMAGE model. This model has no fractional land use: i.e. a grid cell is covered either by agricultural land or natural vegetation, and each grid cell is assigned one natural land-cover type. To increase the spatial detail, we combined this data with the Global Land Cover 2000 (GLC 2000) map (Bartholome et al., 2004). GLC 2000, derived from the VEGA2000 dataset with a daily global image from the Vegetation sensor on board the SPOT4 satellite representing the year 2000, has a resolution of about 0.5 by 0.5 minutes. GLC 2000 has also been used in combination with other data to develop a land-cover base map for IMAGE (chapter 6).

We calculated the proportion of each land-cover/land-use type within each IMAGE grid cell from GLC 2000. The GLC 2000 map has 10 forest classes, 5 classes of low vegetation (grasslands and scrubland), 3 cultivated land classes, ice and snow, bare areas and artificial surfaces (Bartholome et al., 2004). This classification is based on the Land Cover Classification System developed by FAO and United Nations Environment Programme (UNEP) (Di Gregorio and Jansen, 2000).

To calculate the impact of agricultural production intensity we assigned the categories 'intensive agriculture' and 'low input agriculture' to the GLC class of 'cultivated and managed areas', using estimates of the distribution of intensive and low-input agricul-

*Table 10.4. Percentage of forest-use classes derived from FAO (2001) and GLC2000 for various world regions. The proportion of lightly used forest, which could not be estimated, is included in the primary forest category.*

World region	Primary forest	Secondary forest	Forest plantation	Total
	(%)	(%)	(%)	(1000 km <sup>2</sup> )
Canada	55	45	0	4830
USA	56	39	5	3462
Central America	85	14	1	1154
South America	84	15	1	8278
North Africa	31	31	38	45
Western Africa	92	7	1	4070
Eastern Africa	92	4	4	559
Southern Africa	97	2	1	2435
OECD Europe	60	35	5	1454
Eastern Europe	56	40	4	370
Former USSR	91	7	2	9260
Middle East	31	36	33	145
South Asia	53	7	40	857
East Asia	65	15	20	2230
Southeast Asia	75	15	10	2039
Oceania	91	7	2	1505
Japan	20	34	46	232
Greenland	0	0	0	0
<b>Total</b>	<b>78</b>	<b>17</b>	<b>5</b>	<b>42925</b>

ture in different regions of the world from Dixon et al. (2001) (Table 10.3). For all other regions we assumed 100% intensive agriculture. The change in agricultural land calculated by IMAGE for each world region for the future is distributed proportionally to current land use over all grid cells. Hence, expansion of agriculture, as determined by GLC 2000, leads to a loss of area in all (natural) land-cover types within the grid cell.

The GLC 2000 class containing a mosaic of cropland and forest has been assigned to the land-use category 'agroforestry' (Table 10.2), with grazing areas estimated by IMAGE for current and future years and distributed proportionally to all GLC 2000 classes containing low vegetation. We assign this mosaic to the category of 'livestock grazing'. The GLC 2000 class of 'herbaceous cover' is found within areas where forest is a potential vegetation type according to the potential vegetation map generated by IMAGE based on the BIOME model (Prentice et al., 1992) is classified as artificial pastures.

To calculate the impact of forestry we need to assign the land-use categories 'slightly disturbed or managed forest', 'secondary forest' and 'forest plantations' to the GLC 2000 classes. We use data on forest use from FAO (2001) to derive fractions of primary and secondary forest, and forest plantations, of the total forest area for different world regions (Table 10.4). These fractions are applied to all grid cells that contain

Table 10.5. Regression equations for the relationship between atmospheric N deposition exceedance (NE)<sup>a</sup> and MSA<sub>N</sub> for three ecosystems.

Ecosystem	Equation	Applied to GLC 2000 classes (see Table 10.2)
Arctic-Alpine ecosystem	$MSA_N = 0.9 - 0.05 \text{ NE}$	Snow and ice (20)
Boreal coniferous forest	$MSA_N = 0.8 - 0.14 \ln(\text{NE})$	Forests (1-10)
Grassland	$MSA_N = 0.8 - 0.08 \ln(\text{NE})$	Grassland and shrub (11-15)

<sup>a</sup> NE is calculated as N deposition minus critical load.

one or more GLC 2000 forest classes. For future calculations we use calculated timber demands to derive the fractional area needed to produce the timber and distributed the new fraction to each grid cell.

Furthermore, water bodies are excluded from the analysis, while all artificial surfaces are considered to be built-up areas. Bare areas are assigned to primary vegetation if the potential vegetation type is ice and snow, tundra or desert (where bare rocks or sand are abundant). Shrub classes are assumed to be secondary vegetation if the potential vegetation is forest (except for boreal forests).

**Atmospheric N deposition.** We reviewed some 50 studies on experimental addition of N in natural systems and the effects on species richness and species diversity. Based on this review, dose–response relationships were established between the annual rate of atmospheric N deposition exceeding the empirical critical load level and relative MSA. We assumed that the addition of N in these studies is equivalent to N deposition occurring in the field. The N deposition pressure factor applies only to natural land and not to cropland, because the addition of N in agricultural systems is assumed to be much higher than the additional N deposition. Table 10.5 presents the regression equations for the biomes developed by Bobbink (2004).

Global atmospheric N deposition fields were calculated by using emission inventories for N gases for the corresponding years as input for the TM5 chemistry-transport model. Deposition rates for historical and future years were obtained by scaling the current deposition fields for the mid-1990s using emission inventories for N gases for the corresponding years (see chapter 8).

Effects of N deposition are based on the critical load values for major ecosystems, as described by Bouwman et al. (2002), who used the soil map of the world and sensitivity of ecosystems to N inputs to produce a critical load map. The exceedance of N deposition in excess of critical load is calculated from global N deposition fields (see chapter 8) and the critical load map, while the N exceedance and the dose–response relationships for the different biomes are used to assess the effects of N deposition on the species abundance.

Table 10.6. Zones (in km) along linear infrastructural objects and their impact on relative mean species abundance (MSA) based on UNEP/RIVM (2004).

Vegetation cover	High impact (MSA <sub>I</sub> =0.50)	Medium impact (MSA <sub>I</sub> =0.75)	Low impact (MSA <sub>I</sub> =0.9)	No-impact (MSA <sub>I</sub> =1.0)
Cropland	0.0-0.5	0.5-1.5	1.5-5.0	>5.0
Grassland	0.0-0.5	0.5-1.5	1.5-5.0	>5.0
Boreal forest	0.0-0.3	0.3-0.9	0.9-3.0	>3.0
Temperate deciduous forest	0.0-0.3	0.3-0.9	0.9-3.0	>3.0
Tropical forest	0.0-1.0	1.0-3.0	3.0-10.0	>10.0
Desert and semi-desert	0.0-0.5	0.5-1.5	1.5-5.0	>5.0
Wetland	0.0-0.5	0.5-1.5	1.5-5.0	>5.0
Arctic tundra	0.0-1.0	1.0-3.0	3.0-10.0	>10.0
Ice and snow	0.0-0.5	0.5-1.5	1.5-5.0	>5.0

**Infrastructural development.** The impact of infrastructural development is based on the GLOBIO 2 model. GLOBIO 2 includes relationships between the distance to roads and MSA for various biomes based on over 300 peer-reviewed articles comprising information on more than 200 different species (UNEP, 2001). The impact of infrastructural development includes direct effects of disturbance on wildlife, fragmentation due to barrier effects, increased hunting activities and small-scale encroachment along roads.

The dose–response relationships were used to construct impact zones along linear infrastructure (roads, railways, power lines, pipelines) based on data from the Digital Chart of the World (DCW) (DMA, 1992). Buffers of different width were calculated and assigned to impact zones which were aggregated to 0.5 by 0.5 degree grid cells. MSA values were assigned to each impact zone (Table 10.6).

**Fragmentation.** If the unfragmented area of a land-cover type is large, all original species may find sufficient area suitable for supporting at least a minimal viable population, whereas a small unfragmented area may only support a minimal viable population of a few species (Verboom et al., 2006). The minimal area requirement of 156 mammal and 76 bird species, i.e. the minimal area that species need to support a minimal viable population, is used to construct a general relationship between the percentage of species with sufficient area and patch size. Data are taken from Allen et al. (2001), Bouwman et al. (2002) and Woodroffe and Ginsberg (1998). For plant species we assume a much smaller area requirement (1 km<sup>2</sup>) than for animals. Table 10.7 shows the fractions of original species having sufficient area to maintain a minimal viable population. These figures are assumed to represent the relative MSA.

**Climate change.** The treatment of climate change is different to that of the other pressure factors, as the available empirical evidence is limited to areas that are already experiencing significant impacts of change (such as the Arctic and montane forests). The current implementation in the model is based on estimates from EUROMOVE

Table 10.7. The relationship between area and corresponding fraction of species ( $MSA_F$ ) assumed to meet the minimal area requirement.

Area (km <sup>2</sup> )	$MSA_F$
1	0.55
10	0.75
100	0.85
1000	0.95
>10000	1

Table 10.8. Slopes of the regression equations relating mean stable area relative to original area and temperature change (relative to pre-industrial) for calculating the  $MSA_{CC}$  for different biomes.

Biome	Image	Slope (°C <sup>-1</sup> ) <sup>a</sup> EuroMove
Ice	0.023*	0.05
Tundra	0.154	0.07*
Wooded tundra	0.284	0.051*
Boreal forest	0.043*	0.079
Cool conifer forest	0.168	0.080*
Temperate mixed forest	0.045*	0.101
Temperate deciduous forest	0.100*	0.109
Warm mixed forest	0.052*	0.139
Grassland and steppe	0.098*	0.193
Hot desert	0.036*	-
Scrubland	0.129*	0.174
Savanna	0.093*	-
Tropical woodland	0.039*	-
Tropical forest	0.034*	-

<sup>a</sup> Slopes marked with ‘\*’ are used in the GLOBIO 3 model to calculate the correction factor for calculating the  $MSA_{CC}$ , starting from the values presented in Table 10.2 according to:  $MSA_{CC} = 1 - \text{Slope} * \Delta\text{Temperature}$ .

(Bakkenes et al., 2002; 2006), in which the proportion of species lost per biome in response to climate change is a function of temperature. These model results are compared with the predicted biome shifts in the IMAGE model (Leemans and Eickhout, 2005). Table 10.8 shows the slopes of the linear regression equations describing the global relationships between increase of temperature and stable area for each biome (IMAGE), or group of plant species occurring within a biome (EUROMOVE), which is considered to be an estimate of MSA. We used the regression lines that predict the smallest effects yielding conservative estimates (Table 10.8).

#### **Calculation of biodiversity loss and relative contributions of each driver**

The GLOBIO 3 model calculates the overall MSA value by multiplying the MSA values for each driver for each IMAGE 0.5 by 0.5 degree grid cell according to:

$$MSA_i = MSA_{LU_i} MSA_{N_i} MSA_{I_i} MSA_{F_i} MSA_{CC_i} \quad (1)$$

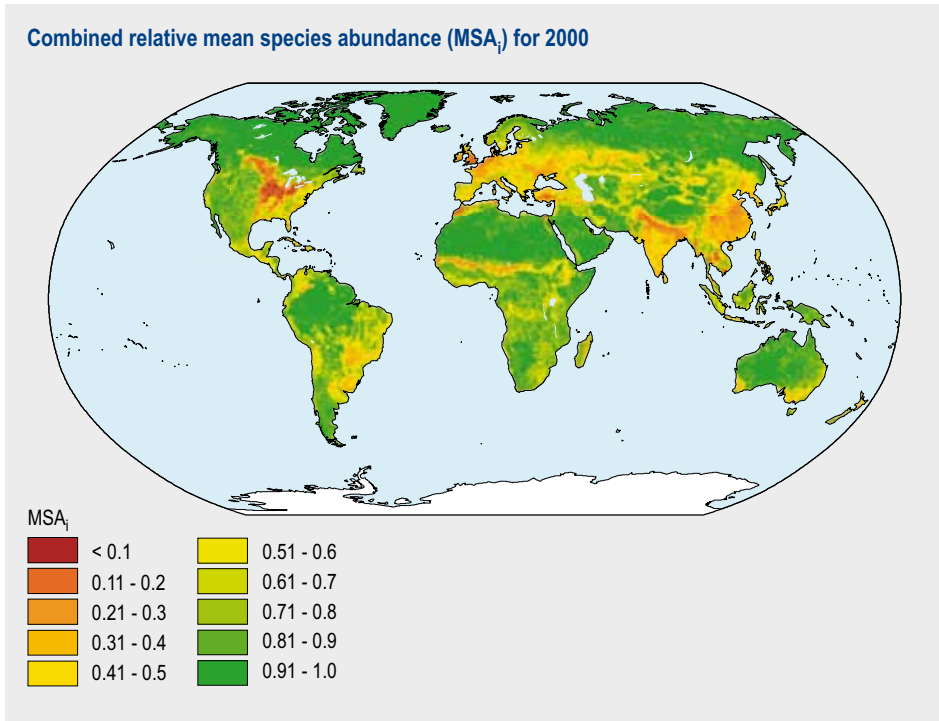


Figure 10.1. Combined relative mean species abundance ( $MSA_i$ ) for the year 2000 using all pressure factors in this study. Land-use effects are dominant in this map. The spreading effect of infrastructure is also visible, especially in Northern Asia and Africa. Climate and nitrogen deposition are minor factors.

where  $i$  is the index for the grid cell,  $MSA_{x_i}$  relative mean species abundance corresponding to the drivers LU (land cover/use), N (atmospheric N deposition), I (infrastructural development), F (fragmentation) and CC (climate change).  $MSA_{LU_i}$  is the area-weighted mean over all land-use categories within a grid cell. Figure 10.1 shows the overall MSA for the world for the year 2000.

The regional  $MSA_r$  is calculated as the area-weighted mean of  $MSA_i$  values of all grid cells located within a region:

$$MSA_r = \frac{\sum_i MSA_i A_i}{\sum_i A_i} \quad (2)$$

where  $A_i$  is the land area occupied by grid-cell  $i$ .

The relative contribution of each driver to the loss of MSA was calculated from equations (1) and (2), as shown for the world in Figure 10.2. Agriculture is the most important factor worldwide in reducing MSA and thus biodiversity. This is because agricultural production systems cover vast areas and most agricultural practices imply a drastic change in the original land cover (clearing, cultivation, use of agro-chemicals, fertilizers, etc.). On

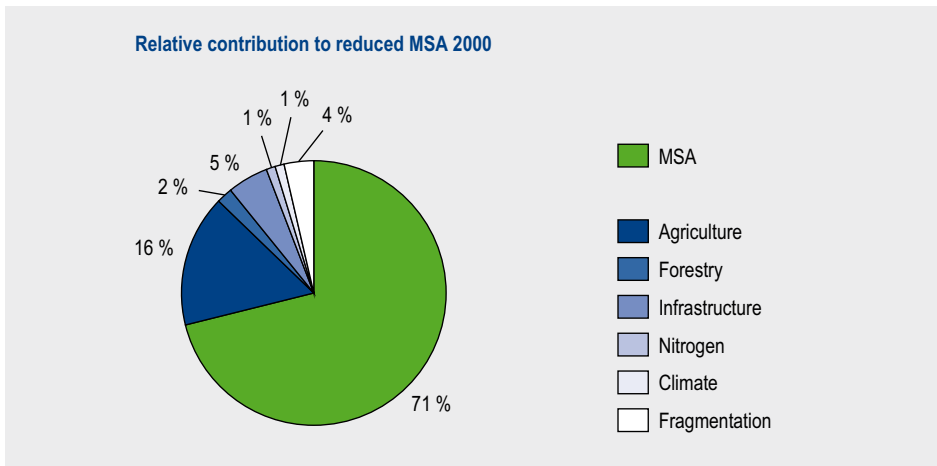


Figure 10.2. Relative global contribution of the different pressure factors to reduced MSA for the year 2000.

the global scale, the second most impact factor is infrastructure, followed by fragmentation. Atmospheric N deposition, climate change and forestry are minor factors on global scale, but do play more prominent roles in some regions. In scenarios too, their role may become increasingly important. The relatively small contribution of forestry is partly explained by the assignment of the effects of deforestation to agriculture, since cleared forests are generally converted to crop or pasture land.

Figure 10.2 also shows that the global MSA is about 70%, indicating that large parts of the world are still in a more or less pristine state. Regionally, however, there are striking differences (Figure 10.3). The regions that include large areas of desert (e.g. Northern Africa and Australia), ice cover (e.g. Greenland) or boreal forest and tundra (e.g. Canada and former USSR), which are not suitable for agriculture, show the highest MSA values.

### 10.3 Implementation of the SRES scenarios

We assessed the development of biodiversity for four different scenarios for the period up to 2030. These are A1b, A2, B1 and B2 from the IPCC Special Report on Emissions Scenarios (SRES) (Nakicenovic et al., 2000), which were implemented with the IMAGE 2.2 model on global scale (IMAGE-team, 2001). The infrastructural development was derived from the GLOBIO 2 model (UNEP, 2001). Here we summarize some of the main elements of the SRES scenarios relevant to global biodiversity. For further details please refer to Nakicenovic et al. (2000). The storylines of the SRES scenarios describe developments in many different social, economic, technological, and environmental and policy dimensions. None of the scenarios include new explicit climate or biodiversity policies.

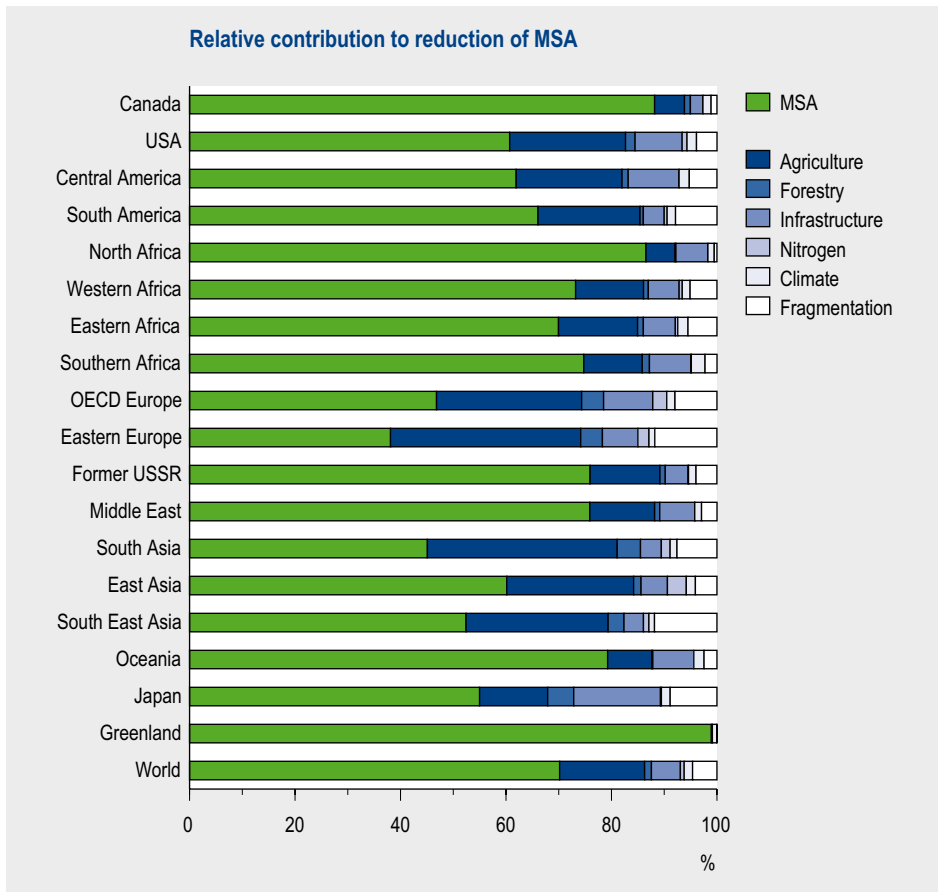


Figure 10.3. Regional differences of the relative contribution to reduced MSA of different pressure factors for the year 2000.

The A1 scenario describes a future world of very rapid economic growth, low population growth, and the rapid introduction and transfer of new and more efficient technologies. Major underlying themes are convergence among regions, capacity building and increased cultural and social interactions, with a substantial reduction in regional differences in per capita income.

The A2 scenario describes a heterogeneous world. The underlying theme is self-reliance and preservation of local identities. Fertility patterns across regions converge slowly, which results in high population growth. Economic development is primarily regionally oriented and per capita economic growth and technological changes are more fragmented and slower than in other storylines.

The B1 scenario assumes continuing globalization and economic growth, and a focus on the environmental and social (immaterial) aspects of life. The scenario can be interpreted as the continuation of a balanced modernization process. Governance at

Table 10.9. Comparison of the late 1990s situation with the SRES scenarios for world population, global arable land area, temperature change, infrastructure development and forestry.

Characteristic	Late 1990s	SRES scenario			
		A1	A2	B1	B2
Human population (x billion)	6.1	8.2	9.3	8.2	8.4
Area agricultural land (Mkm <sup>2</sup> )	17	20	21	19	20
Global temperature change <sup>a</sup>	0.61	1.25	1.33	1.31	1.33
Infrastructural development		high	high	moderate	moderate
Forestry		no change	no change	no change	no change

<sup>a</sup> Relative to pre-industrial

Table 10.10. Global MSA values (%) and reduction (%) caused by different pressure factors for projected land use and climate in 2030 according to the four SRES scenarios as implemented in the IMAGE model (version 2.2).

	A1	A2	B1	B2
MSA remaining	64.2	66.0	66.9	66.9
Reduction by pressure factor				
Agriculture	15.4	16.1	15.2	16.1
Forestry	3.0	3.1	3.2	3.1
Infrastructure	9.4	7.1	7.1	6.1
Nitrogen	1.5	1.4	1.0	1.2
Climate	2.9	2.8	3.0	3.0
Fragmentation	3.6	3.6	3.6	3.6
Total	100.0	100.0	100.0	100.0

all levels and regulated forms of market capitalism are seen as the way forward. It includes the strengthening of non-governmental organizations concerned about issues of sustainability and equity. The B1 scenario represents a modest and decent world, bureaucratic and regulated, but also in search of fairness and sustainability.

The B2 scenario portrays a world in which the emphasis is on local solutions to economic, social, and environmental sustainability. It is a world with moderate population growth, intermediate levels of economic development, and less rapid and more diverse technological change than in the B1 and A1 storylines. While the scenario is oriented towards environmental protection and social equity, it also focuses on local and regional levels.

Since the future infrastructural development is not an explicit part of the SRES scenarios, we assumed a large increase in infrastructure in the A1 and A2 scenarios, whereas infrastructural development is less rapid in B1 and B2. These assumptions are based on the Global Environmental Outlook 3 (UNEP, 2002b). Changes in land use, especially the increase in agricultural land, change in atmospheric N deposition and expected climate change were calculated with the IMAGE model.

There are clear differences between the four scenarios in the future development of the main driving forces of global biodiversity (Table 10.9). The future MSA values and the relative contribution of the pressure factors calculated using the procedures described above lead to decreases of the MSA in all scenarios (Table 10.10). Most biodiversity loss is seen in the A1 scenario (remaining MSA of 64%), while in the B1 and B2 scenarios the decrease of MSA is much less (remaining MSA is 67%).

Expansion of agricultural land is the most prominent factor causing MSA decrease in all scenarios (Table 10.10). Results of Sala et al. (2000) are not entirely comparable, as they use a different set of pressure factors; however, they also state that land-use change will be the most important threat to biodiversity in coming decades. The most severe changes are expected in A1, with more rapid economic growth than in other scenarios. In this scenario land-use changes in combination with infrastructural development will cause biodiversity depletion. The effect of climate change is expected to increase in 30 years but still remains relatively small. Climate change is expected to have major impact on biodiversity in the longer term.

## 10.4 Concluding remarks

The GLOBIO 3 model framework is static rather than dynamic, and deterministic rather than stochastic. It is an operational tool to assess the combined effects of the most important pressure factors on biodiversity. The link with the integrated model IMAGE allows for analysis of scenarios, evaluation of policy measures at the international level and analysis of different potential policy options.

The advantage of the GLOBIO 3 approach is the use of quantitative dose–response relationships for different factors, which allows for estimating (i) biodiversity expressed as a proxy for the mean species abundance and (ii) the quantification of the relative contribution of different pressure factors to the loss of biodiversity. Since GLOBIO 3 also calculates changes of the areas of different ecosystems, it can provide information on changes in distribution and abundance of selected species, and changes in the extent of selected ecosystems and habitats.

There are a number of limitations and uncertainties related to the dose–response relationships, the driving forces considered, and the underlying data used in GLOBIO 3 that we wish to address in the coming years. The dose–response relationships are now based on a limited set of studies that were published and interpreted in a uniform framework. The set of studies does not cover all biomes nor does it represent all important species groups. It is rather a compilation of existing knowledge biased in the direction of specific biomes. Reducing the uncertainty of the estimated effects will require more studies covering a wider range of environmental conditions and vegetation types.

Quantitative information on the interaction between pressure factors is scarce. To assess possible interactions, assumptions can be made that range from 'all interact completely' (only the maximum response is delivered) to 'no interaction' (the responses to each pressure factor are cumulative). Such interactions will be explored in the coming years.

Important factors that may affect biodiversity are not included. Sala et al. (2000) considered the impact of (both intended and unintended) biotic exchange of species and invasion of exotic species, as well as increased atmospheric CO<sup>2</sup> concentration, as major factors. Dose–response relationships were not established in GLOBIO 3 for these factors due to lack of data. Other factors like fire incidence, extreme events and pollution (except atmospheric N deposition) are not addressed either.

Another way to improve the methodology is the use of species distribution and abundance data. Long-term time series of species occurrence and abundance may help to partially validate the GLOBIO 3 results (De Heer et al., 2005). Models for distribution of species can be developed using different statistical techniques combining the drivers behind species distributions, as suggested by Guisan and Zimmermann (2000).

Apart from the dose–response relationships, the GLOBIO 3 model results depend largely on the quality of the input data, particularly the spatial distribution for the different land-use classes. We recognize that the areas of agricultural land use differ significantly between the FAO statistics (FAO, 2005) and satellite imagery (Klein Goldewijk et al., 2006), while the combination of IMAGE-simulated land cover with satellite data also causes inconsistencies. In addition, the GLC 2000 map may not be correct for use in combination with scenarios, because of land-use changes and climate change affecting the distribution of ecosystems.

In spite of all these problems and uncertainties, the results of GLOBIO 3 are in line with the results of other global studies. Patterns of human disturbance reflected by population density, degrees of human domination of ecosystems (McKee et al., 2003; Cardillo et al., 2004; Hannah et al., 1994), patterns of the 'human footprint' (Sanderson et al., 2002) and patterns of human appropriation of net primary production (Imhoff et al., 2004) are in agreement with the MSA estimates of GLOBIO 3. The similarity of the different analyses is not surprising, because all methods are dominated by factors related to land use and land conversion.

In addition to improvements of the approach described in this chapter, we are also working on a similar approach (based on driving forces) to assess changes in biodiversity in freshwater systems and coastal marine ecosystems.



## 11 FAIR: A MODEL FOR ANALYZING ENVIRONMENTAL AND COST IMPLICATIONS OF FUTURE COMMITMENT REGIMES

- The policy decision-support model FAIR, which is part of the IMAGE 2.4 framework, is widely used to assess the environmental and abatement-cost implications of international regimes for the differentiation of future emission reductions of greenhouse gases (GHGs). The model links long-term climate targets and global reduction objectives with regional emission allowances and abatement costs and, as such, accounts for the Kyoto mechanisms.
- FAIR consists of three sub-models: a simple climate model (basically the IMAGE 2.4 climate model), an emission allocation model and a cost model. The cost model uses marginal abatement cost curves of both the energy- and industry-related carbon dioxide emissions modelled by the TIMER 2.0 model and the carbon sinks of the IMAGE model.
- The FAIR model has been used in a recent study to assess different policy regimes and allocation schemes for stabilizing greenhouse gas concentrations at 550 ppm CO<sub>2</sub>-eq. The two regimes that provide the best prospects in terms of reduction targets and abatement costs for most of the countries were found to be the Multi-Stage approach (with a gradual increase in the number of countries adopting emission intensity or reduction targets) and the so-called Triptych approach (with sectoral targets for all countries).

### 11.1 Introduction

The Kyoto Protocol, which entered into force in February 2005, is the first step towards achieving the long-term objective of the UNFCCC: stabilizing atmospheric GHG levels at non-dangerous levels (Article 2) (UNFCCC, 1992). According to the Kyoto Protocol (Article 9.2), international negotiations on the design of a post-2012 climate agreement were due to start in 2005. One of the most contentious issues facing these negotiations is that of (international) burden sharing – or differentiation – of the post-2012 commitments with respect to reducing global GHG emissions: what is the time frame of the contribution (when) and how much should be contributed – and by whom? The answers to these questions are not only related to technical capabilities and economic costs, but also to such moral considerations as responsibility and equity. Within this framework, we developed the policy decision-support tool ‘Framework to Assess International Regimes for the differentiation of commitments’ (FAIR) version 2.0 with the aim of providing a tool which integrates most of these issues in a quantitative manner. More specifically, the model has been developed to explore and evaluate the environmental and abatement cost implications of various international regimes with respect to the differentiation of future commitments for meeting long-term climate targets, such as the stabilization of atmospheric GHG concentrations (Den Elzen and Lucas, 2005).

Many proposals for differentiating commitments among countries have been put forward, both in the literature and from Parties to the UNFCCC (see for an overview Aldy et al., 2003; Bodansky, 2004; Kameyama, 2004; Torvanger and Godal, 2004). The FAIR 2.0 model includes about ten approaches, all of which define the differentiation of commitments based on criteria and rules for the distribution of emission allowances (also referred to as assigned amounts, emission permits or emission endowments). The model was not developed to promote any particular approach to international burden sharing, but rather to support policy makers by quantitatively evaluating the environmental and cost implications of a range of approaches and linking these to targets for global climate protection. It has also been used to support dialogues between scientists, NGOs and policy makers (e.g. Berk et al., 2001). To this end the model is set up as an interactive tool with a graphical user interface, which enables interactive changing and viewing of model input and output. A demonstration version of the model can be downloaded at: [www.mnp.nl/fair](http://www.mnp.nl/fair).

## 11.2 FAIR 2.0 Model description

### General

The FAIR model consists of three linked models (Figure 11.1): a climate model, an emission allocation model and an abatement costs model. The climate model calculates the

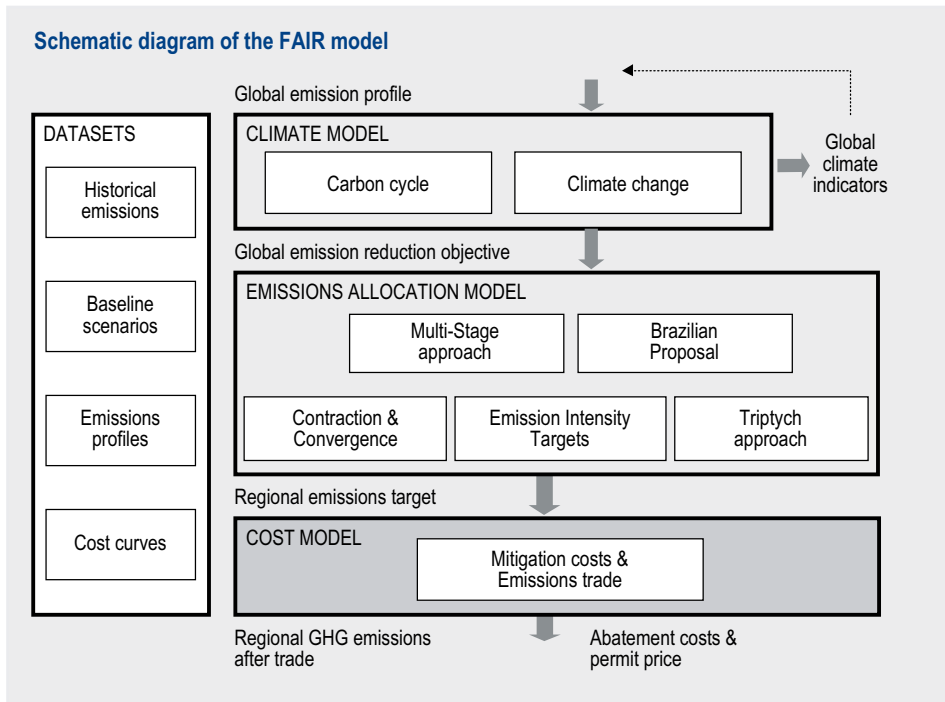


Figure 11.1. Schematic diagram of the FAIR model showing its framework and linkages (Den Elzen and Lucas, 2003).

*Table 11.1. World regions and the different aggregated levels.*

Annexes	Income class <sup>a</sup>	Aggregated regions
Annex I	High	North America, EU plus, Japan, Oceania
	Lower medium	Former Soviet Union (FSU)
Non-annex I	Medium	Latin America
	Lower medium – upper medium	Middle East and Turkey
	Low – lower medium	Southeast and East Asia, northern and southern Africa
	Low	South Asia, western and eastern Africa

<sup>a</sup> High income (US\$9266 or more), upper medium (\$2996-9265), lower medium (\$756-2995) and low income (\$755 or less) (WorldBank, 2001).

climate impacts of global emission profiles and emission scenarios, and determines the global emission reduction objective based on the difference between the global emissions scenario (without climate policy) and a global emission profile (including climate policy).

The emission allocation model calculates the regional GHG emission allowances for different regimes for the differentiation of future commitments within the context of the global reduction objective derived from the climate model.

The abatement costs model calculates the regional abatement costs and emission levels after trading off the emission allowances derived from the emission allocation model following a least-cost approach. The model makes full use of the flexible Kyoto mechanisms for emissions trading and the substitution of reductions between the different gases and sources.

Model calculations have been carried out for 17 world regions or for aggregates of these 17 regions (Table 11.1). The GHG emissions are converted to CO<sub>2</sub>-equivalents, similar to those in the Kyoto Protocol, i.e. the sum of the Global Warming Potential (GWP; a 100-year time horizon is used) weighted emissions of the six GHGs or groups of GHGs specified in the Kyoto Protocol. These are carbon dioxide (CO<sub>2</sub>), methane (CH<sub>4</sub>), nitrous oxide (N<sub>2</sub>O), hydrofluorocarbons (HFCs), perfluorocarbons (PFCs) and sulphur hexafluoride (SF<sub>6</sub>). Various datasets of historical emissions, baseline scenarios, emission profiles and marginal abatement cost (MAC) curves are included in the model framework to assess the sensitivity of the outcomes to variations in these key inputs.

The historical regional emissions are based on CDIAC-ORNL data (Marland et al., 2003) and the EDGAR database (Van Aardenne et al., 2001). The CDIAC-ORNL database includes CO<sub>2</sub> emissions from fossil fuel combustion and cement production (for the period 1751–2000), while the CO<sub>2</sub> emissions from land-use changes are based on Houghton (2003) (1890–2000). The EDGAR database includes the emissions of the Kyoto GHGs (CO<sub>2</sub>, CH<sub>4</sub>, N<sub>2</sub>O and the hydrochlorofluorocarbons (HCFCs), HFCs, PFCs and SF<sub>6</sub>), other halocarbons (e.g. chlorofluorocarbons (CFCs)), sulphur dioxide (SO<sub>2</sub>) and the ozone precursors (NO<sub>x</sub>, CO and volatile organic compounds (VOC)) from fossil fuel com-

Table 11.2. Description of the global climate model.

Sub-module	Model
Carbon cycle	Mass balance equation of the anthropogenic CO <sub>2</sub> emissions minus the terrestrial uptake (i.e. Net Ecosystem Productivity <sup>a</sup> are based on IMAGE 2.2 scenarios (IMAGE-team, 2001)) and the oceanic uptake (i.e. box-diffusion type model is from Joos et al. (1999)).
Methane	Tropospheric loss depends on the OH concentration (parameterized as a function of CH <sub>4</sub> , CO, VOC and NO <sub>x</sub> ), and stratospheric and biospheric loss based on IPCC-TAR (Prather et al., 2001).
Tropospheric ozone	Related to CH <sub>4</sub> concentrations and emissions of reactive gas emissions from IPCC-TAR (Prather et al., 2001).
Halocarbons	For CFCs, PFCs and SF <sub>6</sub> constant lifetimes, and HCFCs and HFCs variable lifetimes (Prather et al., 2001).
Aerosols and ozone forcing	Forcings from sulphate aerosols (direct and indirect), fossil fuel black carbon, fossil fuel organic carbon and biomass burning aerosols, tropospheric and stratospheric ozone (O <sub>3</sub> ) and water vapour are calculated as described in the IPCC Third Assessment Report (TAR).
GHGs forcing	The non-linear concentration-forcing relations for CO <sub>2</sub> , N <sub>2</sub> O and CH <sub>4</sub> (including overlap terms) are based on IPCC-TAR.
Temperature increase and sea level rise	Upwelling-Diffusion Climate Model of the MAGICC model (Wigley and Raper, 1992), with IPCC-TAR parameter values, using a climate sensitivity of 2.5°C equilibrium surface temperature change for a doubling of CO <sub>2</sub> concentration.

<sup>a</sup> From regrowth vegetation (assumed to be an anthropogenic activity) and full-grown vegetation (a natural process)

bustion, industrial and agricultural sources, biomass burning and land-use changes (1890–1995).

Different baseline scenarios are used for future (1995–2100) projections of the regional population and gross domestic product (GDP) along with the anthropogenic baseline emissions of the Kyoto GHGs, SO<sub>2</sub> and the ozone precursors. The baseline scenarios include the IMAGE 2.2 implementation of the six IPCC-SRES scenarios (IMAGE-team, 2001) and the Common POLES-IMAGE baseline emission scenario (Van Vuuren et al., 2003).

The global emission profile discussed in this chapter results in a stabilization of the GHG concentrations at 550 ppm CO<sub>2</sub>-eq. in 2100 (S550e). Other emission profiles are discussed elsewhere (Den Elzen and Lucas, 2005).

MAC curves reflect the costs of abating the last ton of CO<sub>2</sub>-equivalent emissions. Consequently, they describe the potential and costs of the different abatement options considered. For the energy- and industry-related CO<sub>2</sub> emissions we derived MAC curves from the energy models TIMER (Van Vuuren et al., 2004) and POLES (Criqui et al., 1999) and from the macro-economic model WorldScan (CPB, 1999). For CO<sub>2</sub> sequestration, MAC curves derived from the IMAGE 2.2 model can be used. For the non-CO<sub>2</sub> gases, two sets of MACs are included in FAIR: one from Criqui (2002) and EMF21 (DeAngelo et al., 2004; Delhotal et al., 2004; Schaefer et al., 2004). These MAC curves for the non-

CO<sub>2</sub> gases are primarily based on detailed abatement options for different sectors and sources.

### *Climate model*

The simple climate model (Den Elzen and Schaeffer, 2002) calculates global GHG concentrations, radiative forcing, temperature increase and sea level rise using the global emission scenarios and profiles (Table 11.2). For the default calculations, the model uses the stand-alone IMAGE 2.2 climate model (Eickhout et al., 2004), which consists of an oceanic carbon, an atmospheric chemistry and a climate model (see Chapter 9). The UNFCCC – Assessment of Contributions to Climate Change (ACCC) climate model (UNFCCC, 2002) – is included for alternative global climate calculations. This model is based on Impulse Response Functions (IRFs) for the calculations of GHG concentrations, temperature change and sea level rise and on the IPCC-TAR functions for radiative forcing. An IRF mathematically describes a transient climate model response to external forcing (Hasselmann et al., 1993). In addition, eight IRFs derived from simulation experiments with general circulation models (GCM) (Den Elzen, 2002) are included for alternative climate calculations.

The climate attribution model calculates the regional contribution to climate indicators (GHG concentrations, radiative forcing, temperature change and sea level rise) on the basis of historical GHG emissions (Den Elzen et al., 2002) using the UNFCCC-ACCC methodology (UNFCCC, 2002).

### *Emission allocation model*

The emission allocation model calculates regional emission allowances for different international future commitment regimes (hereafter referred to as regimes). Within the framework of the FAIR model a regime is a set of rules for defining international emission reduction commitments and participation thresholds. Table 11.3 provides a brief description of the ten regimes included in the model, five of which are discussed in more depth here below.

**Multi-Stage (MS).** This regime consists of a system which divides countries into groups according to level of effort and type of commitments (stages). This regime results in an incremental evolution of the regime, i.e. a gradual expansion over time of the different groups of countries with commitments, where countries adopt different levels and types of commitments according to participation and differentiation rules (Gupta, 1998; Berk and Den Elzen, 2001; Den Elzen, 2002). The regime is based on four consecutive stages for the non-Annex I regions: (i) no quantitative commitments – the regions follow their baseline emission trajectories; (ii) intensity targets – the regions adopt emission intensity improvement targets defined by the rate of reduction in the emission intensity of their economies, i.e. GHG emissions per unit of economic activity; (iii) stabilization of emissions – the regions stabilize emissions for a period of time; (iv) emission reduction targets – the regions share the remaining reduction effort needed to achieve the global emission profile on the basis of a burden-sharing key.

*Table 11.3. Brief description of the ten different regimes implemented in the FAIR model.*

Regime	Operational rule for allocation of emission allowances
Multi-Stage regime (MS)	A gradual increase in the number of Parties involved adopting either emission intensity or reduction targets (Berk and Den Elzen, 2001).
Brazilian Proposal (BP)	Reduction targets based on a country's contribution to temperature increase (UNFCCC, 1997); participation in emission reductions based on a per capita income threshold (Den Elzen et al., 2003).
Ability to Pay (AP)	Emission reduction allocation and participation in emission reduction based on per capita income thresholds (Jacoby et al., 1999).
Contraction & Convergence (C&C)	Emission targets based on a convergence of per capita emission levels of all Parties under a contraction of the global emission profile (Meyer, 2000).
CSE convergence (CSE)	Per capita emission convergence (C&C) combined with basic sustainable emission rights (Centre of Science and Environment, 1998).
Global Compromise (GC)	Allocation of the global emission allowances based on a population-weighted preference score voting for either emission (grandfathering) or per capita allocation (Müller, 1999).
Grandfathering (GF)	Allocation of the global emission reduction proportional to their present emission share, with participation in reduction based on an income threshold (Rose et al., 1998).
Multi-Criteria Convergence (MCC)	Allocation of the global emission allowances based on different weighting of criteria, i.e. emissions, population and GDP.
Emission Intensity Targets (EIT)	Emission reductions related to improvements in the emission per unit GDP output (Den Elzen and Berk, 2003).
Triptych (TT)	Emission allowances based on various differentiation rules to different sectors for all Parties (Phylipsen et al., 1998).

All Annex I regions (including the U.S.A.) are assumed to start in the fourth stage, immediately after the Kyoto period (2012), while the non-Annex I regions enter the different stages according to various participation thresholds. Stage 3 is excluded from the cases analyzed here. The participation thresholds are based on the Capability-Responsibility (CR) index, which is defined as the normalized sum of per capita income (in PPP\$1000 per capita) and CO<sub>2</sub>-equivalent emissions (in ton CO<sub>2</sub> per capita; the index reflects the historical responsibility for climate change (Criqui and Kouvaritakis, 2000)). Purchase Power Parity (PPP) is an alternative indicator for GDP per capita based on the relative purchasing power of individuals in various regions. For Stage 2, the intensity improvement targets are defined as a linear function of per capita income with a chosen maximum rate that reflects the stringency of the overall climate target, while concurrently avoiding de-carbonization rates in any region that would outpace those of economic growth. The underlying factors determining the MS regime are described in detail by Den Elzen et al. (2006a).

**Contraction & Convergence (C&C).** This regime defines emission rights on the basis of a convergence of per capita emissions in which all countries participate immediately after 2012, with their per capita emission permits (rights) converging towards equal levels over time (Meyer, 2000). More specifically, all regional emission allowance shares converge from actual proportions in emissions to shares based on the distribution of the population in the convergence year. In the S550e example the convergence year is 2050.

**Centre for Science and Environment (CSE) Convergence.** CSE Convergence combines the C&C concept with basic sustainable emission rights (CSE, 1998). The basic assumption is that there is a global sustainable emission level, which is defined as the amount of CO<sub>2</sub> that can be emitted over the very long term without raising the atmospheric CO<sub>2</sub> concentration. This global emission (6 Pg CO<sub>2</sub>-eq. per year is the S550e example) is allocated to all regions on a per capita basis in accordance with the egalitarian equity principle that every human being has the right to a basic emission quatum irrespective of nationality. Given future population development, the per capita basic emission quatum will change over time. In addition to the basic quatum, each person has a remaining quatum, which is calculated by subtracting the global sustainable emission level from the global emission profile using the linear convergence methodology. In the S550e example the convergence year is 2050.

**Global Compromise (GC).** To solve conflicts between Parties, the GC regime creates a weighted arithmetic mean for base proposals and Party preferences (Müller, 1999), in which consensus is sought based on a voting procedure that combines preferences for a distribution of global emission allowances according to emission levels (grandfathering) or population levels (per capita allocation). The calculation takes place in two steps: a voting step, followed by an allocation of emissions on the basis of a population-weighted averaging of the preferences. In the voting step, each region determines its preferred distribution method (per capita or grandfathering). The emission shares per region are then calculated as the (population) weighted mean between the population and grandfathering shares using the calculated weights. In our model implementation, the emissions and population shares and weights depend on a specified policy delay ( $p_d$ ), i.e. the values of the shares at time  $t$  are calculated based on the data of  $t - p_d$  (Den Elzen et al., 2003). In the S550e example the policy delay is ten years.

**Triptych (TT).** The TT regime is a sector- and technology-oriented bottom-up approach that accounts for differences in specific situations within countries. It has been used for supporting decision making in internal target differentiation in the EU, both before and after Kyoto (COP-3) (Phylipsen et al., 1998). In its original form it only included energy-related CO<sub>2</sub> emissions; however, Groenenberg (2002) extended this approach with other GHG emissions and sources and addressed a number of shortcomings. The overall emission allowances are determined by applying various rules for differentiation to three distinct sectors – the internationally oriented energy-intensive industry sector, the domestic sector and the electricity production sector.

The industrial emission allowances are calculated on the basis of a future growth of production. The growth rates are estimated by assuming per capita physical production to be a function of per capita PPP income, with the latter derived from historical trends based on Groenberg (2002). The improvement rates in energy intensity for all regions are calculated on the basis of a world-wide convergence in energy efficiency levels, which are expressed in an aggregated Energy Efficiency Indicator (EEI) (Phylipsen et al., 1998) that varies over time. These improvement rates depend on the initial (2010) values of the indicator, the year of convergence and the final convergence level. The latter is a fraction (in the S550e example, this is 50%) of the EEI value obtained under the best current practices or best available technologies in the convergence year.

The domestic emission allowances depend on the population growth and a convergence of per capita domestic emissions (in the S550e example, 1.5 ton CO<sub>2</sub>-eq. per year). The emission allowances from electricity production are defined by a growth in the electricity consumption and are estimated by the weighted sum of the emission growth in the energy-intensive industry and the domestic sectors, and a convergence in the intensity of the electricity production (emissions per unit of kilowatt-hour; in the S550e example 125 g CO<sub>2</sub>-eq. per kWh). This approach includes the non-CO<sub>2</sub> GHG emissions from two other sectors – fossil fuel production and agriculture (with a maximum reduction of non-CO<sub>2</sub> GHG emissions of 90% below the baseline for fossil fuel and 35% for agriculture). For a more detailed description of this model, the reader is referred to Den Elzen (2002).

### ***Abatement cost model***

The cost calculations in the abatement cost model use aggregated permit demand and supply curves that are derived from the MAC curves for the different regions, gases and sources. Assuming a least-cost approach, these supply curves enable simple and transparent calculations of the costs to be undertaken by different regions in reaching their respective emission targets, as set in the emission allocation model. The intersection formed by the aggregated MAC curves (total supply) and emission reduction objectives (total demand) of Parties determines the international market equilibrium permit price (henceforth referred to as permit price).

Depending on the national or regional MAC curves and the reduction objectives, this market price determines whether Parties will import permits to meet their individual targets or whether they will abate more than is required to sell this surplus on the international permit trading market. This methodology distributes the regional emission reduction objectives over the different gases and sources following a least-cost approach, taking full advantage of the flexible Kyoto Mechanisms, i.e. International Emissions Trading (IET), Joint Implementation (JI) and the Clean Development Mechanism (CDM). The permit price is subsequently used to determine the buyers and sellers on the international trading market as well as the accompanying financial flows of permit trading and the regional abatement costs resulting from domestic and external abatements. As the lion's share of the reduction effort is generally taken domestically,

*Table 11.4. Marginal Abatement Cost (MAC) curves and the parameter setting for the Kyoto mechanisms used for the cost calculations (Van Vuuren et al., 2003).*

MAC curves	Settings
CO <sub>2</sub> energy- and industry-related MAC curves	TIMER
CO <sub>2</sub> AR <sup>a</sup> MAC curves	IMAGE 2.2
Non-CO <sub>2</sub> MAC curves – set	GECS
• Technological improvement	2% per 5-year period
Non-CO <sub>2</sub> agricultural emissions	No MAC curves available
• Maximum reduction (below baseline)	35%
• Target year	2040
Kyoto mechanisms – parameters	
Transaction costs	Sum of a constant \$2 per tCO <sub>2</sub> -eq. plus 2% of the total abatement costs
CDM accessibility factor	10% of the theoretical maximum in 2010 increasing to 30% in 2030

<sup>a</sup> AR, Afforestation and Reforestation

the ratio of abatement costs to GDP measured in PPP terms (referred to as the ‘effort rate’) is a useful indicator of potential economic impacts of emission reduction. For a more detailed description of this model, the reader is referred to Den Elzen and Lucas (2003).

The MAC curves and main parameter settings used in the analysis in this chapter are presented in Table 11.4 and briefly discussed below (for details, see Van Vuuren et al., 2003). FAIR uses impulse response curves from the TIMER energy model (de Vries et al., 2001) for CO<sub>2</sub> abatement options and cost estimates for energy- and industry-related emissions (energy, feedstock and cement production). The TIMER energy model calculates regional energy consumption, energy-efficiency improvements, fuel substitution and the supply and trade of fossil fuels and renewable energy technologies as well as carbon capture and storage. A carbon tax on fossil fuels is imposed for constructing the MAC curves to induce emission abatements, taking into account technological developments, learning effects and system inertia (Van Vuuren et al., 2004). The potential of CO<sub>2</sub> sinks for application in Afforestation and Reforestation (AR) projects, as determined by the IMAGE model (see chapter 7), are extended with conservative estimates of sinks from Forest Management together with negligible costs.

For the non-CO<sub>2</sub> GHG emissions, the set of MAC curves from Criqui (2002) is used, including curves for CH<sub>4</sub> and N<sub>2</sub>O emissions from both energy- and industry-related emissions and from some agricultural sources, as well as abatement options for the halocarbons. The non-CO<sub>2</sub> MAC curves have been corrected for measures already applied under our baseline scenario in order to increase consistency within the analysis (see Van Vuuren et al., 2003, for the methodology used). In addition to the end-of-pipe measures on which the non-CO<sub>2</sub> MAC curves are based, CH<sub>4</sub> and N<sub>2</sub>O emissions can be reduced by systemic changes in the energy system (for example, the reduction in the use of coal and/or gas reduces CH<sub>4</sub> emissions during the production and transport of

these fuels). In Van Vuuren et al. (2006) we account for these effects by a coupled analysis of the FAIR and TIMER models. It should be noted, however, that the total impact of these indirect reductions are relatively small (at the most, about 0.1-0.2 Pg C compared to the overall reduction objective of more than 10 Pg C in 2050) and have therefore not been taken into account in the analysis here.

As the model includes different sets of MAC curves, several additional assumptions need to be taken to use them together within the FAIR framework. The non-CO<sub>2</sub> MAC curves are constructed for the year 2010 only and do not change in time. Therefore, a technological improvement factor is included that increases the abatement potential per dollar invested over time. Furthermore, no MAC curves are currently available for several non-CO<sub>2</sub> land-use emission sources (mainly wetland rice, animals and fertilizer use). Since several abatement options already exist for these sources, exogenous assumptions are made for their reduction potentials.

Transaction costs are included for the use of the Kyoto mechanisms. The non-participating regions that have no commitments in the regimes (MS, BP, AP, EIT and GF) can only participate through CDM projects. For these projects we used an accessibility factor, as only a limited amount of the total CDM abatement potential is assumed to be accessible to the market.

The description of costs of climate policies using marginal abatement costs is transparent and flexible and allows for a description of emission trading, including possible limitations in the use of flexible instruments (e.g. transaction costs and accessibility of reduction options). Furthermore, the approach takes all six Kyoto GHGs into account and allows for full flexibility in both the abatement of these gases (the so-called multi-gas approach) and in other options such as sinks.

There are also a number of limitations inherent to the MAC curves approach: (i) they only represent direct cost effects and provide no feedback to the overall economy; as such, there is no direct link with macroeconomic indicators such as GDP or utility losses; (ii) MAC curves are as yet not available for all sources; (iii) the MAC curves for the non-CO<sub>2</sub> sources do not fully account for the dynamics of the technological developments, learning effects and system inertia as a function of time-pathways of the earlier abatements.

### **11.3 Model analyses with FAIR 2.0**

FAIR evaluates the allocation of the necessary emission reductions and the accompanying abatement cost implications of the ten regimes included in the FAIR model. In the analysis presented here only one global emission stabilization profile is used, that of stabilizing atmospheric GHG concentrations at 550 ppm CO<sub>2</sub>-eq.

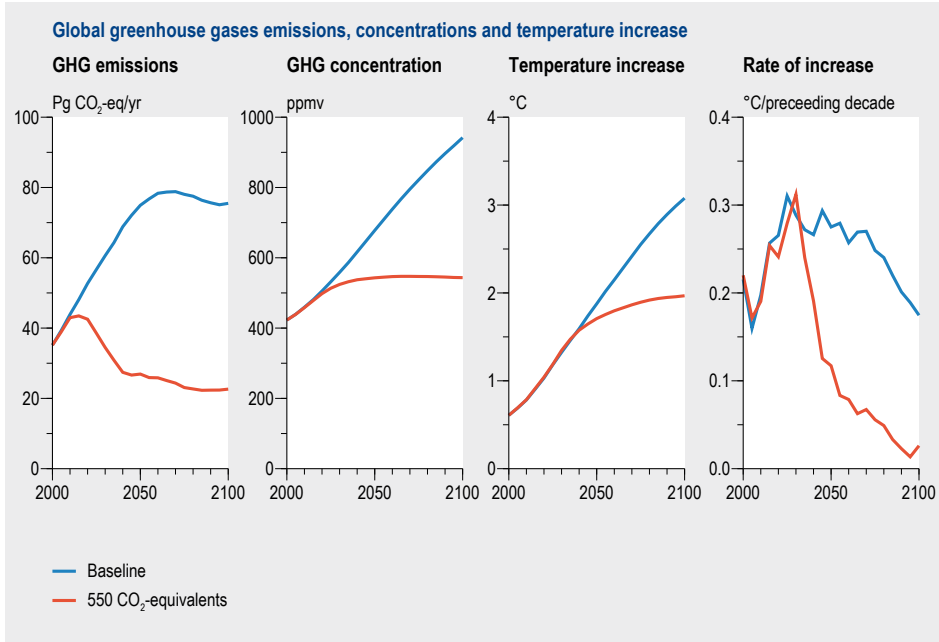


Figure 11.2. Global GHG emissions (left) and concentrations (second left), total temperature increase (second right) and rate of temperature increase (most right) for the 550 CO<sub>2</sub> eq. emission profile and the baseline scenario.

### Climate impacts

We used the Common POLES-IMAGE scenario (Criqui et al., 2003; Van Vuuren et al., 2003) as the baseline scenario (Figure 11.2). This scenario describes a continued process of globalization, medium technology development and a strong dependence on fossil fuels. GHG emissions increase from 35 Pg CO<sub>2</sub>-eq. in 2000 to more than 90 Pg CO<sub>2</sub>-eq. in 2050, which corresponds to a medium-level scenario when compared to the IPCC SRES emissions scenarios.

The S550e stabilization profile leads to a long-term stabilization of the GHG concentration at 550 ppm CO<sub>2</sub>-eq. in 2100 (Eickhout et al., 2003). Up to 2010, S550e includes the implementation of the Annex I Kyoto targets for Canada, Japan and western and eastern Europe, and an optimal level of banking of excess emissions by the former Soviet Union (FSU). The U.S.A. follows the Bush plan (emission intensity target), but this leads to emissions which do not significantly differ from their baseline values (Van Vuuren et al., 2002). The Annex I region, Oceania (including Australia), and the non-Annex I regions are assumed to follow their baseline emissions. After 2010, the profiles are designed in such a way that they meet the long-term CO<sub>2</sub>-equivalence stabilization targets. The GHG emissions continue to rise during the first decades of the simulation, after which they need to be reduced. For the S550e profile, the global anthropogenic GHG emissions would have to peak before 2020 and be back to 1990 levels around 2035.

Table 11.5. Average of the absolute reductions over all regimes and standard deviation of the average, and regional reduction with respect to the default average<sup>a</sup> for 17 world regions<sup>b</sup> for the different regimes in 2025 for the S550e profile<sup>d</sup>.

2025, S550e	Average	SD	GC	CSE	AP	MS	C&C	TT	BP	EIT	GF	MCC
Canada	55.0	10.4	74.3	67.3	61.3	54.8	53.5	39.8	52.6	53.8	50.5	42.5
USA	47.5	15.0	77.9	65.3	55.0	50.9	43.3	42.1	35.0	40.5	35.1	29.7
OECD Europe	40.2	10.8	53.5	51.8	51.2	38.4	39.2	35.4	45.6	23.1	39.8	23.6
Eastern Europe	32.4	7.8	46.4	44.1	24.4	29.0	29.9	35.2	31.7	26.7	30.8	23.3
Former USSR	46.0	10.0	65.7	59.3	31.8	44.2	43.8	43.1	41.4	50.8	41.1	39.4
Oceania	45.0	13.1	73.1	62.1	44.9	46.9	43.7	36.7	37.3	33.0	38.6	33.3
Japan	44.4	9.4	55.4	55.1	55.7	42.9	43.8	41.1	45.1	31.1	44.6	28.7
Central America	33.5	8.0	22.5	24.1	37.4	34.0	29.4	27.1	40.4	41.5	47.1	31.9
South America	36.2	5.1	34.8	33.6	36.7	37.2	33.3	27.1	40.3	40.6	45.4	32.9
Northern Africa	13.0	12.1	-2.0	3.8	0.0	11.6	19.1	16.0	24.5	27.1	0.0	30.1
Western Africa	-13.1	34.1	-78.8	-69.7	0.0	0.0	-13.4	-6.2	0.0	9.2	0.0	28.0
Eastern Africa	-29.3	52.3	-130.5	-117.7	0.0	0.0	-44.1	-15.0	0.0	3.7	0.0	10.2
Southern Africa	18.2	14.3	28.1	23.3	2.7	9.1	32.5	20.1	20.3	0.3	2.7	43.3
Middle East	46.3	5.3	55.7	49.6	43.4	47.7	46.0	41.0	39.5	41.1	52.9	46.2
South Asia	-3.2	22.6	-51.7	-33.0	0.0	1.1	3.4	12.6	0.0	10.7	0.0	25.1
East Asia	31.5	2.6	28.1	31.8	27.1	30.4	32.2	34.7	30.4	31.6	35.7	32.6
South East Asia	22.7	11.1	6.2	13.9	17.4	10.2	27.0	22.5	42.2	28.5	25.2	34.0
Annex-I	44.8	10.7	66.5	59.3	47.4	45.1	42.2	40.2	39.8	38.0	38.5	30.7
non-Annex I	23.1	7.2	8.3	13.3	21.5	23.1	25.0	25.8	26.6	27.3	27.6	32.9

#### Fewer non-Annex I reductions

decrease relative to average reduction > 50%  
 decrease relative to average contribution > 25%  
 decrease > 10%  
 decrease < 10%

-XX	XX

#### More non-Annex I reductions

increase relative to average reduction > 50%  
 increase relative to average contribution > 25%  
 increase > 10%  
 increase < 10%

XX is absolute reduction compared to the baseline

<sup>a</sup> The colour of each cell and number is a function of the relative change of a regional reduction with respect to the default average reductions of the particular region. For example, the absolute reduction for Canada under the GC case is 74.3%, which represents a change in reduction of 19.3% compared to the averaged reduction (55%). The relative difference between 19.3% and 55% is now 35% ( $=100 \cdot 19.3/55$ ), and so occurs in the (25–50)% range; this indicates that the GC case is not really attractive for Canada.

<sup>b</sup> Columns are sorted from left to right, with increasing reductions for non-Annex-I.

### Regional emission reduction

The global emission reduction objective required is defined by the difference between the baseline emissions and the stabilization profile. The emission reductions under the various regimes are summarized for S550e in Table 11.5. Since the differences between the regimes are most pronounced over the short term, the focus is on the year 2025.

The regime resulting in the smallest emission reductions or highest emission allowances are indicated by the darkly shaded cells with white numbers. These can be classified as the most favourable or most attractive regimes. The regime resulting in the largest

emission reductions, relatively speaking, or the lowest emission allowances can be classified as the least favourable or least attractive regime; these are indicated by darkly shaded cells with black numbers. The attractiveness of a regime is known to depend on the policy parameter settings chosen and – in some cases – on the stringency of the global emission profile to be met. The parameter settings can be as important as the choice of the regime (Den Elzen et al., 2002; Den Elzen et al., 2003), with the most important policy parameters being threshold levels, burden-sharing key and convergence dates.

Regimes should not lead to disproportional burdens (Article 3.1 UNFCCC). Based on such extreme (disproportional) results, defined here as a relative difference of more than 50% (i.e., the dark-grey cells with the white numbers in Table 11.5), the regimes can be divided into three groups.

The first group represents those cases resulting in disproportional burdens, such as GC, CSE, MCC and GF. GC and CSE are clearly the most attractive regimes for the non-Annex I regions with the exception of the Middle East and Turkey. In the short term, these cases not only lead to large excess emission allowances for the low income non-Annex I regions but also for northern Africa due to the initial re-allocation of emission allowances towards a better division in emissions per capita. MCC and GF represent the most attractive regimes for the Annex I regions, while leading to high reductions for the low- and medium-income non-Annex I regions.

The second group is the most attractive in terms of reductions for certain Parties (AP, EIT and BP), while clearly being unattractive for some other Parties. The AP case with a burden sharing based on per capita income is attractive to most low- and medium-income countries. The EIT case is, in general, attractive to the regions of the Organization for Economic and Co-operative Development (OECD) with relatively low emission intensities, in particular for OECD-Europe and Japan, but it is particularly unattractive for South Asia and northern Africa due to their early entry into commitments to emission reductions. Furthermore, for the latter two regions, the adopted intensity improvement rates exceed the trend in their baselines. The BP regime is not only unattractive to OECD-Europe due to its relatively large historical contribution to temperature increase but also to Latin America. Southern Africa, South Asia and northern Africa benefit from the no-binding commitments that are conditional to their participation in emission reductions, which specifically makes the BP regime attractive to these three regions (see comment 1).

The third group comprises the MS, the TT and C&C, which occupy a position more to the middle (Table 11.5). Hence, the MS and TT regimes are the most acceptable ones in terms of reduction targets. The MS regime leads to high reductions for the U.S.A. and Central and South America. It is less restrictive for South Asia, which can follow the baseline emissions, and also for East Asia, as its per capita emissions are close to the world average. However, for eastern and western Africa, this case is less attractive than C&C, because they do not experience excess emission allowances.

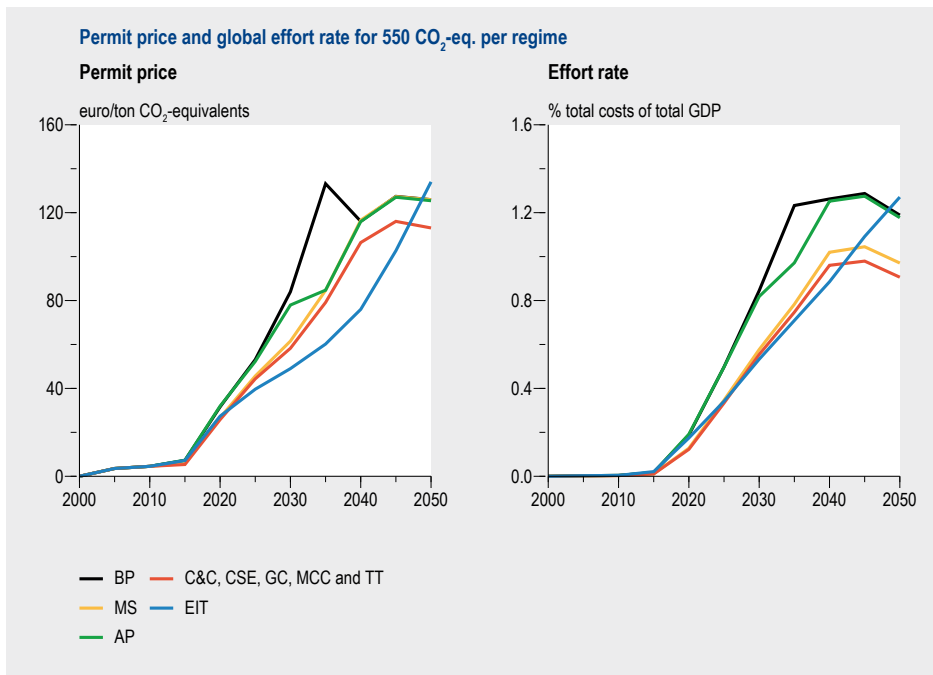


Figure 11.3. Permit price (left) and global effort rate (right) for the various regimes for the 550-eq. emission profile. Note that the delayed participation of South Asia under the BP case in 2040 leads to a sudden decrease in the permit price.

The C&C case is attractive to OECD-Europe and Japan because of their relatively low per capita emissions and the fact that under C&C all countries contribute to emission reductions. The earlier contribution of the non-Annex I regions makes C&C a relatively less attractive regime for South Asia and East Asia. Since the per capita emissions for East Asia are close to the world average per capita emissions, they do not gain in the C&C regime. In the short term, it is eastern and western Africa who stand to gain from the excess emissions.

In general, the TT regime is attractive to the OECD regions with relatively low emission intensities, i.e. OECD-Europe and Japan. The regime is also attractive to the medium-income regions, Latin America, the Middle East and Turkey. In contrast, the TT regime is particularly unattractive to South Africa, South Asia and East Asia due to their relative inefficiency in the electricity and industrial sector and their high dependency on carbon-intensive coal.

### **Regional abatement costs**

Compared to the regimes with full participation in the emission permit trading market, such as C&C and MCC, the permit prices and effort rates remain somewhat below the prices and effort rates in the gradual participation regimes (Figure 11.3). For the full participation cases, all non-Annex I regions are assumed to fully participate in emissions trading after 2012, whereas for the other cases, participation increases with

Table 11.6. Effort rate for the ten regimes explored in 2025 for the S550e profile<sup>a</sup>.

2025, \$550e	Average	SD	GC	CSE	AP	MS	C&C	TT	BP	EIT	GF	MCC
Canada	0.77	0.23	1.27	1.08	1.01	0.76	0.72	0.41	0.74	0.63	0.68	0.43
USA	0.69	0.31	1.48	1.16	0.96	0.79	0.58	0.52	0.36	0.43	0.36	0.23
OECD Europe	0.40	0.18	0.60	0.57	0.63	0.37	0.38	0.32	0.52	0.10	0.42	0.13
Eastern Europe	0.28	0.18	0.70	0.63	0.02	0.21	0.24	0.35	0.27	0.14	0.23	0.05
Former USSR	1.01	0.41	2.10	1.75	0.17	0.93	0.91	0.93	0.79	1.05	0.76	0.66
Oceania	0.67	0.29	1.51	1.18	0.73	0.75	0.64	0.35	0.47	0.24	0.52	0.34
Japan	0.42	0.16	0.58	0.58	0.65	0.39	0.40	0.35	0.45	0.17	0.44	0.16
Central America	0.39	0.20	0.10	0.14	0.51	0.40	0.28	0.22	0.60	0.50	0.80	0.34
South America	0.53	0.17	0.48	0.45	0.57	0.56	0.44	0.27	0.69	0.54	0.86	0.43
Northern Africa	-0.07	0.29	-0.60	-0.41	-0.26	-0.18	0.08	-0.02	0.23	0.33	-0.26	0.43
Western Africa	-2.32	2.39	-8.22	-7.47	-0.63	-0.51	-2.80	-2.14	-0.61	-0.76	-0.63	0.64
Eastern Africa	-3.11	3.37	-11.32	-10.32	-0.36	-0.29	-4.62	-2.32	-0.35	-0.78	-0.36	-0.42
Southern Africa	-0.26	1.27	0.61	0.23	-1.87	-0.95	0.96	0.01	-0.20	-1.31	-1.86	1.84
Middle East	1.44	0.27	1.85	1.57	1.39	1.51	1.40	1.15	1.17	0.99	1.92	1.41
South Asia	-0.49	0.40	-1.78	-1.31	-0.24	-0.49	-0.41	-0.17	-0.23	-0.17	-0.24	0.14
East Asia	0.28	0.09	0.20	0.30	0.11	0.26	0.32	0.39	0.23	0.23	0.39	0.33
South East Asia	0.10	0.28	-0.32	-0.12	-0.10	-0.24	0.22	0.10	0.66	0.26	0.14	0.40
World	0.34	0.04	0.34	0.34	0.39	0.35	0.33	0.32	26.6	0.27	0.39	0.33
XX	costs 4 times world average											
XX	costs 2 times world average											
XX	costs 20% above world average											
XX	costs about world average											
XX	costs less than 80% world average											
-XX	low gains (50% world average)											
-XX	average gains less world average											
-XX	high gains 2 times world average											
-XX	very high gains 3 times world average											
value	absolute change in contribution											

<sup>a</sup> The sequence of the regimes is similar to those in Table 11.5. The first and second columns give the average and the standard deviations (SD) of the effort rates for the ten regimes per region.

time. The non-participating non-Annex I regions have no commitments and can therefore only participate through CDM. CDM allows the participating regions to fulfill part of their reduction objective by purchasing emission reductions of non-participating regions on a project basis. The limited accessibility of viable CDM projects lowers the supply of emission reductions on the international market, thereby increasing the permit price. As shown in Den Elzen and Lucas (2005), both the international permit price and the global effort rate depend more on the stabilization level chosen than on the regimes considered.

The estimation of the costs of emission reduction for the different regimes is fraught with uncertainties (Van Vuuren et al., 2003), even for very short-term cost calculations of the Kyoto Protocol. We therefore focus on the year 2025 (Table 11.6). The effort rates vary greatly across the various regimes and regions. This heterogeneity can be explained by the differences in regional reduction objectives (Table 11.5), reduction potentials and income levels.

The effort rates of the OECD regions are about 0.2–1%, with the exception of the CSE and GC cases. Although the differences are small, total abatement costs tend to be relatively high for Canada, the U.S.A. and Oceania (regions with the highest per capita emissions) and somewhat lower for Europe and Japan (regions with medium per capita emissions). The costs for the FSU are much higher due to relatively high emissions per capita and medium-income levels.

The costs for non-Annex I regions are more variable than for the Annex I regions, primarily due to the more differentiated emission reduction targets in the group of non-Annex I compared to the Annex I regions. The Middle East and Turkey are confronted with the highest effort rates (1–2%), caused primarily by their relatively high per capita emissions and medium-income levels, while the effort rates of Latin America are about the same as those of the OECD regions for both profiles. With the exception of the MCC case, the low-income regions gain in all regimes and under both profiles. These gains range from 0 to 3% of their GDP and are the highest for the CSE, C&C and GC cases. Finally, for the low- to lower-medium income regions (Southeast and East Asia), the effort rates are below the world average (about 0.3% of GDP), mainly due to their relatively high gains from emissions trading, which partly compensate for the costs of emissions control.

In general, the differences in costs between regions reflect the differences in reduction targets presented in Table 11.5. For example, in most Annex I regions the GC case leads to the highest reduction targets as well as to the highest costs. However, due to a limited reduction potential and a low income, regimes with low reduction efforts – for example, the MS case for the Middle East and Turkey – can still lead to high abatement costs and may therefore not be that attractive.

Den Elzen et al. (2005b) have systematically analyzed the regional effort rates of the BP, MS and C&C. By comparing the effort rates with the world average, they identified four groups of regions with similar efforts that were in line with the income classes (Table 11.1): (i) high-income regions generally show intermediate cost levels compared to other regions; (ii) medium-income regions in group 2 are confronted with the highest costs; (iii) low- to lower-medium-income regions in group 3 are faced with low to average costs; (iv) low-income regions show net gains from emissions trading. This grouping also holds for the ten regimes (Table 11.6).

The pattern of attractive regimes is quite similar for the reductions and the abatement costs (Tables 11.5 and 11.6). It can be concluded that for the high-income regions, MCC and EIT and, to a lesser extent, MS, TT and C&C are the most attractive regimes; BP and particularly AP are the least attractive ones. For the Middle East and FSU (medium-income regions), almost all of the regimes are unattractive, since most of them lead to high costs. For Latin America (also medium income), GF is the least attractive regime, while the other regimes show moderate costs. For the low- to lower-medium-income regions, southern Africa in particular, the C&C and MCC regimes are less attractive than regimes with income thresholds (MS and AP). Finally, for the low-income regions,

all regimes except MCC are reasonably attractive and lead to high gains, in particular C&C.

Hence, the MS and TT regimes result in a more even distribution of costs than the other regimes, particularly among the Annex I regions (with the exception of the FSU, with high effort rates for most regimes). Within each income class, MS and TT also show the smallest differences compared to the average costs for the income class, and for this reason they would seem to provide the best prospects for a negotiation outcome based on compromises of all Parties. However, it is recognized that the results depend strongly on the policy parameter settings, marginal abatement cost curves, the baseline emission scenarios chosen and the climate target set (Den Elzen et al., 2005b). In practice, regime proposals will be evaluated on the basis of a much wider range of considerations. Therefore, multi-criteria analysis on the basis of environmental, political, economic and technical criteria could be a useful tool for identifying the relative strengths and weakness of each regime (e.g. Den Elzen et al. (2003) and Höhne et al. (2003)).

## 11.4 Caveats

The FAIR model has several strengths and weaknesses. Its main strengths are outlined below. The integration of the climate model enables the direct climate impacts of the different emission profiles and baseline scenarios to be determined, taking into account the uncertainties of the climate sensitivity. Regimes can be compared with respect to their environmental and cost implications for the different world regions, as the model includes many regimes already proposed in academic, non-governmental and policy circles. The model provides a complete and detailed description of the different sources of GHG emissions and their abatement options and potentials, thereby allowing for flexible substitution between abatement of sources, gases and regions. Finally, the description of costs of climate policies using the methodology based on marginal abatement cost curves is transparent and flexible, allowing for a description of emissions trading, including possible limitations in the use of the flexible instruments (e.g. transaction costs and accessibility of reduction options).

The main weaknesses of the FAIR model are also outlined here. First, the abatement costs represent the direct-cost effects based on MAC curves but do not consider the various linkages and rebound effects via the economy. Second, the model uses GWPs to determine total CO<sub>2</sub> equivalent emissions and a cost-effective distribution of the different reduction options. Although this GWP concept has some shortcomings, it is consistent with the current GHG emission reduction targets formulation of climate policies (e.g. Kyoto Protocol). And third, as the model combines different sets of MAC curves from different sources, not all interactions and co-benefits are taken into account.

## 11.5 Concluding remarks

The FAIR model can be applied to obtain a consistent and quantitative comparison of various allocation-based, multi-lateral regime proposals. This has been done for the EU DG Environment project 'Greenhouse gas reduction pathways in the UNFCCC post-Kyoto process up to 2025' (Criqui et al., 2003). The model has also been used to evaluate the Kyoto Protocol under the Bonn and Marrakesh agreements in terms of environmental effectiveness and costs (Den Elzen and de Moor, 2002; Lucas et al., 2005), the Bush Climate Change Initiative (Van Vuuren et al., 2002) and the Brazilian Proposal (Den Elzen et al., 2002). Furthermore, the mode has been used in combination with the integrated assessment model IMAGE and the energy model TIMER for the analysis of multi-gas mitigation scenarios in the Energy Modelling Forum (EMF 21) (Van Vuuren et al., 2006).

The model is used here for a consistent and quantitative comparison of ten regimes. These ten international regimes are rule-based approaches for defining international emission reduction commitments, and they act as effective schemes for deriving emission targets systematically on the basic principle of a fair distribution of emission reduction obligations. The key difficulty in designing post-2012 regimes lies in the acceptability of the corresponding emission reduction targets to the different Parties. The regimes should not lead to extreme results (for example, when regional costs as a percentage of the GDP far exceed the world's average costs) or be particularly attractive or unattractive only to certain Parties.

A comparison of the resulting reduction targets showed that the GC, CSE and AP regimes are the most attractive regimes for most non-Annex I regions. Conversely, the MCC and GF regimes are the most attractive for the Annex I regions. The EIT regime is, in general, attractive to OECD regions with relatively low emission intensities – OECD-Europe and Japan in particular. The MS and the TT regimes and, to a lesser extent, the C&C regime occupy a kind of middle position in terms of reduction targets. It should be acknowledged that the attractiveness of a regime depends on the policy parameter settings chosen and, in some cases, also on the stringency of the global emission profile to be met.

With respect to the abatement costs, MS and C&C are attractive regimes for the Annex I regions with high incomes (excluding the FSU), whereas the GC, CSE and, to a lesser extent, the BP regimes are unattractive to these regions. In contrast, all regimes seem to be unattractive for the Middle East and Turkey, the FSU and, to a lesser extent, Latin America (medium-income regions), since all lead to high costs; this is particularly true for the GC regime. For Southeast Asia, East Asia, northern Africa and especially southern Africa (low- to lower-medium-income regions), C&C can be less attractive than regimes with income thresholds (the MS and the BP). For western and eastern Africa and South Asia (low-income regions), all regimes appear to be attractive, in particular those in which the allowable emission levels are higher than the baseline emissions (excess emission allowances), as under C&C, CSE and GC.

When reduction targets and abatement costs are combined, the MS, TT and, to a lesser extent, the C&C regimes seem to result in the most even distribution of costs amongst all Parties and, therefore, would appear to provide the best prospects for a negotiation outcome based on compromises from all Parties. However, although the reduction targets seem to be moderate for some regions, the abatement costs can be quite high. Therefore, an in-depth analysis of the accompanying costs is required when regional reduction objectives are being assessed for different regimes in order to identify and subsequently avoid disproportional results.

In conclusion, since the finalization of the FAIR 2.0 model (2003), developmental work has continued in five areas of the model, which has resulted in a new version of the FAIR model, the FAIR 2.1. These five areas are: (i) multi-gas emission pathways (and envelopes) corresponding to a stabilization of GHG concentration at levels of about 450, 550 and 650 ppm CO<sub>2</sub>-eq. (Den Elzen et al., 2006b); (ii) abatement cost calculations for mitigation scenarios based on updated MAC curves for all GHG emissions from the TIMER 2 and IMAGE 2.3 models (Den Elzen et al., 2006a); (iii) updated climate attribution calculations (Den Elzen et al., 2005a); (iv) an updated Triptych approach (based on the work of Phylipsen et al., 2005), two additional post-2012 regimes for post-2012 commitments (i.e. Common-but-differentiated convergence (Höhne et al., 2004), and the South-North Dialogue Proposal (Den Elzen, 2005), and (v) country-scale calculation of emission allowances and abatement costs, referred to as the FAIR-world model (Den Elzen, 2005).



## REFERENCES

### Chapter 1

- Alcamo J. (Editor) (1994) *IMAGE 2.0: Integrated modeling of global change*. Kluwer Academic Publishers, Dordrecht, 318 pp.
- Alcamo J., Leemans R. and Kreileman E. (Editors) (1998) *Global change scenarios of the 21st century. Results from the IMAGE 2.1 model*. Elsevier Science, Oxford, 296 pp.
- Alcamo J., Döll P., Henrichs T., Kaspar F., Lehner B., Rösch T. and Siebert S. (2003) Development and testing the WaterGap 2 model of water use and availability. *Hydrological Sciences*, 48:317-337.
- Alkemade R., Bakkenes M., Ten Brink B., Eickhout B., De Heer M., Kram T., Manders T., Van Oorschot M., Smout F., Clement J., Van Vuuren D., Westhoek H., Miles L., Lysenko I., Fish L., Nellemann C., Van Meijl H. and Tabeau A. (2006) *Cross-roads of Planet Earth's Life. Exploring means to meet the 2010-biodiversity target*. Report 555050001, Netherlands Environmental Assessment Agency, Bilthoven, The Netherlands, 92 pp.
- Batjes N.H. (1997) A world dataset of derived soil properties by FAO-UNESCO soil unit for global modelling. *Soil Use and Management*, 13:9-16.
- Batjes N.H. (2002) Revised soil parameter estimates for the soil types of the world. *Soil Use and Management*, 18:232-235.
- Belward A. and Loveland T. (1995) The IGBP-DIS 1 km land cover project. In: Curran P. and Robertson Y.C. (Editors), *Remote sensing in action*. University of Southampton, Southampton, pp. 1099-1106.
- CPB (1999) *WorldScan: the core version*. CPB Netherlands Bureau for Economic Policy Analysis, The Hague, 137 pp.
- De Vries B., Bollen J., Bouwman L., Den Elzen M., Janssen M. and Kreileman E. (2000) Greenhouse gas emissions in an equity, environment- and service-oriented world: An IMAGE-based scenario for the 21st Century. *Technological Forecasting and Social Change*, 63:137-174.
- De Vries H.J.M., Van Vuuren D.P., Den Elzen M.G.J. and Jansen M.A. (2001) *The Targets Image Energy Regional (TIMER) model*. Report 461502024, National Institute for Public Health and the Environment, Bilthoven, The Netherlands, 188 pp.
- Eickhout B., Den Elzen M. and Kreileman E. (2004) *The atmosphere-ocean system in IMAGE 2.2. A global model approach for atmospheric concentrations, and climate and sea level projections*. Report 481508017, National Institute for Public Health and the Environment, Bilthoven, The Netherlands.
- Eickhout B., Van Meijl H., Tabeau A. and Van Rheenen R. (2006) *Economic and ecological consequences of four European land use scenarios*. Land Use Policy (in press).
- European Commission (1992) *Development of a framework for the evaluation of policy options to deal with the greenhouse effect*. Commission of the European Community, Directorate General for Environment, Nuclear Safety and Civil Protection, Brussels.
- European Commission (2005) *Winning the battle against global climate change*. Communication from the Commission to the Council, the European Parliament, the European Economic and Social Committee and the Committee of the Regions. COM 2005/35, European Commission, Brussels 17 pp. ([http://europa.eu.int/comm/environment/climat/future\\_action.htm](http://europa.eu.int/comm/environment/climat/future_action.htm)).
- FAO (1978-1981) *Reports of the agro-ecological zones project*. World Soil Resources Project No. 48, Vol. 3 - South and Central America. Food and Agriculture Organization of the United Nations, Rome.
- Hilderink H.B.M. (2001) *World population in transition: an integrated regional modelling framework*. Thela Thesis. Rozenberg, Amsterdam, 256 pp.
- IMAGE-team (2001a) *The IMAGE 2.2 implementation of the SRES scenarios. A comprehensive analysis of emissions, climate change and impacts in the 21st century*. CD-ROM publication 481508018, National Institute for Public Health and the Environment, Bilthoven, The Netherlands. Reprinted by Netherlands Environmental Assessment Agency (MNP), Bilthoven, as CD-ROM publication 500110001.
- IMAGE-team (2001b) *The Image 2.2 implementation of the SRES scenarios. Climate change scenarios resulting from runs with several GCMs*. CDROM publication 481508019, National Institute for Public Health and the Environment, Bilthoven, The Netherlands.

- Klein Goldewijk K., Van Drecht G. and Bouwman A.F. (2006) Contemporary global cropland and grassland distributions on a 5 by 5 minute resolution. *Journal of Land Use Science* (submitted).
- Kram T. (2003) An IMAGE of the future. Strategienota IMAGE ontwikkeling. Report 481508023/2002, National Institute of Public Health and the Environment, Bilthoven, The Netherlands, 38 pp.
- Millennium Ecosystem Assessment (2006a) Ecosystems and human well-being. Synthesis report. Island Press, Washington, DC, 160 pp.
- Millennium Ecosystem Assessment (Edited by Carpenter S.R., Pingali P.L., Bennett, E.M. and Zurek M.B.) (2006b) Ecosystems and human well-being: scenarios, Volume 2. Island Press, Washington, DC
- Nakicenovic N., Alcamo J., Davis G., De Vries B., Fenhann J., Gaffin S., Gregory K., Grübler A., Jung T.Y., Kram T., Emilio la Rovere E., Michaelis L., Mori S., Morita T., Pepper W., Pitcher H., Price L., Riahi K., Roehrl A., Rogner H., Sankovski A., Schlesinger M., Shukla P., Smith S., Swart R., Van Rooyen S., Victor N. and Dadi Z. (2000) Special report on emissions scenarios. IPCC Special Reports, Cambridge University Press, Cambridge, 599 pp.
- Netherlands Environmental Assessment Agency (2004a) Kwaliteit en toekomst. Verkenning van duurzaamheid, Netherlands Environmental Assessment Agency, Bilthoven, The Netherlands, 226 pp.
- Netherlands Environmental Assessment Agency (2004b) Quality and the future. Sustainability outlook (summary), Netherlands Environmental Assessment Agency, Bilthoven, The Netherlands, 28 pp.
- Prentice I.C., Cramer W., Harrison S., Leemans R., Monserud R.A. and Solomon A.M. (1992) A global biome model based on plant physiology and dominance, soil properties and climate. *Journal of Biogeography*, 19:117-134.
- Rotmans J. (1990) IMAGE. An integrated model to assess the greenhouse effect. Kluwer Academic Publishers, Dordrecht, 289 pp.
- Schlesinger M.E., Malyshev S., Rozanov E.V., Yang F., Andronova N.G., De Vries B., Grübler A., Jiang K., Masui T., Morita T., Nakicenovic N., Penner J., Pepper W., Sankovski A. and Zhang Y. (2000) Geographical distributions of temperature change for scenarios of greenhouse gas and sulphur dioxide emissions. *Technological Forecasting and Social Change*, 65:167-193.
- Seitzinger S.P., Harrison J.A., Dumont E., Beusen A.H.W. and Bouwman A.F. (2005) Sources and delivery of carbon, nitrogen, and phosphorus to the coastal zone: an overview of Global NEWS models and their application. *Global Biogeochemical Cycles*, 19, GB4S, doi:10.1029/2004GB002453, 2005.
- Tinker B. (2000) Report of the third session of the IMAGE advisory board. Report 481508014, National Institute of Public Health and the Environment, Bilthoven, The Netherlands.
- UNEP (2002) GEO-3. Past, present and future perspectives. Earthscan, London, 446 pp.
- UNEP/RIVM (Potting J. and Bakkes J., Editors) (2004) The GEO-3 scenarios 2002-2032: Quantification and analysis of environmental impacts. Report UNEP/DEWA/RS.03-4 and RIVM 402001022, Division of Early Warning and Assessment (DEWA), United Nations Environment Programme (UNEP) / National Institute for Public Health and the Environment, Nairobi / Bilthoven, 216 pp.
- Van Vuuren D.P., Den Elzen M., Lucas P., Eickhout B., Strengers B., Van Ruijven B., Woinink S. and Van Houdt R. (2006) Stabilizing greenhouse gas concentrations at low levels: an assessment of reduction strategies and costs. *Climatic Change* (in press).

## Chapter 2

- Bongaarts J. and Potter R.G. (1983) Fertility, biology and behavior: an analysis of the proximate determinants. *Studies in population*. Academic Press, New York, 244 pp.
- CIESIN and CIAT (2005) Gridded Population of the World Version 3 (GPWv3). Socio-economic Data and Applications Center (SEDAC), Columbia University. sedac.ciesin.columbia.edu/gpw.
- Coleman J.S. (1990) Foundations of social theory. Belknap Press of Harvard University Press, Cambridge, MA.
- Cotts Watkins S. (1987) The fertility transition: Europe and the Third World compared. *Sociological Forum*, 2:645-673.
- Davis K. (1945) The world demographic transition. *Ann. Am. Academy of Political and Social Science*, 237:1-11.
- De Bruijn B.J. (1999) Foundations of demographic theory: choice, process, context, Faculty of spatial sciences, University of Groningen, Groningen, 298 pp.
- Easterlin R.A. (1983) Modernization and fertility: a critical essay. In: Bulatao R.A. and Lee R.D. (Editors), *Determinants of fertility in developing countries* (volume 2). Academic Press, New York, pp. 562-586.

- Eurostat (2005) New Cronos. Eurostat, Luxembourg (<http://epp.eurostat.cec.eu.int>).
- Ezzati M., Lopez A., Rodgers A., Van Der Hoorn S. and Murray C.J.L. (2002) Selected major risk factors and global and regional burden of disease. *Lancet*, 360:1347-60.
- Forrester J.W. (1971) *World Dynamics*. Wright-Allen Press, Cambridge, MA, 160 pp.
- Frejka T. (1996) Long-range global population projections. In: Lutz W. (Editor), *The future population of the world. What can we assume today?* Earthscan Publications Ltd., London, pp. 3-13.
- Frenk J., Bobadilla J.L., Stern C., Frejka T. and Lozano R. (1993) Elements for a theory of the health transition. In: Chen L.C., Kleinman A. and Ware N.C. (Editors), *Health and social change in international perspective*. Harvard University Press, Boston MA, pp. 25-49.
- Gray A. (2001) Definitions of crowding and the effects of crowding on health: a literature review. Ministry of Social Policy, Wellington, 40 pp.
- Gross R., Solomons N.W., Barba C.V.C., De Groot L. and Khor G.L. (1997) Overview of ageing, urbanization, and nutrition in developing countries and the development of the reconnaissance project. *Food and Nutrition Bulletin*, 18(3) (UNU, [www.unu.edu/unu-press/food/V183e/index.htm](http://www.unu.edu/unu-press/food/V183e/index.htm)).
- Harpam T., Reed H., Montgomery M., Satterthwaite D., Moser C. and Cohen B. (2003) Mortality and morbidity: is city life good for your health? In: Montgomery M.R., Stren R., Cohen B. and Reed H.E. (Editors), *Cities transformed: Demographic changes and its implications in the developing world*. National Academies Press, Washington, DC, pp. 259-299.
- Hilderink H.B.M. (2000a) PHOENIX pluss: the population user support system version 1.0, <http://www.mnp.nl/phoenix>.
- Hilderink H.B.M. (2000b) World population in transition: an integrated regional modeling framework. Thela Thesis / Rozenberg, Amsterdam, 256 pp.
- LandScan (2001) Global Population Database. Oakridge National Laboratory, Oakridge.
- Loveland T.R., Reed B.C., Brown J.F., Ohlen D.O., Zhu Z., Yang L. and Merchant J.W. (2000) Development of a global land cover characteristics database and IGBP DISCover from 1 km AVHRR data. *International Journal of Remote Sensing*, 21:1303-1330.
- Lutz W. (1996) *The future population of the world. What Can We Assume Today?* (Revised and updated edition 1996). Earthscan Publications Ltd., London, 500 pp.
- Lutz W. and Goujon A. (2001) The World's Changing Human Capital Stock: Multi-State Population Projections by Educational Attainment. *Population and Development Review*, 27:323-339.
- Millennium Institute (1996) *Documentation for Threshold 21*, Millennium Institute, Arlington, VA.
- Montgomery M., Reed H. and White M. (2003) Fertility and reproductive health. In: Montgomery M.R., Stren R., Cohen B. and Reed H.E. (Editors), *Cities transformed: Demographic changes and its implications in the developing world*. National Academies Press, Washington DC, pp. 199-258.
- Nakicenovic N., Alcamo J., Davis G., De Vries B., Fenhann J., Gaffin S., Gregory K., Grubler A., Jung T.Y., Kram T., Emilio la Rovere E., Michaelis L., Mori S., Morita T., Pepper W., Pitcher H., Price L., Riahi K., Roehrl A., Rogner H., Sankovski A., Schlesinger M., Shukla P., Smith S., Swart R., Van Rooyen S., Victor N. and Dadi Z. (2000) Special report on emissions scenarios. IPCC Special Reports. Cambridge University Press, Cambridge, 599 pp.
- Notestein F.W. (1945) Population, the long view. In: Schultz T.W. (Editor), *Food for the world*, Chicago, pp. 36-57.
- Parry M.L., Arnell N.W., McMichael A.J., Nicholls R.J., Martens P., Kovats R.S., Livermore M.T.J., Rosenzweig I.A. and Fischer G. (2001) Millions at risk: defining critical climate change threats and targets. *Global Environmental Change*, 11:181-93.
- Rogers A. (1985) Regional population projection models. *Scientific geography series*, 4. SAGE Publications, New Delhi, 96 pp.
- Rotmans J. and De Vries B. (Editors) (1997) *Perspectives on global change: the TARGETS approach*. Cambridge University Press, Cambridge, 463 pp.
- Rotmans J., Van Asselt M.B.A., De Vries H.J.M., Beusen A.H.W., Den Elzen M.G.J., Hilderink H.B.M., Hoekstra A.Y., Janssen M.A., Köster H.W., Niessen L.W. and Strengers B.J. (1997) The TARGETS model. In: Rotmans J. and De Vries B. (Editors), *Perspectives on global change: The TARGETS approach*. Cambridge University Press, Cambridge, pp. 33-54.
- Szreter S. (1993) The idea of demographic transition and the study of fertility change. *Population and Development Review*, 19:659-702.
- UN (1974) *Methods for projection of urban and rural population*. United Nations, New York, 126 pp.
- UN (1980) *Patterns of urban and rural population growth*. United Nations, New York, 176 pp.

- UN (2003) World urbanization prospects: the 2003 revision. United Nations Population, Division Department of Economic and Social Affairs, New York.
- UN (2004) World population prospects: the 2004 revision. United Nations, Department for Economic and Social Information and Policy Analysis, New York.
- UNEP (2002) Global environmental outlook 3. United Nations Environmental Programme, EarthScan, London, 446 pp.
- UNSD (2003) Demographic yearbook 2003. United Nations, New York (<http://unstats.un.org/unsd/demographic/default.htm>).
- Van Vuuren D., Lucas P. and Hilderink H.B.M. (2005) Downscaling drivers of global environmental change scenarios: Enabling use of the IPCC SRES scenarios at the national and grid level. *Global Environmental Change* (in press).
- White M., Montgomery M.R., Brennan-Galvin E. and Visaria P. (2003) Urban population dynamics: models, measures, and forecasts. In: Montgomery M.R., Stren R., Cohen B. and Reed H.E. (Editors), *Cities transformed: Demographic changes and its implications in the developing world*. National Academies Press, Washington DC, pp. 108-154.
- World Bank (2004) World development indicators. World Bank, Washington DC ([www.worldbank.org/data](http://www.worldbank.org/data)).
- De Vries H.J.M., Van Vuuren D.P., Den Elzen M.G.J. and Janssen M.A. (2002) The Targets Image Energy model regional (TIMER) - Technical documentation. Report 461502024, National Institute for Public Health and the Environment, Bilthoven, The Netherlands, 187 pp.
- De Vries H.J.M., Hoogwijk M. and Van Vuuren D.P. (2006) The potential supply of renewable energy: wind, solar and bio-energy. *Energy Policy* (in press).
- Grubler A., Nakicenovic N. and Victor D.G. (1999) Dynamics of energy technologies and global change. *Energy Policy*, 27:247-280.
- Hendriks C., Graus W. and Van Bergen F. (2002a) Global carbon dioxide storage potential and costs. Report EEP-02001, Ecofys, Utrecht.
- Hendriks C., Harmelink M., Hofmans Y. and De Jager D. (2002b) Climate neutral energy carriers in the regulatory energy tax. Ecofys, Utrecht, 60 pp.
- Hendriks C., Harmelink M., Burges K. and Ransel K. (2004) Power and heat productions: plant developments and grid losses. Report EEP-03038, Ecofys, Utrecht.
- Hoogwijk M. (2004) On the global and regional potential of renewable energy sources. PhD thesis, Utrecht University, Utrecht, 256 pp.
- Junginger M., Faaij A. and Turkenburg W.C. (2005) Global experience curves for wind farms. *Energy Policy*, 33:133-150.
- Lucas P., Van Vuuren D.P., Den Elzen M.G.J., Olivier J.G.J. and Bouwman A.F. (2006) Long-term reduction potential of non-CO<sub>2</sub> greenhouse gases. *Environmental Science and Policy* (in press).
- Mastandrea M.D. and Schneider S.H. (2004) Probabilistic Integrated Assessment of dangerous climate change. *Science*, 304:571-574.
- Meinshausen M. (2006) On the risk of overshooting 2°C. In: Schellnhuber H.J., Cramer W., Nakicenovic N., Wigley T. and Yohe G. (Editors), *Avoiding Dangerous Climate Change*. Cambridge University Press, Cambridge, pp. 265-281.
- MIT (2003) The future of nuclear power - an interdisciplinary MIT study. Massachusetts Institute of Technology, Cambridge MA, 180 pp.
- New M., Hulme M. and Jones P. (1999) Representing twentieth century space-time climate variability, Part I: Development of a 1961-91 mean monthly terrestrial climatology. *Journal of Climate*, 12:829-856.

- Reijnders H.T.J., De Groot A. and Lako P. (2001) *Evaluatie van waterstof-gebaseerde concepten en systemen*. ECN-C-01-019, ECN, Petten, The Netherlands, 41 pp.
- Rogner H.H. (1997) An assessment of World Hydrocarbon Resources. *Annual Review of Energy and the Environment*, 22:217-262.
- Rotmans J. and De Vries B. (1997) *Perspectives on Global Change: The TARGETS approach*. Cambridge University Press, Cambridge, 463 pp.
- Sims R.E.H., Rogner H.H. and Gregory K. (2003) Carbon emission and mitigation cost comparisons between fossil fuel, nuclear and renewable energy resources for electricity generation. *Energy Policy*, 31:1315-1326.
- UNEP (2002) *Global Environment Outlook 3*. United Nations Environment Programme, EarthScan, London, 446 pp.
- Van Ruijven B., Van Vuuren D.P. and De Vries B. (2006) The potential role of hydrogen in energy systems with and without climate policy. *International Journal of Hydrogen Energy* (in press).
- Van Vuuren D.P. and De Vries H.J.M. (2001) Mitigation scenarios in a world oriented at sustainable development: the role of technology, efficiency and timing. *Climate Policy*, 1:189-210.
- Van Vuuren D.P., Den Elzen M.G., Berk M.M., Lucas P.L., Eickhout B., Eerens H. and Oostenrijk R. (2003) Regional costs and benefits of alternative post-Kyoto climate regimes. Report 728001025/2003, National Institute for Public Health and the Environment, Bilthoven, The Netherlands, 117 pp.
- Van Vuuren D.P., Den Elzen M.G.J., Lucas P., Eickhout B., Strengers B.J., Van Ruijven B., Wonink S. and Van Houdt R. (2006) Stabilizing greenhouse gas concentrations at low levels: an assessment of reduction strategies and costs. *Climatic Change* (in press).
- Wene C.O. (2000) Experience curves for energy technology policy, OECD/IEA, Paris, 133 pp.
- Weyant, J., Delacheyne, P and Blanford, G. (2006). An overview of EMF-21: multigas mitigation and climate change. *Energy Journal* (in press).
- Wurster R. and Zittel D.W. (1994) Hydrogen energy. L-B systemtechnik, Ottobrun, Germany. Workshop on energy technologies to reduce CO<sub>2</sub> emissions in Europe: prospects, competition, synergy, 11-12 April 1994. *Energieonderzoek Centrum Nederland (ECN), Petten, The Netherlands*.
- ## Chapter 4
- Abler D. (2003) Adjustment at the Sectoral Level. An IAPRAP workshop on Policy Reform and Adjustment. The Wye Campus of Imperial College, October 23-25. ([http://agadjust.aers.psu.edu/Workshop\\_files/Abler\\_presentation.pdf](http://agadjust.aers.psu.edu/Workshop_files/Abler_presentation.pdf)).
- Alcamo J., Leemans R. and Kreileman G.J.J. (1998) Global change scenarios of the 21st century. Results from the IMAGE 2.1 model. Elsevier Science, London, 296 pp.
- Alkemade R., Bakkenes M., Ten Brink B., Eickhout B., De Heer M., Kram T., Manders T., Van Oorschot M., Smout F., Clement J., Van Vuuren D., Westhoek H., Miles L., Lysenko I., Fish L., Nellemann C., Van Meijl H. and Tabeau A. (2006) Cross-roads of Planet Earth's Life. Exploring means to meet the 2010-biodiversity target. Report 555050001, Netherlands Environmental Assessment Agency, Bilthoven, The Netherlands, 92 pp.
- Bouwman A. F., Van Der Hoek K.W., Eickhout B. and Soenario I. (2005) Exploring changes in world ruminant production systems. *Agricultural Systems*, 84:121-153.
- Bruinsma J. (2003) World Agriculture: Towards 2015/2030. An FAO perspective. Earthscan, London, 432 pp.
- Brundtland G. (1987) *Our Common Future: The World Commission on Environment and Development*. Oxford University Press, Oxford, 318 pp.
- Bulte E.H. and Barbier E.B. (2004) Trade and renewable resources in a second best world: An overview. Paper based on keynote address by Erwin Bulte, 12th annual conference of the European Association of Environmental and Resource Economists, Bilbao (Spain), June 28-30, 2003.
- CBD (2002) Assessing the impact of trade liberalization on the conservation and sustainable use of agricultural biological diversity. Document no. UNEP/CBD/COP/6/INF/2, Convention on Biological Diversity, United Nations Environment Programme, Montreal, Canada (<http://www.biodiv.org/doc/meetings/cop/cop-06/information/cop-06-inf-02-en.pdf>)
- De Janvry A., Fafchamps M. and Sadoulet E. (1991) Peasant household behavior with missing markets: Some paradoxes explained. *Economic Journal*, 101:1400-17.
- Eickhout B., Van Meijl H., Tabeau A. and Van Zeijts H. (2004) Between liberalization and protection: Four long-term scenarios for trade, poverty and the environment. Presented at the Seventh Annual Conference on Global Economic Analysis, June 2004, Washington DC.

- Eickhout B., Van Meijl H., Tabeau A. and Van Rheenen R. (2006a) Economic and ecological consequences of four European land use scenarios. *Land Use Policy* (in press).
- Eickhout B., Kram T., Manders T., Van Meijl H. and Tabeau A. (2006b) How do trade, poverty and climate policies affect biodiversity? Presented at the 9th Annual Conference on Global Economic Analysis, June 2006, Addis Ababa, Ethiopia.
- EPA (1994) International anthropogenic methane emissions: estimates for 1990. Report EPA 230-R-93-010, U.S. Environmental Protection Agency, Washington, DC.
- Fischer G., Shah M. and Van Velthuisen H. (2002) Climate Change and Agricultural Vulnerability. Special report prepared for the World Summit on Sustainable Development, Johannesburg 2002, International Institute of Applied Systems Analysis, Vienna, 152 pp.
- Hertel T. (1997) *Global Trade Analysis. Modelling and Applications*. Cambridge University Press, 403 pp.
- Hertel T.W. and Keeney R. (2003) Assessing the impact of WTO reforms on world agricultural markets: A new approach. Paper presented at the Conference on New Developments in Commodity Market Research, December 15-16, Food and Agriculture Organization of the United Nations, Rome.
- Huang H. and Labys W.C. (2001) Environment and trade: Theories and methods. Research Paper 2001-1. West Virginia University - Regional Research Institute, Morgantown, WV.
- Huang H., Van Tongeren F., Dewbre F. and Van Meijl H. (2004) A new representation of agricultural production technology in GTAP. Paper presented at the Seventh Annual Conference on Global Economic Analysis, June, Washington, DC, USA.
- IEA (2004) *World energy outlook 2004*. International Energy Agency, Paris, 2004.
- Leemans R. and Van Den Born G.J. (1994) Determining the potential distribution of vegetation, crops and agricultural productivity. In: Alcamo J. (Editor), *IMAGE 2.0-integrated modeling of global climate change*. Kluwer Academic Publishers, Dordrecht, pp. 133-161.
- Millennium Ecosystem Assessment (2005) *Ecosystems and Human well-being: Synthesis*. Island press, Washington DC, U.S.A., 160 pp.
- OECD (2003) *PEM technical Document (Draft)*, Paris.
- Parry M., Arnell N., McMichael T., Nicholls R., Martens P., Kovats S., Livermore M., Rosenzweig C., Iglesias A. and Fischer G. (2001) Millions at Risk: Defining Critical Climate Change Threats and Targets. *Global Environment Change*, 11:1-3.
- Rosenzweig C., Parry M. and Fischer G. (1995) World Food Supply. In: Strzepek, K.M. and Smith, J.B. (Editors), *As climate changes: International impacts and implications*. Cambridge University Press, pp. 27-56.
- Strengers B.J. (2001) The agricultural economy model in IMAGE 2.2. Report 481508015. National Institute for Public Health and the Environment, Bilthoven, The Netherlands (<http://www.mnp.nl/image>).
- Tabeau A., Eickhout B. and Van Meijl H. (2006) Endogenous agricultural land supply: Estimation and implementation in the GTAP model. Presented at the Ninth Annual Conference on Global Economic Analysis, June 2006, Addis Ababa, Ethiopia.
- United Nations (2001) Road map towards the implementation of the United Nations Millennium Declaration. Report to the secretary general. Report A/56/326, United Nations General Assembly, New York.
- Van Meijl H., Van Rheenen T., Tabeau A. and Eickhout B. (2006) The impact of different policy environments on agricultural land use in Europe. *Agriculture, Ecosystems and Environment*, 114:21-38.

## Chapter 5

- Alcamo J., Kreileman E., Krol M., Leemans R., Bollen J., Van Minnen J., Schaeffer M., Toet S. and De Vries B. (1998) Global modelling of environmental change: an overview of IMAGE 2.1. In: Alcamo J., Leemans R. and Kreileman E. (Editors), *Global change scenarios of the 21st century. Results from the IMAGE 2.1 model*. Elsevier Science Ltd., Oxford, pp. 3-94.
- Bouwman A.F., Van Der Hoek K.W., Eickhout B. and Soenario I. (2005) Exploring changes in world ruminant production systems. *Agricultural Systems*, 84:121-153.
- Bouwman A.F., Van Der Hoek K.W., Van Drecht G. and Eickhout B. (2006) World livestock and crop production systems, land use and environment between 1970 and 2030. In: Brouwer F. and McCarl B. (Editors), *Rural lands, agriculture and climate beyond 2015: A new perspective on future land use patterns*. Springer, Dordrecht, pp. 75-89.
- Bruinsma J.E. (2003) *World agriculture: towards 2015/2030. An FAO perspective*. Earthscan, London, 432 pp.
- De Haan C., Steinfeld H. and Blackburn H. (1999) *Livestock and the environment. Finding a balance*. Food and Agriculture Organization of the United Nations, Rome.

- Delgado C., Rosegrant M., Steinfeld H., Ehui S. and Courbois V. (1999) Livestock to 2020. The next food revolution. Food, Agriculture and the Environment Discussion paper 28, International Food Policy Research Institute, Food and Agriculture Organization of the United Nations, International Livestock Research Institute, Washington, DC, 72 pp.
- Eickhout B., Bouwman A.F. and Van Zeijts H. (2006) The role of nitrogen in world food production and environmental sustainability. *Agriculture, Ecosystems and the Environment*, 116:4-14.
- FAO (1978-1981) Reports of the Agro-Ecological Zones Project. World Soil Resources Project No. 48, Vol. 3 - South and Central America. Food and Agriculture Organization of the United Nations, Rome.
- FAO (2005) FAOSTAT database collections, Food and Agriculture Organization of the United Nations, Rome ([www.apps.fao.org](http://www.apps.fao.org)).
- Hoogwijk M. (2004) On the global and regional potential of renewable energy sources, PhD thesis, Utrecht University, 256 pp.
- IMAGE-team (2001) The IMAGE 2.2 implementation of the SRES scenarios. A comprehensive analysis of emissions, climate change and impacts in the 21st century. CD-ROM publication 481508018, National Institute for Public Health and the Environment, Bilthoven. Reprinted by Netherlands Environmental Assessment Agency (MNP), Bilthoven as CD-ROM publication 500110001.
- Nakicenovic N., Alcamo J., Davis G., De Vries B., Fenhann J., Gaffin S., Gregory K., Grubler A., Jung T.Y., Kram T., Emilio la Rovere E., Michaelis L., Mori S., Morita T., Pepper W., Pitcher H., Price L., Riahi K., Roehrl A., Rogner H., Sankovski A., Schlesinger M., Shukla P., Smith S., Swart R., Van Rooyen S., Victor N. and Dadi Z. (2000) Special Report on emissions scenarios. IPCC Special Reports. Cambridge University Press, Cambridge, 599 pp.
- Seré C. and Steinfeld H. (1996) World livestock production systems. Current status, issues and trends. Animal Production and Health Paper 127, Food and Agriculture Organization of the United Nations, Rome, 83 pp.
- Van Vuuren D.P., Den Elzen M.G.J., Lucas P., Eickhout B., Strengers B.J., Van Ruijven B., Wonink S. and Van Houdt R. (2006) Stabilizing greenhouse gas concentrations at low levels: an assessment of reduction strategies and costs. *Climatic Change* (in press).
- USDA (2006) National Agricultural Statistics Service (NASS) (<http://www.nass.usda.gov>).
- Allen, R.C. (1998) Agricultural Output and Productivity in Europe, 1300-1800. Discussion Paper 98-14. University of British Columbia, Department of Economics, Vancouver, Canada.
- Auslig (1997) Pre-settlement map for 1788, Australian Surveying and Land Information Group (AUSLIG) (<http://www.auslig.gov.au>).
- Bartholome E., Belward A.S., Achard F., Bartalev S., Carmonamoren C., Eva H., Fritz S., Gregoire J.-M., Mayaux P. and Stibig H.-J. (2002) GLC2000. Global land cover mapping for the year 2000. Project status November 2002. Report EUR 20524 en, Institute for Environment and Sustainability, Joint Research Centre, ISPRA, Italy (<http://www-gvm.jrc.it/glc2000/defaultglc2000.htm>).
- Betts R.A. (2001) Biogeophysical impacts of land use on present-day climate: near surface temperature and radiative forcing. *Atmospheric Science Letters*, 1, doi: 10.1006/asle.2001.0023.
- Bertrand C., Loutre M.F., Crucifix M. and Berger A. (2002) Climate of the last millennium: a sensitivity study. *Tellus*, 54: 221-244.
- Brovkin V., Sitch S., Von Bloh W., Clausen M., Bauer E. and Cramer W. (2004) Role of atmospheric CO<sub>2</sub> increase and climate change during the last 150 years. *Global Change Biology*, 10:1-14, doi: 10.1111/j.1365-2486.2004.00812.
- Brovkin V., Clausen M., Driesschaert E., Fichefet T., Kicklighter D., Loutre M.F., Matthews H.D., Ramankutty N., Schaeffer M. and Sokolov A. (2006) Biogeophysical effects of historical land cover changes simulated by six earth system models of intermediate complexity. *Climate Dynamics*, 26:587-600.
- Chase T.N., Pielke Sr. R.A., Kittel T.G.F., Nemani R.R., Running S.W. (2000) Simulated impacts of historical land cover changes on global climate in northern winter. *Climate Dynamics*, 16:93-105.
- China National Bureau of Statistics (2006a) China Agricultural Statistics, Beijing (<http://www.stats.gov.cn/english/>).
- China National Bureau of Statistics (2006b) China Statistical Yearbooks, Beijing (<http://www.stats.gov.cn/english/>).
- Cramer W., Bondeau A., Woodward F.I., Prentice I.C., Betts R.A., Brovkin V., Cox P.M., Fisher V., Foley J.A., Friend A.D., Kucharik C., Lomas M.R., Ramankutty N., Sitch S., Smith B., White A. and Young-Molling C. (2001) Global response of terrestrial ecosystem structure and function to CO<sub>2</sub> and climate change: results from six dynamic global vegetation models. *Global Change Biology*, 7:357-373.

## Chapter 6

- Crumley C. (2000) From garden to globe: linking time and space with meaning and memory. In: McIntosh R.J., Tainter J.A., and Keech McIntosh S. (Editors), *The way the wind blows: climate, history, and human action*. Columbia Series in Historical Ecology. Columbia University Press, New York, pp. 193-208.
- DCW (1993), Digital Chart of the World, ESRI (<http://www.esri.com>).
- Demeny, P. (1990) Population. In: Turner B.L., Clark W.C., Kates R.W., Richards, J.F., Mathews J.T. and Meyer W.B. (Editors), *The earth as transformed by human action*, Cambridge University Press, Cambridge, pp. 41-54.
- Defries R.S., Field C.B. and Fung I. (1999) Combining satellite data and biogeochemical models to estimate global effects of human-induced land cover change on C emissions and primary productivity. *Global Biogeochemical Cycles*, 13:803-815.
- Etter A. and Van Wyngaarden W. (2000) Patterns of landscape transformation in Colombia, with emphasis in the Andean region. *Ambio*, 29:432-439.
- FAO (2006) FAOSTAT database collections, Food and Agriculture Organization of the United Nations, Rome ([www.apps.fao.org](http://www.apps.fao.org)).
- FAO (2005) Global forest resources assessment. Forestry Paper 147, Food and Agriculture Organization of the United Nations, Rome.
- Feddema J., Oleson K., Bonan G., Mearns L., Washington W., Meehl G. and Nycha D. (2005) A comparison of a GCM response to historical anthropogenic land cover change and model sensitivity to uncertainty in present-day land cover representations. *Climate Dynamics*, 25:581-609.
- GAEZ (2000) Jointed Global Agro-Ecological Zones Project (Global-AEZ), FAO-IIASA, Laxenburg, Austria (<http://www.fao.org/ag/agl/agll/gaez/index.htm>).
- GLOBE (1999) Global Land One-kilometer Base Elevation map (GLOBE), A 3-arc second (1 km) gridded, quality-controlled global Digital Elevation Model (DEM), National Geophysical Data Center (NGDC) (<http://www.ngdc.noaa.gov/mgg/topo/globe.html>).
- Grigg D. (1987) The industrial revolution and land transformation. In Wolman M.G. and Fournier F.G.A. (Editors), *Land transformation in agriculture*, Wiley and Sons, New York, pp. 79-109.
- Hansen J.E., Sato M., Lacs A., Ruedy R., Tegen I. and Matthews E. (1998) Climate forcings in the industrial era. *Proceedings of the National Academy of Sciences*, 95:12753-12758.
- Henderson-Seller A., Dickinson R.E., Durbridge T.B., Kennedy P.J., McCuffie K. and Pitman A.J. (1993) Tropical deforestation – modeling local-scale to regional-scale climate change. *Journal of Geophysical Research*, 98:7289-7315.
- Houghton R.A. (1999) The annual net flux of C to the atmosphere from changes in land use 1850-1990. *Tellus*, 51B:298-313.
- Houghton R.A. (1991) Tropical deforestation and atmospheric carbon dioxide. *Climatic Change* 19:99-118.
- Houghton R.A. (2003) Revised estimates of the annual net flux of carbon to the atmosphere from changes in land use and land management 1850-2000. *Tellus*, 55B:378-390.
- Houghton R.A. and Hackler J.L. (2002) Carbon flux to the atmosphere from land-use changes. In: *Trends. A Compendium of Data on Global Change*. Carbon Dioxide Information Analysis Center, Oak Ridge National Laboratory, U.S. Department of Energy, Oak Ridge, Tennessee, TN.
- Houghton J.T., Ding Y., Griggs D.J., Noguera M., Van Der Linden P.J., Dai X., Maskell K., Johnson C.A. (Editors) (2001), *Climatic change 2001. The scientific basis. Contribution of Working Group I to the third assessment report of the Intergovernmental Panel on Climate Change*. Cambridge University Press, Cambridge, 881 pp.
- Demographia (2006) Global urban areas and urbanization, Wendell Cox Consultancy, <http://www.demographia.com> (visited July 2006).
- Klein Goldewijk K. (2001) Estimating global land use change over the past 300 years: the HYDE database. *Global Biogeochemical Cycles*, 15:417- 433.
- Klein Goldewijk K. (2005) Three centuries of global population growth: A spatial referenced population density database for 1700-2000. *Population and Environment*, 26:343-367.
- Klein Goldewijk K. and Ramankutty N. (2004). Land cover change over the last three centuries due to human activities: the availability of new global data sets. *Geojournal*, 61:335-344.
- Klein Goldewijk K., Van Drecht G. and Bouwman A.F. (2006). Mapping contemporary global cropland and rangeland maps on a 5' resolution grid. *Journal of Land Use Science* (submitted).
- Landscan (2006) LandScan™ Global population database. The 2004 revision. Oak Ridge National Laboratory, Oak Ridge, Tennessee, TN. (<http://www.ornl.gov/landscan/>).

- Loveland T.R., Reed B.C., Brown J.F., Ohlen D.O., Zhu Z., Yang L. and Merchant J.W. (2000) Development of a global land cover characteristics database and IGBP DISCover from 1 km AVHRR data. *International Journal of Remote Sensing*, 21:1303-1330.
- Lucas D. (2003) *World Population Growth. Beginning Australian Population Studies*. National Centre for Development Studies, The Australian National University, Canberra (<http://demography.anu.edu.au/Publications/Books>).
- Matthews E. (1983) Global Vegetation and Land Use: New High-Resolution Data Bases for Climate Studies, *Journal of Applied Meteorology*, 22: 474-487.
- Matthews H.D., Weaver A.J., Eby M. and Meisner K. (2003) Radiative forcing of climate by historical land cover change. *Geophysical Research Letters*, 30, doi: 10.1029/2002GL016098.
- Matthews H.D., Weaver A.J., Meisner K.J., Gillet N.P. and Eby M. (2004) Natural and anthropogenic climate change: incorporating historical land cover change, vegetation dynamics and the global carbon cycle. *Climate Dynamics*, 22:461-479.
- Maizel M., White R.D., Root R., Gage S., Stitt S., Osborne L. and Muehlbach G. (1998) Historical interrelationships between population settlement and farmland in the conterminous United States, 1790 to 1990. In: T.D. Sisk (Editor), *Perspectives on the land use history of North America: a context for understanding our changing environment*, Biological Science Report USGS/BRD/BSR 1998-0003, U.S. Geological Survey, Biological Resources Division.
- McEvedy, C. and R. Jones (1978) *Atlas of world population history*. Penguin Books, Harmondsworth, UK, 368 pp.
- McGuire A.D., Prentice I.C., Ramankutty N., Reicheau T., Schloss A., Tian H., Williams L.J. and Wittenberg U. (2001) Carbon balance of the terrestrial biosphere in the twentieth century: Analyses of CO<sub>2</sub>, climate and land use effects with four process-based ecosystem models. *Global Biogeochemical Cycles*, 15:183-206.
- Pacala S.W., Hurtt G.C. and Bake D. (2001) Consistent land and atmosphere-based U.S. carbon sink estimates. *Science*, 292:2316-2320.
- Petit C.C. and Lambin E. (2002) Long-term land-cover changes in the Belgian Ardennes (1775-1929): model-based reconstruction vs. historical maps. *Global Change Biology*, 8:616 -631.
- Pielke Sr R.A., Marland G., Betts R.A., Chase T.N., Eastman J.L., Niles J.O., Niyogi D.D.O. and Running S. (2002) The influence of land-use change and landscape dynamics on the climate system: relevance to climate-change policy beyond the radiative effect of greenhouse gases. *Philosophical Transactions of the Royal Society (London) A*, 360: Issue 1797.
- Pitman A.J. and Zhao, M. (2000) The relative impact of observed change in land cover and carbon dioxide as simulated by a climate model. *Geophysical Research Letters*, 27:1267-1270.
- Pitman A.J. (2003) The evolution of, and revolution in, land surface schemes designed for climate models. *International Journal of Climatology*, 23:479-510.
- Prentice I.C., Cramer W., Harrison S.P., Leemans R., Monserud R.A. and Solomon A.M. (1992) A global biome model based on plant physiology and dominance, soil properties and climate. *Journal of Biogeography*, 19:177-134.
- Ramankutty N. and Foley J.A. (1998) Characterizing patterns of global land use: An analysis of global croplands data. *Global Biogeochemical Cycles*, 12:667-685.
- Ramankutty N. and Foley J.A. (1999) Estimating historical changes in global land cover: croplands from 1700 to 1992. *Global Biogeochemical Cycles*, 13:997-1027.
- Richards J.F. (1990) Land transformation. In: Turner II B.L., Clark W.C., Kates R.W., Richards J.F., Mathews J.T., Meyer W.B. (Editors), *The earth as transformed by human action*, Cambridge Univ. Press, New York, pp.163-178.
- Richards J.F. and Flint E. (1994) Historic land use and carbon estimates for South and Southeast Asia 1880-1980, Data set NDP-046 CDIAC/ORNL, Carbon Dioxide Information Analysis Center, Oak Ridge National Laboratory, Oak Ridge, Tennessee, TN.
- Ruddiman W.F.R. (2003) The anthropogenic greenhouse era began thousands of years ago. *Climatic Change*, 61:261-293.
- UN (2004) United Nations Population Division, 2004 Revision of World Population Prospect. UN Population Division, New York.
- USDA (2006) Data and Statistics. United States Department of Agriculture (<http://www.nass.usda.gov/>).
- Williams M. (2000) Dark ages and dark areas: global deforestation in the deep past, *Journal of Historical Geography*, 26: 28-46.
- Wilson M.F. and Henderson-Sellers A. (1985) A global archive of land cover and soils data for use in general circulation climate models. *Journal of Climatology*, 5:119-143.

## Chapter 7

- Achard F., Eva H.D., Stibig H.J., Mayaux P., Gallego J., Richards T. and Malingreau J.-P. (2002) Determination of Deforestation Rates of the World's Humid Tropical Forests. *Science*, 297:999-1002.
- Alexandrov G.A., Oikawa T. and Yamagata Y. (2003) Climate dependence of the CO<sub>2</sub> fertilization effect on terrestrial net primary production. *Tellus B*, 55:669-675.
- Araujo M.B., Cabeza M., Thuiller W., Hannah L. and Williams P.H. (2004) Would climate change drive species out of reserves? An assessment of existing reserve-selection methods. *Global Change Biology*, 10:1618-1626.
- Baker T., Phillips O.L., Malhi Y., Almeida S., Arroyo L., Di Fiore A., Erwin T., Higuchi N., Killeen T.J., Laurance S.G., Laurance W.F., Lewis S.L., Monteagudo A., Neill D.A., Vargas P.N., Pitman N.C.A., Silva N.M. and Martínez R.V. (2004) Increasing biomass in Amazonian forest plots. *Philosophical Transactions of the Royal Society, Series B*, 359:353-365.
- Brinkman S., Strengers B., Van Minnen J.G., Nabuurs G.J. and Trines E. (2005) IMAGE 2.2. Carbon cycle analysis. MNP working paper, Netherlands Environmental Assessment Agency, Bilthoven, The Netherlands.
- Cannell M.G.R. (1982) *World Forest Biomass and Primary Production Data*. Academic Press, New York, 391 pp.
- Cao M. and Woodward F.I. (1998) Dynamic responses of terrestrial ecosystem carbon cycling to global climate change. *Nature*, 393:249-252.
- CDIAC (2006) Carbon dioxide information analysis center, Oak Ridge National Laboratory, Oak Ridge (<http://cdiac.ornl.gov>).
- Cox P.M., Betts R.A., Collins M., Harris P.P., Huntingford C. and Jones C.D. (2004) Amazon dieback under climate-carbon cycle projections for the 21st century. *Theoretical Applied Climatology*, 78:137-156.
- Cramer W., Bondeau A., Schaphoff S., Lucht W., Smith B. and Sitch S. (2004) Tropical forests and the global carbon Cycle: Impacts of atmospheric carbon dioxide, climate change and rate of deforestation. *Philosophical Transactions of the Royal Society, Series B*:331-343.
- Cramer W. and Solomon A.M. (1993) Climatic classification and future global redistribution of agricultural land. *Climate Research*, 3:97-110.
- Cramer W., Bondeau A., Woodward I., Prentice I.C., Betts R., Brovkin V., Cox P., Fisher V., Foley J.A., Friend A.D., Kucharik C., Lomas M., Sitch S., Smith B., White A. and Young-Molling C. (2001) Global response of terrestrial ecosystem structure and function to CO<sub>2</sub> and climate change: results from six dynamic global vegetation models. *Global Change Biology*, 7:357-373.
- Davidson E.A. and Janssens J.A. (2006) Temperature sensitivity of soil carbon decomposition and feedbacks to climate change. *Nature*, 440:165-173.
- Davidson E.A., Janssens J.A. and Luo Y. (2006) On the variability of respiration in terrestrial ecosystems: moving beyond Q<sub>10</sub>. *Global Change Biology*, 12:154-164.
- Davis M.B. (1981) Quaternary history and the stability of forest communities. In: West D.C., Shugart H.H. and Botkin D.B. (Editors), *Forest Succession: Concepts and Application*. Springer-Verlag, New York, pp. 132-154.
- Del Lungo A. (2003) *Planted forest database: Analysis of annual planting trends and silvicultural parameters for commonly planted species*. Planted Forest and Trees Working Papers, Working Paper 26, Forest Resources Division, Food and Agriculture Organization of the United Nations, Rome, 60 pp.
- FAO (2001) *Global forest resources assessment 2000: Main report*. Forestry Paper 140, Food and Agriculture Organization of the United Nations, Rome, 479 pp.
- Friedlingstein P., Dufresne J.-L., Cox P.M. and Rayner P. (2003) How positive is the feedback between climate change and the carbon cycle? *Tellus B*, 55:692-700.
- Gracia C. and Sabate S. (2002) Aboveground biomass expansion factors and biomass equations of forests in Catalonia, CREAM expert meeting on biomass expansion factors (BEF), Valencia, 5 pp.
- Guisan A. and Thuiller W. (2005) Predicting species distribution: Offering more than simple habitat models. *Ecological Letters*, 8:993-1009.
- Harvey L.D.D. (1989) Transient climatic responses to an increase of greenhouse gases. *Climatic Change*, 15:15-30.
- Heath J., Ayres E., Possell M., Bardgett R.D., Black H.I.J., Grant H., Ineson P. and Kerstiens G. (2005) Rising atmospheric CO<sub>2</sub> reduces sequestration of root-derived soil carbon. *Science*, 309:1711-1713.
- Houghton R.A. (2003) Revised estimates of the annual flux of carbon to the atmosphere from changes in land use and land management 1950-2000. *Tellus B*, 55:378-390.

- Huntley B. and Webb T., III (1989) Migration: Species' response to climatic variations caused by changes in the earth's orbit. *Journal of Biogeography*, 16:5-19.
- Ilic J., Boland D., McDonald M., Downes G. and Blakemore P. (2000) *Woody Density Phase 1 - State of Knowledge*. 18, Australian Greenhouse Office 234 pp.
- IMAGE-team (2001) The IMAGE 2.2 implementation of the SRES scenarios. A comprehensive analysis of emissions, climate change and impacts in the 21st century. CD-ROM publication 481508018, National Institute for Public Health and the Environment, Bilthoven, The Netherlands. Reprinted by Netherlands Environmental Assessment Agency (MNP), Bilthoven as CD-ROM publication 500110001.
- IPCC (2004) *Good Practice Guidance for Land Use, Land-Use Change and Forestry*, IPCC Special Report, Institute for Global Environmental Studies (IGES), Hayama, Kanagawa, Japan, 599 pp.
- Jenny H., Gessel S.P. and Bingham F.T. (1949) Comparative study of decomposition rates of organic matter in temperate and tropical regions. *Soil Science*, 68:419-432.
- Joos F., Prentice I.C., Sitch S., Meyer R., Hooss G., Plattner G.-K., Gerber S. and Hasselmann K. (2001) Global warming feedbacks on terrestrial carbon uptake under the Intergovernmental Panel on Climate Change (IPCC) emission scenarios. *Global Biogeochemical Cycles*, 15(4):891-908.
- Klein Goldewijk K., Van Minnen J.G., Kreileman G.J.J., Vloebeld M. and Leemans R. (1994) Simulation of the carbon flux between the terrestrial environment and the atmosphere. *Water, Air and Soil Pollution*, 76:199-230.
- Knorr W., Prentice I.C., House J.I. and Holland E.A. (2005) Long-term sensitivity of soil carbon turnover to warming. *Nature*, 433:298-301.
- Körner C., Asshoff R., Bignucolo O., Hattenschwiler S., Keel S.G., Pelaez-Riedl S., Pepin S., Siegwolf R.T.W. and Zotz G. (2005) Carbon flux and growth in mature deciduous forest trees exposed to elevated CO<sub>2</sub>. *Science*, 309:1360-1362.
- Krankina O.N., Harmon M.E., Cohen W.B., Doug R. Oetter, Zyrina O. and Duane M.V. (2004) Carbon stores, sinks, and sources in forests of Northwestern Russia: Can we reconcile forest inventories with remote sensing results? *Climatic Change*, 67:257-272.
- Larcher W. (2003) *Physiological Plant Ecology*. Springer-Verlag, 303 pp.
- Leemans R. and Eickhout B. (2004) Another reason for concern: regional and global impacts on ecosystems for different levels of climate change. *Global Environmental Change*, 14: 219-228.
- Leemans R., Eickhout B.J., Strengers B., Bouwman A.F. and Schaeffer M. (2002) The consequences for the terrestrial carbon cycle of uncertainties in land use, climate and vegetation responses in the IPCC SRES scenarios. *Science in China*, 43:1-15.
- Li Z., Apps M.J., Kurz W.A. and Banfield E. (2003) Temporal changes of forest net primary production and net ecosystem production in west central Canada associated with natural and anthropogenic disturbances. *Canadian Journal of Forestry Research*, 33:2340-2351.
- Lloyd J. and Taylor J.A. (1994) On the temperature dependence of soil respiration. *Functional Ecology*, 8(3):315-323.
- Mitchell J.F.B., Karoly D.J., Hegerls G.C., Zwiers F.W., Allen M.R. and Marengo J. (2001) Detection of climate change and attribution of causes. In: Houghton J.T., Ding Y., Griggs D.J., Noguer M., Van Der Linden P.J., Dai X., Maskell K., Johnson C.A. (Editors), *Climatic change 2001. The scientific basis. Contribution of Working Group I to the third assessment report of the Intergovernmental Panel on Climate Change*. Cambridge University Press, Cambridge, pp. 695-738.
- Nabuurs G.J. and Mohren G.M.J. (1993) Carbon fixation through forestation activities. A study of the carbon sequestration potential of selected forest types. IBN Research Report 93/4, Institute for Forestry and Nature Research, Wageningen, 205 pp.
- Nakicenovic N., Alcamo J., Davis G., de Vries B., Fenhann J., Gaffin S., Gregory K., Grübler A., Jung T.Y., Kram T., Emilio la Rovere E., Michaelis L., Mori S., Morita T., Pepper W., Pitcher H., Price L., Riahi K., Roehrl A., Rogner H.-H., Sankovski A., Schlesinger M.E., Shukla P.R., Smith S., Swart R.J., van Rooyen S., Victor N. and Dadi Z. (Editors) (2000) *IPCC Special Report on Emissions Scenarios*. Cambridge University Press, Cambridge, 599 pp.
- Nilsson S. and Schopfhauser W. (1995) The carbon-sequestration potential of a global afforestation program. *Climatic Change*, 30:267-293.
- Prentice I.C., Cramer W., Harrison S.P., Leemans R., Monserud R.A. and Solomon A.M. (1992) A global biome model based on plant physiology and dominance, soil properties and climate. *Journal of Biogeography*, 19:117-134.

- Prentice I.C., Farquhar G.D., Fasham M.J.R., Goulden M.L., Heimann M., Jaramillo V.J., Khashgi H.S., Le Quéré C., Scholes R.J. and Wallace D.W.R. (2001) The carbon cycle and atmospheric carbon dioxide. In: Houghton J.T., Ding Y., Griggs D.J., Noguer M., Van Der Linden P.J., Dai X., Maskell K., Johnson C.A. (Editors), *Climatic change 2001. The scientific basis. Contribution of Working Group I to the third assessment report of the Intergovernmental Panel on Climate Change*. Cambridge University Press, Cambridge, pp. 183-237.
- Schaphoff S., Lucht W., Gerten D., Sitch S., Cramer W. and Prentice I.C. (2006) Terrestrial biosphere carbon storage under alternative climate projections. *Climatic Change*, 74: 97-122, doi 10.1007/s10584-005-9002-5.
- Schober R. (1975) *Ertragstabeln wichtiger Baumarten*. J.D. Sauerländer's Verlag, Frankfurt am Main, 154 pp.
- Sitch S., Smith B., Prentice I.C., Arneth A., Bondeau A., Cramer W., Kaplan J.O., Levis S., Lucht W., Sykes M.T., Thonicke K. and Venevski S. (2003) Evaluation of ecosystem dynamics, plant geography and terrestrial carbon cycling in the LPJ Dynamic Global Vegetation Model. *Global Change Biology*, 9:161-185.
- Sitch S., Brovkin V., Von Bloh W., van Vuren D.P., Eickhout B. and Ganopolski A. (2005) Impacts of future land cover changes on atmospheric CO<sub>2</sub> and climate. *Global Biogeochemical Cycles*, 19: GB2013, doi 10.10129/2004GB002311.
- Strengers B., Van Minnen J.G. and Eickhout B. (2006) The costs and uncertainties in establishing C plantations in order to mitigate climate change. *Climatic Change* (in press).
- UNFCCC (1992). United Nations General Assembly, United Nations Framework Convention on Climate Change, United Nations, New York (<http://www.unfccc.int/resources>).
- Van Minnen J.G., Klein Goldewijk K. and Leemans R. (1995) The importance of feedback processes and vegetation transition in the terrestrial carbon cycle. *Journal of Biogeography*, 22:805-814.
- Van Minnen J.G., Leemans R. and Ihle F. (2000) Assessing consequences of dynamic changes in global vegetation patterns, using the IMAGE 2.1 model. *Global Change Biology*, 6:595-611.
- Van Minnen J.G., Eickhout B., Strengers B.J., Brinkman S., Van den Houdt R. and Leemans R. (2006a) The consequences of uncertainties in the vegetation response to climate change on the global and regional terrestrial C cycle. *Global Change Biology* (submitted).
- Van Minnen J.G., Strengers B.J. and Eickhout B. (2006b) Evaluating the role of carbon plantations in climate change mitigation including land-use requirements. *Carbon Balance and Management* (submitted).
- Van Vuuren D., Den Elzen M., Lucas P., Eickhout B., Strengers B., Van Ruijven B., Wonink S., Van den Houdt R., Berk M. and Oostenrijk R. (2006) Stabilizing greenhouse gas concentrations. Assessment of different strategies and costs using an integrated assessment framework. *Climatic Change* (in press).
- White A.M., Cannell M.G.R. and Friend A.D. (2000) CO<sub>2</sub> stabilization, climate change and the terrestrial carbon sink. *Global Change Biology*, 6:817-833.
- Woodward F.I., Smith T.M. and Emanuel W.R. (1995) A global land primary productivity and phytogeography model. *Global Biogeochemical Cycles*, 9: 471-490.
- Zaehle S., Sitch S., Smith B. and Hatterman F. (2005) Effects of parameter uncertainties on the modeling of terrestrial biosphere dynamics. *Global Biogeochemical Cycles*, 19: GB3020, doi:10.1029/2004GB002395.

## Chapter 8

- AAPFCO/TFI (2006) Commercial fertilizers 2005, Association of American Plant Food Control Officials / The Fertilizer Institute, Washington, D.C. ([www.aapfco.org](http://www.aapfco.org)).
- American Geophysical Union (2006) Global nutrient export from watersheds (reprint volume from *Global Biogeochemical Cycles*). American Geophysical Union, Washington, DC.
- Batjes N.H. (1997) A world dataset of derived soil properties by FAO-UNESCO soil unit for global modelling. *Soil Use and Management*, 13:9-16.
- Batjes N.H. (2002) Revised soil parameter estimates for the soil types of the world. *Soil Use and Management*, 18:232-235.
- Beusen A.H.W. and Bouwman A.F. (2006) Nutrient balances in global agricultural systems and natural ecosystems. Documentation and manual (internal report), Netherlands Environmental Assessment Agency (MNP), Bilthoven, The Netherlands.
- Beusen A.H.W., Dekkers A.L.M., Bouwman A.F., Ludwig W. and Harrison J. (2005) Estimation of global river transport of sediments and associated particulate C, N and P. *Global Biogeochemical Cycles*, 19, GB4505, doi:10.1029/2005GB002453.

- Bobbink R., Hornung M. and Roelofs J.G.M. (1998) The effects of air-borne nitrogen pollutants on species diversity in natural and semi-natural European vegetation. *Journal of Ecology*, 86:717-738.
- Bouwman A.F., Fung I., Matthews E. and John J. (1993) Global analysis of the potential for N<sub>2</sub>O production in natural soils. *Global Biogeochemical Cycles*, 7:557-597.
- Bouwman A.F., Lee D.S., Asman W.A.H., Dentener F.J., Van Der Hoek K.W. and Olivier J.G.J. (1997) A global high-resolution emission inventory for ammonia. *Global Biogeochemical Cycles*, 11:561-587.
- Bouwman A.F., Boumans L.J.M. and Batjes N.H. (2002a) Estimation of global NH<sub>3</sub> volatilization loss from synthetic fertilizers and animal manure applied to arable lands and grasslands. *Global Biogeochemical Cycles*, 16(2):1024, doi:10.1029/2000GB001389.
- Bouwman A.F., Boumans L.J.M. and Batjes N.H. (2002b) Modeling global annual N<sub>2</sub>O and NO emissions from fertilized fields. *Global Biogeochemical Cycles*, 16(4):1080 doi:10.1029/2001GB001812.
- Bouwman A.F., Van Drecht G. and Van Der Hoek K.W. (2005a) Surface N balances and reactive N loss to the environment from intensive agricultural production systems for the period 1970-2030. *Science in China Ser. C. Life Sciences*, 48 Supp. 1-13.
- Bouwman A.F., Van Drecht G., Knoop J.M., Beusen A.H.W. and Meinardi C.R. (2005b) Exploring changes in river nitrogen export to the world's oceans. *Global Biogeochemical Cycles*, 19, doi:10.1029/2004GB002314.
- Bouwman A.F., Van Der Hoek K.W., Eickhout B. and Soenarso I. (2005c) Exploring changes in world ruminant production systems. *Agricultural Systems*, 84(2):121-153, doi:10.1016/j.agsy.2004.05.006.
- Bouwman A.F., Van Drecht G. and Van Der Hoek K.W. (2005d) Nitrogen surface balances in intensive agricultural production systems in different world regions for the period 1970-2030. *Pedosphere*, 15(2):137-155.
- Bouwman A.F., Beusen A.H.W., Van Der Hoek K.W., Asman W.A.H. and Van Drecht G. (2006) Global Inventory of Ammonia Emissions from Global Livestock Production and Fertilizer Use. In: Schlesinger W. and Aneja V. (Editors), *Agricultural Air Quality*, Potomac, MD.
- Bruinsma J.E. (2003) *World agriculture: towards 2015/2030. An FAO perspective*. Earthscan, London, 432 pp.
- Carpenter S.R., Pingali P.L., Bennett E.M. and Zurek M.B. (Editors) (2006) *Ecosystems and human well-being: scenarios*, Volume 2. Island Press, Washington DC.
- China National Bureau of Statistics (2006a) *China Agricultural Statistics*, Beijing.
- China National Bureau of Statistics (2006b) *China Statistical Yearbook*, Beijing.
- Cleveland C.C., Townsend A.R., Schimel D.S., Fisher H., Howarth R.W., Hedin L.O., Perakis S.S., Latty E.F., Fisher J.C.V., Elserod A. and Wasson M.F. (1999) Global patterns of terrestrial biological nitrogen (N<sub>2</sub>) fixation in natural ecosystems. *Global Biogeochemical Cycles*, 13:623-645.
- Collins W.J., Stevenson D.S., Johnson C.E. and Derwent R.G. (1997) Tropospheric ozone in a global-scale three-dimensional Lagrangian model and its response to NO<sub>x</sub> emission controls. *Journal of Atmospheric Chemistry*, 26:223-274.
- Conley D. (2002) Terrestrial ecosystems and the global biogeochemical silica cycle. *Global Biogeochemical Cycles*, 16(4):68-1 to 68-8 (1121, doi:10.1029/2002GB001894).
- Davidson E.A. and Kingerlee W. (1997) A global inventory of nitric oxide emissions from soils. *Nutrient Cycling in Agroecosystems*, 48:37-50.
- Dentener F., Stevenson D., Ellingsen K., Noije T.v., Schultz M., Amann M., Atherton C., Bell N., Bergmann D., Bey I., Bouwman L., Butler T., Cofala J., Collins B., Drevet J., Doherty R., Eickhout B., Eskes H., Fiore A., Gauss M., Hauglustaine D., Horowitz L., Isaksen I.S.A., Josse B., Lawrence M., Krol M., Lamarque J.F., Montanaro V., Müller J.F., Peuch V.H., Pitari G., Pyle J., Rast S., Rodriguez J., Sanderson M., Savage N.H., Shindell D., Strahan S., Szopa S., Sudo K., Dingenen R.V., Wild O. and Zeng G. (2006) *The global atmospheric environment for the next generation*. *Environment Science and Technology*, 40:3586-3594.
- EEA (1998) *Europe's Environment. Statistical compendium for the second assessment*, European Environmental Agency, Copenhagen.
- Eurostat (2000) *NewCronos*. Eurostat, European Communities ([www.europa.eu.int/comm/eurostat/](http://www.europa.eu.int/comm/eurostat/)).
- FAO (2005) *FAOSTAT database collections*, Food and Agriculture Organization of the United Nations, Rome ([www.apps.fao.org](http://www.apps.fao.org)).
- FAO (2006) *World Agriculture: Towards 2030/2050. Interim Report. Prospects for food, nutrition, agriculture and major commodity groups*, Global Perspectives Studies Unit. Food and Agriculture Organization of the United Nations, Rome, 71 pp.

- Galloway J.N., Dentener F.J., Capone D.G., Boyer E.W., Howarth R.W., Seitzinger S.P., Asner G.P., Cleveland C.C., Green P.A., Holland E.A., Karl D.M., Michaels A.F., Porter J.H., Townsend A.R. and Vörösmarty C.J. (2004) Nitrogen cycles: Past, present, and future. *Biogeochemistry*, 70:153-226.
- Hansen J. (2000) Nitrogen balances in agriculture. *Statistics in focus. Environment and energy*, theme 8-16/2000, European Communities, Brussels, 7 pp.
- Heathwaite A.L. (1993) Nitrogen cycling in surface waters and lakes. In: Burt T.P. and Trudgill S.T. (Editors), *Nitrate: processes, patterns and management*. Wiley and Sons, Chichester, pp. 99-140.
- IFA/IFDC/FAO (2003) *Fertilizer use by crop*. 5th edition, Food and Agriculture Organization of the United Nations, Rome.
- IMAGE-team (2001) *The IMAGE 2.2 implementation of the SRES scenarios. A comprehensive analysis of emissions, climate change and impacts in the 21st century*. CD-ROM publication 481508018, National Institute for Public Health and the Environment, Bilthoven, The Netherlands. Reprinted by Netherlands Environmental Assessment Agency (MNP) as CD-ROM publication 500110001.
- IPCC (2006) *IPCC Guidelines for National Greenhouse Gas Inventories* (in press), IPCC NGGIP Programme, IPCC-TSU/IGES, Japan.
- Klepper O. and Van Drecht G. (1998) *WARiBAS, Water assessment on a river basin scale; a computer program for calculating water demand and water satisfaction on a catchment basin level for global-scale analysis of water stress*. Report 402001009, National Institute for Public Health and the Environment, Bilthoven, The Netherlands, 124 pp.
- Kolenbrander G.J. (1981) Leaching of nitrogen in agriculture. In: Brogan J.C. (Editor), *Nitrogen losses and surface runoff from landspreading of manures*. Developments in Plant Sciences Vol. 2. Martinus Nijhoff/Dr. W. Junk Publishers, The Hague, pp. 199-216.
- Kragt J.F., De Vries W. and Breeuwisma A. (1990) Modelling nitrate leaching on a regional scale. In: Merckx R.H., Vereecken H. and Vlassak K. (Editors), *Fertilization and the environment*. Leuven University Press, Leuven, Belgium, pp. 340-347.
- Meinardi C.R. (1994) *Groundwater recharge and travel times in the sandy regions of The Netherlands*. Report 715501004, National Institute for Public Health and the Environment, Bilthoven, The Netherlands.
- Mosier A.R., Kroeze C., Nevison C., Oenema O., Seitzinger S. and Cleemput O.V. (1998) Closing the global atmospheric N<sub>2</sub>O budget: nitrous oxide emissions through the agricultural nitrogen cycle. *Nutrient Cycling in Agroecosystems*, 52:225-248.
- OECD (2001) *Environmental indicators for agriculture*. Volume 3. Methods and results. Organization for Economic Co-operation and Development, Paris.
- Olivier J.G.J., Berdowski J.M., Peters J.A.H.W., Bakker J., Visschedijk A.J.H. and Bloos J.P.J. (2001) *Applications of EDGAR. Including a description of EDGAR V3.0: reference database with trend data for 1970-1995*. Report 773301001, National Institute for Public Health and the Environment (RIVM)/Netherlands Organization for Applied Scientific Research (TNO), Bilthoven, The Netherlands.
- Rabalais N.N. (2002) Nitrogen in aquatic ecosystems. *Ambio*, 31:102-112.
- Seitzinger S.P., Harrison J.A., Dumont E., Beusen A.H.W. and Bouwman A.F. (2005) Sources and delivery of carbon, nitrogen, and phosphorus to the coastal zone: an overview of Global NEWS models and their application. *Global Biogeochemical Cycles*, 19, GB4S01, doi:10.1029/2005GB002606, 2005.
- Seitzinger S.P., Harrison J.A., Böhlke J.K., Bouwman A.F., Lowrance R., Peterson B., Tobias C. and Van Drecht G. (2006) Denitrification across landscapes and waterscapes: a synthesis. *Ecological Applications* (in press).
- Simmelsgaard S.E., Kristensen K., Andersen H.E., Grant R., Jørgensen J.O. and Østergaard H.S. (2000) An empirical model for calculation of root zone nitrate leaching. *DJF rapport Markbrug no. 32* (in Danish), Danmarks Jordbrugsforskning, 67 pp.
- Singh B., Yadvinder-Singh and Sekhon G.S. (1995) Fertilizer use efficiency and nitrate pollution of groundwater in developing countries. *Journal of Contaminant Hydrology*, 20:167-184.
- Smil V. (1999) Nitrogen in crop production: An account of global flows. *Global Biogeochemical Cycles*, 13:647-662.
- Smith S.V., Swaney D.P., Talaue-McManus L., Bartley D.D., Sandhei P.T., McLaughlin C.J., Dupra V.C., Crossland C.J., Buddemeier R.W., Maxwell B.A. and Wulff F. (2003) Humans, hydrology, and the distribution of inorganic nutrient loading to the ocean. *BioScience*, 53:235-245.

- Stehfest E. and Bouwman A.F. (2006) N<sub>2</sub>O and NO emission from agricultural fields and soils under natural vegetation: summarizing available measurement data and modeling of global annual emissions. *Nutrient Cycling in Agroecosystems*, 74: 207-228, doi 10.1007/s10705-006-9000-7.
- Turner R.E., Rabelais N.N., Justic D. and Dortch Q. (2003) Global patterns of dissolved N, P and Si in large rivers. *Biogeochemistry*, 64:297-317.
- UNEP (2002) GEO-3. Past, present and future perspectives. United Nations Environment Programme, Earthscan, London, 446 pp.
- US-EPA (2006) Inventory of U.S. Greenhouse Gas Emissions and Sinks 1990-2004, United States Environmental Protection Agency, Washington, DC.
- USDA (2006) China Agricultural and Economic Data: Provincial Data, United States Department of Agriculture. Economic Research Service ([www.ers.usda.gov](http://www.ers.usda.gov)).
- Van Der Hoek K.W. (1998) Nitrogen efficiency in global animal production. In: Van Der Hoek K.W., Erisman J.W., Smeulders S., Wisniewski J.R. and Wisniewski J. (Editors), *Nitrogen, the Confer-N-s*. Elsevier, Amsterdam, pp. 127-132.
- Van Der Hoek K.W. and Bouwman A.F. (1999) Upscaling of nutrient budgets from agroecological niche to global scale. In: Smaling E.M.A., Oenema O. and Fresco L.O. (Editors), *Nutrient disequilibria in agroecosystems*. CAB International, Wallingford, pp. 57-73.
- Van Drecht G., Bouwman A.F., Knoop J.M., Beusen A.H.W. and Meinardi C.R. (2003) Global modeling of the fate of nitrogen from point and nonpoint sources in soils, groundwater and surface water. *Global Biogeochemical Cycles*, 17(4):1115, doi:10.129/2003GB002060.
- Vitousek P.M., Aber J.D., Howarth R.W., Likens G.E., Matson P.A., Schindler D.W., Schlesinger W.H. and Tilman D.G. (1997) Human alteration of the global nitrogen cycle: sources and consequences. *Ecological Applications*, 7:737-750.
- Vollenweider R.A. (1992) Coastal marine eutrophication: principles and control. *Science of the Total Environment*, Supplement 1992:1-20.
- WHO/UNICEF (2000) Water supply and sanitation assessment 2000, World Health Organization (WHO) / United Nations Children's Fund (UNICEF), Geneva ([www.child\\_info.org/eddb/sani](http://www.child_info.org/eddb/sani) and [www.who.int/docstore/water\\_sanitation\\_health/Globassessment/](http://www.who.int/docstore/water_sanitation_health/Globassessment/)).
- ## Chapter 9
- Barford C.C., Wofsy S.C., Goulden M.L., Munger J.W., Pyle E.H., Urbanski S.P., Hutrya L., Scott R. Saleska, Fitzjarrald D., Moore D.K. (2001). Factors controlling long- and short-term sequestration of atmospheric CO<sub>2</sub> in a mid-latitude forest. *Science*, 294, 1688-1691.
- Betts R.A. (2000). Offset of the potential carbon sink from boreal forestation by decreases in surface albedo. *Nature*, 408 :187-190.
- Bonan G.B., Chapin F.S. III, and Thompson, S.L. (1995). Boreal forest and tundra ecosystems as components of the climate system. *Climatic Change*, 29:145-167.
- Bond G., Kromer B., Beer J., Muscheler R., N. Evans M.N., Showers W., Hoffmann S., Lotti-Bond R., Hajdas I., Bonani G. (2001). Persistent solar influence on North Atlantic climate during the holocene. *Science*, 294:2130-2136.
- Brovkin V., Claussen M., Driesschaert E., Fichefet T., Kicklighter D., Loutre M.-F., Matthews H. D., Ramankutty N., Schaeffer M., Sokolov A. (2006). Biogeophysical effects of historical land cover changes simulated by six Earth system models of intermediate complexity. *Climate Dynamics*, 26:587-600.
- Chapin F.S. III, Sturm M., Serreze M.C., McFadden J.P., Key J.R., Lloyd A.H., McGuire A.D., Rupp T.S., Lynch A.H., Schimel J.P., Beringer J., Chapman W.L., Epstein H.E., Euskirchen E.S., Hinzman L.D., Jia G., Ping C.-L., Tape K.D., Thompson C.D.C., Walker D.A., and Welker J. M. (2005) Role of land-surface changes in arctic summer warming. *Science*, 310:657-660.
- Claussen M., Brovkin V., Ganopolski A., Kubatzki C., and Petoukhov V. (2003). Climate change in northern Africa: the past is not the future. *Climatic Change*, 57:99-118.
- Collatz G.J., Berry J.A., and Clark J.S. (1998). Effects of climate and atmospheric CO<sub>2</sub> partial pressure on the global distribution of C4 grasses: Present, past, and future. *Oecologia*, 114:441-454.
- Cox PM, Betts RA, Jones C.D., Spall S.A., Totterdell I.J. (2000). Acceleration of global warming due to carbon-cycle feedbacks in a coupled climate model. *Nature*, 408:184-187.
- Cox P.M., Betts R.A., Collins M., Harris P. P., Huntingford C. and Jones C. D. (2004). Amazonian forest dieback under climate-carbon cycle projections for the 21<sup>st</sup> century. *Theoretical and Applied Climatology*, 78:137-156.

- Easterling D.R., Meehl G.A., Camille Parmesan C., Stanley A. Changnon S.A., Thomas R. Karl T.R., Linda O. Mearns L.O. (2000). Climate Extremes: Observations, Modeling, and Impacts. *Science*, 289:2068-2074.
- Eickhout B., Den Elzen M.G.J. and Kreileman G.J.J. (2004). The Atmosphere-ocean system of IMAGE 2.2: A global model approach for atmospheric concentrations, and climate and sea level projections. Report 481508017, National Institute for Public Health and the Environment, Bilthoven, The Netherlands.
- Feddema J.J., Oleson K.W., Bonan G.B., Mearns L.O., Buja L.E., Meehl G.A., Washington W.M. (2005). The Importance of Land-Cover Change in Simulating Future Climates. *Science*, 310:1674-1678.
- Foley J.E. (2005) Tipping Points in the tundra. *Science*, 310:627-628.
- Haarsma R.J., Selten F.M., Opsteegh J.D., Lenderink G. and Liu Q. (1996) ECBILT: A coupled atmosphere ocean sea-ice model for climate predictability studies. Report, TR-195, Netherlands Meteorological Institute (KNMI), De Bilt, The Netherlands.
- Haarsma R.J., Campos A.J.D., Hazaleger W., Severijns C., Piola A.R., Molteni, F. (2005) Dominant modes of variability in the South Atlantic: A study with a hierarchy of ocean-atmosphere models. *Journal of Climate*, 18:1719-1735.
- Harding R.J. and Pomeroy J.W. (1996). The energy balance of the winter Boreal landscape. *Journal of Climate*, 9:2778-2787.
- Hoogwijk M., Faaij A., Eickhout B., De Vries B. and Turkenburg W. (2005) Potential of biomass energy out to 2100, for four IPCC SRES land-use scenarios. *Biomass and Bioenergy*, 29:225-257.
- Houghton J.T., Ding Y., Griggs D.J., Noguer M., Van Der Linden P.J., Dai X., Maskell K. and Johnson C.A. (2001) Climatic change 2001. The scientific basis. Contribution of Working Group I to the third assessment report of the Intergovernmental Panel on Climate Change. Cambridge University Press, Cambridge, 881 pp.
- Hughes T.P., Baird A.H., Bellwood D.R., Card M., Connolly S.R., Folke C., Grosberg R., Hoegh-Guldberg O., Jackson J.B.C., Kleypas J., Lough J.M., Marshall P., Nyström M., Palumbi S.R., Pandolfi J.M., Rosen B., Roughgarden J. (2003). Climate Change, Human Impacts, and the Resilience of Coral Reefs. *Science*, 301:929-933.
- Hutjes R.W.A., Dolman A.J., Nabuurs G.J., Schelhaas M.J., Maat H.W. ter, Kabat P., Moors E., Huygen J., Haarsma R., Ronda R., Schaeffer M., Opsteegh J.D., Leemans R., Bouwman L., Busch G., Eickhout B., Kreileman E., Schaeffer M., Strengers B., De Vries B., Verhagen A., Vleeshouwers, Corre W.J., Jongschaap R.E.E., Kruseman G., Ierland E. van, Holtslag A.A.M., Ronda R., Willemsen F., Dorland C., Van Tol R.S.J. (2001). Feedback land surface with atmosphere at global scales. In Land use, climate and biogeochemical cycles: Feedbacks and options for emission reduction. Global Change NOP-NRP report 410200107. Bilthoven, The Netherlands.
- IMAGE-team (2001) The IMAGE 2.2 implementation of the SRES scenarios. A comprehensive analysis of emissions, climate change and impacts in the 21st century. CD-ROM publication 481508018, National Institute for Public Health and the Environment, Bilthoven, The Netherlands. Reprinted by Netherlands Environmental Assessment Agency (MNP), Bilthoven as CD-ROM publication 500110001.
- Kabat P., Claussen M., et al., Dirmeyer P.A., Gash J.H.C., Bravo De Guenni L., Meybeck M., Pielke Sr. R., Vörösmarty C.J., Hutjes R.W.A., and Lütkeemeier S. (2004). Vegetation, water, humans and the climate. A new perspective on an interactive system. Springer Verlag, Berlin.
- Katz R.W. and Brown B.G. (1992). Extreme events in a changing climate: variability is more important than averages. *Climatic Change*, 21:289-302.
- Kiehl J.T. and Trenberth K.E. (1997). Earth's annual global mean energy budget. *Bulletin of the American Meteorological Society*, 78:197-208.
- Knutti R. and Stocker T.F. (2002). Limited predictability of the future thermohaline circulation close to an instability threshold. *Journal of Climate*, 15:179-186.
- Manabe S. and Stouffer R.J. (1988). Two stable equilibria of a coupled ocean-atmosphere model. *Journal of Climate*, 1:841-866.
- Manabe S. and Stouffer R.J. (1993). Century-scale effects of increased atmospheric CO<sub>2</sub> on the ocean-atmosphere system, *Nature*, 364:215-218.
- Manabe S. and Stouffer R.J. (1995). Simulation of abrupt climate change induced by freshwater input to the North Atlantic Ocean. *Nature*, 378:165-167.
- Molteni F. (2003). Atmospheric simulations using a GCM with simplified physical parametrizations. I: Model climatology and variability in multi-decadal experiments. *Climate Dynamics*, 20:175-191.

- Müller C. and Lucht W. (2006) Robustness of terrestrial carbon and water cycle simulations against variations in spatial resolution. *Journal of Geophysical Research* (in press).
- Oppenheimer M. and Alley R.B. (2004). The West Antarctic ice sheet and long term climate policy. *Climatic Change*, 64:1-10.
- Opsteegh J.D., Haarsma R.J., Selten F. M. and Kattenberg A. (1998). ECBILT: a dynamic alternative to mixed boundary conditions in ocean models. *Tellus*, 50A:348-367.
- Parmesan C., Root T.L., and Willig M.R. (2000). Impacts of extreme weather and climate on terrestrial biota. *Bulletin of the American Meteorological Society*, 81:443-450.
- Pielke R.A. Sr., Marland G., Betts R.A., Chase T.N., Eastman J.L., Niles J.O., Niyogi D.S. and Running S.W. (2002). The influence of land-use change and landscape dynamics on the climate system: relevance to climate-change policy beyond the radiative effect of greenhouse gases. *Philosophical Transactions of the Royal Society of London*, 360:1705-1719.
- Rahmstorf S. and Ganopolski A. (1999). Long-term global warming scenarios computed with an efficient coupled climate model. *Climatic Change*, 43:353-367.
- Riha S.J., Wilks D.S. and Simoens P. (1996). Impact of temperature and precipitation variability on crop model predictions. *Climatic Change*, 32:293-311.
- Robinson D.A. and Kukla G. (1985). Maximum surface albedo of seasonally snow-covered lands in the Northern hemisphere. *Journal of Climate and Applied Meteorology*, 24:402-411.
- Ronda R.J., Haarsma R.J., and Holtslag A.M. (2003). Modelling the atmospheric boundary layer in a climate model of intermediate complexity. *Climate Dynamics*, 21:327-335.
- Russell G.L. and Rind D. (1999). Response to CO<sub>2</sub> transient increase in the GISS coupled model: regional coolings in a warming climate. *Journal of Climate*, 12:531-539.
- Schaeffer M., Selten F.M., Opsteegh J.D. and Goosse H. (2002). Intrinsic limits to predictability of abrupt regional climate change in IPCC SRES scenarios. *Geophysical Research Letters*, 29(16), 14:1-14:4.
- Schaeffer M., Selten F.M., Goosse H. and Opsteegh J.D. (2004). The influence of ocean convection patterns on high-latitude climate projections. *Journal of Climate*, 17:4316-4329.
- Schaeffer M., Selten F.M. and Opsteegh J.D. (2005). Shifts of means are not a proxy for changes in extreme winter temperatures in climate projections. *Climate Dynamics*, 25:51-63.
- Schaeffer M., Eickhout B., Hoogwijk M., Strengers B., Van Vuuren D., Leemans R. and Opsteegh T. (2006) CO<sub>2</sub> and albedo climate impacts of extratropical carbon and biomass plantations. *Global Biogeochemical Cycles*, 20, GB2020, doi:10.1029/2005GB002581.
- Scheffer M., Carpenter S.R., Foley J.A., Folke C., and Walker B. (2001). Stochastic events can trigger large state shifts in ecosystems with reduced resilience. *Nature*, 413:591-596.
- Sharrat B.S. (1998). Radiative exchange, near-surface temperature and soil water of forest and cropland in interior Alaska. *Agricultural and Forest Meteorology*, 89:269-280.
- Sitch S., Smith B., Prentice I.C., Arneth A., Bondeau A., Cramer W., Kaplans J.O., Levis S., Lucht W., Sykes M.T., Thonicke K., and Venesky S. (2003) Evaluation of ecosystem dynamics, plant geography and terrestrial carbon cycling in the LPJ dynamic global vegetation model. *Global Change Biology*, 9:161-185.
- Van Den Hurk B.J.J.M., Viterbo P., Beljaars A.C.M. and Betts A.K. (2000) Offline validation of the ERA40 surface scheme. Technical Memorandum 295, European Centre for Medium-Range Weather Forecasts, Reading, U.K., 42 pages.
- Van Ulden A.P. and Van Oldenborgh G.J. (2006). Large-scale atmospheric circulation biases and changes in global climate model simulations and their importance for climate change in Central Europe. *Atmospheric Chemistry and Physics*, 6:863-881.
- Van Vuuren D.P. and De Vries H.J.M. (2001). Mitigation scenarios in a world oriented at sustainable development: the role of technology, efficiency and timing. *Climate Policy*, 24:1-22.

## Chapter 10

- Allen C.R., Pearlstine L.G., Kitchens W.M. (2001) Modeling viable populations in Gap analyses. *Biological Conservation*, 99:135-144
- Bakkenes M., Alkemade J.R.M., Ihle F., Leemans R. and Latour J.B. (2002) Assessing effects of forecasted climate change on the diversity and distribution of European higher plants for 2050. *Global Change Biology*, 8:390-407.
- Bakkenes M., Eickhout B. and Alkemade R. (2006) Impacts of different climate stabilisation scenarios on plant species in Europe. *Global Environmental Change*, 16:19-28.

- Bartholome E., Belward A.S., Achard F., Bartalev S., Carmonamorenno C., Eva H., Fritz S., Gregoire J.-M., Mayaux P. and Stibig H.-J. (2002) GLC 2000; Global Land Cover mapping for the year 2000. Project status November 2002. Report EUR 20524 EN, Institute for Environment and Sustainability, Joint Research Centre, Ispra, Italy, 58 pp. (<http://www-gvm.jrc.it/glc2000/default-GLC2000.htm>).
- Bobbink R. (2004) Plant species richness and the exceedance of empirical nitrogen critical loads: an inventory. Internal report. Utrecht University.
- Bouwma I.M., Jongman, R.H.G. and Butovsky R.O. (Editors) (2002) The Indicative Map of Pan-European Ecological Network. Technical background document. ECNC Technical report series, ECNC, Tilburg, The Netherlands/Budapest.
- Bouwman A.F., Van Vuuren D.P., Derwent R.G. and Posch M. (2002) A global analysis of acidification and eutrophication of terrestrial ecosystems. *Water, Air and Soil Pollution*, 141:349-382.
- Cardillo M., Purvis A., Sechrest W., Gittleman J.L., Bielby J. and Mace G.M. (2004) Human population density and extinction risk in the world's carnivores. *PLoS Biology*, 2:909-914.
- De Heer M., Kapos V. and Ten Brink B.J.E. (2005) Biodiversity trends in Europe: Development and testing of a species trend indicator for evaluating progress towards the 2010 target. *Phil. Transactions of the Royal Society B (Biological Sciences)*, 360:297-308.
- DMA (1992) The digital chart of the world. Defense Mapping Agency, Fairfax, Virginia.
- Di Gregorio A. and Jansen L.J.M. (2000) Land cover classification system. Classification concepts and user manual, Report GCP/RAF/287/ITA Africover, including CD-ROM, Food and Agriculture Organization of United Nations, Rome, 179 pp.
- Dixon J., Gulliver A. and Gibbon D. (2001) Farming Systems and poverty. Improving farmers' livelihoods in a changing world. Food and Agriculture Organization of the United Nations/World Bank, Rome/Washington, DC, 412 pp.
- FAO (2001) Global forest resources assessment 2000. FAO Forestry Paper 140. Food and Agriculture Organization of the United Nations, Rome.
- FAO (2005) FAOSTAT database collections. Food and Agriculture Organization of the United Nations, Rome ([www.apps.fao.org](http://www.apps.fao.org)).
- Guisan A. and Zimmermann N.E. (2000) Predictive habitat distribution models in ecology. *Ecological Modelling*, 135:147-186.
- Hannah L., Lohse D., Hutchinson C., Carr J.L. and Lankerani A. (1994) A preliminary inventory of human disturbance of world ecosystems. *Ambio*, 23:246-250.
- IMAGE-team (2001). The IMAGE 2.2 implementation of the SRES scenarios. A comprehensive analysis of emissions, climate change and impacts in the 21<sup>st</sup> century. CDROM publication 481508018, National Institute for Public Health and the Environment, Bilthoven The Netherlands. Reprinted by Netherlands Environmental Assessment Agency (MNP), Bilthoven as CD-ROM publication 500110001.
- Imhoff M.L., Bounoua L., Ricketts T., Loucks C., Hariss R. and Lawrence W.T. (2004) Global patterns in human consumption of the net primary production. *Nature*, 429:870-873.
- Klein Goldewijk K., Van Drecht G. and Bouwman A.F. (2006) Contemporary global cropland and grassland distributions on a 5 by 5 minute resolution. *Journal of Land Use Science* (submitted).
- Leemans R. and Eickhout B. (2004) Another reason for concern: regional and global impacts on ecosystems for different levels of climate change. *Global Environmental Change*, 14:219-228.
- Loh J., Green R.E., Ricketts T., Lamoreux J., Jenkins M., Kapos V. and Randers J. (2005) The living planet index: using species population time series to track trends in biodiversity. *Philosophical Transactions of the Royal Society of London B: Biological Sciences*, 360: 289-295.
- Majer J.D. and Beeston G. (1996) The biodiversity Integrity Index: An illustration using ants in Western Australia. *Conservation Biology*, 10:65-73.
- McKee J.K., Sciulli P.W., Fooce C.D. and Waite T.A. (2003) Forecasting global biodiversity threats associated with human population growth. *Biological Conservation*, 115:161-164.
- Millennium Assessment (2003) Ecosystems and Human Well-being. A framework for assessment. Millennium Ecosystem Assessment. Island Press, Washington, 245 pp.
- Nakicenovic N., Alcamo J., Davis G., De Vries B., Fenhann J., Gaffin S., Gregory K., Grubler A., Jung T.Y., Kram T., Emilio la Rovere E., Michaelis L., Mori S., Morita T., Pepper W., Pitcher H., Price L., Riahi K., Roehrl A., Rogner H., Sankovski A., Schlesinger M., Shukla P., Smith S., Swart R., Van Rooyen S., Victor N. and Dadi Z. (2000) Special Report on emissions scenarios. IPCC Special Report. Cambridge University Press, Cambridge, 599 pp.

- Petit S., Firbank L., Wytt B. and Howard D. (2001) MIRABEL: Models for integrated review and assessment of biodiversity in European landscapes. *Ambio*, 30:81-88.
- Prentice C., Cramer W., Harrison S.P., Leemans R., Monserud R.A. and Solomon A.M. (1992) A global biome model based on plant physiology and dominance, soil properties and climate. *Journal of Biogeography*, 19:117-134.
- Sala O.E., Chapin III F.S., Armesto J.J., Berlow E., Bloomfield J., Irzo R., Huber-Samwald E., Huenneke, K.L.F., Jackson R.B., Kinzig A., Leemans R., Lodge D.M., Mooney H.A., Oesterheld M., Poff N.L., Sykes M.T., Walker B.H., Walker M. and Wall D.H. (2000) Global biodiversity scenarios for the year 2100. *Science*, 287:1770-1774.
- Sanderson E.W., Jaiteh M., Levy M.A., Redford K.H., Wannebo, A.V. and Woolmer G. 2002. The Human footprint and the last of the wild. *BioScience*, 52:891-904.
- Scholes R.J. and Biggs R. (2005) A biodiversity intactness index. *Nature*, 434:45-49.
- UNEP (2001) GLOBIO. Global methodology for mapping human impacts on the biosphere. Report UNEP/DEWA/TR 25, United Nations Environment Programme, Nairobi.
- UNEP (2002a) Decision VI/26 Strategic plan for the Convention on Biological Diversity. Sixth Conference of the Parties to the Convention of Biological Diversity, The Hague.
- UNEP (2002b) Global Environment Outlook 3. Earthscan Publications Ltd., London, 446 pp.
- UNEP (2004) Decision VII/30 Strategic plan: future evaluation of progress. Seventh Conference of the Parties to the Convention on Biological Diversity, Kuala Lumpur.
- UNEP/RIVM (Potting J. and Bakkes J., Editors) (2004) The GEO-3 scenarios 2002-2032: Quantification and analysis of environmental impacts. Report UNEP/DEWA/RS.03-4 and RIVM 402001022, Division of Early Warning and Assessment (DEWA), United Nations Environment Programme (UNEP) / National Institute for Public Health and the Environment, Nairobi / Bilthoven, The Netherlands, 216 pp.
- Verboom J., Alkemade R., Klijn J., Metzger M.J. and Reijnen R. (2006) Combining biodiversity modeling with political and economic development scenarios for 25 EU countries. *Ecological Economics* (in press).
- Wackernagel M., Schulz N.B., Deumling D., Callejas Linares A., Jenkins M., Kapos V., Monfreda C., Loh J., Myers N., Norgaard R. and Randers J. (2002) Tracking the ecological overshoot of the human economy. *Proceedings of the National Academy of Sciences*, 99:9266-9271.
- Woodroffe R. and Ginsberg J.R. (1998) Edge effects and the extinction of populations inside protected areas. *Science*, 280:2126-2128.

## Chapter 11

- Aldy J.E., Ashton J., Baron R., Bodansky D., Charnovitz S., Diringier E., Heller T.C., Pershing J., Shukla P.R., Tubiana L., Tudela F. and Wang X. (2003) Beyond Kyoto, Advancing the international effort against climate change. Pew Center on Global Climate Change, Arlington, VA.
- Berk M.M. and Den Elzen M.G.J. (2001) Options for differentiation of future commitments in climate policy: how to realize timely participation to meet stringent climate goals? *Climate Policy*, 1(4):465-480.
- Berk M.M., Van Minnen J.G., Metz B., Moomaw W., Den Elzen M.G.J., Van Vuuren D.P. and Gupta J. (2001) Climate options for the long term (COOL) Global dialogue synthesis report. Report 490200003, National Institute for Public Health and the Environment, Bilthoven, The Netherlands.
- Bodansky D. (2004) International climate efforts beyond 2012: a survey of approaches, Pew Center on global climate change, Arlington, VA. ([www.pewclimate.org](http://www.pewclimate.org))
- CPB (1999) WorldScan: the core version. Netherlands Bureau for Economic Policy Analysis (CPB), The Hague, 137 pp.
- Criqui P. (2002) GECS Final Report Section 6: Detail report. GECS - Research Project N° EVK2-CT-1999-00010, Thematic Programme: Environment and Sustainable Development, DG Research Fifth Framework Programme, CNRS-IEPE, Grenoble.
- Criqui P., Kitous A., Berk M.M., Den Elzen M.G.J., Eickhout B., Lucas P., Van Vuuren D.P., Kouvaritakis N. and Vanregemorter D. (2003) Greenhouse gas reduction pathways in the UNFCCC Process up to 2025 - Technical Report. B4-3040 /2001 /325703 /MAR /E.1 for the DG Environment, CNRS-IEPE, Grenoble.
- Criqui P. and Kouvaritakis N. (2000) World energy projections to 2030. *International Journal of Global Energy Issues*, 14(1-4):116-136.
- Criqui P., Mima S. and Viguier L. (1999) Marginal abatement costs of CO<sub>2</sub> emission reductions, geographical flexibility and concrete ceilings: an assessment using the POLES model. *Energy Policy*, 27(10):585-601.
- CSE (1998). Definitions of equal entitlements. CSE-dossier, fact sheet 5, Centre for Science and Environment (CSE), Delhi.

- De Vries H.J.M., D.P. Van Vuuren, Den Elzen M.G.J. and Janssen M.A. (2001) The Targets Image Energy model regional (TIMER) - Technical documentation. Report 461502024, National Institute for Public Health and the Environment, Bilthoven, The Netherlands, 188 pp.
- DeAngelo B.J., De la Chesnaye F.C., Beach R.H., Sommer A. and Murray B.C. (2004) Methane and nitrous oxide mitigation in agriculture. *Energy Journal*, (in press).
- Delhotal K.C., De la Chesnaye F.C., Gardiner A., Bates J. and Sankovski A. (2004) Mitigation of methane and nitrous oxide emissions from waste, energy and industry. *Energy Journal*, (in press).
- Den Elzen M.G.J. (2002) Exploring climate regimes for differentiation of future commitments to stabilise greenhouse gas concentrations. *Integrated Assessment*, 3(4):343-359.
- Den Elzen M.G.J. (2005) Analysis of future commitments and costs of countries for the "South-North Dialogue" Proposal using the FAIR 2.1 world model. Report 728001032, Netherlands Environmental Assessment Agency (MNP), Bilthoven, The Netherlands ([www.mnp.nl/en](http://www.mnp.nl/en)).
- Den Elzen M.G.J. and De Moor A.P.G. (2002) Analysing the Bonn Agreement and Marrakesh Accords: Economic efficiency & environmental effectiveness. *Ecological Economics*, 43:141-158.
- Den Elzen M.G.J. and Schaeffer M. (2002) Responsibility for past and future global warming: uncertainties in attributing anthropogenic climate change. *Climatic change*, 54:29-73.
- Den Elzen M.G.J. and Berk M.M. (2003) How can the Parties fairly and effectively establish future obligations under long-term objectives? In: Michel D. (Editor), *Climate policy for the 21st century: meeting the long-term challenge of global warming*. Center for Transatlantic Relations, Washington, DC, pp. 79-112.
- Den Elzen M.G.J. and Lucas P. (2003) FAIR 2.0: a decision-support model to assess the environmental and economic consequences of future climate regimes. Report 550015001, National Institute for Public Health and the Environment, Bilthoven, The Netherlands ([www.mnp.nl/fair](http://www.mnp.nl/fair)).
- Den Elzen M.G.J. and Lucas P. (2005) The FAIR model: a tool to analyse environmental and costs implications of climate regimes. *Environmental Modeling and Assessment*, 10(2):115-134.
- Den Elzen M.G.J., Schaeffer M. and Eickhout B. (2002) Responsibility for past and future global warming: time horizon and nonlinearities in the climate system. Report 728001022, National Institute for Public Health and the Environment, Bilthoven, The Netherlands.
- Den Elzen M.G.J., Berk M.M., Lucas P., Eickhout B. and Van Vuuren D.P. (2003) Exploring climate regimes for differentiation of commitments to achieve the EU climate target. Report 728001023, National Institute for Public Health and the Environment, Bilthoven, The Netherlands.
- Den Elzen M.G.J., Fuglestedt J.S., Höhne N., Trudinger C.M., Lowe J., Matthews B.J.H., Romstadt B., Pires De Campos C. and Andranova N. (2005a) Analysing countries' contribution to climate change: Scientific uncertainties and methodological choices. *Environmental Science and Policy*, 8:614-636.
- Den Elzen M.G.J., Lucas P. and Van Vuuren D.P. (2005b) Abatement costs of post-Kyoto climate regimes. *Energy Policy*, 33(16):2138-2151.
- Den Elzen M.G.J., Berk M.M., Lucas P., Criqui C. and Kitous A. (2006a) Multi-Stage: a rule-based evolution of future commitments under the Climate Change Convention. *International Environmental Agreements: Politics, Law and Economics*, 6:1-28.
- Den Elzen M.G.J., Meinshausen M. and Van Vuuren D.P. (2006b) Multi-gas emission envelopes to meet greenhouse gas concentration targets: costs versus certainty of limiting temperature increase. *Global Environmental Change* (in press).
- Eickhout B., Den Elzen M.G.J. and Van Vuuren D.P. (2003) Multi-gas emission profiles for stabilizing greenhouse gas concentrations. Report 728001026, National Institute for Public Health and the Environment, Bilthoven, The Netherlands.
- Eickhout B., Den Elzen M.G.J. and Kreileman G.J.J. (2004) The Atmosphere-ocean system of IMAGE 2.2: A global model approach for atmospheric concentrations, and climate and sea level projections. Report 481508017, National Institute for Public Health and the Environment, Bilthoven, The Netherlands.
- Groenenberg H. (2002) Development and convergence: a bottom-up analysis for the differentiation of future commitments under the Climate Convention. PhD Thesis, Utrecht University.

- Gupta J. (1998) Encouraging developing country participation in the climate change regime, Institute for Environmental Studies, Free University of Amsterdam.
- Hasselmann K., Sausen R., Maier-Reimer E. and Voss R. (1993) On the cold start problem in transient simulations with coupled atmosphere-ocean models. *Climate Dynamics*, 9:53-61.
- Höhne N., Den Elzen M.G.J. and Weiss M. (2004) Common but differentiated convergence (CDC), a new conceptual approach to long-term climate policy. *Climate Policy* 6 (in press).
- Höhne N., Galleguillos C., Blok K., Harnisch J. and Phylipsen D. (2003) Evolution of commitments under the UNFCCC: Involving newly industrialized countries and developing countries. Report 20141255, UBA-FB 000412, ECOFYS GmbH, Berlin.
- Houghton R.A. (2003) Revised estimates of the annual net flux of carbon to the atmosphere from changes in land use and land management 1850–2000. *Tellus*, 55B:378–390.
- IMAGE-team (2001) The IMAGE 2.2 implementation of the SRES scenarios. A comprehensive analysis of emissions, climate change and impacts in the 21<sup>st</sup> century. CD-ROM publication 481508018, National Institute for Public Health and the Environment, Bilthoven, The Netherlands. Reprinted by Netherlands Environmental Assessment Agency (MNP), Bilthoven as CD-ROM publication 500110001.
- Jacoby H.D., Schmalensee R. and Wing I.S. (1999) Toward a useful architecture for climate change negotiations. Report 49, MIT, Cambridge, MA.
- Joos F., Plattner G.-K., Stocker T.F., Marchal O. and Schmittner A. (1999) Global warming and marine carbon cycle feedbacks on future atmospheric CO<sub>2</sub>. *Science*, 284:464-467.
- Kameyama Y. (2004) The future climate regime: a regional comparison of proposals. *International Environmental Agreements: Politics, Law and Economics*, 4:307-326.
- Lucas P.L., Den Elzen M.G.J. and Van Vuuren D.P. (2005) A Multi-gas abatement analysis of the Marrakesh Accords. Report 550006001, Netherlands Environmental Assessment Agency (MNP), Bilthoven, The Netherlands, 34 pp.
- Marland G., Boden T.A. and Andres R.J. (2003) Global, regional, and national fossil fuel CO<sub>2</sub> Emissions. In: ORNL Carbon Dioxide Information Analysis Center, U.S. Department of Energy, Trends: A Compendium of data on global change, Oak Ridge, Tennessee, TN. ([http://cdiac.esd.ornl.gov/trends/emis/meth\\_reg.htm](http://cdiac.esd.ornl.gov/trends/emis/meth_reg.htm)).
- Meyer A. (2000) Contraction & convergence. The global solution to climate change. Schumacher Briefings, 5. Green Books, Bristol, UK.
- Müller B. (1999) Justice in global warming negotiations - How to achieve a procedurally fair compromise. Oxford Institute for Energy Studies, Oxford.
- Phylipsen G.J.M., Bode J.W., Blok K., Merkus H. and Metz B. (1998) A Triptych sectoral approach to burden differentiation; GHG emissions in the European bubble. *Energy Policy*, 26(12):929-943.
- Phylipsen G.J.M., Höhne N. and Janzic R. (2005) Implementing Triptych 6.0. Report DM 70046/ICC03080, Ecofys, Utrecht.
- Prather M., Ehhalt D., Dentener F.J., Derwent R., Dlugokencky E., Holland E., Isaksen I., Katima J., Kirchhoff V., Matson P., Midgley P. and Wang M. (2001) Atmospheric chemistry and Greenhouse Gases. In: Houghton J.T., Ding Y., Griggs D.J., Noguera M., Van Der Linden P.J., Dai X., Maskell K., Johnson C.A. (Editors), *IPCC Third Assessment - Climate Change 2001, The Scientific Basis*. Cambridge University Press, Cambridge.
- Rose A., Stevens B., Edmonds J. and Wise M. (1998) International Equity and differentiation in Global Warming policy. *Environmental and Resource Economics*, 12(1):25-51.
- Schaefer D.O., Godwin D. and Harnisch J. (2004) Estimating future emissions and potential reductions of HFCs, PFCs and SF6. *Energy Journal* (in press).
- Torvanger A. and Godal O. (2004) An evaluation of pre-Kyoto differentiation proposals for national greenhouse gas abatement targets. *International Environmental Agreements: Politics, Law and Economics*, 4(65-91).
- UNFCCC (1992) United Nations General Assembly, United Nations Framework Convention on Climate Change, United Nations, New York (<http://www.unfccc.int/resources>).
- UNFCCC (1997) Paper no. 1: Brazil; Proposed Elements of a Protocol to the United Nations Framework Convention on Climate Change. Report UNFCCC/AGBM/1997MISC.1Add.3GE.97, Bonn.
- UNFCCC (2002) Assessment of contributions to climate change, Terms of Reference (<http://unfccc.int/program/mis/brazil/index.html>).
- Van Aardenne J.A., Dentener F.J., Olivier J.G.J., Klein Goldewijk C.G.M. and Lelieveld J. (2001) A 1 x 1 degree resolution dataset of historical anthropogenic trace gas emissions for the period 1890-1990. *Global Biogeochemical Cycles*, 15(4):909-928.

- Van Vuuren D.P., De Vries H.J.M., Eickhout B. and Kram T. (2004) Responses to technology and taxes in a simulated world. *Energy Economics*, 26(579-601).
- Van Vuuren D.P., Den Elzen M.G.J. and Berk M.M. (2002) An evaluation of the level of ambition and implications of the Bush Climate Change Initiative. *Climate Policy*, 2:293-301.
- Van Vuuren D.P., Den Elzen M.G.J., Berk M.M., Lucas P., Eickhout B., Eerens H. and Oostenrijk R. (2003) Regional costs and benefits of alternative post-Kyoto climate regimes. Report 728001025, National Institute for Public Health and the Environment, Bilthoven, The Netherlands.
- Van Vuuren D.P., Eickhout B., Lucas P.L. and Den Elzen M.G.J. (2006) Long-term multi-gas scenarios to stabilise radiative forcing - exploring costs and benefits within an integrated assessment framework. *Energy Journal* (in press).
- Wigley T.M.L. and Raper S.C.B. (1992) Implications for climate and sea-level of revised IPCC emissions scenarios. *Nature*, 357:293-300.
- WorldBank (2001) World development report 2000/2001: Attacking poverty. Oxford University Press, Oxford.